UNIVERSITY OF NEWCASTLE UPON TYNE

DEPARTMENT OF CIVIL ENGINEERING

THE TRANSFER OF OXYGEN FROM AIR ENTRAINED BY JETS ENTERING A FREE WATER RECIPIENT

by

S.T. AVERY, B.Sc.

A thesis submitted for the Degree of Doctor of Philosophy, 1976

CONTENTS

ACKNOWLEDGEMENTS

The author wishes to express appreciation to all whose assistance has led to the production of this thesis.

Particular thanks are due to:

Professor P. Novak for the many hours spent in discussion and, thankfully, for his patience. The technical staff of the Department of Civil Engineering, both for their technical assistance and welcome company during the many months spent in the laboratory. To mention but a few: Alan Jefferson, Dave Innes, John Cuthbert, John Hamilton, Vic Henderson, Neil Baldridge, John Allen and Mr. E. Armstrong.

The following individuals and organisations for their cooperation and kind provision of supplementary data without which this project would have been incomplete: Mr. A.L.H. Gameson of the Water Research Centre, Mr. A.G. Holler of the U.S. Corps of Engineers, the firm of Lawler, Matusky and Skelly of New York, the Minnesota Power and Light Company, U.S.A., Mr. J.J. McKeown of the NCASI, New York, and Bauassessor K.R. Imhoff of the Ruhrverband and Ruhrtalsperrenverein, West Germany.

Miss Kathy Gray for performing the arduous task of producing a typed draft from my notes and Mrs. Dorreen Moran for typing the final script.

The Science Research Council for the award of a research studentship.

Messrs. Waterhouse and Partners, Consulting Engineers, for provision of financial assistance by way of part-time employment.

The University for the remission of fees for the session 1974/75.

My fellow research students for their occasionally inspiring company.

And finally, my parents, for their moral support throughout.

ABSTRACT

A detailed study has been made of the oxygen transfer resulting from the air entrained into a free water recipient by water jets. Particular attention has been paid to various free falling jets entering a pool for a variety of conditions of this pool, also to a guided jet terminating in the formation of an hydraulic jump. These features are common to a number of hydraulic structures.

An extensive laboratory programme has been conducted, the effect of all important hydraulic variables has been investigated together with water quality effects, in particular the effect of dissolved salts.

Dimensionless correlation equations have been developed and some success has been achieved in determining the modelling laws governing the oxygen transfer in an air entrainment situation. Modelling according to the Froude law of similarity has shown that the oxygen transfer expressed as a deficit ratio varied as a simplified function of the scale. For the first time, the laboratory measurements of oxygen transfer due to a free falling jet entering a free water recipient have been successfully correlated with data received for a number of prototype dam and weir structures. Similar success has been achieved in correlation with published laboratory work on free overfall weirs, and a wider range of applicability to multi crested and cascade weirs has been shown subject to certain conditions.

LIST OF FIGURES AND PLATES

LIST OF PLATES

LIST OF TABLES

LIST OF PRINCIPAL SYMBOLS WITH DIMENSIONS

a	water quality index, Equation 2.11
A	area of gas/liquid interface, (L^2)
A_c	cross sectional area of flow, (L^2)
b	river structure parameter, Equation 2.11
B	channel or weir crest width (L)
B_J	jet width, (L)
c	constant ($y = cx^2$) constant, Equation 2.41
C_{ac}	aeration capacity, Equation 1.34
C_i	gas concentration in liquid film at gas/liquid interface, Equation 1.9, (ML^{-3})
C_L	gas concentration in the body of liquid beyond the liquid film, Equation 1.9, (ML^{-3})
C_n	constant, Equation 2.41
C_s	gas saturation concentration, (ML^{-3})
C'_s	gas saturation concentration in saline water, (ML^{-3})
C_t	gas concentration at time t, (ML^{-3})
C_{tx}	gas concentration at time t and distance x from the gas/liquid interface, (ML^{-3})
C_o	gas concentration at time $t = 0$, (ML^{-3})
C_1	oxygen concentration prior to aeration, (ML^{-3})
C_2	oxygen concentration after aeration, (ML^{-3})
d	stilling pool depth, (L)
d'	optimum depth of stilling pool, (L)
d_b	bubble diameter, (L)
d_g	thickness of gas film, (L)
d_L	thickness of liquid film, (L)
d_o	depth of flow over weir crest, (L)
D	jet diameter, (L)
D_E	coefficient of eddy diffusion, (L^2T^{-1})
D_L	longitudinal mixing coefficient, Equation 4 Table 2.1, (L^2T^{-1})
D_m	coefficient of molecular diffusion, (L^2T^{-1})
D_T	overall coefficient of diffusion, (L^2T^{-1})
E	specific energy ($y + \alpha v^2/2g$), (L)
E_d	energy dissipation per unit mass of fluid, Equation 5 Table 2.1

E_o specific energy upstream of sluice gate ($y_o + \alpha_o v_o^2/2g$), (L)

E_1 specific energy at the initial hydraulic jump conjugate depth section ($y_1 + \alpha_1 v_1^2/2g$), (L)

E_2 specific energy at the sequent hydraulic jump conjugate depth section ($y_2 + \alpha_2 v_2^2/2g$), (L)

f friction factor, Equation 1.3

Fr Froude number ($v/\sqrt{gy}$)

Fr_1 Froude number at the initial hydraulic jump conjugate depth section ($v_1/\sqrt{gy_1}$)

Fr_J jet Froude number, Equation 7.4

g acceleration due to gravity, (LT^{-2})

Δh change in water surface elevation, Equation 13 Table 2.1, (L)

h height of fall (difference between upstream and downstream water surface elevations), (L)

H height of fall (difference between the pool crest and stilling pool bed elevations), (L)

k_g gas film diffusion coefficient, (LT^{-1})

k_j constant, Equation 4.5

k_{J1} k_{J2} k_{J3} functions of specific discharge, Equations 4.24, 4.25, 4.26

k_L liquid film diffusion coefficient, (LT^{-1})

k_r constant, Equation 4.5

k_1 k_2 functions of specific discharge, Equations 4.15, 4.16

K constant, Equation 1.30 also Equation 2.1

K_d constant, Equation 1.4 also Equation 7.10

K_I deoxygenation rate constant, Equation 2.44

K_J constant, Equation 7.16

K_L overall film coefficient, (LT^{-1})

K_{La} overall gas transfer coefficient ($K_L A/V$), (T^{-1})

K_m constant, Equation 2.17

K_p constant, Equation 2.17

K_s constant, Equation 7.20

K_{sa} constant, Equation 1.39

ℓ Prandtl mixing length, (L)

L_j length of aerated zone of hydraulic jump, (L)

L_o distance to point of total jet disintegration measured along jet centre line, Equation 2.7, (L)

L_r length of roller zone of hydraulic jump, (L)

L_t BOD at time t, (ML^{-3})

L_1 initial BOD (Biochemical Oxygen Demand), (ML^{-3})

m	depth exponent, Equation 2.36
M	mass of gas transferred, (M)
$M_{\Delta E}$	energy loss scale
M_{K_L}	liquid film coefficient scale $((K_L)_1/(K_L)_2)$
M_L	length scale
M_o	rate of gas transfer, (MT^{-1})
M_{r-1}	r-1 scale $((r-1)_1/(r-1)_2)$
M_t	time scale
n	number of steps in a cascade
n_1	exponent, Equation 2.37
N	number of jets discharged from a notch
N_o	Avogadro's number
P	jet perimeter, (L)
P_g	concentration (partial pressure) of solute in main body of gas, $(ML^{-1}T^{-2})$
P_i	concentration (partial pressure) of solute in gas at gas/liquid interface, $(ML^{-1}T^{-2})$
P_o	barometric pressure, $(ML^{-1}T^{-2})$
P_{vp}	saturated water vapour pressure at T^oC, $(ML^{-1}T^{-2})$
q	water discharge per unit notch or channel width, (L^2T^{-1})
q_a	air discharge per unit channel width, (L^2T^{-1})
q_J	water discharge per unit jet perimeter, (L^2T^{-1})
Q	water discharge, (L^3T^{-1})
Q'	water discharge computed from channel velocity traverse, (L^3T^{-1})
Q_a	air discharge, (L^3T^{-1})
r	deficit ratio (C_s-C_2/C_s-C_1) at T^oC
r_c	constant rate of surface renewal, (T^{-1})
r_{15}	deficit ratio at 15^oC
R	hydraulic radius (A_c/P), (L)
R_e	Reynolds number, Equation 2.5
R_o	universal gas constant
s	rate of surface production, Equation 1.20 (T^{-1})
S	channel slope
S_a	salinity
S_c	Schmidt number
t	time of contact, (T)
t'	time of bubble rise, (T)
t''	time of bubble descent, (T)

t_c constant time of exposure of fluid elements, (T)

t_f time of flow, (T)

t_J jet thickness, (L)

T temperature, (^oC)

T_o absolute temperature, (^oK)

u_* shear velocity, Equation 11 Table 2.1, (LT^{-1})

$\bar{u}$ average velocity with respect to time, (LT^{-1})

U velocity of free falling jet, (LT^{-1})

U_e minimum jet velocity for the entrainment of air, (LT^{-1})

v channel velocity, (LT^{-1})

v_n mean velocity in segmental area dA, (LT^{-1})

v_1, v_2 velocity at initial sequent hydraulic jump conjugate depth sections (LT^{-1})

V volume of body of liquid, (L^3)

V_a volume of entrained air, (L^3)

x horizontal distance coordinate, (L) perpendicular distance from a point in the fluid to the air/water interface, (L)

y mean depth of stream, (L)
vertical distance coordinate, (L)

y_e effective depth of flow (surface area/surface width), (L)

y_o depth of flow in channel upstream of sluice gate, (L)

y_1, y_2 initial sequent conjugate depth of the hydraulic jump, (L)

α Coriolis coefficient, Equation 3.7

α_o Coriolis coefficient upstream of sluice gate

α_1, α_2 Coriolis coefficients at the initial sequent conjugate depth sections of the hydraulic jump

β ratio of air/liquid discharge (Q_a/Q)

β_B Boussinesq coefficient, Equation 3.8

β_m a maximum ratio of air/liquid discharge, Equation 2.3

$\beta_o \beta_1 \beta_2$ constants, Equations 2.36, 2.38, 2.39

γ surface tension, (M/T^2)

γ_1 constant, Equation 2.41

Δ increment of or change in

η efficiency of oxygen transfer (M/ML^2T^3)

θ temperature coefficient

μ dynamic viscosity, ($ML^{-1}T^{-1}$)

ν kinematic viscosity, (L^2T^{-1})

π circle circumference/diameter ratio

ρ fluid density, (ML^{-3})

ϕ_s a function of channel geometry, Equation 10 Table 2.1

ϕ_v a function of surface velocity, Equation 10 Table 2.1

INTRODUCTION

Pollution has recently become an emotive term symbolising man's interference with the delicate balance otherwise efficiently maintained by nature. A healthy stream will contain a great number of species of flora and fauna with none predominant, pollution will become apparent by a reduction in the number of species with an increasing abundance of individual species among those surviving. Various biological and chemical indices of pollution have been developed requiring considerable time and expertise in analysis and evaluation. Whilst highly polluted streams have been observed with no oxygen sag, and, although oxygen is only one of many stream resources susceptible to depletion, it is generally regarded as the most important. The maintenance of oxygen levels in a stream is essential for the aerobic breakdown of organic matter into simple inorganic compounds containing oxygen (e.g. H_2O, CO_2, NO_3, SO_4, P_2O_5). In the absence of oxygen, decomposition is taken over by anaerobic bacteria resulting in the production of compounds which are toxic to life (e.g. CH_4, NH_3, H_2S).

Any effluent can be rendered harmless by suitable treatment, but the cost of doing so will add to the price of the article being manufactured, a factor which might render impossible the sale of that article due to competition from some country in which there is less concern about natural amenities. The choice between clean and polluted rivers is thus essentially a political and social one.

In the meantime, more efficient management of watercourses, for instance in more efficient utilisation of head losses to aerate water, can add significantly to the assimilative capacity of a river at little extra cost.

The studies reported herein are aimed at identifying the parameters controlling the oxygen transfer occurring at two features common to a large number of hydraulic structures, the hydraulic jump and free falling jet. These studies thus aim at providing general equations describing the mechanics of the transfer processes and thus a tool with which predictions may be made as to the oxygen that will be transferred as a result of air entrainment at an hydraulic structure, and, also to assist in identifying suitable modifications to optimise such a situation.

An extensive literature review has been presented to permit an understanding of the principles of gas transfer and subsequent attempts to apply these to practical situations such as free overfall weirs. The limitations of these attempts have been recognised and a suitable programme of laboratory work devised.

CHAPTER 1

THE PROCESSES OF GAS TRANSFER

1.1 OXYGENATION OF WATER - GENERAL

The oxygenation of turbulent water is a purely physical process involving the entry of oxygen molecules at an air/water interface followed by the distribution of this oxygen throughout the volume of the liquid. The air/water interface may be at the exposed water surface or may be created by the entrainment of air.

Two distinct processes are identified above, that of molecular diffusion and that of the physical mixing. Diffusion of gas from one medium to another will only occur if there is a difference between the active partial pressures of the gas in the two mediums. The actual process of diffusion will always occur in a direction such that it tends to reduce the partial pressure gradient. In other words, if water is oxygen deficient then oxygen will diffuse into it. If the active partial pressure gradient between air and the liquid is zero then the liquid is said to be saturated. This state of affairs is the ultimate state of equilibrium, but, it does not mean that diffusion ceases. The movement of molecules in both directions is equalised. The process of diffusion into quiescent water is very slow since it relies only on the inherent energy of the gas molecules themselves, but the whole process is speeded up by the application of some external force to cause rapid mixing of the oxygen saturated elements and dispersion into the main body of the fluid.

1.2 MOLECULAR DIFFUSION

If a quiescent body of liquid has an air/water contact area then the rate of mass transfer can be quantified by FICK's first Law of Diffusion :

$$\frac{\partial M}{\partial t} = - D_m A \frac{\partial C}{\partial x} \quad (g/s) \tag{1.1}$$

where D_m = coefficient of Molecular Diffusion (m^2/s)

x = distance from air/water Interface

$\frac{\partial C}{\partial x}$ = concentration gradient

A = air/water contact area

The equation is expressed as a partial differential equation since the concentration gradient varies during the diffusion. The minus sign indicates that the diffusion proceeds in a direction such that it offsets the concentration gradient. Clearly, for a particular gas, the law of diffusion states that the rate of diffusion per unit area is solely governed by the concentration gradient.

An equation to evaluate the molecular diffusion coefficient was developed by Albert EINSTEIN from his studies of Brownian motion:

$$D_m = \frac{R_o T_o}{N_o f} \tag{1.2}$$

R_o = Universal Gas constant

T_o = Absolute Temperature

N_o = Avogadro's Number

f = friction factor (related to the ability of the surrounding medium to impede the progress of the diffusing molecule)

A little later on, the friction factor f was re-defined by STOKES. Spherical particles falling freely through water were considered and STOKES showed that:

$$f = 6\pi\mu r_b \tag{1.3}$$

μ = viscosity of the medium

r_b = radius of the falling sphere

Thus combining Equations 1.2 and 1.3 it is seen that the coefficient of molecular diffusion of the diffusing matter is a function of the viscosity of the fluid, the absolute temperature and the size of the diffusing particle.

A solution by a Fourier Series ("POPEL) to Equation 1.1 enables the concentration of a diffusing gas to be obtained at a depth x below the gas liquid interface. Thus:

$$C_{tx} = C_s^{-0.811} (C_s - C_o).(e^{K_d} + \frac{1}{9} e^{K_d} + \frac{1}{25} e^{25K_d} + ...) \quad (1.4)$$

C_o = gas concentration at time t = o

C_{tx} = gas concentration at time t and distance x from the gas/liquid interface

C_s = saturation concentration of gas in liquid

$K_d = \pi^2 D_m t/4x^2$

For very short times of exposure (a matter of seconds), the concentration C_{tx} can be approximated by:

$$C_{tx} = C_s - \frac{C_s - C_o}{\sqrt{\pi D_m t}} x \ (g/m^3) \quad (1.5)$$

This approximate solution is indicated by the dotted lines in Figure 1.1 along with the curves given by Equation 1.4.

During an exposure time t, the amount of gas absorbed through the gas/liquid interfacial area is given by:

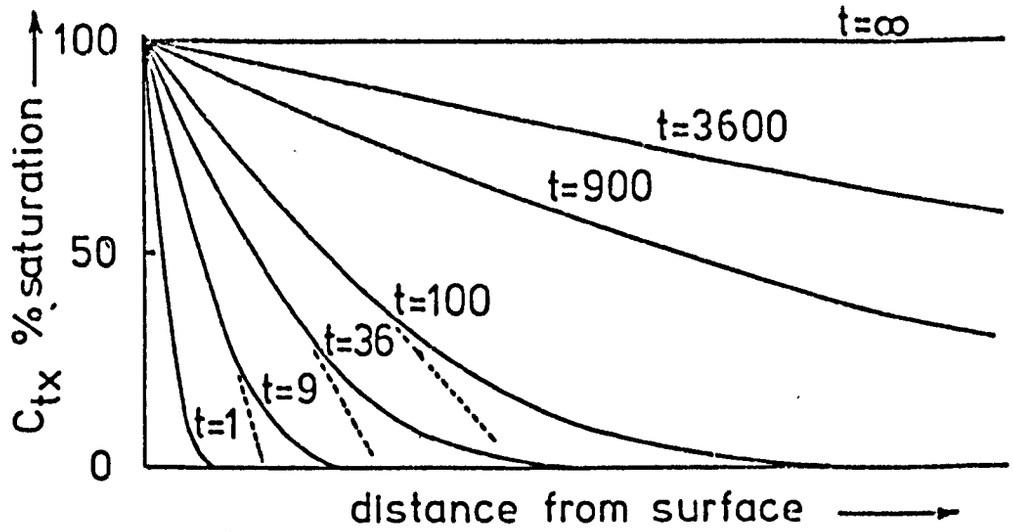

fig. 1.1 gas concentration in liquid due to molecular diffusion at various time intervals since exposure (reproduced - HIGBIE (1935))

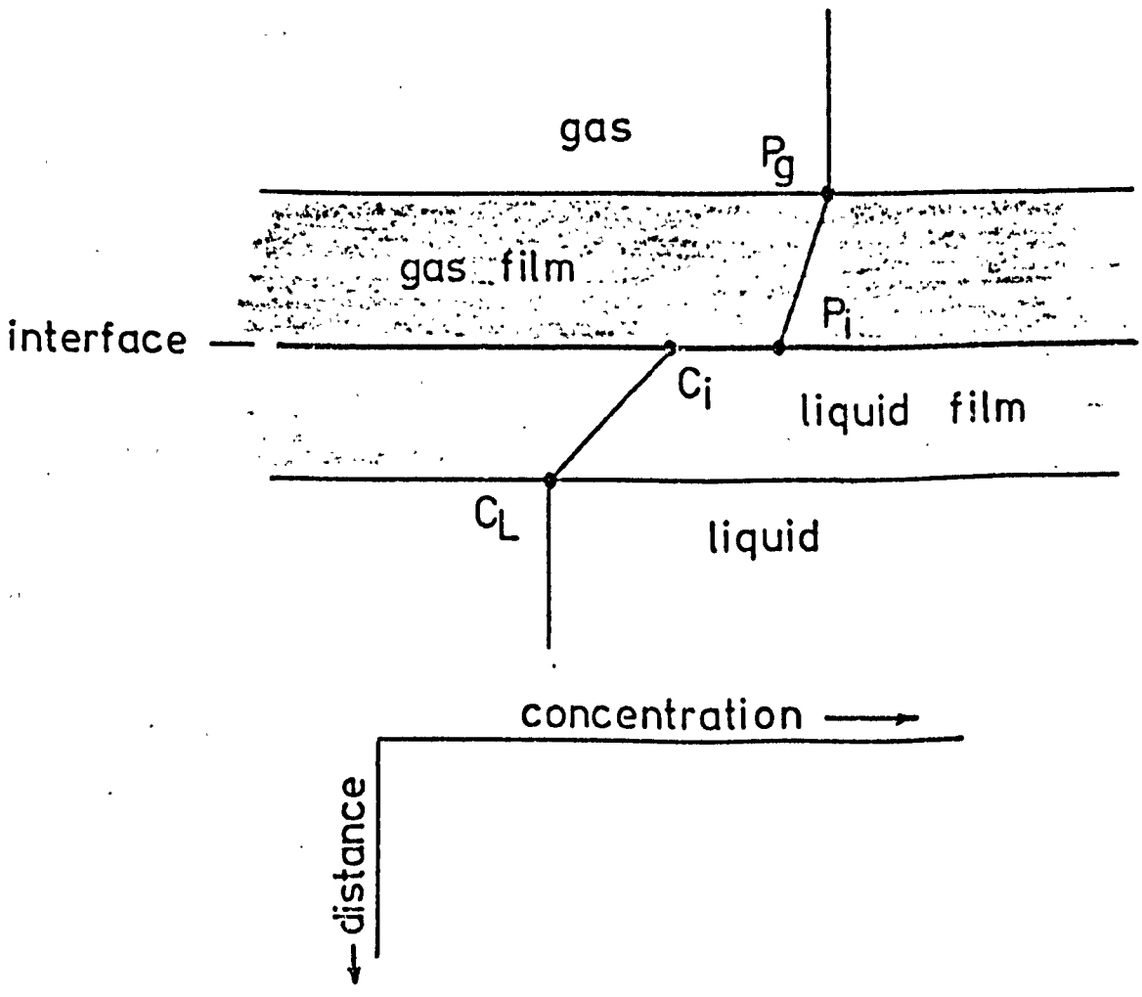

fig. 1.2 gas/liquid interface - two film model

$$M = 2A(C_s - C_o)\sqrt{\frac{D_m \cdot t}{\pi}} \qquad (g) \qquad (1.6)$$

This process is very slow, stagnant water will absorb in one hour a quantity of gas equivalent to a saturated water layer only 2mm thick (DANCKWERTS).

1.3 EDDY DIFFUSION

In dealing with molecular diffusion a quiescent body of fluid and gas was assumed. Furthermore, no reaction between the gas and liquid is assumed. This situation is analogous to laminar flow in which no eddies are present in the body of liquid and no renewal of the gas interface occurs.

Turbulent flow is characterised by a motion of particles, totally random with respect to time, direction or magnitude. The PRANDTL theory assumes that eddies move with a mean velocity $\bar{u}$ perpendicular to the net flow over a mean distance given by the Prandtl mixing length. The means are measured with respect to time.

The interchange of fluid particles associated with these turbulent eddies aids the distribution of solute throughout a solution, a process started by the molecular diffusion of solute.

The process of solute distribution or mixing by eddies is known as eddy diffusion and a simply defined coefficient of eddy diffusion in terms of the Prandtl mixing length and mean velocity is:

$$D_E = \bar{u} \cdot \ell \qquad (m^2/s) \qquad (1.7)$$

ℓ = Prandtl mixing length

D_E is thus a function of the hydrodynamic conditions existing.

1.4 TOTAL DIFFUSION

The effects of molecular diffusion and eddy diffusion are additive and therefore an overall diffusion coefficient can be expressed as:

$$D_T = D_E + D_m \tag{1.8}$$

The effect of eddy diffusion has one other important effect. It will aid the distribution of gas molecules throughout the liquid mass, but, in so doing it speeds up the process of molecular diffusion. The rate of molecular diffusion falls as the concentration gradient falls, but, if eddies are present then it is probable that bodies of fluid with high concentrations of solute are "whisked" away from the surface and replaced with solute deficient fluid bodies. Thus, the more eddies there are, or, the more turbulent the body of the fluid, the greater will be the tendency to maintain homogeneity within the fluid and therefore to maintain the maximum concentration gradient. The tendency is therefore to fully exploit the molecular diffusion capability.

A distinction is made between the two effects of turbulence, namely, it aids the diffusion of gas through the body of the liquid and secondly it maintains a high transfer across the gas/liquid interface by keeping high the concentration gradient across the interface.

Conversely, the higher the turbulence the shorter will be the exposure time of an element of fluid.

1.5 THEORIES OF GAS TRANSFER

1.5.1 Film Theory - LEWIS and WHITMAN (1924)

LEWIS and WHITMAN visualised a model of contact between liquid and gas consisting of two stagnant films of gas and liquid on either side of the gas/liquid interface. The transfer of gas must therefore be effected by the relatively slow process of diffusion through these films. The quantity of diffusion occurring may be given by:

$$\frac{1}{A}\frac{dM}{dt} = k_g\ (P_g - P_i) = k_L(C_i - C_L) \qquad (1.9)$$

k_g = diffusion coefficient through gas film

k_L = diffusion coefficient through liquid film

P = concentration of solute in gas (mm. Hg)

C = concentration of solute in liquid (ppm)

Subscript g applies to conditions in main body of gas

Subscript i applies to conditions at gas/liquid interface

Subscript L applies to conditions in main body of liquid

This film model is illustrated in Figure 1.2.

In the case of insoluble gases, such as oxygen, the gas film resistance is generally held to be insignificant compared to the liquid film resistance. Therefore it can be stated that $P_i = P_g$ and therefore that C_i is equal to the concentration for a liquid saturated with the diffusing gas i.e. $C_i = C_s$. Equation 1.9 becomes:

$$\frac{1}{A} \cdot \frac{dM}{dt} = K_L\ (C_s - C_L) \qquad (1.10)$$

K_L represents the overall film coefficient, referred to as the Liquid Film Coefficient (m/s).

The Two-film theory is criticised because of the assumption of stagnant films which, it is argued, is hardly representative of a practical situation. Furthermore, if FICK's Law of Diffusion is applied to the liquid film of thickness d_L, then

$$\frac{1}{A} \cdot \frac{dM}{dt} = D_m \frac{C_s - C_L}{d_L} \quad \text{(from Eq. 1.1)} \tag{1.11}$$

Hence, from Equations 1.10 and 1.11,

$$K_L = \frac{D_m}{d_L} \tag{1.12}$$

Equation 1.12 provides further ground for disagreement with LEWIS & WHITMAN since K_L in practice shows a much lower dependence on D_m.

1.5.2 Penetration Theory - HIGBIE (1935)

HIGBIE's investigations were concerned mainly with the liquid film coefficient and are therefore applicable where gas solubilities are low. He criticised the LEWIS & WHITMAN film mechanism which he stated would not be applicable for periods of gas/liquid contact which are less than the time it takes for the gas to penetrate the liquid film, i.e. steady state transfer through the film must be achieved before the equations of LEWIS & WHITMAN can be applied.

HIGBIE points out that steady state conditions are not reached in most industrial equipment, therefore the liquid film resistance depends on what occurs during the penetration period.

HIGBIE's model visualises fluid elements briefly exposed to gas at the interface. During this brief time of exposure the gas diffuses into the liquid, but, in contrast to the film theory, this gas "penetration" is one of unsteady diffusion and will remain so

unless the time of exposure becomes great enough to permit achievement of the steady state. Fig. 1.3 depicts HIGBIE's model of gas penetration. The initial gas concentration in the liquid element is that in the main body of the fluid $C_o = C_L$. The gas film is assumed non-existent (by using a pure gas) and the element interface is thus instantaneously saturated with the gas, $C_i = C_s$. The history of the penetration of the liquid film by dissolved gas is shown by dashed lines in Figure 1.3. If penetration is uninterrupted then the condition indicated by the full line is attained. This line represents the state of steady state diffusion upon which the theory of LEWIS & WHITMAN was based.

The time of exposure is small so the approximate solution to Fick's Law (Equation 1.5) may be applied, whence the depth of penetration:

$$x = \sqrt{\pi D_m t} \tag{1.13}$$

The concentration gradient is:

$$\frac{\partial C}{\partial x} = \frac{C_i - C_L}{x} = \frac{C_s - C_L}{\sqrt{\pi D_m t}}$$

and by applying Fick's Law, Equation 1.1:

$$\frac{1}{A}\frac{dM}{dt} = \sqrt{\frac{D_m}{\pi . t}}\,(C_s - C_L) \quad (g/s) \tag{1.14}$$

which gives the unsteady gas transfer rate during the time of exposure.

The penetration theory assumes a constant time of exposure for all fluid elements, $t = t_c$, the amount of gas transferred to the fluid element in time t_c is thus:

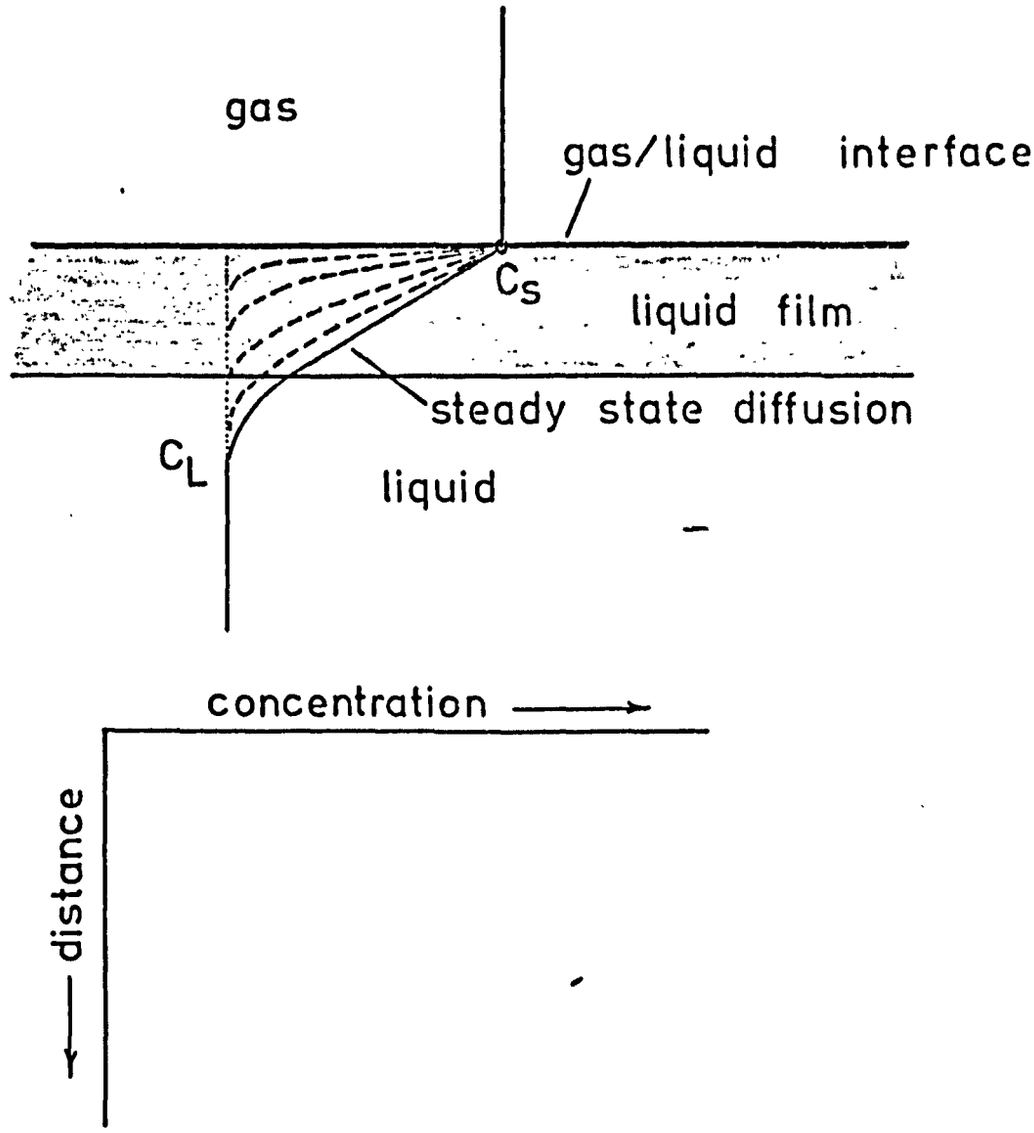

fig. 1.3 steady and unsteady state diffusion through a liquid film (after HIGBIE)

$$M = \int_0^{t_c} \sqrt{\frac{D_m}{\pi . t}}\, A\, (C_s - C_L).dt \qquad (1.15)$$

$$= 2A\, (C_s - C_L) \sqrt{\frac{D_m . t_c}{\pi}} \quad (g) \qquad (1.16)$$

The mean rate of transfer during this time t_c is given by:

$$M_o = \frac{M}{t_c} = 2\sqrt{\frac{D_m}{\pi . t_c}}\, A\, (C_s - C_L) \quad (g/s) \qquad (1.17)$$

The penetration theory leads to:

$$K_L = 2\sqrt{\frac{D_m}{\pi\, t_c}} \qquad (1.18)$$

Since a constant time of exposure t_c has been assumed then the rate of surface renewal r_c has also been assumed constant. Equation 1.18 can be re-written:

$$K_L = 2\sqrt{\frac{D_m\, r_c}{\pi}} \qquad (1.19)$$

1.5.3 Surface Renewal Theory - DANCKWERTS (1951)

In common with HIGBIE, DANCKWERTS abandoned the concept of a stagnant film stating the improbability of the existence of such a film in a turbulent fluid. He does however refer to this as a "harmless and convenient usage" as measured absorption rates do indeed conform to relationships of the form of Equation 1.10 with the liquid film mass transfer coefficient being constant for a given liquid under given conditions.

DANCKWERTS supposes the liquid surface to be continually replaced with fresh liquid. This is a case of unsteady diffusion of gas into the liquid element and DANCKWERTS assumes the rate of gas

absorption to be as given by Equation 1.14.

The average rate of production of surface s is constant, and the chance of a surface element being replaced within a given time is assumed to be independent of its age. The possible time of exposure may vary from zero to infinity - in this respect the theory differs from HIGBIE's assumption of constant time of exposure. The fraction of the surface having ages between t and t + dt is assumed to be $f(t).dt = se^{-st}.dt$. The rate of absorption into those surface elements of age t and of fraction $se^{-st}.dt$ of the area is found from Equation 1.14 to be:

$$\frac{dM}{dt} = A\, se^{-st} \sqrt{\frac{D_m}{\pi t_c}}\, (C_s - C_L).dt \qquad (1.20)$$

whence the average absorption rate will be:

$$M_o = \int_o^\infty A\, se^{-st} \sqrt{\frac{D_m}{\pi t_c}}\, (C_s - C_L)\, dt \qquad (1.21)$$

$$\therefore \qquad M_o = (C_s - C_L) \sqrt{D_m.s} \qquad (1.22)$$

The surface renewal theory predicts that

$$K_L = \sqrt{D_m s} \qquad (1.23)$$

1.5.4 Film/Surface Renewal Theory - DOBBINS (1962)

This theory combines the film and surface renewal theories into one equation.

For conditions of very low turbulence such as a slow flowing river, the exposure of surface elements may be long enough to permit the attainment of steady state diffusion. Also, during unsteady

diffusion under these conditions the depth of penetration may reach beyond the surface element and into the main body of the fluid and thus into the region of molecular and eddy diffusion, i.e. the film theory will apply.

The theory applies the concept of surface renewal and the gas transfer coefficient is expressed as a function of the average rate of surface renewal s and maximum depth of penetration (film thickness), $x = d_L$:

$$K_L = \sqrt{D_m s}\ \operatorname{Coth}\sqrt{\frac{s\ d_L^2}{D_m}} \qquad (1.24)$$

Note for low turbulence, s tends to zero, the film theory ($K_L = D_m/d_L$ - Equation 1.12) will apply. For high turbulence the coth term in Equation 1.24 tends to unity and K_L becomes governed by surface renewal theory, Equation 1.23.

1.5.5 Relative merits of the Gas Transfer Theories

The assumption of steady state diffusion and of stagnant surface films by the film theory makes this an unrealistic theory since the periods of exposure usually occurring in practice are too short to enable a steady state of diffusion to be attained. Further, the existence of a stagnant film is a convenient but unrealistic one in view of the conditions of turbulence usually prevailing. Also, the dependence of K_L on D_m as predicted by Equation 1.12 is not borne out by practical experience.

The first three theories discussed all have one unknown and the fourth has two. Of the first three theories, one has been discredited, which leaves the penetration theory (unknown constant time of

exposure, t_c) and the surface renewal theory (unknown average rate of surface renewal, s). Of these two, t_c is more readily measured in practice, but s can only be obtained by measurements of K_L and substitution into Equation 1.23.

It is generally accepted that K_L is a function of turbulence, the more turbulent the body of fluid the higher will K_L be, (a particular gas is assumed).

This effect is readily explained by the various theories discussed: The effect of increasing turbulence is to reduce the thickness d_L of the liquid film, to reduce the time of exposure to gas of the fluid elements, t_c, to increase the rate of surface renewal, s, and in the last theory d_L is decreased and s is increased.

All the theories can therefore be said to satisfactorily explain the effect of turbulence on the gas transfer coefficient.

In contrast to the above theories, KISHINEVSKI (1955) has concluded that the value of K_L is independent of the gas diffusion coefficient being solely dependent on the turbulence intensity at the interface.

1.6 FACTORS AFFECTING THE GAS TRANSFER COEFFICIENT

1.6.1 Temperature

In keeping with EINSTEIN's equation, Equation 1.2, the coefficient of molecular diffusion will increase as the temperature rises and thus will increase the value of K_L given by the various gas transfer theories. The viscosity of the water will be decreased by a temperature rise and this will enable the bubbles in an air entrainment situation to rise more rapidly with consequent reduction in the time of exposure t_c (assume K_L given by HIGBIE's model - Equation 1.18). This reduction in t_c will result in a higher value of K_L.

Two other quite separate temperature effects must be noted. A rise in temperature results in a drop in the solubility of a gas in a liquid (Section 1.9.1), the saturation concentration C_s is reduced, the concentration gradient is therefore reduced with a consequent lowering of the rate of gas transfer. Secondly, a rise of temperature in a situation of air entrainment results in a reduction of the surface tension of the liquid. The bubbles will thus tend to expand and in so doing they create a larger air/water interface which should promote aeration. Conversely, the expansion of the bubble will result in a fall in the partial pressure of gas within the bubble with consequent lowering of the driving force.

The effects of temperature are generally taken into account by a temperature function, this will be discussed later (Section 1.10).

1.6.2 Surface Active Agents

These agents are seen to have a variety of conflicting effects. Generally they are visualised as forming a diffusion inhibiting film at interfacial surfaces although there is evidence to suggest that in highly turbulent situations this film is effectively destroyed and thus no effect on the aeration performance is noted, (MANCY & OKUN, 1965).

However, if a film is formed, then the surface active agent will not only lower the surface tension of the fluid but it will also modify the hydrodynamic properties of the surface layer (POPEL). The normal random motion is reduced to one of surface stagnation or to a viscous layer with a lowering of the rate of surface renewal.

Two conflicting effects of surface active agents are possible. On the one hand they form inhibiting films at gas transfer interfaces

and on the other they reduce surface tension and thus increase the gas/liquid interface. The resultant effect cannot be predicted since it must depend on the concentrations involved and on the dynamics of the aerating system. Hence it is not surprising that a literature review will reveal that surfactants may have no effect or they may increase or decrease aeration.

Under highly turbulent conditions, the surface active agents will probably have no effect on the liquid film coefficient K_L and thus the overall effect will be governed by the effect on the air/water interface. MANCY & OKUN's (1960) studies on bubble aeration showed a reduced K_L but increased $K_L\frac{A}{V}$. Similarly the experiments of ZIEMINSKI, GOODWIN & HILL (1960) showed that the addition of alcohols and carboxylic acids can increase the aeration efficiency by up to 100%, this effect increased progressively as the length of the carbon chain. Tests on anionic commercial surface active agents revealed a lesser improvement in aeration efficiency but two non-ionic surface active agents tested resulted in a marked decrease in absorption efficiency. In this latter case the advantage offered by the reduced size of air bubbles was more than offset by the decreased transfer or liquid film coefficient K_L.

It is clearly useless to attempt a generalisation.

1.6,3 Suspended Solids

VAN DER KROON (1968) has shown that the rate of oxygen transfer in a mixed liquor and an aluminium hydroxide suspension depends on the concentration of suspended solids and decreases with increase in suspended solids concentration.

MANCY & OKUN (1968) attributed this effect to an increase in the liquid viscosity and the fact that turbulent eddies will tend to

be dissipated by the presence of suspended solids. The increase in viscosity will of course tend to decrease the oxygen diffusivity coefficient. The dissipation of the kinetic energy of liquid eddies will tend to result in a thicker boundary layer, larger values of diffusion time, smaller frequency of surface renewal - the resultant conclusion in the light of the various transfer theories already discussed is a net reduction in the transfer coefficient K_L. For most practical applications it is believed that the main effect of suspended solids is the interference with the liquid hydrodynamics rather than the reduction in oxygen diffusivity coefficient.

However, the effect of suspended solids is reduced by mechanical agitation or highly turbulent situations (BOWERS 1955, also BRIERLEY & STEEL 1959) and there will be some critical degree of turbulence beyond which the effect of solids on the rate of aeration will become negligible.

The parallel turbulence dependent behaviour displayed by temperature, surface active agents, suspended solids is interesting and it is probable that for a turbulent air entrainment situation the detrimental effects of contaminants may safely be assumed negligible. The temperature effects are discussed in Section 1.10.

1.7 A GENERAL EQUATION OF GAS TRANSFER

All the theories of gas transfer discussed earlier have taken FICK's Law as the basic equation describing the transfer of oxygen from the gas to the liquid phase. The differences between the individual theories lie in the different approaches to predicting the liquid film gas transfer coefficient, (the physical presence of a liquid film is not being implied).

The basic equation expressing the rate of mass transfer is given by Equation 1.14 as:

$$\frac{dM}{dt} = A.K_L\ (C_s - C_L) \qquad (g/s) \tag{1.24}$$

If V is the volume of fluid into which mass of gas dM diffuses in time dt then Equation 1.24 may be re-expressed as a rate of change of concentration:

$$\frac{dC}{dt} = \frac{1}{V} \cdot \frac{dM}{dt} = K_L.\frac{A}{V}.(C_s - C_L) \tag{1.25}$$

Equation 1.25 represents an instantaneous rate - to determine concentration changes for a given time, it is necessary to integrate Equation 1.25 between the limits of zero and t for time and between C_o and C_t for concentration. C_o corresponds to initial concentration, i.e. $C_L = C_o$ when t = o. Integrating: (C_t = gas concentration after time t)

$$-\int_{C_o}^{C_t} \frac{-dC}{C_s - C_L} = K_L \frac{A}{V} \int_o^t dt \tag{1.26}$$

$$\text{Log}_e \frac{C_s - C_t}{C_s - C_o} = K_L \frac{A}{V} \cdot t \tag{1.27}$$

$$\frac{C_s - C_t}{C_s - C_o} = e^{-K_L \frac{A}{V}.t} \tag{1.28}$$

Equations 1.27 and 1.28 are probably the most widely quoted equations of gas transfer and the ratio $(C_s - C_o)/(C_s - C_t)$ has been frequently used as a measure of oxygen uptake and is usually referred to as the "deficit ratio" (GAMESON, 1957). Equation 1.28 may be re-expressed,

$$C_t = C_s - (C_s - C_o)\ e^{-K_L \frac{A}{V}.t} \tag{1.29}$$

and in this form it is essentially the same as the relationship of ADENEY & BECKER (1919 and 1920) derived from experiments on the rate of gas transfer from bubbles.

VAN DER KROON & SCHRAM (1969) expressed the oxygen uptake in terms of what they termed the "aeration capacity", C_{ac}.

Assuming that for a particular aeration situation:

$$e^{-K_L \frac{A}{V} t} = \text{Constant} = 1 - K \tag{1.30}$$

and the oxygen levels above and below the aeration system are C_1 and C_2, then Equation 1.28 may be re-expressed:

$$\frac{C_s - C_2}{C_s - C_1} = 1 + \frac{C_1 - C_2}{C_s - C_1} = 1 - K$$

or

$$C_2 = KC_s + C_1 \frac{C_s(1 - K)}{C_s} \tag{1.31}$$

or $$C_2 = C_1 + KC_s \left(1 - \frac{C_1}{C_s}\right) \tag{1.32}$$

or $$C_2 = C_1 + C_{ac} \left(1 - \frac{C_1}{C_s}\right) \tag{1.33}$$

The aeration capacity, C_{ac}, is expressed in Equation 1.33 and expressed in words the aeration capacity of a particular system is defined as the oxygen level that would be achieved by the system if the oxygen level in the water arriving at the system were zero (See Figure 1.4).

The aeration capacity is related to the deficit ratio by Equation 1.34:

$$C_{ac} = C_s \left(1 - \frac{C_s - C_2}{C_s - C_1}\right) = C_s \left(1 - \frac{1}{r}\right) \tag{1.34}$$

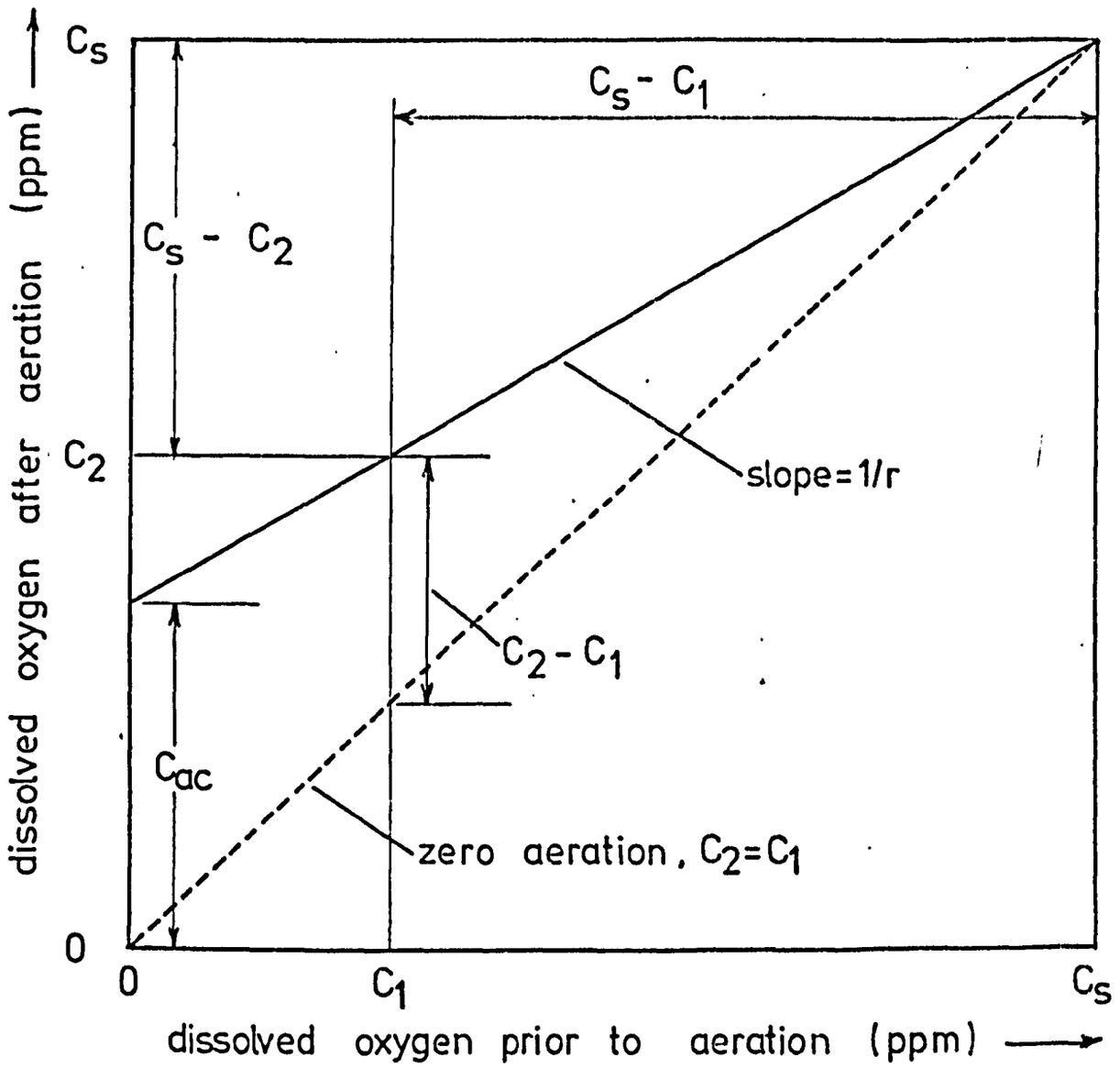

fig. 1.4 relationship between oxygen levels above and below a weir system

Both the deficit ratio and aeration capacity are presented graphically in Figure 1.4 which depicts the relationship between oxygen levels above and below a particular weir system for constant hydraulic conditions.

1.8 THE APPLICATION OF GAS TRANSFER EQUATIONS

The reciprocal of the deficit ratio could be predicted for a particular system of aeration by the application of Equation 1.28. This would require an accurate knowledge of the oxygen solubility which depends on prevailing conditions of temperature and pressure and on the presence of dissolved salts (Section 1.9). According to gas theories (except that of KISHINEVSKI) the liquid film coefficient depends on the diffusion coefficient of the gas, the time of exposure or rate of surface renewal and on the presence of surface active agents. The volume of fluid and the time over which aeration occurs can be stated but the interfacial area would require an estimation based on air flow, bubble size, bubble velocity etc.

Clearly, for practical purposes such as aeration at a weir the precise application of Equation 1.28 is impossible and it is for this reason that recourse is made to experiment to estimate the aeration possibilities of a particular situation.

In general, an overall gas transfer coefficient K_{La} is used, re-writing Equation 1.28:

$$\frac{C_s - C_2}{C_s - C_1} = \frac{1}{r} = e^{-K_L \frac{A}{V} t} = e^{-K_{La} \cdot t} \qquad (1.35)$$

or

$$\text{Log}_e\, r = K_L \cdot \frac{A}{V} \cdot t = K_{La} \cdot t \qquad (1.36)$$

In all the experimental work reported in this thesis, the oxygen uptake has been expressed as the deficit ratio and attempts have been made to correlate the deficit ratio with the hydraulic parameters controlling the values of K_{La} and t. The success of such correlations would have to be tested outside the laboratory and can only be expected to be successful if all parameters that influence K_{La} and t appear in the correlation.

All the theories discussed so far relate to gas transfer in general. In these studies interest is focused on oxygen transfer and the factors affecting it in a situation of air entrainment.

1.9 THE SOLUBILITY OF OXYGEN IN WATER

1.9.1 The Effects of Temperature and Pressure

A liquid can be said to be saturated with a gas when equilibrium is reached between the concentration of gas dissolved in the liquid and the partial pressure of the gas above the liquid. This is a statement of HENRY's Law.

Sparingly soluble gases are generally held to obey the gas laws and KLOTS and BENSON (1963) have confirmed this by observing no deviations from HENRY's Law for the solubility of oxygen, nitrogen and argon at partial pressures up to 1 atmosphere. Furthermore BENSON & PARKER (1961) have shown that oxygen and nitrogen conform to DALTON's Law at 1 atmosphere.

For a given atmospheric pressure, the oxygen partial pressure in air will vary with temperature because of the increase in the saturated water vapour pressure:

$$P_g = (P_o - P_{vp}) \times 0.21 \qquad (1.37)$$

where P_g = oxygen partial pressure in air

P_o = atmospheric pressure

P_{vp} = saturated water vapour pressure at temperature T°C

0.21 = proportion by volume of oxygen in air

The partial pressure of oxygen and therefore also the solubility of oxygen in water will both vary with changes in temperature and pressures.

For temperatures ranging from 0°C to 35°C HATFIELD (1941) expressed the solubility of atmospheric oxygen in water by the equation:

$$C_s = \frac{0.678\ (P_o - P_{vp})}{T + 35} \qquad (1.38)$$

C_s = solubility of oxygen (ppm)

Much work has been carried out to determine the solubility of oxygen in water. Among the most recent work, the results of MONTGOMERY, THOM & COCKBURN (1964) are in good agreement with KLOTS & BENSON (1963). Doubts have been expressed (GREEN) about the accuracies of the results of TRUESDALE, DOWNING & LOWDEN (1955). A convenient nomogram which enables the calculation of dissolved oxygen contents in water has been presented by HART (1967) based on the saturation valves of MONTGOMERY and co-workers. This nomogram, reproduced in Figure 1.5, gives values of C_s in agreement with those calculated from Equation 1.38.

The reduction in solubility with increase in temperature is consistent with the principle of LE CHATELIER since the dissolving of a gas is associated generally with an evolution of heat.

1.9.2 The Effect of Added Salts

The solubilities of most gases in water are reduced by adding salts to the water. This salting out effect of an electrolyte is

connect T and P to give intersection on R , connect point of intersection and $\%C_S$, read C

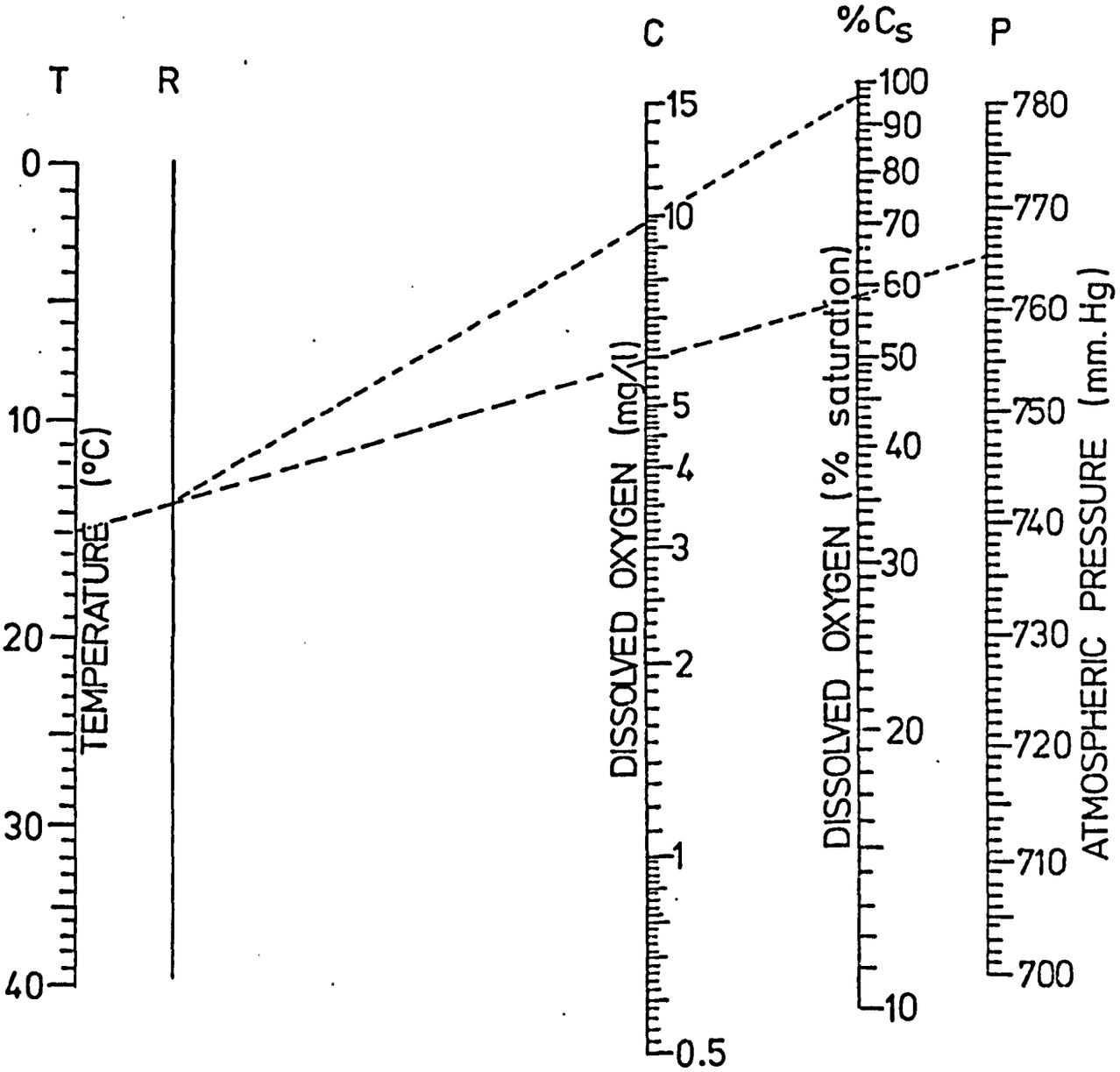

fig. 1.5 nomogram to calculate dissolved oxygen content (mg/l) from dissolved oxygen (% saturation) at temperature T °C and atmospheric pressure P mm. Hg - after HART (1967)

attributed to the congregation of dipolar molecules of the polarizable solvent, for instance water, around the ions of the added electrolyte. The net effect is a reduction in the amount of free water available to the solution of gas.

It has been generally accepted that solubility changes linearly with salinity (FOX 1909, TRUESDALE and others, 1955), although GREEN's results (1965) were best fitted by a relationship proposed by SETSCHENOW in 1875:

$$\text{Log.}\frac{C_s'}{C_s} = - K_{sa}\,(T).S_a \qquad (1.39)$$

S_a is the salt concentration and C_s' is the solubility in this solution. K_{sa} is a constant.

The equation proposed by TRUESDALE and co-workers (1955) for sea water is given by Equation 1.40:

$$C_s' = 14.161 - 0.3943\,T + 0.007714\,T^2 - 0.0000646\,T^3 - S_a\,(0.0841 - 0.00256\,T + 0.0000374\,T^2) \qquad (1.40)$$

with C_s' in ppm and salinity S_a in parts per thousand.

Equation 1.40 is very cumbersome to apply and this resulted in a simpler equation being produced by GAMESON & ROBERTSON (1955):

$$C'_s = \frac{475 - 2.65\,S_a}{33.5 + T} \qquad (1.41)$$

In the range 0 - 30° this equation is stated to fit the experimental data of TRUESDALE and others with the same precision as Equation 1.40. For pure water Equation 1.41 reduces to:

$$C_s = \frac{475}{33.5 + T} \qquad (1.42)$$

which is of the same form as Equation 1.38 - Note that the experiments of TRUESDALE and others were carried out at a pressure 760 mm. Hg., also that GREEN suggested that these results were about 3% too low.

1.9.3 The Effect of Suspended Solids

A drop of less than 5% in the oxygen saturation value has been found by VAN DER KROON (1968) for a mixed liquor and a suspension of aluminium hydroxide. MANCY & OKUN (1968) questioned this finding and suggested that perhaps salting out effects had been ignored. In any event, there is no other evidence to support this finding.

1.10 THE EFFECTS OF TURBULENCE ON TEMPERATURE INFLUENCE

The effects of temperature on the interfacial area and on the liquid film coefficient have already been discussed in Section 1.6.1. The temperature dependence of Equation 1.36 is generally described by a temperature function of the form:

$$\left(K_L \frac{A}{V}\right)_{T_2} = \left(K_L \frac{A}{V}\right)_{T_1} . \theta^{T_2 - T_1} \qquad (1.43)$$

or

$$(K_{La})_{T_2} = (K_{La})_{T_1} . \theta^{T_2 - T_1} \qquad (1.44)$$

A survey of the literature will reveal a variety of values for the "constant" θ. These vary from 1.00 to 1.047 and this variation has been shown to be due to different degrees of turbulence. GAMESON, VANDYKE & OGDEN (1958) suggested a coefficient of $\theta = 1.018$ for an experimental weir system and they also found that this coefficient was not affected by the presence of surface active agents. TRUESDALE and VANDYKE (1958) found a value of 1.015 for flowing water. The results

of CHURCHILL (1961) are those generally applied to surface aeration:

$$(K_{La})_{T^o} = (K_{La})_{20^o} \times 1.0241^{(T-20)} \qquad (1.45)$$

In common with but prior to CHURCHILL, DOWNING and TRUESDALE (1955) carried out experiments in a stirred vessel and reported $\theta = 1.0212$ which is similar to CHURCHILL's reported value. They also indicated lower values of θ for higher stirring rates and reported no evidence to suggest a different coefficient for saline water.

The reduction in θ with increase in turbulence was further reported by DRESNACK and METZGER (1968). It is therefore conceivable that extrapolation to high degrees of turbulence or mixing will result in θ tending to unity and thus it follows from Equations 1.43 and 1.35 that the oxygen transfer expressed as deficit ratio would theoretically become independent of the temperature.

The varying temperature effects can best be understood by visualising the following model describing the two phases of gas transfer. (a) On exposure to an air interface, the water molecular boundary layer is instantaneously saturated with oxygen whatever the initial deficit (PASVEER, 1955 (ii)). (b) The dispersal of this oxygen throughout the fluid can be effected either by diffusion into the fluid body, or by the intensive mixing of the oxygen saturated particles with oxygen deficient water, or by a combination of these latter two processes. In phase (a), the temperature is important in that it determines the saturation value. In phase (b) the diffusion processes will be accelerated by temperature increases whereas the mixing process is not believed to change with temperature (IMHOFF & ALBRECHT 1972). Therefore it is the degree of mixing (or turbulence) in the fluid body which will determine

the relative temperature influence in phase (b), since, the greater the mixing, the lower will be the dependence on diffusion for the distribution of oxygen throughout the fluid and thus the lower the temperature influence.

This is illustrated in Figure 1.6 where the oxygen transfer (mg) at various temperatures is expressed as a ratio of the oxygen transfer at 10°C and plotted against the temperature. For surface aeration (Curve A - CHURCHILL) and an increased temperature, the increased diffusion rate outweighs the reduced solubility, for diffused aeration or low turbulence systems (Curve B - PASVEER, also BEWTRA, NICHOLAS & POLOKOWSKI) the reduction in oxygen solubility with increased temperature is almost equally compensated by the increased diffusion. For higher turbulence systems, as illustrated by the experimental weir studies of GAMESON, VANDYKE & OGDEN (1958), the influence of the diffusion processes on the oxygen movement becomes progressively less significant, an overall reduction in relative oxygen transfer being felt as a result of the relative reduction in solubility. Curve C depicts the relative oxygen saturation variation with temperature (1.0 at 10°C) and this curve represents the limit at which the contribution to oxygen distribution by the diffusion processes becomes negligible.

IMHOFF & ALBRECHT (1972) believed that the prototype structures they studied (a weir, two turbine aerators, two surface rotary aerators) exhibited the temperature dependence displayed by curve C. They also suggested that an energy expenditure of 20 watt/m^3 represented the lowest limit for temperature dependence described by Curve C. This view is not consistent with the results of GAMESON, VANDYKE & OGDEN, and will be discussed in more detail in Section 4.5.

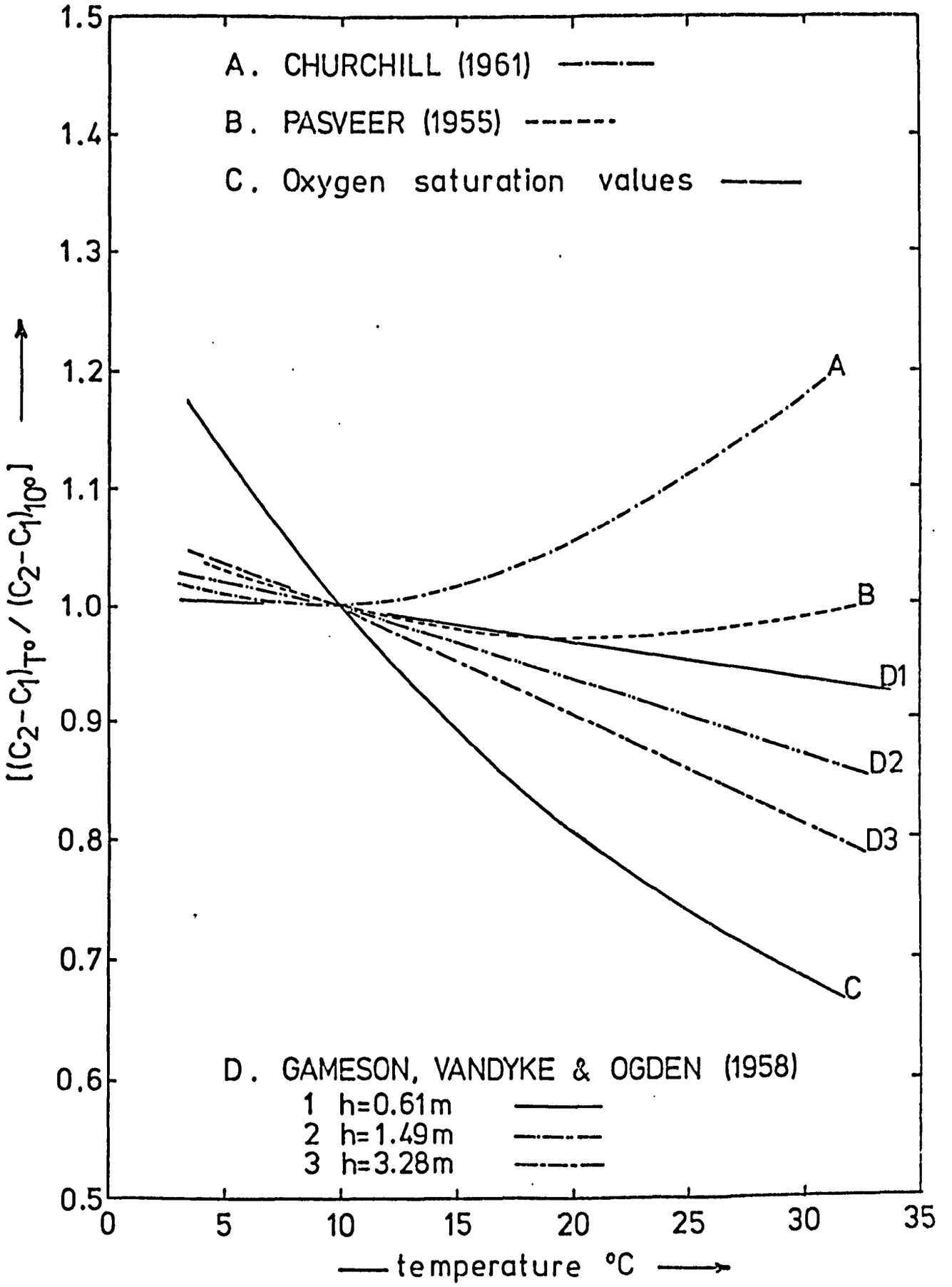

fig. 1.6 the effect of temperature on the relative dissolved oxygen transfer (1.0 at 10°C).
[partly reproduced from IMHOFF & ALBRECHT (1972)]

CHAPTER 2

THE AERATION OF FLOWING WATERS

2.1 INTRODUCTION

The assimilative capacity of a river has been the subject of research since the early work of BLACK & PHELPS (1911) when first attempts were made to predict reaeration capacity.

The oxygen balance of a river system depends on a number of variables some of which are noted in Section 2.5. The use of a river as a convenient recipient for human and industrial wastes places considerable strains on the river's natural assimilative capacity and times of low flow are critical since the dilution ratio is low. Similarly during high temperature periods when the gas solubility in water is reduced and the bacterial growth stimulated. At such times a need for supplemental aeration is realised, preferably at the lowest point on the oxygen sag curve. The location of such facilities is however usually dictated by the adaptability of existing structures (usually those involving a head loss e.g. turbines) or by the availability of either power or supervisory personnel. An oxygen level of 40% saturation has been suggested as an upper limit for economical supplemental aeration (THACKSTON & SPEECE, 1966).

A review is presented of means of estimating the reaeration capacity of a river and various ways of supplementing river oxygen levels are noted.

Particular attention has been paid to two air entraining phenomena common to many hydraulic structures, namely the hydraulic jump and free falling water jet.

2.2 NATURAL REAERATION THROUGH A STREAM SURFACE

The aeration equation developed by STREETER & PHELPS (1925) (basically Equation 1.25) has formed the basis of all studies of stream assimilative capacity and numerous formulations have been proposed to enable estimates of the reaeration rate coefficient K_{LV}^{A} or K_{La} for gas transfer through the surface of a stream. Table 2.1 summarises most of the major contributions in this field.

In their early work STREETER & PHELPS proposed that K_{La} depended upon many variables such as mean stream velocity v_m, depth y, slope S, and channel irregularity. This is reflected in Equation 1 of Table 2.1 where C and n are constants for a particular river stretch whose values depend in part on the channel slope and roughness. STREETER & PHELPS indicated that wide variations in the empirical coefficients are to be expected and indeed this has been amply demonstrated by most of the subsequently developed models in Table 2.1, almost all of which follow the form of the original equation of STREETER & PHELPS. Of the two equations developed by O'CONNOR & DOBBINS, Equation 2 of Table 2.1 applies to streams exhibiting a pronounced vertical velocity gradient, a condition of non-isotropic turbulence (Chezy Coefficient $v_m/\sqrt{RS} < 20$), whilst the second equation is relevant to comparatively deep channels where a condition of isotropic turbulence may be approached (Chezy Coefficient > 20).

ISAACS & MAAG (1969) introduced additional empirical factors for channel shape ϕ_s and surface velocity ϕ_v. From the data of CHURCHILL, ELMORE & BUCKINGHAM (1962), they obtained mean values $\phi_s = 1.078$ and $\phi_v = 1.16$.

KRENKEL & ORLOB (1962) attempted to explain reaeration in terms of a longitudinal mixing coefficient D_L whilst in the second model Equation 5, Table 2.1, the energy dissipation per unit mass of fluid

TABLE 2.1

Various Equations Relating the Surface Reaeration Rate Coefficient to Hydraulic Parameters

AUTHOR(S)	REAERATION RATE COEFFICIENT		UNITS
STREETER & PHELPS (1925)	$K_{La} = Cv_m^{\,n}\, y^{-2}$	(1)	K_{La} day^{-1}, v_m ft/s, y ft
O'CONNOR & DOBBINS (1956)	$K_{La} = 480\, D_m^{\frac{1}{2}} S^{\frac{1}{4}} y^{-5/4}$	(2)	K_{La} day^{-1}, S ft/ft, y ft
	$K_{La} = D_m^{\frac{1}{2}} v_m^{\frac{1}{2}} y^{-3/2}\, 2.31^{-1}$	(3)	D_m ft^2/day, v_m ft/s
KRENKEL & ORLOB (1962)	$K_{La}(20^oC) = 0.00004302\, D_L^{1.15} y^{-1.915}$	(4)	K_{La} min^{-1}, D_m ft^2/min, y ft
	$K_{La}(20^oC) = 0.000141\, E_d^{0.408} y^{-0.66}$	(5)	
OWENS, EDWARDS & GIBBS (1964)	$K_{La}(20^oC) = 9.41\, v_m^{0.67} y^{-1.85}$	(6)	
CHURCHILL, ELMORE & BUCKINGHAM (1962)	$K_{La}(20^oC) = 5.026\, v_m^{0.969} y^{-1.673}$	(7)	v_m ft/s, y ft
ISAACS (1967)	$K_{La} = cv_m\, (1.0241)^{T-20} y^{-1.5}$	(8)	K_{La} day^{-1}, v_m ft/s, y ft
LANGBEIN & DURUM (1967)	$K_{La} = 3.3\, v_m y^{-1.33}$	(9)	K_{La} day^{-1}, v_m ft/s, y ft
ISAACS & MAAG (1969)	$K_{La} = 2.98\, \phi_s \phi_v\, v_m y^{-1.5}$	(10)	K_{La} day^{-1}, v_m ft/s, y ft
THACKSTON & KRENKEL (1969)	$K_{La} = 0.000125\, (1 + v_m/\sqrt{gy}) u_* y^{-1}$	(11)	
NEGULESCU & ROJANSKI (1969)	$K_{La} = 0.0153\, D_m\, v_m^{1.63} y^{-1.63}$	(12)	D_m cm^2/s, v_m m/s, ym
TSIVOGLOU & WALLACE (1972)	$K_{La}(25^oC) = 0.054\, \Delta h/t_f$	(13)	K_{La} hr^{-1}, Δh ft, t_f hr

was introduced where $E_d = v_m Sg$. THACKSTON & KRENKEL (1969) produced another modified form of the STREETER & PHELPS model when they introduced the Froude number $v_m/\sqrt{gy}$ and a shear velocity u_*. The studies of CHURCHILL and co-workers (1962) are among the most extensive carried out. They produced nineteen models involving some eight to ten hydraulic parameters and all exhibited similar correlation. The model recommended was the simplest but gave equally good correlation of the data.

TSIVOGLOU & WALLACE (1972) utilised a recently developed field tracer procedure for measuring stream reaeration, a radioactive form of the noble gas krypton serving as a tracer for oxygen. The field results collected encompassed a wide variety of conditions and were considered as representative of most non tidal fresh water streams. The early predictive models given by Equations (3), (7), (9), (11) and (6) in Table 2.1 were tested against observed results. None proved capable of prediction within acceptable limits the differences between predicted and observed values of K_{La} proving to be consistently large for highly turbulent stream reaches where flow was not uniform.

The change in water surface elevation Δh and time of flow t_f were demonstrated to be primary hydraulic properties related to reaeration. The mean forward flow velocity and stream depth were not found to be related to stream reaeration in a primary way and similarly the stream bottom roughness and longitudinal dispersion were not found to serve as useful indicators of stream reaeration capacity.

The constant 0.054 in Equation 13 Table 2.1, referred to as the escape coefficient, is affected by pollution as indeed are all the models in Table 2.1. The value given is for a typical stream, reasonably well mixed and moderately polluted (5 day BOD approximately 15 mg/l).

2.3 SUPPLEMENTAL REAERATION

2.3.1 Diffused Air Aeration

The injection of air into a body of water through diffusers is an important constituent of the activated sludge waste treatment process (BEWTRA & NICHOLAS 1964) and as a result has provoked much research, particularly with regard to the suitable design of diffusers. The technique has also been employed to aerate streams (TYLER, 1946; PALLADINO, 1961) but reported efficiencies were low and the costs, both capital and operating, were high. However, the technique has been recommended (SPEECE & RAYYAN, 1973) for the aeration of the hypolimnion(cold water layer) of stratified impounded waters since this could be achieved without disturbance of the stratification. De-stratification by pumping hypolimnion waters to the surface is a method commonly used to aerate the hypolimnion, but, this involves pumping huge quantities of water and the distribution of nutrients from the hypolimnion with undesirable increases in algal activity.

2.3.2 Mechanical Aeration

This is another system used where no head losses are available. The water surface is churned up by a series of rotating vanes, or alternatively a system whereby water is pumped from the river and subsequently sprayed out by the turbines was tested by KAPLOVSKY, WALTERS & SOSEWITZ (1964). The system has an advantage of mobility since the aerators can be mounted on readily movable pontoons. However, the capital costs involved are probably greater than any other system whilst the running costs are comparable to those encountered with diffused air aeration (THACKSTON & SPEECE, 1966).

2.3.3 Turbine Aeration

This is a case where existing structures have been modified in favour of supplementing aertation. Many power turbines set above tail-water level are fitted with spring loaded air vents to alleviate the vibration and cavitation which develop in the turbine draft tubes as a result of high vacuums at low flows. The wisdom of permanent venting was initially doubted because of possible increases in cavitation and corrosion together with the destruction of tailwater vacuum. However, the damage feared did not materialise and power losses of only 5% for heads 6 to 9m were reported (THACKSTON & SPEECE) whilst significant aeration was achieved. Alternative techniques such as the injection of compressed air immediately before the turbine impeller have been reported (IMHOFF & ALBRECHT, 1972).

2.3.4 U-Tube Aeration

A more recent development, this is a conceptually simple system, consisting of two basic elements - a device for introducing air to a flowing water stream (an aspirator, or a compressor linked to a diffuser) followed by a vertical u-shaped flow path to provide contact time under conditions of above atmospheric pressure thus providing a favourable driving force for the transfer of oxygen. The u-shaped flow path may take various forms, possibly a pair of vertical pipes connected at the bottom by a 180^{o} bend, or, a pair of concentric pipes with flow down one passage and up the other.

The U-Tube, first reported by BRIUZN & TUINZAAD in 1958, is a highly attractive aerator requiring little maintenance, minimal operating labour, and offering considerable flexibility in the choice of

configurations. In cases where a head loss was available, MITCHELL (1973) demonstrated that the cost per unit oxygen dissolved was very significantly less than for mechanical or diffused air aeration. Even when the head had to be created by pumping, the U-Tube proved the most economical at a discharge 10 mgd whilst for a higher discharge 100 mgd it proved comparable to mechanical aeration whilst slightly less economical than diffused air aeration.

2.3.5 Weir Aeration

Since weirs are rarely constructed specifically for aeration purposes, they must constitute the cheapest most effective and most reliable source of oxygen available. The superior oxygen transfer capability of a weir compared to a turbine was noted by THACKSTON & SPEECE together with the possibility of improving the aeration performance by breaking a single fall into a number of steps. The value of a weir as a source of oxygen for ice-bound rivers was stated by LE BOSQUET. Aeration is achieved by the weir in addition to breaking the ice cover over the stream below the weir and thus promoting the surface aeration possible.

The aeration at weirs, either by a free falling jet or by a spillway controlled jet culminating in an hydraulic jump, forms the basis of this thesis and will shortly be discussed in some detail.

2.4 NATURAL REAERATION THROUGH AIR ENTRAINMENT

2.4.1 Introduction

The capability of free surface flows to entrain air is very much in evidence in nature and because of the engineering problems associated with this phenomenon, it has already provoked much research. An understanding of the mechanics of air entrainment is necessary before attempting to comprehend and quantify the processes governing the transfer of gases from the air to the water.

2.4.2 Similarity and Aerated Flows

The difficulties encountered in the modelling of air entraining flows stem from the well proven fact (HAINDL, 1958; RAO & KOBUS,1975) that irrespective of model scale the size of air bubble entrained remains relatively constant. This means that the conditions of geometric and kinematic similarity cannot be satisfied.

The conditions required for perfect similarity of geometrically similar air/water flows have been demonstrated by RAO & KOBUS (1975) from a dimensional analysis. Perfect similarity is achieved if the Froude number, Reynolds number and Weber number are simultaneously equal in the model and prototype. As it is usual to use the same fluid in both model and prototype and also keep the gravitational acceleration constant, then only one of the numbers can be kept constant at any one time. Under these conditions perfect similarity is theoretically not possible and the success of modelling air entrainment situations will depend on the relative influence of the conditions not satisfied.

The Reynolds number describes the viscous forces associated with the flow of a real fluid and these forces are most prominent when the

velocities are low or if the flow section is restricted. For relatively high velocity water flows and relatively large flow sections the viscous forces are insignificant in comparison with other forces.

The effects of surface tension at fluid interfaces are described by the Weber number. These effects are similarly only significant for low velocities and narrowed flow sections. Thus, for fully turbulent flow conditions, the effects described by the Reynolds and Weber numbers become relatively insignificant and therefore model similarity may be achieved directly by keeping the Froude number (the ratio of inertial to gravitational forces) constant.

A review of various investigations into the entrainment of air by free surface flows led RAO & KOBUS to conclude that the process of air entrainment could be described very well by similarity according to Froude's law. It was also suggested that those cases where scale effects were observed had in common the fact that the process of air entrainment was being influenced by the limitations in the transport capacity of the flow.

Evidence for the two air entraining situations relevant specifically to this thesis will be reviewed, namely, for an hydraulic jump and free falling jet. The air entraining capability of other free surface flows is not reviewed here.

A most comprehensive review recently edited by RAO & KOBUS, reference to which has already been made, deals more broadly with air entraining free surface flows.

An excellent review of various air entrainment studies involving shaft spillways, plunging jets, hydraulic jumps etc. is provided by RENNER (1973).

2.4.3 Air entrained by Hydraulic Jumps

If an air pocket is formed, for instance, in a pipeline, then an hydraulic jump will form at the end of the air pocket thus entraining air and ultimately removing the air pocket. It was this phenomenon which prompted the studies of KALINSKE & ROBERTSON (1942).

From studies they carried out on a laboratory scale circular pipeline they found the ratio β, of air discharge Q_a to water discharge Q to be a function of the Froude Number as follows:

$$\beta = \frac{Q_a}{Q} = K\ (Fr_1 - 1)^{1.4} \qquad (2.1)$$

where $Fr_1 = v_1/\sqrt{gy_e}$ is the Froude number of the supercritical flow

y_e = effective approach depth (water area divided by surface width)

K = 0.0066 for these tests

With a view to improving the existing design criteria for air vents CAMPBELL & GUYTON (1953) studied the air demand resulting from hydraulic jumps formed in pressure conducts downstream of dam outlet gates for $Fr_1 < 30$. The air discharge ratios they obtained were consistently higher than those predicted by Equation 2.1 and they suggested this could be due to: (1) entrainment of air into the stream before reaching the jump; (2) entrainment of air by the intensely fluctuating turbulent front of the jump; (3) the higher velocities downstream facilitating more efficient removal of air.

The equation describing the results of CAMPBELL & GUYTON is:

$$\beta = 0.04\ (Fr_1 - 1)^{0.65} \qquad (2.2)$$

where $Fr_1 = v_1/\sqrt{gy_e} = v_1/\sqrt{gy_1}$

FASSO (1956) on the other hand arrived at air quantities considerably less than predicted by Equation 2.1.

However, Equation 2.1 was verified by the laboratory experiments of HAINDL and SOTORNIK (1957) in a closed rectangular conduit. Their flow section was approximately three times larger than that employed by KALINSKE & ROBERTSON and they concluded that this therefore indicated a wide range of applicability of Equation 2.1. Taking into account the scatter of his points HAINDL (1958) noted a maximum value K = 0.012 in Equation 2.1.

WISNER (1965) further compared the field measurements of YUKIO (1959), GUYTON (1958), PETRIKAT (1958), and concluded that these results were in good agreement with the model of KALINSKE & ROBERTSON with a maximum value of K = 0.014. This is in good agreement with the maximum K noted by HAINDL (1958) for his model tests. These results confirmed WISNER's supposition that it is possible to model air entrainment according to the Froude criterion in locally turbulent situations only. WISNER stated a lower limit of validity for the prototype to be satisfactorily modelled according to model results, namely, for hydraulic jumps, $Fr_1 > 8$. WISNER states that Equation 2.2 gives values of β erring on the low side for $Fr_1 > 8$.

In contrast, RAJARATNAM (1962) investigated the aeration characteristics of jumps formed in open conduits and noted that the air is entrained at the toe of the jump. The mean air concentration in a vertical section was observed to attain a maximum value within a very short distance of the toe of the jump and thereafter it was seen to decrease as air was lost to atmosphere through the surface roller. Similar results were noted by others and most recently by RESCH & LEUTHEUSSER (1971), also LEUTHEUSSER, RESCH & ALEMU (1973).

RAJARATNAM showed a similar dependence on Froude number thus:

$$\beta_m = 0.018\ (Fr_1 - 1)^{1.245} \qquad (2.3)$$

where β_m is the maximum relative air discharge which was recorded close to the toe of the jump.

RENNER (1973) compared the measurements of RESCH & LEUTHEUSSER (1972) in an open conduit with those of RAJARATNAM and showed them to be higher. However, RESCH & LEUTHEUSSER used an anemometric technique which produced results of dubious accuracy as discussed in Section 5.2.4.

2.4.4 Air Entrained by Liquid Jets

SHIRLEY (1950) was possibly the first to quantify the air entrained by a plunging liquid jet. He investigated the air entrained by an inclined circular jet issuing from five different nozzle sizes. SHIRLEY reported a separate relationship between air entrained and jet velocity for each jet diameter studied.

TONG JOE LIN & DONNELLY (1966) principally studied plunging laminar jets, namely, those jets having a flat velocity profile at the point of entry into the fluid. Although such laminar jets are not likely to occur in practical situations, some interesting conclusions are made and these will be reviewed.

In contrast to the mechanical bubble trapping device of SHIRLEY, LIN & DONNELLY employed high speed cine photography. The volumetric gas flow rate was thus determined from the bubble size distribution data and frequency of bubble occurrence data obtained from photographic analysis. Spherical bubbles were assumed. A minimum entrainment velocity was defined as the minimum jet velocity, based on the jet

diameter at plunging point, required to entrain bubbles in a given system. This was expressed by the correlation:

$$U_e = 6.22 \frac{\gamma^{0.794}}{D^{0.206} \rho^{0.206} \mu^{0.587}} \quad (m/s) \qquad (2.4)$$

A minimum velocity U_e is required to entrain air and this is shown to be a function of fluid density ρ, viscosity μ, and surface tension γ, and, also of the diameter D of the jet at the plunging point.

Equation 2.4 is applicable in the laminar region up to a REYNOLD's number (defined in Equation 2.5 below) 1500. Above this value the jet becomes unstable and the entrainment mechanism changes.

$$R_e = \frac{\rho U D}{\mu} \qquad (2.5)$$

where U is the jet velocity.

Entrainment by laminar jets is effected by a thin film of gas formed around the jet. The jet and film enter into the liquid intact. As the jet penetrates further into the liquid, oscillations develop and this subsequently leads to the breakup of the gas film into bubbles. In contrast, the turbulent jet, occurring for R_e > 1500, is characterised by instability in the gas phase with visible disturbances on the jet surfaces. These disturbances are responsible for the entrainment of air, visual observations showed that in contrast to the laminar jet no gas film was entrained intact into the liquid body. The addition of a surface active agent was observed to reduce the minimum entraining velocity. This is due to the lowering of the solution surface tension. The presence of more than 0.2% surface active agents did not produce any further effect on U_e or surface tension, while the initial addition of 0.02% had the most dramatic effect.

The dominant factor affecting both bubble size and bubble frequency was the jet velocity. The average bubble size decreased and the bubble frequency increased sharply as the jet velocity was increased above the minimum entraining velocity. An increase in the jet diameter has a lesser effect, but, it resulted in increases in both bubble size and frequency with a more pronounced effect on the latter. The addition of 0.02% surface active agent resulted in reduced bubble size but increased frequency at minimum entrainment velocity.

WISNER (1965) was mainly concerned with the design of venting orifices to provide adequate ventilation behind the jet falling from a weir. WISNER demonstrated for prototype and model situations that the relative air entrainment was a function of the Froude number of the jet at impact. It is worth noting that the air uptake measured by WISNER was that due to the underside of the jet (i.e. the venting required). The total relative air entrainment into the tailwater will thus be far greater, or, approximately twice as much.

More recently, ERVINE & ELSAWY (1975) reported experiments on the air entrained by rectangular nappes falling freely to a downstream pool. They produced an empirical relationship between the maximum ratio air to water discharge and the nappe parameters width B_J, perimeter P, thickness t_J, velocity U, and impacting with a pool after fall h.

$$\frac{Q_a}{Q} = 0.26 \left(\frac{B_J}{P}\right) \left(\frac{h}{t_J}\right)^{0.446} \left(1 - \frac{U_e}{U}\right) \qquad (2.6)$$

where U_e was the minimum velocity to entrain air (approximately 1.1 m/s).

For low values (< 10) of Froude number $(U/\sqrt{gt_J})$, the ratio Q_a/Q was not constant but varied as the jet thickness varied. This was

attributed to noticeable surface tension and viscous effects in the thinnest jets giving a reduced rate of entrainment. This is possible, but the design of the apparatus was such that entrained air may not have been readily removed and thus scale effects introduced. The apparatus as illustrated by ERVINE & ELSAWY provided that the water left the pool at the same end as the inclined jet entered, in other words, the horizontal velocity components of the inclined jet and the mass of fluid in the pool were opposed. The comments of RAO & KOBUS on scale effects mentioned in Section 2.2 might therefore apply. It is interesting to add that for the thinnest jets, ERVINE & ELSAWY obtained values of β as high as unity which is surprising since this represents the upper limit of β which is in general physically possible. A value of $\beta = 1$ corresponds to the maximum possible air concentration of approximately 50% (the ratio of air volume to the total volume of air and water) (RAO & KOBUS), the exact maximum being dependent on the distribution of bubble sizes.

For values of Froude number > 10, ERVINE & ELSAWY stated that the ratio air to water discharge tended to a maximum as given by Equation 2.6.

The work of CHARLTON (1970) was also mentioned. CHARLTON found a clear correlation between the Froude number and the air water discharge ratio of a circular jet plunging into a pool of water and he similarly recorded a tendency towards a constant ratio air to water discharge for higher values of Froude number (> 10).

In all the work discussed so far, only LIN & DONNELLY classified the nature of their jets. In their case a distinction was made between laminar and turbulent jets, but no one has distinguished between solid and disintegrated jets which is surprising since this must radically alter the air entrainment process.

The behaviour in air of free falling jets formed by rectangular crests was studied in detail by HORENI (1956). The co-ordinates of the passage of these jets through air were shown to be expressed by a parabola of the second order, i.e. $y = cx^2$, and for these experiments the coefficients of velocity at the exit section were found to vary between 0.93 and 0.98. At the point at which disintegration occurred in the whole width of the jet, a distinct change in the jet outlines was observed. Horeni conveniently expressed this point of disintegration as a function of the specific discharge at the crest:

$$L_o = 31.19\ q^{0.319} \qquad (2.7)$$

q = specific discharge (cm^2/s)

L_o = distance measured along the jet centre line to the point of total disintegration (cm)

2.4.5 Oxygen Uptake in an Hydraulic Jump

As already discussed, the air entrainment qualities of the hydraulic jump have long been recognised with much work being done to quantify the air uptake.

Very little has been done to record the oxygen uptake which is clearly one of the major attributes of the hydraulic jump. JARVIS (1970) recognised this need during his field survey of weirs which included Crump weirs and sloping aprons. In such cases the quantity of oxygen absorbed depended on whether or not an hydraulic jump was formed. JARVIS demonstrated in the laboratory the significant aeration achieved by an hydraulic jump by comparing the aeration achieved by a sloping apron without an hydraulic jump to that with an hydraulic jump. Furthermore, detailed work was recommended and a possible correlation with

Froude number was suggested.

APTED (1975) followed on and carried out experiments with an hydraulic jump formed in the narrowed section of a flume (10 cm wide) downstream of an underflow sluice gate. Downstream of the jump the narrowed section expanded abruptly to the full width of the flume (30.5 cm).

APTED's experiments were for one discharge (approximately 4 l/s) and he suggested it was not possible to express the relationship between the oxygen uptake (expressed as the deficit ratio (defined in Section 1.7, Equation 1.35) adjusted to 15°C by use of Equation 2.13), and the upstream Froude number by a simple mathematical equation.

Instead, he proposed a correlation with the measured energy loss ΔE:

$$r_{15} = 10^{0.0024\Delta E} \quad (\Delta E \text{ cm}) \tag{2.8}$$

or

$$\text{Log } r_{15} = 0.0024\ \Delta E \quad (\Delta E \text{ cm}) \tag{2.9}$$

The hydraulic jump was also studied by HOLLER (1971) using a discharge of 1.2 cfs (33.98 l/s) in a 15 inch (38.1cm) wide channel (Private Communication, 1974). HOLLER correlated the deficit ratio corrected to 20°C with Δv the difference in measured velocities before and after the jump:

$$r_{20} = 1 + 0.0043\ \Delta v^2 \quad (\Delta v \text{ ft/s}) \tag{2.10}$$

The information available on the oxygen transfer within an hydraulic jump is obviously limited and inconclusive with more work being called for.

2.4.6 Oxygen Uptake at Weirs

GAMESON (1957) made the first serious attempt to provide a means of predicting the aeration occurring at a weir system. GAMESON expressed the oxygen change in terms of the deficit ratio (Equation 1.35). A survey of various prototype weir systems led to an approximate relation between deficit ratio and height of fall (difference between water levels).

$$r = 1 + \frac{abh}{2} \quad \text{(h in metres)} \qquad (2.11)$$

'a' is an arbitrary measure of water quality with suggested values 1.25, 1.00, 0.85 respectively for slightly, moderately and grossly polluted waters.

'b' is a function of the type of weir being 1.0, 1.3 respectively for a free overfall and cascade (step weir).

GAMESON also expressed the degree of aeration in terms of a weir coefficient r-1/h for comparison of different weir systems since this coefficient was apparently independent of h. It was also reported that despite changes in discharge, water temperature and concentration of surface active agents at a particular weir system, there was no recorded change in the degree of aeration. Tests on an experimental weir system verified that the rate of escape of oxygen from supersaturated water is equal to the rate of entry of oxygen into water which is less than saturated with oxygen.

The effect of temperature was further studied by GAMESON, VANDYKE & OGDEN (1958) and found to be significant at an experimental weir system. As a result the following equation was suggested to replace Equation 2.11:

$$r = 1 + 0.11\ ab(1 + 0.046T)h \qquad (2.12)$$

where r is the deficit ratio at $T^{o}C$.

The equation used for adjusting data to a standard value at $15^{o}C$ was

$$r_{15} = 1 + \frac{r - 1}{1 + 0.027\ (T-15)} \qquad (2.13)$$

Additional tests indicated that the temperature coefficient was not affected by the presence of surface active agents.

Further work by BARRETT, GAMESON & OGDEN (1960) at four weir systems confirmed the equality of rates of invasion and evasion of oxygen. In studies at Teddington weir on the River Thames, observed values of r-1 were 17% greater than those predicted by Equation 2.12. The need to investigate the effects of discharge and depth of receiving water was acknowledged, although the omission of these effects was not considered to greatly affect the validity of Equation 2.12.

OWENS & EDWARDS (1963) studied three free overfall weirs in the River Lark and concluded that the oxygen transfer is essentially predictable in a manner described by Equation 2.12. Close examination of their data shows that an increase in deficit ratio was recorded for a reduction in discharge. At another weir, the opposite effect was indicated by their data, although, at this weir considerable leakage occurred through the boards forming the weir on the occasion of the lower discharge. The height of fall at these weirs was small (approximately 0.6m).

The effect of discharge was also noted separately by NATERMAN (1952) and LONDONG (1967) - a reduction in aeration with increasing discharge being observed.

GANNON (1967) illustrated the significance of aeration at waste treatment plant overfall structures and compared observations with predictions from Equation 2.12.

In one free overfall, observed values of r-1 were only 6% higher than predicted while in another the predicted r-1 was 58% too high.

MASTROPIETRO (1968) reported a technique credited to QUIRK, LAWLER & MATUSKY (1966) which was developed to predict aeration at the Upper Gate House on the St. Louis River. Discharge Q was considered an important variable, steady state conditions were assumed i.e. $\frac{dC}{dt} = 0$ and the mixing was assumed complete, i.e. $C_s - C_t = C_s - C_2$.

A mass balance of dissolved oxygen at the dam was considered:

$$K_{La}.V(C_s - C_2) = QC_2 - QC_1 \qquad (2.14)$$

C_1, C_2 are dissolved oxygen concentrations above, below the dam.

For constant volume V of system, K_{La} will vary with Q, thus:

$$K_{La}.\frac{V}{Q} = f(Q) = \frac{C_2 - C_1}{C_s - C_2} \qquad (2.15)$$

or

$$C_2 = \frac{C_1}{1 + f(Q)} + \frac{f(Q).C_s}{1 + f(Q)} \qquad (2.16)$$

The second method review by MASTROPIETRO assumed a linear relationship between per cent saturation above and below the dam and that this relationship is independent of discharge, i.e.:

$$\frac{C_2}{C_s} \times 100 = K_m \times 100 + K_p.\frac{C_1}{C_s} \times 100 \qquad (2.17)$$

or

$$C_2 = K_m C_s + K_p C_1 \qquad (2.18)$$

Equation 2.17 was verified for dams of height 7 and 15 feet and K_m and K_p were tentatively shown to vary linearly with the dam height:

$$K_m = 0.037h \text{ and } K_p = 1 - 0.043h \quad (h \text{ ft}) \tag{2.19}$$

A comparison with the deficit ratio is interesting. Re-arranging the deficit ratio yields:

$$C_2 = (1 - \frac{1}{r})\ C_s + \frac{1}{r}\ C_1 \tag{2.20}$$

Equations 2.20, 2.18 and 2.16 are identical if

$$\frac{1}{r} = K_p = \frac{1}{1 + f(Q)} \tag{2.21}$$

and

$$1 - \frac{1}{r} = K_m = \frac{f(Q)}{1 + f(Q)} \tag{2.22}$$

whence

$$\frac{1}{r} + (1 - \frac{1}{r}) = \frac{1}{1 + f(Q)} + \frac{f(Q)}{1 + f(Q)} \tag{2.23}$$

If f(Q) is constant for a given dam height then $K_m + K_p = 1$ and Equations 2.21 and 2.22 hold true.

The experimental results as indicated in Equation 2.19 indicate an approximate validity. Note that temperatures effects were ignored, the equations were developed for temperatures in the range 20–25°C.

The prediction equations were derived for use with specific structures and were not intended for general use, but, the principles embodied could be applied elsewhere.

JARVIS (1970) showed that the values of 'a' given by GAMESON (1957) for use with Equation 2.11 were incorrectly derived and should be 1.52, 1.04, 0.68 respectively. From his own field survey of weirs,

JARVIS derived the following values of a = 1.23, 0.91, 0.59 for slight, moderate and gross degrees of pollution.

JARVIS also experimented using a 22½° V-Notch discharging at the rate of 0.65 1/s into a 61cm square downstream pool. He related the deficit ratio to the height of fall (difference between water levels) by the equation:

$$r_{15} = 2.05\ h^{0.434} \quad (h\ m) \tag{2.24}$$

Deficit ratios were corrected to 15°C by Equation 2.13. JARVIS, and earlier the DEPARTMENT OF SCIENTIFIC & INDUSTRIAL RESEARCH (1958), showed that as the depth of downstream pool increases (for constant height of fall, h) then the deficit ratio increases until an optimum value of depth is reached beyond which the deficit ratio is independent of depth. This depth is approximately the depth to which bubbles penetrate (D.S.I.R., 1958) and is termed the optimum depth. JARVIS reported a relationship between the optimum depth d' and the distance H between the upstream water surface and the bed of the downstream pool:

$$d' = 8.46\ \log_e (H/14.14) \quad (cm) \tag{2.25}$$

with H in cm.

For optimum depth conditions:

$$r_{15} = 0.009H + 1.00 \quad (H\ cm) \tag{2.26}$$

JARVIS also obtained an increase in aeration for a reduction in his downstream pool width.

VAN DER KROON & SCHRAM (1969) experimented with a variety of notches. They demonstrated partitioning of a weir nappe could lead

to considerable increases in the aeration occurring with an optimal result being achieved with about six jets per metre width of weir crest. Their results also showed that an increase in discharge was accompanied by a small reduction in aeration. It is worth noting that the depth of water in their downstream pool was 0.6m for the majority of their experiments. In one experiment at a height of fall 0.9m the depth was reduced to 0.4m, in this case a slight reduction in aeration was obtained for notches consisting of up to three partitions but for greater than three partitions no change was observed. The width of the downstream pool was 0.75m and the length was reduced to 0.5m without influencing the aeration occurring. The discharge used in most of the tests was 8.33 l/s with a maximum notch width of 0.75m.

An almost direct proportionality was observed between the aeration capacity (see Equation 1.34 and Figure 1.4 for definition) and the height of fall. This constant of proportionality decreased abruptly irrespective of the weir type at a height of fall 0.7 to 0.8m.

These studies made no attempt to provide prediction equations.

A reduction in aeration with increased discharge was observed by TEBBUTT (1972) during studies on a laboratory cascade weir.

HOLLER (1971) experimented with sharp crested weirs in a 15 inch (38 cm) wide channel over a height of fall range 8 inch (20.3cm) to 22.5 inches (57.15cm), (details obtained by private communication). The water jet impacted on the bed of the channel, and, the aeration was expressed in terms of the deficit ratio corrected to 20°C standard and the impact velocity of the jet:

$$U = \sqrt{2gh} \qquad (2.27)$$

where U = impact velocity after height of fall h.

and

$$r_{20} = 1 + 0.0043\ U^2 \qquad (U\ ft/s) \tag{2.28}$$

Using Equation 2.27, Equation 2.28 may be expressed in terms of h:

$$r_{20} = 1 + 0.0091\ h \qquad (h\ cm) \tag{2.29}$$

The similarity between Equations 2.26 and 2.29 is somewhat fortuitous since $H = h+d'$ in Equation 2.26. HOLLER's experiments did not consider the effect of depth below the weir. Furthermore, the implied linear variation between deficit ratio and height of fall is contrary to that given by Equation 2.24 or Equation 2.33. The discharge used in HOLLER's experiments was 0.2 cfs (5.66 1/s). For one height of fall (36.8cm) the effect of discharge ranging from 2.7 to 7.25 1/s was tested with no significant effect on the oxygen uptake (details by private communication). HOLLER also obtained aeration measurements for three prototype weir structures involving heights of fall 12, 27.5 and 35 feet and tailwater depths up to 16 feet. The aeration achieved by these structures was expressed by:

$$r_{20} = 1 + 0.0010\ U^2 \qquad (U\ ft/s) \tag{2.30}$$

This can be re-expressed in terms of the height of fall:

$$r_{20} = 1 + 0.0021\ h \qquad (h\ cm) \tag{2.31}$$

The reduction in the coefficient 0.0043 in Equation 2.28 to 0.001 in Equation 2.30 was suggested to be due to the cushioning effect of tailwater below the prototype structures. The ratio prototype to

model for values of r-1 is 0.23 and is approximately half the same ratio observed by the D.O.E. (1973) (to be discussed shortly). In the latter's work the ratio 0.55 was attributed to difference in water quality, but, it is probable that neither reasoning is correct.

The DEPARTMENT OF THE ENVIRONMENT (1973) published further data on the deficit ratio achieved with optimum depth of receiving water for their experimental weir. For these experiments (for falls up to 3m):

$$r_{15} = 1 + 1.17h\ (1 - 0.11\ h) \qquad (h\ m) \qquad (2.32)$$

or, if the temperature coefficient is incorporated (Equation 2.13):

$$r = 1 + 0.69\ h\ (1 - 0.11\ h)\ (1 + 0.046\ T) \quad (h\ m) \qquad (2.33)$$

This experimental weir utilised a 0.22m wide rectangular notch and a 30cm square lower pool. Oxygen levels were determined by titration and the discharge employed was about 1.82 l/s (private communication).

Additions of synthetic anionic detergents were shown to significantly reduce r - 1 by up to 16% at the experimental weir. The D.O.E. then took the results of 12 weirs previously observed in moderately polluted rivers as well as 5 studied by JARVIS, and on the assumption of optimum depth conditions, these observations were compared with those predicted by Equation 2.33. An average ratio of observed to predicted r-1 of 0.55 was obtained, and as a result an amended equation was recommended:

$$r = 1 + 0.38\ ah\ (1 - 0.11\ h)(1 + 0.046\ T) \qquad (2.34)$$

in which h is in metres and 'a' has the values 1.8, 1.6, 1.0, 0.65 for clean, slightly polluted, moderately, grossly polluted water.

The effect of discharge was further studied by APTED (1975) who used a 100mm wide notch with a downstream pool of width 1.00m, length 1.5m and variable depth up to a maximum 0.5m. For a fixed position of the receiving basin greater aeration was observed at the lower discharges for shallow pool depths. The peak values of deficit ratio achieved at different discharges did not differ significantly. These peaks were attained at the optimum depth which for this set of experiments was related to the discharge (Q 1/s) by the expression:

$$d' = 25 \log Q + 24.2 \quad \text{(cm)} \tag{2.35}$$

Among the most recent work on weir aeration is that of NAKASONE (1975) in Japan. Experiments were conducted using weir notches 0.14, 0.2, 0.28m wide approximately, with a range of discharges from 2.5 to 10 1/s discharging into a pool 300cm long and 20 cm wide. The pool depth was varied between 13.6 and 43.6cm and the height of fall between 40 and 110cm.

The model developed by ECKENFELDER (1959) for diffused aeration was adapted to describe the aeration occurring at a weir:

$$\frac{\frac{dC}{dt}}{C_s - C_L} = K_{La} = \frac{\beta_o Q_a d^{1-m}}{V.d_b.S_c^{0.5}} \tag{2.36}$$

Q_a = Gas flow rate

S_c = Schmidt number relating diffusivity and kinematic viscosity

V = Volume of fluid being aerated

d = Depth of fluid

d_b = bubble diameter

β_o = constant

m = depth exponent

For high air-flow rates ECKENFELDER states that

$$d_b \alpha Q_a^{n_1} \tag{2.37}$$

where the exponent n_1 relates to the variation of bubble size with air-flow rate and also to turbulence as dictated by tank geometry. Hence Equation 2.36 becomes:

$$K_{La} = \frac{\beta_1 Q_a^{1-n_1} d^{1-m}}{V S_c^{0.5}} \tag{2.38}$$

β_1 is a combination of the constants from Equations 2.36 and 2.37.

NAKASONE assumed that for air entrainment by a jet that:

$$Q_a = f(U, t_j) = \beta_2 . U^x t_j^y \tag{2.39}$$

$$U = \sqrt{2gh} = \frac{Q}{Bt_j} = \frac{q}{t_j} \tag{2.40}$$

where U, t_j are the jet velocity and thickness at impact. The jet width appears to have been assumed equal to the weir crest width B at all heights of fall.

Substituting into Equation 2.38:

$$K_{La} . V = C_n . h^{\alpha} . q^c d^{\gamma_1} \tag{2.41}$$

where

$$C_n = \frac{\beta_1 \beta_2^{(1-n_1)}}{S_c^{0.5}} (2g)^{\alpha}$$

$$\alpha = (0.5x-y)(1-n)$$

$$\gamma_1 = (1-m)$$

From his experiments, NAKASONE obtained values for the exponents and the constant in Equation 2.41: (all results were corrected to 20°C using the temperature correction given by Equation 2.13),

$$K_{La}.V = 0.0675\ h^{1.28}\ q^{1.62}\ d^{0.439} \qquad (2.42)$$

where $K_{La}.V$ has units $m^3/h.m$, d and h metres, q m^2/h.

Equation 2.42 re-expressed in terms of the deficit ratio at 20°C:

$$\text{Log}_e\ r_{20} = 0.0675 h^{1.28}\ q^{0.62}\ d^{0.439} \qquad (2.43)$$

None of the equations so far discussed is dimensionless. The choice of ECKENFELDER's general diffused aeration equation as a basis for developing the Equation 2.42 proposed by NAKASONE is surprising as ECKENFELDER states clearly that the exponents n_1 and m in Equation 2.38 are variables affected by pool geometry etc. The exponents derived by NAKASONE from his experiments therefore relate solely to his experimental apparatus and Equation 2.42 will certainly not be a general equation of oxygen uptake at free overfalls as claimed.

Furthermore, Equation 2.43 predicts that the natural logarithm of the deficit ratio will vary as the depth to the power 0.439 providing all other conditions are kept constant. This is physically possible only over a limited range as it is well established /D.O.E. (1973), JARVIS (1970), APTED (1975)/ that once the pool depth exceeds the depth of bubble penetration (i.e. the optimum depth) then the oxygen uptake becomes independent of the pool depth for constant height of fall.

Despite the limitations of NAKASONE's work, his experimental results are of interest. An increase in aeration is recorded with

increase in discharge which contrasts with the findings of VAN DER KROON & SCHRAM.

Much work has clearly been done to provide a clearer picture of the mechanics of oxygen transfer at a weir situation, but, as yet, it has not proved possible to bring together all this research or to provide a generally applicable model describing the transfer processes.

2.4.7 Further Attempts to Establish Modelling Laws for Oxygen Transfer at Hydraulic Structures

Recent attempts to determine the model/prototype laws governing the gas transfer at hydraulic structures have not met with much success as evidenced by the efforts of WILHELMS (1975). WILHELMS recommended continued efforts to correlate model and prototype data but concluded that at present, it is still quicker to define the aeration characteristics by large scale collection of prototype data.

This approach was used by JOHNSON and KING (1975), who working from the basic aeration equation, Equation 1.29, suggested means of determining C_s, $K_{LV}\frac{A}{V}$ and t as a result of studies at prototype hydraulic structures. The results they quoted, indicated good estimates of dissolved nitrogen levels after aeration but dissolved oxygen levels observed were in several cases as low as 85% of the predicted levels. Errors such as these would result in dramatic errors in the deficit ratio. Several assumptions were necessary to determine values of C_s, $K_{LV}\frac{A}{V}$ and t and these will be briefly mentioned. In evaluating C_s, JOHNSON and KING rightly allowed for the depth of water in the aeration basin, a value of barometric pressure and two-thirds of the basin depth being assumed. The contact time was determined (a) by considering the tailwater depth and assuming the bubbles to rise at a terminal

velocity of 0.696 ft/sec (an assumed mean bubble diameter of 0.7mm gave the best results) and, (b) by attempting to assess the path travelled by the jet through the basin and assuming the bubbles to be carried along with it. The least value calculated by (a) and (b) was considered the critical one and used in subsequent computation. The value of $K_L \frac{A}{V}$ was judged to be a function of the velocity head of the jet at impact divided by the path length of the jet in the pool (an energy gradient parameter for the flow) and also a function of the ratio jet cross sectional area to jet perimeter at impact. A family of curves was presented based on prototype observations enabling $K_L \frac{A}{V}$ to be determined from the two ratios just mentioned.

Clearly, the assessment of the pool conditions, particularly with regard to estimating $K_L \frac{A}{V}$ and t, is an ambitious project and the results arrived at by any two assessors are unlikely to agree. The approach, however, does provide an interesting interpretation of the most relevant parameters controlling the gas transfer process.

2.5 THE OXYGEN BALANCE IN A RIVER SYSTEM

Various means of aiding the assimilative capacity of a river have been discussed. This picture is incomplete without an understanding of the variables affecting the oxygen balance of a river system.

The addition of oxygen through atmospheric aeration has already been discussed. Consideration should also be given to the daytime photosynthetic contribution of algae and plant life as well as that resulting from dilution of main flows by clean tributary flows. The removal of oxygen is effected by BOD exerted by organic wastes carried with the water, by plants at night, by diffusion into river bottom muds and oxidation of gases escaping from these muds, as well as the additional BOD load inflicted by foul tributary flows.

The effects noted above should be borne in mind when contemplating the improvement of oxygen levels particularly if an impedence to the flow such as a weir is considered since this must have undesirable as well as beneficial effects.

The STREETER & PHELPS (1925) oxygen sag equation forms the basis for estimating the oxygen profile variation with time at a section:

$$C_s - C_t = \frac{K_I L_1}{K_{La} - K_I} (10^{-K_I t} - 10^{-K_{La} t}) + (C_s - C_1) 10^{-K_{La} t} \qquad (2.44)$$

$C_s - C_1$ = initial oxygen deficit

L_1 = initial BOD

$C_s - C_t$ = oxygen deficit after time t

K_I = deoxygenation rate constant

K_{La} = reaeration rate constant

The BOD change follows the relation

$$L_t = L_1 \, 10^{-Kt} \tag{2.45}$$

The use of the STREETER-PHELPS equation will provide an over simplified solution to the oxygen situation in a river. A complete consideration of the effective factors noted above together with stream characteristics poses a difficult problem and much work is still being done using the basic oxygen sag equation (TEBBUTT, 1971).

CHAPTER 3

THE HYDRAULIC JUMP - HYDRAULIC EQUATIONS AND CHARACTERISTICS, AND AN INVESTIGATION OF THE DOWNSTREAM VELOCITY COEFFICIENTS

3.1 A DEFINITION OF THE HYDRAULIC JUMP

It is established in hydraulics that subcritical flow is produced by a downstream control (e.g. weirs) and supercritical flow by an upstream control (e.g. underflow sluice gate).

If two such controls are present in a channel, the one downstream creating subcritical flow in the channel upstream of itself and the one upstream creating supercritical flow downstream of itself, then, a conflict arises between the influence of the two controls. Such a conflict can only be resolved by a transition from supercritical to subcritical flow. This transition which is characterised by considerable turbulence, air entrainment and loss of energy is the feature known as the hydraulic jump.

The formation of an hydraulic jump is illustrated in Figure 3.1a.

3.2 EQUATIONS DESCRIBING THE HYDRAULIC JUMP

The application to an hydraulic jump situation (illustrated in Figure 3.1a)of the simplified equations of continuity, momentum and energy for an homogeneous liquid flowing through a horizontal, resistance-free channel of rectangular cross section will lead to the following well-known equations of the hydraulic jump:

$$\frac{y_2}{y_1} = \frac{1}{2}\left(-1 + \sqrt{1 + 8\,Fr_1^2}\right) \qquad (3.1)$$

where Fr_1 is the Froude No. of the supercritical flow at the toe of the jump:

$$Fr_1 = \frac{v_1}{\sqrt{gy_1}} = \frac{q}{y_1^{1.5}\, g^{0.5}} \qquad (3.2)$$

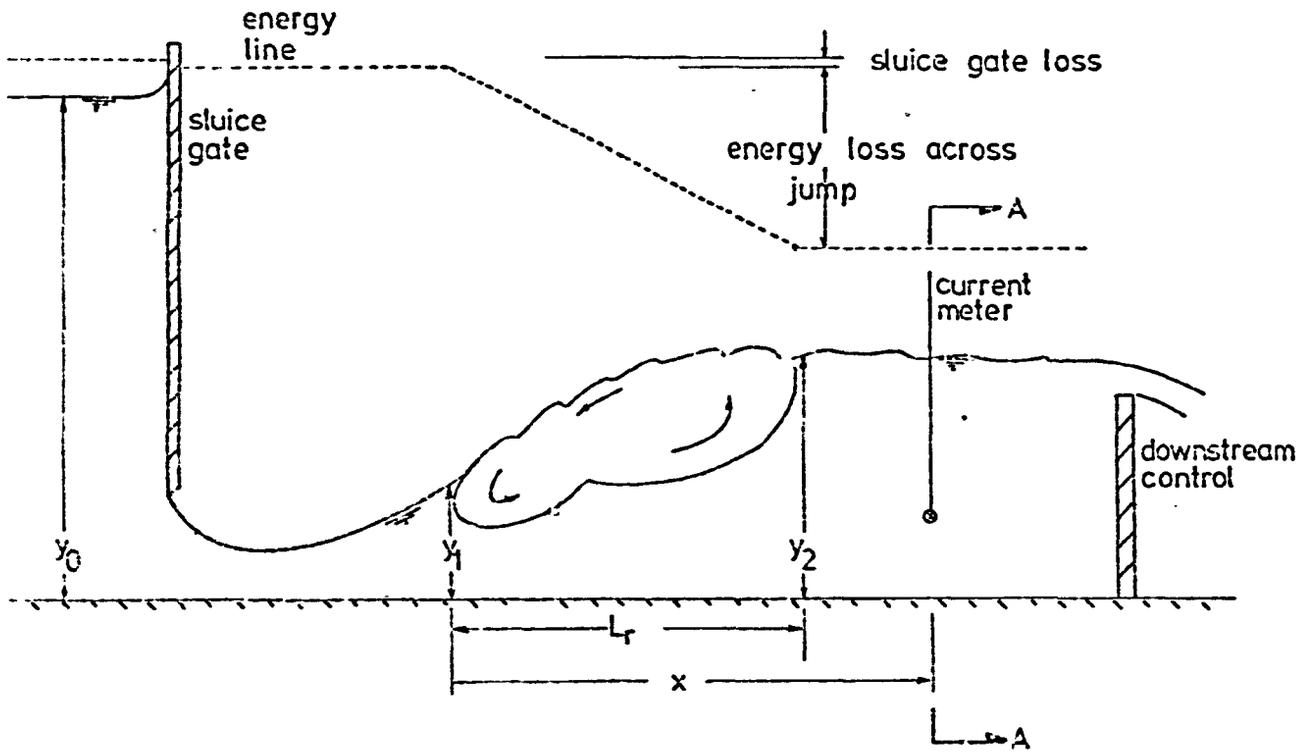

figure 3.1a the hydraulic jump

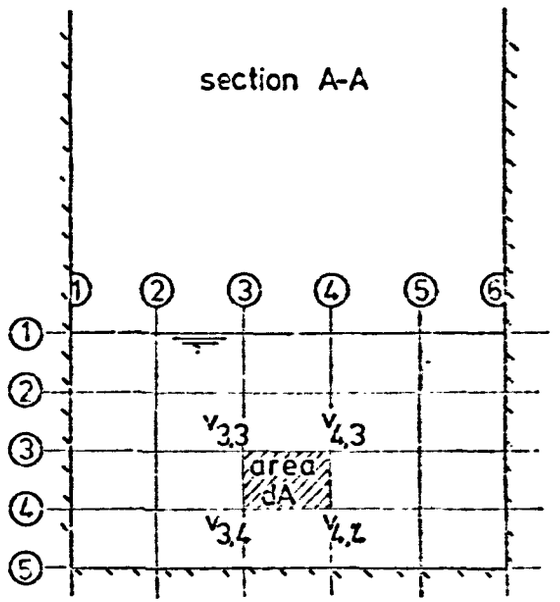

figure 3.1b channel cross section - typical velocity measuring grid

and y_1, y_2 are the conjugate depths of the hydraulic jump (suffices 1, 2 refer to the cross sections before and after the hydraulic jump), v is the mean velocity (q/y), q is the specific discharge flowing.

The Energy Loss ΔE in the hydraulic jump is:

$$\Delta E = (y_1 + \frac{v^2_1}{2g}) - (y_2 + \frac{v^2_2}{2g}) \tag{3.3}$$

or,

$$\Delta E = (y_1 - y_2) + \frac{q^2}{2g\, y^2_1\, y^2_2} (y^2_2 - y^2_1) \tag{3.4}$$

substituting for q:

$$\Delta E = \frac{(y_2 - y_1)^3}{4\, y_2\, y_1} \tag{3.5}$$

3.3 VELOCITY COEFFICIENTS

3.3.1 Velocity Coefficients Defined

In all the above equations it has been assumed that the mean velocity head across a section, $(v^2/2g)_m$, is equal to $v_m^2/2g$ where v_m is the mean velocity across the section.

This can never be true because viscous drag reduces velocities at boundaries below those in the main fluid body.

The true mean velocity head is thus obtained by multiplication by a correction factor.

The mean velocity head, or kinetic energy per unit weight of fluid is equal to:

$$(\frac{v^2}{2g})_m = \frac{\int \frac{v^3}{2g}.dA}{v_m.A_c} = \alpha \cdot \frac{v_m^2}{2g} \tag{3.6}$$

where A_c is the cross sectional area of flow.

The correction coefficient α is sometimes known as the Coriolis Coefficient. α is a correction coefficient to be applied to the velocity head as calculated from the mean velocity i.e.:

$$\alpha = \frac{\int v^3 . dA}{v_m^3 . A_c} \tag{3.7}$$

Similarly, a correction coefficient, the Boussinesq coefficient β_B, is employed to correct the momentum term which has been computed using the mean velocity, v_m, thus:

$$\beta_B = \frac{(\rho Q v)_m}{\rho Q v_m} = \frac{\int v^2 dA}{v_m^2 . A_c} \tag{3.8}$$

The coefficients α and β_B are never less than unity and are both equal to unity when the flow is uniform across the cross section. The further the flow departs from being uniform, the greater become the coefficients α and β_B. It follows from Equations 3.7 and 3.8 that α is more sensitive to velocity variations and thus, for a given channel section, $\alpha > \beta_B$.

3.3.2 Reasons for Attempting to Measure α

It was suggested by APTED that the assumption $\alpha = \beta_B = 1$ was invalid for the hydraulic jump he studied. APTED came to this conclusion because he found that the energy loss as given by Equation 3.3 did not agree with that calculated from Equation 3.5. These equations are of course the same assuming that $\alpha = \beta_B = 1$. Following from APTED's supposition, one of the first objectives of this research was to attempt to quantify the magnitude of the velocity coefficients. APTED calculated β_B to be as high as 3.01 at his downstream conjugate depth section.

3.3.3 The Computation of α

To calculate α from Equation 3.7 it is necessary to obtain a grid of velocity measurements over the whole cross section under consideration.

For simplicity of illustration, consider a cross section of flow, depicted in Figure 3.1b, divided into n segments of flow each of equal area dA by a system of grid lines as shown. Velocity measurements are taken at all the intersection points of the grid lines.

Considering the typical segmental area of flow dA in Figure 3.1b, the mean velocity of flow of the segment is approximately:

$$v_n = \frac{1}{4}(v_{3,3} + v_{4,3} + v_{3,4} + v_{4,4}) \tag{3.9}$$

Thus, considering all segmental areas constituting the whole area A_c, i.e.

$$\sum^{n} dA = A_c \tag{3.10}$$

Also,

$$\sum^{n} (v_n . dA) = Q' \tag{3.11}$$

The Coriolis coefficient may be estimated:

$$\alpha = \frac{\sum^{n} (v_n^{\,3} . dA)}{v_m^{\,3} . A_c} \tag{3.12}$$

where $v_m = Q/A_c = q/y_2$, Q is the recorded discharge and Q' is the discharge as calculated from the velocity traverse. Obviously, the more concentrated the grid pattern, the more accurate will be the estimate of α and Q'.

3.4 EXPERIMENTAL APPARATUS

3.4.1 The Flume and Water Supply System

The hydraulic jump studied was formed downstream of a variable opening underflow sluice gate in a glass walled flume, 3 metre long by 10cm wide.

The water is supplied under constant head from the header tank of the laboratory's re-circulating water system. Water is contained in a 22,000 gallon capacity sump from which it is pumped to the header tank. This header tank supplies all hydraulic apparatus in the laboratory, the available head being approximately 11 metres. After passing through the flume, the water is returned to the sump.

The flume and water circulating system are illustrated in Figure 4.1 and Plate 4.1.

The measurement of flow through the flume was effected by an orifice plate connected to a differential mercury manometer and calibrated to British Standard.

The flume is fitted with a downstream control with which the depth of flow may be regulated. The slope of the channel may be varied, but, for all hydraulic jump experiments the flume was maintained in a horizontal position.

Depth measurements were obtained by means of point gauges mounted on carriages which could be moved along the length of the flume on rails.

3.4.2 The Measurement of Velocity

Some difficulty was experienced in finding a suitable means of accurately measuring velocities.

(a) Pitot - Static Tube

In view of the anticipated fluctuating nature of velocities at a point, the Pitot-Static tube was first tested as it was thought that the velocity oscillations might be effectively damped in the manometer tubes, thus providing an easily read mean velocity at that point.

After numerous tests, the use of the Pitot-Static tube was abandoned and an alternative method sought.

The first objection to the use of the Pitot-Static tube was its interference with the flow. This highlighted one of the disadvantages of working in such a small flume, the obstruction to flow offered by the tube being quite significant relative to the actual cross section of flow. As the pitot-static tube was lowered deeper into the flow, the hydraulic jump was visibly observed to advance towards the sluice gate. An interference of this scale was unacceptable. Secondly, measurements collected and computed, revealed values of the Coriolis Coefficient less than unity, an impossible result. It was established that the Pitot-Static tube was sensitive to boundary conditions and that the calibration could only be applied with confidence when the tube was positioned in the centre of the flow section and thus free from boundary effects.

(b) Miniature Current meter - Wallingford

The miniature Wallingford current meter with a 3mm diameter propeller proved to be the solution required. It provided accurate measurement and retained its calibration near boundaries. By virtue of its small size, it was therefore possible to take measurements within 2mm of the boundary walls and the channel bed, and, no interference with the flow was observed.

The rotation of the meter's propeller was recorded by a counter, and, by measuring the number of rotations over a known period of time,

the mean number of cycles per second recorded at the particular point of measurement could then be translated to the mean velocity via the calibration curve. The meter was calibrated in a towing tank 30 metres in length.

One of the main difficulties encountered with this current meter was the meter's inability to differentiate between forward and reverse velocities. Consequently, if the current meter is placed in a region of reversible flow, such as occurs in the roller region of the hydraulic jump, then, the forward and reverse velocities will be added positively resulting in an over-estimate of the velocity at that point. It was necessary, therefore, to ensure that there were no flow reversals in any selected measuring section. It was thus not possible to take measurements too close to the roller region of the jump.

3.5 EXPERIMENTAL TECHNIQUE

The discharge through the flume was kept constant at 3.45 l/s (as recorded by the orifice plate).

For various openings of the sluice gate, an hydraulic jump was formed just downstream of the sluice gate by suitable adjustment of the gate regulating the tail-water depth.

Depths at the toe of the jump and downstream of the roller were recorded.

Three cross sections were arbitrarily selected (in two cases, only two were studied), the sections all being downstream of the roller of the hydraulic jump. The location of the chosen section was recorded as the horizontal distance x measured from the toe of the jump. (See Figure 3.1a.)

The measurement of velocities was carried out on a 2cm square grid except at the boundaries where measurements were taken within 10mm

and 2mm of the boundary. At each measuring point, the rotation of the current meter propeller was measured over 50 seconds.

3.6 RESULTS

The results collected have been summarised in Table 3.1. The velocity measurements collected were read into a computer program, and, as a check on the accuracy of the data, the discharge was computed (Equation 3.11) and compared with the discharge recorded by the orifice-plate meter. The latter discharge Q was a constant 3.45 l/s and the computed discharges Q' tabulated in Table 3.1 are also plotted in Figure 3.2 against the ratio x/y_2. The bulk of the data indicate that the calculated discharges lie within $\pm$ 1% of the recorded discharge, but, deviations of up to -2% are exhibited by five other points with four further points deviating by 3% and slightly more. It must be concluded that the agreement between recorded and measured flow rate is very good and therefore the velocity measurements were confidently applied for further computation.

The mean velocity distributions across the width of the channel are presented in Figure 3.3. The distributions displayed are fairly typical for turbulent flow, and, as would be expected, the flow is not uniform within the range of these tests. Flow is said to be uniform if the velocity profile does not change in the direction of motion (HENDERSON). The limit between non uniform and uniform flow downstream of a jump was shown by LEUTHEUSSER and KARTHA (1972) to be practically independent of upstream Froude number (for $Fr_1 > 4$) and, for an hydraulic jump formed close to the sluice gate they showed the inflow to the hydraulic jump to be undeveloped, i.e. the boundary layer is still predominant. The experiments reported here were probably conducted

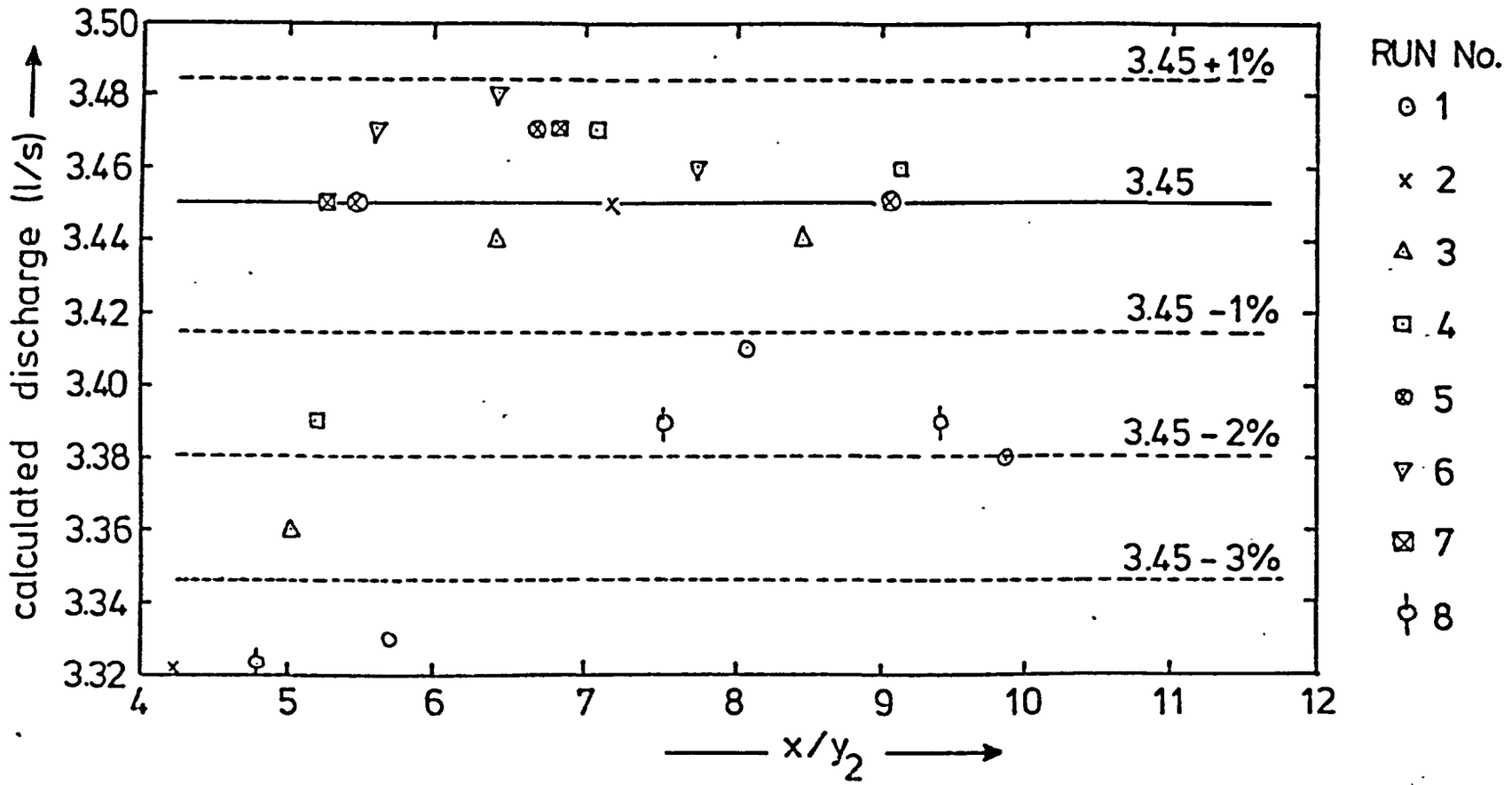

figure 3.2 discharge calculated from velocity measurements (manometer discharge = 3.45 l/s)

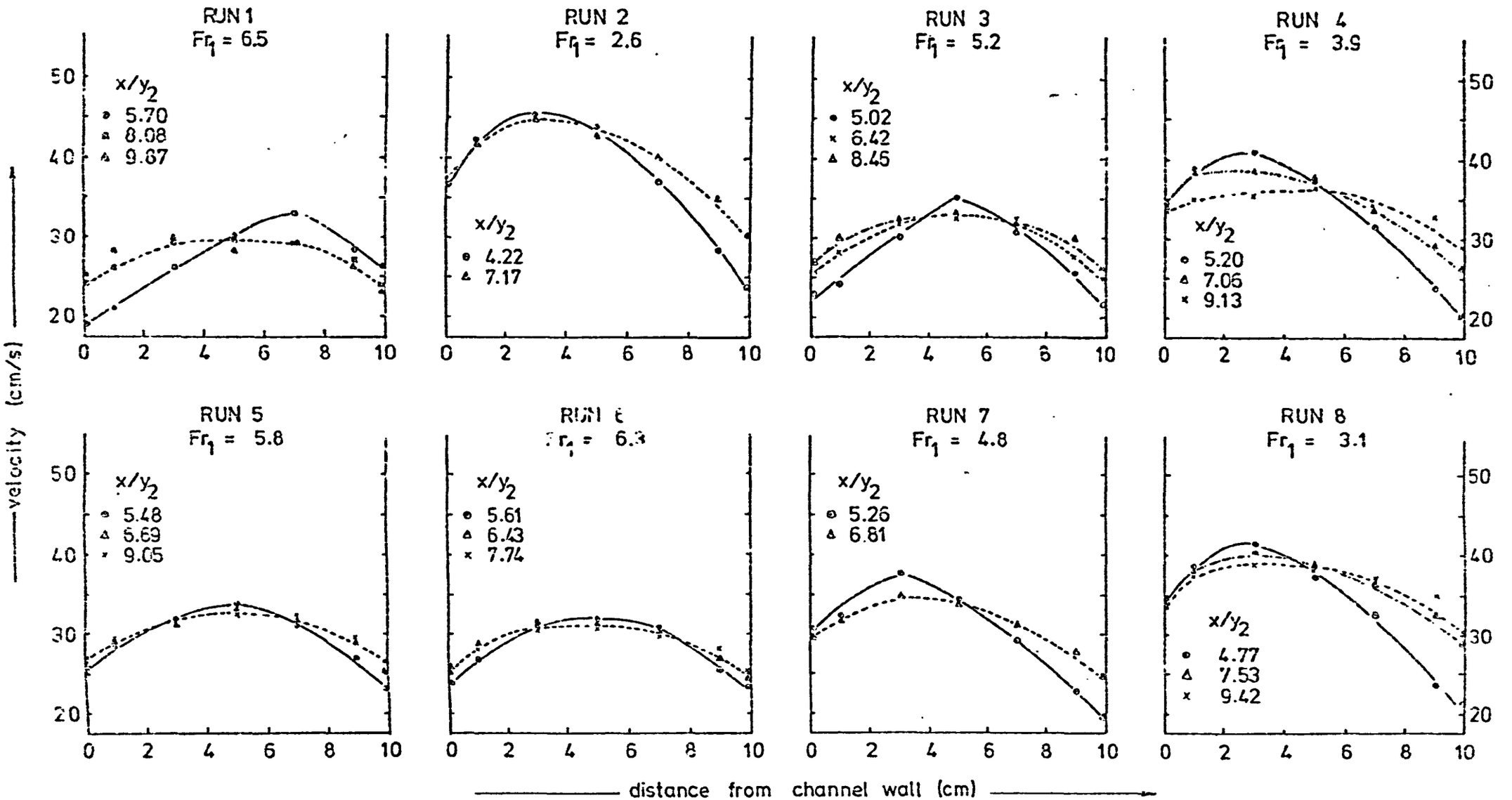

figure 3.3 MEAN VELOCITY DISTRIBUTIONS DOWNSTREAM OF AN HYDRAULIC JUMP

Q = 3.45 l/s

TABLE 3.1

Calculated Values of Coriolis Coefficient

RUN NO.	Q (L/S)	$\frac{x}{y_2}$	α	Q' (L/S)	$\frac{x}{y_2}$	α	Q' (L/S)	$\frac{x}{y_2}$	α	Q' (L/S)
1	3.45	5.70	1.15	3.33	8.08	1.03	3.41	9.87	1.02	3.38
2	3.45	4.22	1.24	3.32	7.17	1.03	3.45	-	-	-
3	3.45	5.02	1.16	3.36	6.42	1.06	3.44	8.46	1.04	3.44
4	3.45	5.20	1.20	3.39	7.06	1.05	3.47	9.13	1.02	3.46
5	3.45	5.48	1.05	3.45	6.69	1.02	3.47	9.05	1.02	3.45
6	3.45	5.61	1.06	3.47	6.43	1.04	3.48	7.74	1.03	3.46
7	3.45	5.26	1.13	3.45	6.81	1.04	3.47	-	-	-
8	3.45	4.77	1.21	3.32	7.53	1.03	3.39	9.42	1.02	3.39

for a condition of undeveloped inflow and for this condition LEUTHEUSSER and KARTHA showed that the flow becomes uniform at a distance downstream of the toe of the jump given by $x/y_2 \approx 12$. The non-uniformity of flow displayed by Figure 3.3 is consistent with this, and, velocity coefficients greater than unity are anticipated. A skewed velocity distribution is present in a number of cases, but as one travels downstream of the jump the influence of the channel begins to predominate over the influence of the jump and the distribution tends to a symmetrical one. The reason for the skew is not clear, but, it can probably be attributed to a variation in the sluice gate opening with width due to imperfections in construction.

It is worth recording here that one run was repeated with an obstruction placed in the water downstream of the measuring section. This was done to investigate the effects on the characteristics of the jump due to the presence of a dissolved oxygen measuring electrode in the flow downstream of the jump. An electrode was inserted, the backing up of flow resulting was compensated for by opening the tailwater control gate until the jump returned to the position it occupied prior to insertion of the electrode. A complete velocity traverse was conducted and to conclude, no significant variation in the velocity distribution due to the obstruction was observed.

The values of Coriolis coefficient computed for these experiments by means of Equation 3.12 are tabulated in Table 3.1 and plotted against the ratio x/y_2 in Figure 3.4. Extrapolation of the results shows that the flow becomes uniform (i.e. $\alpha = 1$) for $x/y_2 \approx 12$ which is in agreement with the limit shown by the experiments of LEUTHEUSSER and KARTHA (discussed above).

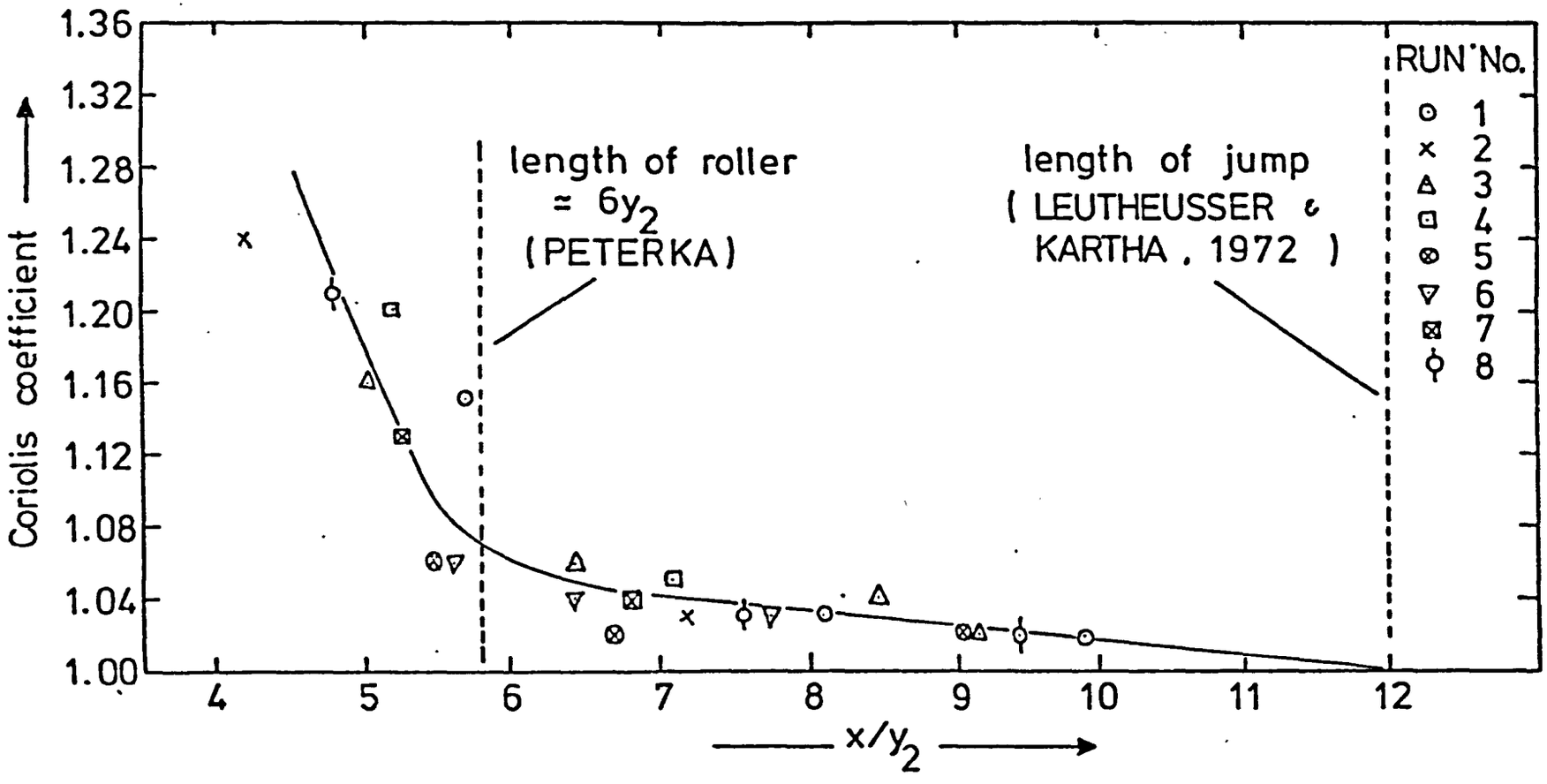

figure 3.4 variation in the Coriolis coefficient with distance downstream of an hydraulic jump

The transition point indicated on Figure 3.4 is consistent with the end of the roller of the hydraulic jump defined by PETERKA (1963), $L_j \simeq 6y_2$. It would appear from these measurements that the Coriolis coefficient for the downstream conjugate depth section is unlikely to exceed 1.05, and, further, this value of α is considerably smaller than the value anticipated by APTED to explain his discrepancy between measured and calculated energy losses.

As confirmation of the above results, the classic air model results of ROUSE, SIAIO & NAGARATNAM (1959) are cited. These revealed that at the end of the hydraulic jump transition, α was within 5% of unity in every case, i.e. $\alpha \leq 1.05$; the agreement is remarkable.

Although the tests reported above were not conducted in the same apparatus as those of APTED, the results obtained here do not support APTED's supposition regarding his discrepancies, and the reasons for these will be sought elsewhere and discussed in Section 3.7.

3.7 AN EXPLANATION OF THE DISCREPANCIES REPORTED BY APTED

The data supplied by APTED have been reproduced in Table 3.2. Also presented in columns 8 and 9 of this Table are the energy losses in the jump as computed from Equations 3.3 and 3.5 respectively.

Comparison of columns 8 and 9 reveal the discrepancy noted by APTED and it can be seen to be very significant. It appears that ΔE computed from Equation 3.3 is consistently higher than that calculated from Equation 3.5. APTED attributed this to the geometry of his flume and an incorrect assumption of velocity coefficients equal to unity. Whilst measurements in Section 3.6 do not support this view, it should be remembered that these were conducted in a different flume. However, close examination of Table 3.2 reveals an impossible situation described by columns 5 and 6. It would appear that a large proportion of APTED's data suggest an increase in the specific energy function across the sluice gate; this is clearly ridiculous and can only be attributed to inaccuracies in the measurement of the depth of super-critical flow below the sluice gate. The larger depths above the sluice gate and downstream of the hydraulic jump are less sensitive to inaccuracies in the depth measurement since the velocity head term in the energy function is relatively small compared to the static head. For the super-critical flow region, even very slight errors in the depth measurement are reflected in very significant changes in the calculated velocity head, which, for this flow regime, constitutes the largest portion of the energy function. To illustrate the extent of the errors in y_1, the ratio y_2/y_1 has been plotted in Figure 3.5 against the Froude number of the supercritical flow. For comparison, the law of Bélanger, Equation 3.1, relating the conjugate depths, is also shown.

TABLE 3.2

APTED's Hydraulic Jump Data and Calculated Energy Losses

y_o (cm)	y_1 (cm)	y_2 (cm)	Q (l/s)	E_o (cm)	E_1 (cm)	E_2 (cm)	E_1-E_2 (cm)	$\frac{(y_2-y_1)^3}{4\,y_2y_1}$
42.48	1.43	12.8	4.16	42.53	44.53	13.34	31.19	20.07
38.68	1.41	11.9	3.94	38.73	41.21	12.46	28.75	17.20
38.60	1.42	12.1	3.95	38.65	40.86	12.64	28.22	17.72
35.56	1.51	12.0	4.08	35.63	38.72	12.59	26.13	15.93
35.32	1.53	12.1	3.97	35.38	35.85	12.65	23.20	25.95
35.29	1.54	11.5	4.06	35.36	36.96	12.13	24.83	13.95
35.02	1.52	12.1	4.01	35.09	36.99	12.66	24.33	16.10
33.73	1.50	11.3	3.90	33.80	35.95	11.91	24.04	13.88
32.00	1.58	12.0	4.04	32.08	34.90	12.58	22.32	14.92
30.93	1.61	11.5	3.98	31.01	32.76	12.11	20.65	13.06
28.65	1.70	11.2	4.01	28.75	30.06	11.85	18.21	11.26
27.14	1.80	11.0	4.00	27.25	26.97	11.67	15.30	9.83
25.47	1.85	10.8	4.00	25.59	25.68	11.5	14.18	8.97
24.59*	1.90	10.8	4.00	24.72	24.49	11.5	12.99	8.69
24.04	1.96	10.6	4.00	24.18	23.19	11.32	11.87	7.76
23.96	2.00	10.6	4.04	24.10	22.79	11.34	11.45	7.50
22.14	2.17	10.3	4.01	22.31	19.57	11.07	8.50	6.01
20.19	2.19	10.0	4.00	20.39	19.19	10.81	8.38	5.44
17.40	2.50	9.5	4.06	17.68	15.94	10.43	5.51	3.61
17.90	2.39	9.6	4.01	18.15	16.74	10.49	6.25	4.08
15.82	2.55	8.9	4.00	16.14	15.09	9.93	5.16	2.82
15.54	2.65	8.6	4.01	15.88	14.32	9.71	4.61	2.31
1	2	3	4	5	6	7	8	9

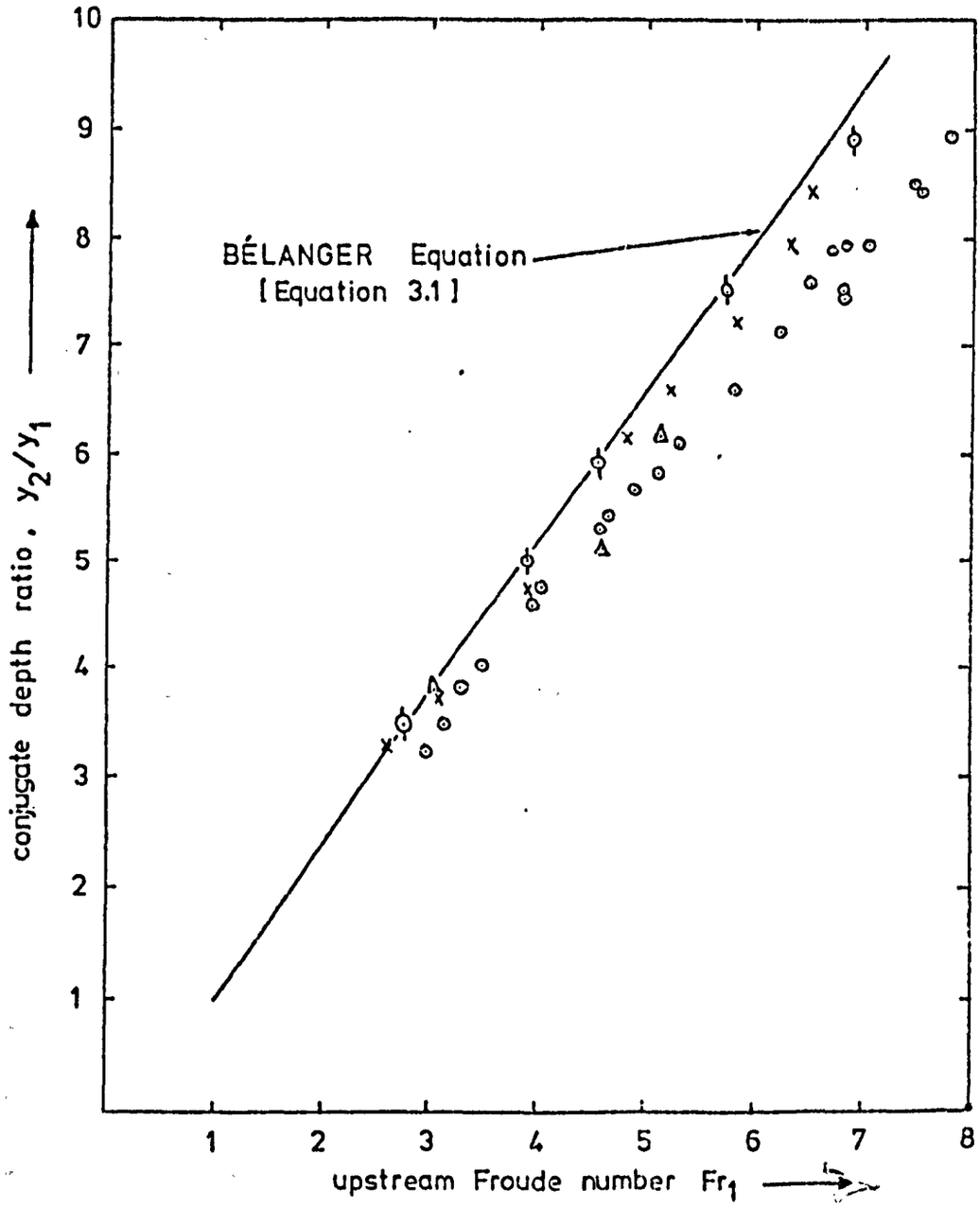

- ⊙ APTED (1975) - Table 3.2
- Δ HOLLER (1971) - Table 4.4
- × these studies - Table 3.3 - y_1 measured in the centre of the channel.
- ϕ these studies - y_1 = mean depth measured across channel width.

figure 3.5 - recorded deviations from the hydraulic jump conjugate depth equation of BÉLANGER.

Deviations from the Bélanger law have been shown to occur by LEUTHEUSSER & KARTHA (1972) but these have been for a situation where the inflow into the hydraulic jump is fully developed. For the inflow to fully develop, the hydraulic jump must be formed a long way downstream from the sluice gate. LEUTHEUSSER & KARTHA referred to a previous finding by KARTHA (1968) indicating that the distance required for inflow to fully develop must be greater than or equal to two hundred times (200 x) the sluice gate opening.

The experiments of this research and those of APTED were conducted for conditions of undeveloped inflow and for such a condition, LEUTHEUSSER & KARTHA concluded from their results that the ratio of conjugate depths is essentially that given by the Bélanger equation, Equation 3.1. RESCH & LEUTHEUSSER (1971) showed this was so since for this inflow condition the energy of turbulence upstream of the jump was negligible.

The deviations from the Bélanger law exhibited by APTED's data in Figure 3.5 are significant particularly as the range of Froude number tested was relatively small.

Also plotted in Figure 3.5 are some data supplied by HOLLER which display similar inaccuracies in the depth measurements.

As a matter of interest, the data discussed in Section 3.6 was treated in the same way as APTED's data resulting in Table 3.3. Curiously, exactly the same observations can be made with regard to this data except to a lesser degree. An increase in specific energy across the sluice gate was similarly implied and discrepancies were revealed between the calculated and measured energy losses. There is a deviation of the conjugate depth ratio from the law of Bélanger (Figure 3.5), but to a much lesser degree than suggested by the data of APTED and HOLLER.

TABLE 3.3

Hydraulic Jump - Depths and Calculated Energy Levels

RUN NO.	y_o (cm)	y_1 (cm)	y_2 (cm)	E_o (cm)	E_1 (cm)	E_2 (cm)	E_1-E_2 (cm)	$\frac{(y_2-y_1)^3}{4y_2y_1}$
1	30.75	1.39	11.75	30.81	32.79	12.19	20.60	17.02
2	11.94	2.54	8.30	12.36	11.94	9.18	2.76	2.26
3	23.70	1.63	10.75	23.81	24.46	11.27	13.19	10.82
4	16.94	1.99	9.42	17.15	17.31	10.10	7.21	5.47
5	25.44	1.53	11.05	25.53	27.44	11.55	15.89	12.76
6	28.53	1.44	11.50	28.60	30.69	11.96	18.73	15.37
7	21.87	1.74	10.65	22.00	21.78	11.18	10.60	9.54
8	14.0	2.33	8.70	14.31	13.50	9.50	4.00	3.19

The belief that these deviations were entirely due to slight errors in y_1 is reinforced by the excellent agreement obtained (Section 3.6) between recorded discharges and the discharge calculated from velocity measurements and the measured downstream depth y_2. If significant errors arose in measuring y_2, then these would have been reflected in the calculated discharges.

Great care was taken in the measurement of depth, but, it must be admitted that the design of the point-gauges precluded any depth measurement other than in the middle of the channel. A special carriage was therefore constructed which enabled the point-gauge to be traversed across the width of the channel as well as along the length of it.

The measurements of y_1 subsequently collected across the channel width, revealed a concave water surface such that the depths near the boundaries were anything up to 25% higher than the minimum depth which generally occurred in the centre of the channel. For five different Froude numbers, the mean supercritical depth across the channel width y_1 was measured along with the corresponding downstream depth y_2. The results, plotted in Figure 3.5, display almost total agreement with the law of Bélanger. This is consistent with the conclusions of LEUTHEUSSER and KARTHA.

It would seem reasonable to suggest that y_1 in APTED's experiments was similarly underestimated, thus explaining the discrepancies he observed.

It is interesting to record here that MOORE (1941) similarly noted the sensitivity of the specific energy of the supercritical flow at the base of a free overfall to small changes in the supercritical depth, and MOORE referred to errors exceeding 25%.

3.8 SUMMARY

An investigation of the velocity coefficients in the flow downstream of an hydraulic jump did not reveal any significant departure of the coefficients from unity. This was shown to be consistent with the findings of ROUSE, SIAIO & NAGARATNAM.

Subsequent tests showed that the conjugate depth ratio was closely described by the law of Bélanger, and that departures from this law observed by APTED, HOLLER, and also by the author of this thesis in earlier tests, were entirely due to inaccurately measured depths in the supercritical region downstream of the sluice gate and just prior to formation of an hydraulic jump. The validity of the law of Bélanger was also demonstrated by LEUTHEUSSER and KARTHA for an hydraulic jump formed just downstream of a sluice gate.

CHAPTER 4

AN ELUCIDATION OF THE FACTORS CONTROLLING THE OXYGEN TRANSFER IN AN HYDRAULIC JUMP

4.1 OBJECTIVES

(a) In view of the inaccuracies in APTED's hydraulic measurements, identified in Chapter 3, it has been considered expedient to repeat all his tests and

(b) to expand on the work begun by APTED by investigating as wide a range of discharges as possible,

(c) to achieve a generally applicable correlation between oxygen transfer and hydraulic characteristics of the hydraulic jump.

4.2 A DESCRIPTION OF THE APPARATUS

4.2.1 The Flume and Water Supply System

This has already been described in Section 3.4.1. However, in addition to the water supply from the main laboratory header tank used in the experiments conducted in Chapter 3, an additional supply line was installed to provide deoxygenated water from the mixing tank on the floor above. The deoxygenation of the water is explained in detail in Appendix B and a schematic layout of the experimental system is detailed in Figure 4.1.

The availability of two water supply lines proved useful in providing higher discharges than were possible from the mixing tank alone. This was effected by mixing deoxygenated water with oxygenated water from the main laboratory header tank.

The operational flume is shown in Plate 4.1.

4.2.2 Hydraulic Measurements

Discharge measurement was effected by a differential water manometer connected to an orifice plate meter in the deoxygenated water supply line. The main water supply from the laboratory header tank was

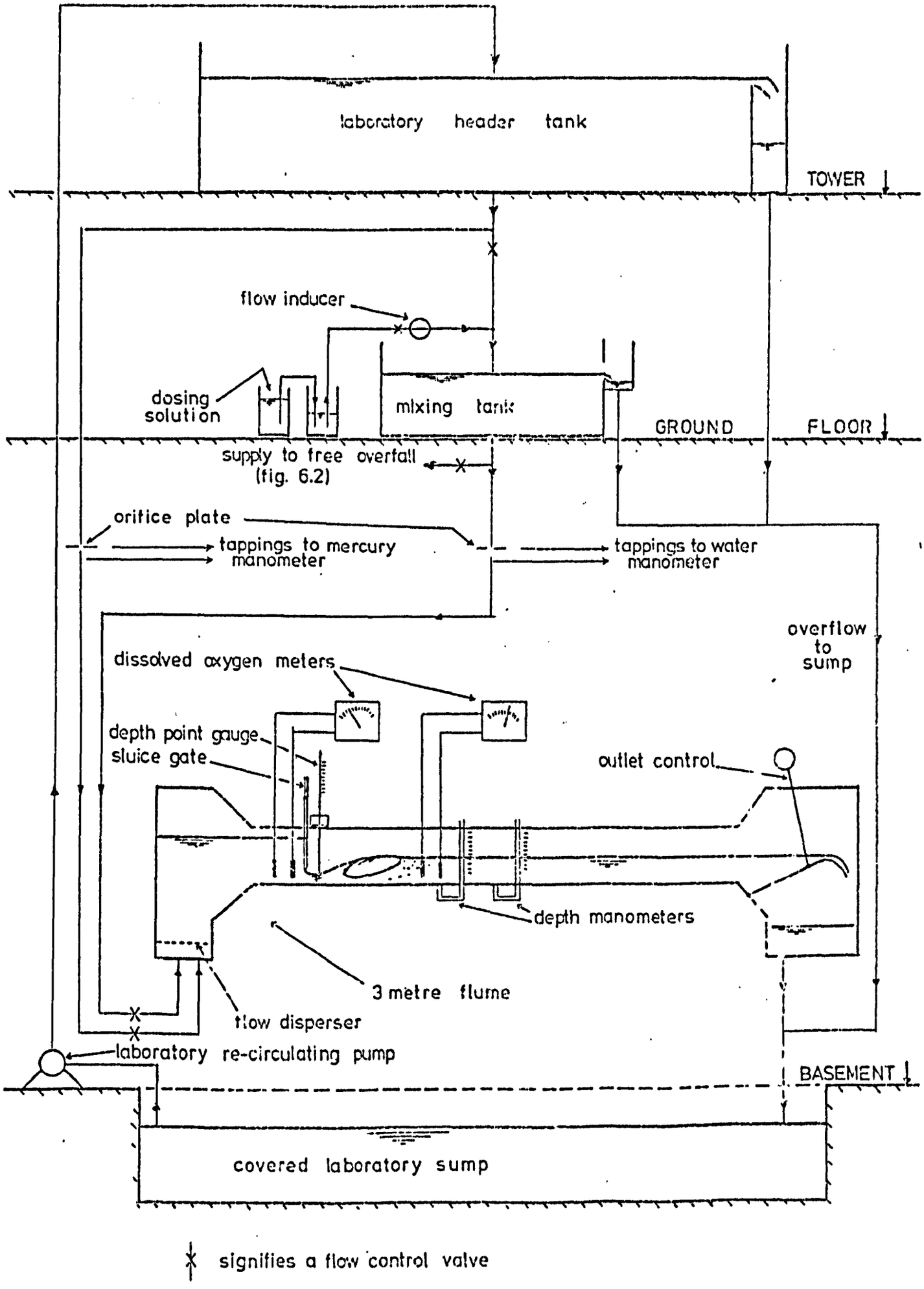

figure 4.1 LABORATORY CIRCUIT - HYDRAULIC JUMP EXPERIMENTS

PLATE 4.1 The operational flume with hydraulic jump

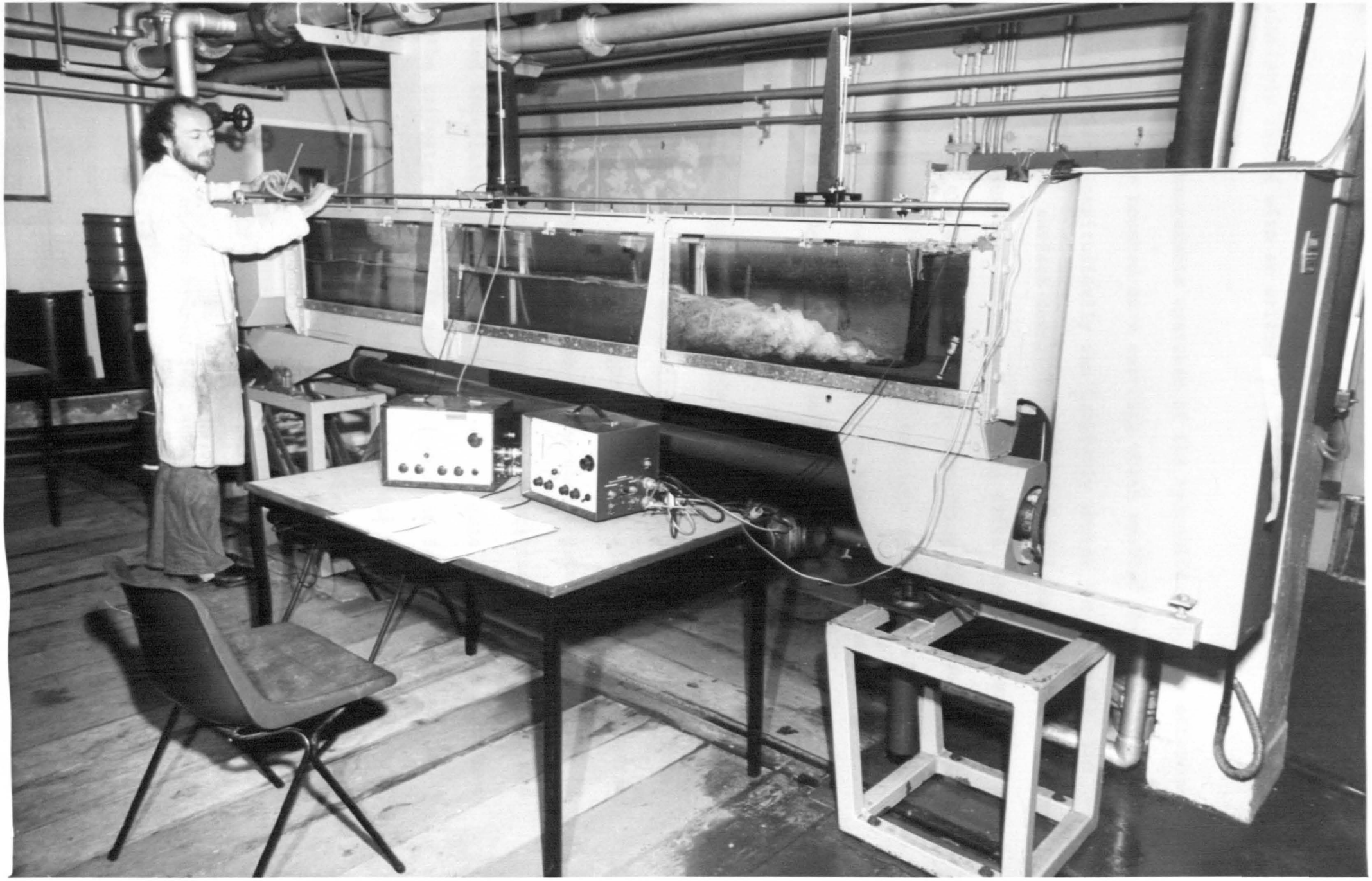

similarly fitted with an orifice plate meter but connected to a mercury manometer.

Depth measurements upstream of the hydraulic jump were effected by a point gauge mounted on a carriage which enabled the gauge to be traversed both longitudinally and laterally across the channel. The fluctuating water surface downstream of the jump made accurate point gauge depth measurement difficult. During these tests, the oscillations were damped and the depth measured by connecting single limb manometers of internal diameter 10mm to several tappings in the bed of the channel. These manometers were calibrated against the point gauges for water flowing freely in the channel for various depths.

4.2.3 Measurement of Oxygen Levels

The equipment used to monitor dissolved oxygen levels has been fully described and tested in Appendix A. The electrodes were immersed in the flow immediately upstream of the sluice gate and in the flow downstream of the hydraulic jump. In all tests the hydraulic jump was formed immediately downstream of the sluice gate by suitable adjustment of the tailwater depth. It was established in Section 3.6 that the presence of the electrode in the tailwater did not alter the velocity distribution in the flow upstream of the electrode.

4.3 THE QUALITY OF THE LABORATORY WATER

The water of the hydraulics laboratory re-circulatory system is treated with quantities of Sodium Nitrite $NaNO_3$ to prevent the corrosion of pipes and other equipment in contact with this water.

For the experiments of JARVIS & APTED the concentration of sodium nitrite in the laboratory water is likely to have been maintained at

approximately 0.6%. Similarly for earlier experiments carried out by the author of this thesis.

During the course of experimental work the concentration of sodium nitrite was reduced to a more economic level of 0.3% and this presented an ideal opportunity to investigate the effects of sodium nitrite on aeration characteristics (Section 4.7 and 7.2). Neither JARVIS nor APTED suspected any effects due to the presence of this salt.

The properties of corrosion inhibition displayed by the nitrite ion NO_3^- are discussed by WEST (1970) and will be reviewed here. The nitrite ion acts as a powerful oxidising agent of ferrous ions and this oxidation gives rise to a stable protective film which inhibits further dissolution. It is classed as an anodic inhibitor since the passivating oxide film is formed primarily at those parts of the metal surface where metal cations are formed, i.e. at the anodes. This type of inhibitor is positively dangerous if used in insufficient quantities as it can then enhance the rate of corrosion. WEST mentions concentrations of nitrite ion of less than 0.05 Molar as deficient.

4.4 AN APPRAISAL OF THE PARAMETERS CONTROLLING THE GAS TRANSFER IN AN HYDRAULIC JUMP

Reference is made to the equation of gas transfer, Equation 1.36. Three controlling factors are apparent for constant temperature and water quality, the liquid film coefficient, the contact time and the ratio air/water interfacial area to volume.

From Equation 2.1:

$$\frac{Q_a}{Q} = \frac{V_a}{V} = \frac{A.\frac{1}{3}\left(\frac{d_b}{2}\right)}{V} = f\,(Fr_1) \qquad (4.1)$$

the mean bubble diameter d_b is relatively constant (HAINDL)

$$\therefore \quad \frac{A}{V} = f_1 (Fr_1) \tag{4.2}$$

K_L is assumed to be a function of the energy loss ΔE which from Equation 3.5 can be re-expressed:

$$\Delta E = \frac{y_1}{16}\left(\frac{-3 + \sqrt{1 + 8\ Fr_1^2}}{-1 + \sqrt{1 + 8\ Fr_1^2}}\right)^3 \tag{4.3}$$

$$\therefore \quad K_L = f_2 (\Delta E) = f_3(y_1, Fr_1) \tag{4.4}$$

An estimate can be made of the contact time, t. An approximate model of the variation in mean velocity through the hydraulic jump is shown in Figure 4.2. L_r represents the length of the roller zone of the hydraulic jump whilst L_j represents the length of the aerated zone which will extend beyond the roller zone. It is shown in Section 5.3.2 that

$$L_r = k_r y_2 \quad \text{and} \quad L_j = k_j y_2 \tag{4.5}$$

where k_r and k_j are relatively constant irrespective of Froude number.

The time of contact will be given by:

$$t = \frac{2L_r}{v_1+v_2} + \frac{L_j - L_r}{v_2} \tag{4.6}$$

$$= \frac{2L_r}{\frac{q}{y_1} + \frac{2q}{y_1}(-1 + \sqrt{1+8Fr_1^2})} + \frac{L_j - L_r}{\frac{2q}{y_1}(-1 + \sqrt{1+8Fr_1^2})} \tag{4.7}$$

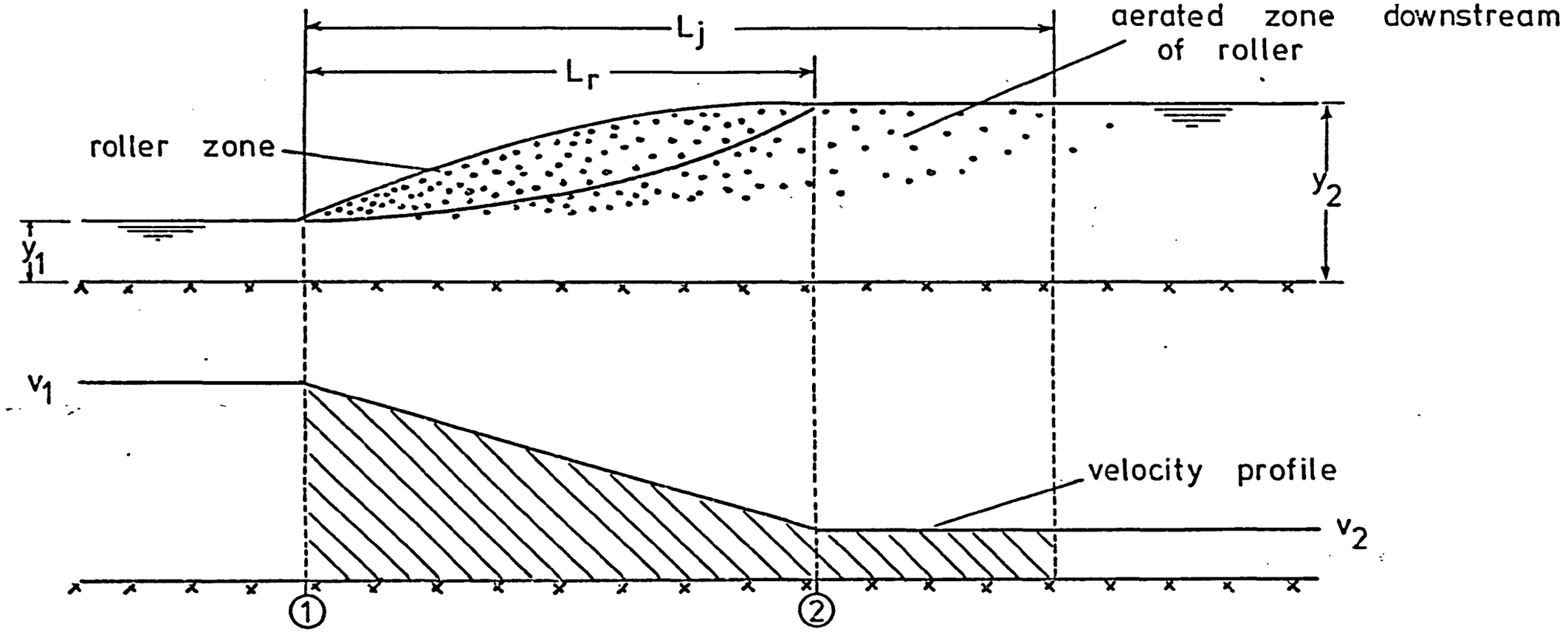

figure 4.2 an approximate velocity profile through the hydraulic jump

$$= \frac{y_1}{q}\left[\frac{2k_r y_2}{1 + 2(-1 + \sqrt{1+8Fr_1^2})} + \frac{(k_j - k_r)\, y_2}{2(-1 + \sqrt{1+8Fr_1^2})}\right] \quad (4.8)$$

$$= \frac{y_1^2}{q}\left[\frac{k_r(-1 + \sqrt{1+8Fr_1^2})}{1 + 2(-1 + \sqrt{1+8Fr_1^2})} + \frac{(k_j-k_r)(-1 + \sqrt{1+8Fr_1^2})}{4(-1 + \sqrt{1+8Fr_1^2})}\right] \quad (4.9)$$

$$= \frac{\sqrt{y_1}}{Fr_1\sqrt{g}}\left[\frac{k_r(-1 + \sqrt{1+8Fr_1^2})}{1 + 2(-1 + \sqrt{1+8Fr_1^2})} + \frac{(k_j-k_r)(-1 + \sqrt{1+8Fr_1^2})}{4\,(-1 + \sqrt{1 + 8Fr_1^2}}\right] \quad (4.10)$$

$$\text{i.e. } t = f_4\,(\sqrt{y_1}\,,\, Fr_1) \quad (4.11)$$

For constant Froude number, the time of contact varies as the square root of the scale. It is clear from Equations 4.2, 4.4 and 4.11 that

$$r = f_5(y_1\,,\, Fr_1), \quad (4.12)$$

i.e. for a constant Froude number, an increase in discharge which results in an increase in energy loss and time of contact will therefore result in an increase in the oxygen transfer according to some function of the length scale y_1.

4.5 ADJUSTMENT FOR TEMPERATURE VARIATIONS

The influence of temperature on oxygen transfer in water was discussed in Section 1.10 and the influence of the degree of mixing was illustrated in Figure 1.6. The experiments of GAMESON, VANDYKE and OGDEN at an experimental weir clearly indicated an increase in the deficit ratio with increase in temperature whereas IMHOFF & ALBRECHT

suggested, for a prototype weir they studied, that the deficit ratio was independent of temperature. If this latter observation was in fact true, then it would jeopardise the validity of modelling an oxygen transfer situation since the modes of transfer would be different in both situations. In the model the diffusion transfer processes are apparent, whereas in the prototype the effect of these is suggested by IMHOFF & ALBRECHT to be absent.

The inconsistency between the results of GAMESON, VANDYKE, OGDEN and IMHOFF & ALBRECHT is highlighted if the energy expended in the former's experiments is compared with that cited by IMHOFF & ALBRECHT for their prototype weir; (see Table 4.1 below).

TABLE 4.1

Energy Expenditure at Two Weir Systems

SOURCE	POOL DIMENSIONS (m)			HEIGHT OF FALL (m)	ENERGY EXPENDITURE watt/m^3
	Length	Width	Depth		
GAMESON, VANDYKE & OGDEN (1958)	0.3	0.3	0.089	3.28	7316
				1.49	3323
				0.61	1360
IMHOFF, ALBRECHT (1972)	Spillenburg weir (Ruhr River)				1200

The energy available was computed from the expression: (MKS units)

$$\frac{\rho\, Q\, g\, h}{1000} \text{ Kw} \qquad (4.13)$$

and the energy expenditure (watt/m^3) quoted by IMHOFF/ALBRECHT was assumed to refer to the energy being expended per unit volume of the stilling pool.

Clearly, the energy expended in the model stilling pool exceeds that quoted by IMHOFF/ALBRECHT for their prototype. Therefore if the latter's observations were correct, then the oxygen transfer dependence on temperature in the model should have been described by curve C in Figure 1.6.

The model tests were carefully controlled, whilst during the measurements of IMHOFF & ALBRECHT the discharge varied between 12 and 28 m^3/s (ALBRECHT, 1968) and therefore the height of fall also varied. The measurements of IMHOFF/ALBRECHT have been recalculated in terms of deficit ratio and plotted in Figure 4.3 along with the model tests of GAMESON & co-workers for three heights of fall and a constant discharge. The scatter displayed by the data of IMHOFF/ALBRECHT is remarkable and not surprising in view of the discharge range of their tests. The original presentation of results by IMHOFF & ALBRECHT has been reproduced in Figure 4.4 along with the data of GAMESON & co-workers for one height of fall (1.49m). The oxygen transfer as a percentage of the initial oxygen level is plotted against the initial oxygen level as a percentage of saturation. Temperature has been marked alongside each point. It is easy to see how IMHOFF & ALBRECHT came to their conclusion from this plot and also to see that for the same temperature range ($13-26^{\circ}$) a similar conclusion might have been drawn from the data of GAMESON, VANDYKE and OGDEN.

It is felt therefore, that IMHOFF & ALBRECHT's recommendation on the influence of temperature in highly turbulent systems (> 20 watt/m^3) is not substantiated and that the measure of oxygen transfer used to present their data was particularly insensitive to changes in oxygen transfer especially when small initial oxygen deficits existed.

Successful modelling of oxygen transfer systems is anticipated and the temperature correction of GAMESON, VANDYKE & OGDEN will apply

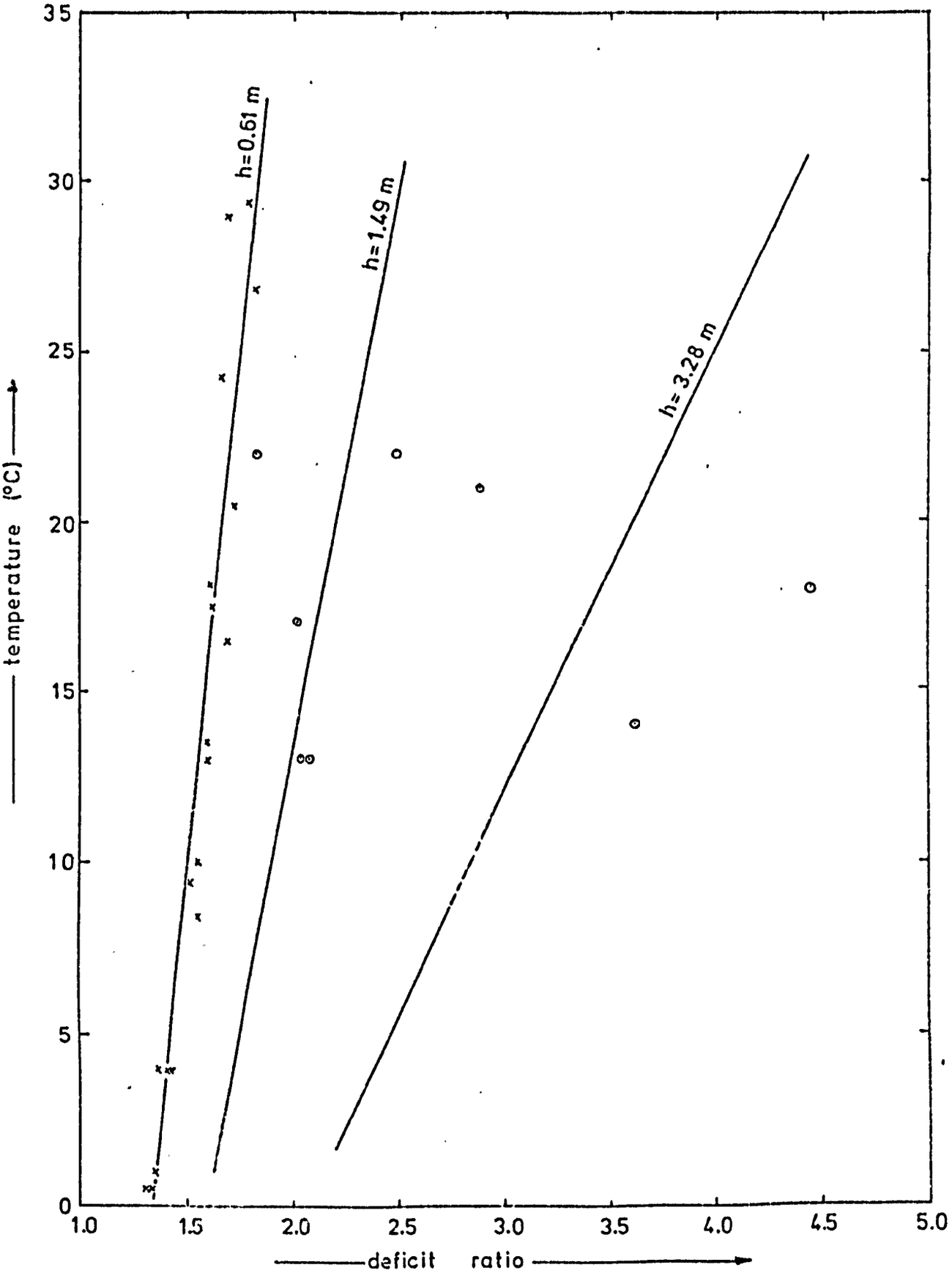

figure 4.3 the effect of temperature on deficit ratio at two weir systems

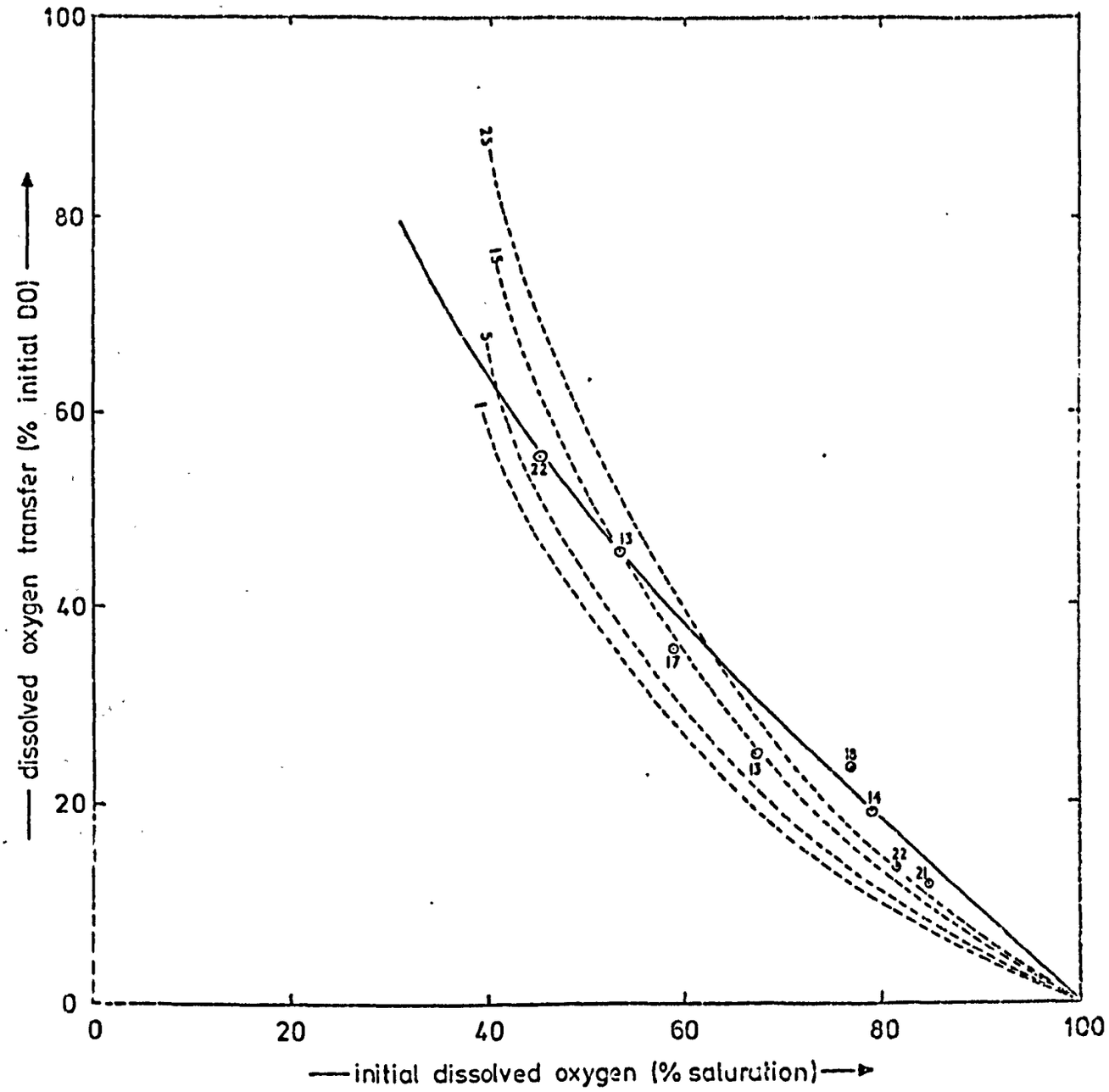

—c— IMHOFF & ALBRECHT (Spillenburg weir, temperatures [°C] indicated beside each point)

---------- GAMESON, VANDYKE & OGDEN (Experimental weir, h=1.49 m, temperature [°C] shown on each curve)

figure 4.4 relative DO transfer v initial DO for various temperatures at two weir systems

broadly to a variety of model and prototype situations.

The application of the temperature correction of GAMESON & co-workers to the current hydraulic jump experiments is justified by the comparable energy expenditure demonstrated in Table 4.2 over most of the range of the tests.

The volume of tailwater has been taken as the volume of the roller region, i.e. between sections (1) and (2) in Figure 4.2. The length of the roller is taken as $6y_2$ (PETERKA) and a linear variation in depth between sections (1) and (2) is assumed. This volume is the volume of air and water, therefore the energy expenditure per unit volume of water will be higher than that shown in Table 4.2.

Whilst the energy expenditure per cubic metre for the low values of Froude number is smaller than the lowest value for the tests of GAMESON & Co-workers (Table 4.1), significant errors in temperature correction are not anticipated.

TABLE 4.2

Energy Expenditure During Hydraulic Jump Tests

Q (1/s)	y_1 (cm)	y_2 (cm)	Fr_1	ΔE (cm)	Energy Expenditure (w/m^3)
1.45	0.64	7.85	9.0	18.5	1316
	0.94	6.3	5.1	6.5	676
3.46	1.35	12.78	7.0	21.6	1353
	2.39	8.98	3.0	3.3	366
6.75	2.61	17.6	5.1	18.3	1136

4.6 THE EFFECT OF DISCHARGE ON OXYGEN TRANSFER-RESULTS

Oxygen transfer has been expressed as the deficit ratio (Equation 1.35) and the temperature correction equation of GAMESON, VANDYKE & OGDEN (Equation 2.13) was used to correct deficit ratios to a standard value at 15°C.

The deficit ratio results have been presented in Figure 4.5 against the dimensionless ratio $\Delta E/y_1$. The separate relationship for each discharge is consistent with comments made in Section 4.4.

$$\text{i.e.} \quad \frac{\Delta E}{y_1} = f\,(Fr_1) \quad \text{whereas} \quad r = f(y_1, Fr_1) \tag{4.14}$$

Similar comments apply to Figure 4.6, the relationship between deficit ratio and supercritical Froude number. It is apparent from both these graphs that the deficit ratio is independent of the initial oxygen deficit as would be expected from the law of ADENEY and BECKER (1919). From Figures 4.7 and 4.8:

$$r_{15} - 1 = k_1 \left(\frac{\Delta E}{y_1}\right)^{0.8} \tag{4.15}$$

$$\text{and} \quad r_{15} - 1 = k_2 \,(Fr_1)^{2.1} \tag{4.16}$$

and k_1 and k_2 are functions of q.

To test the variation of r-1 with scale for constant Froude number, the scale ratio has been expressed as a specific discharge ratio q/345 and plotted against k_1 and k_2 from Equations 4.15, 4.16. ($q = 345\ cm^2/s$ was chosen for comparison since the largest quantity of data was available at this discharge.) See Figure 4.9. It is now possible to express the results by the following two equations:

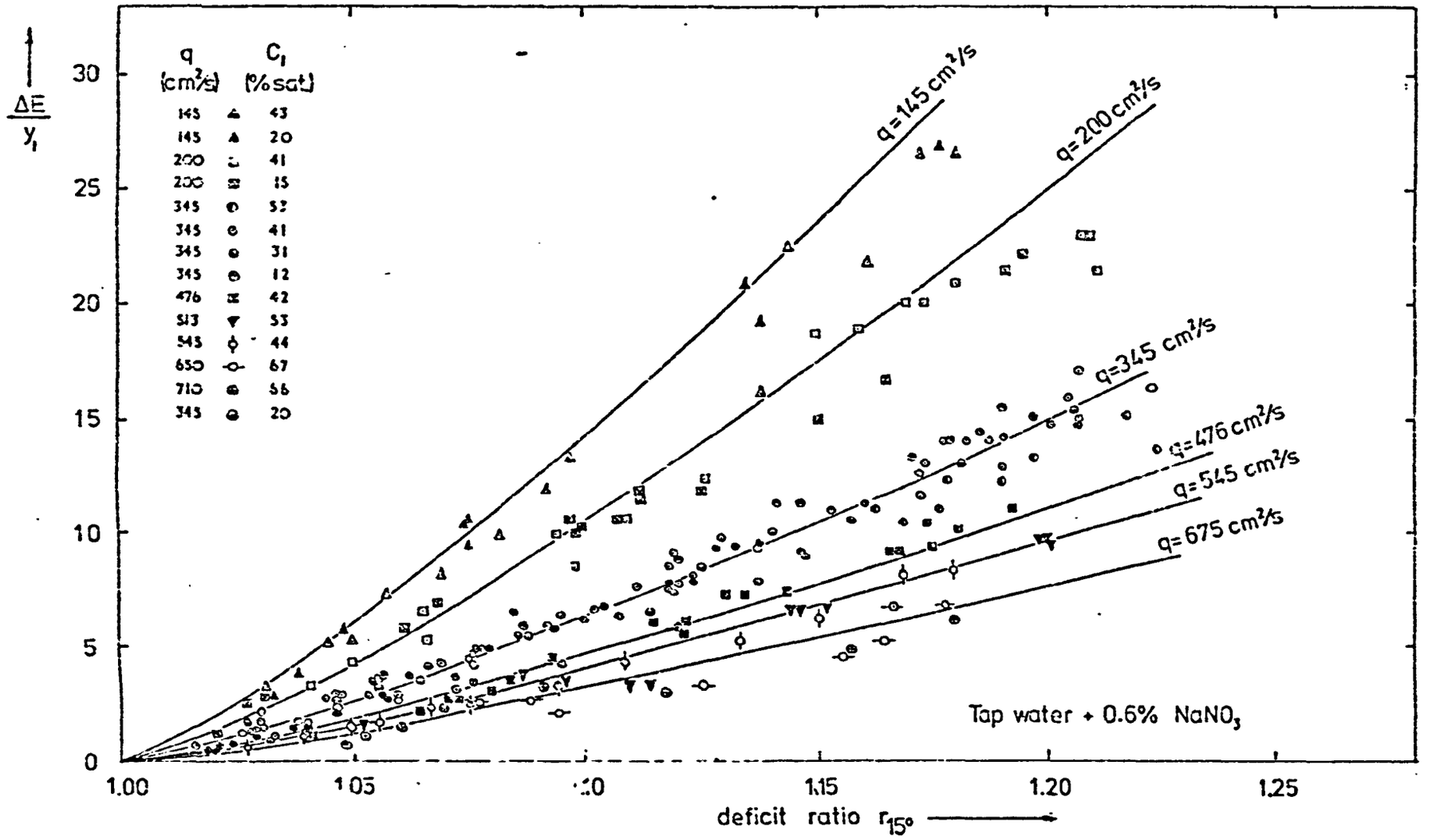

figure 4.5 $\Delta E/y_1$ v deficit ratio for various discharges

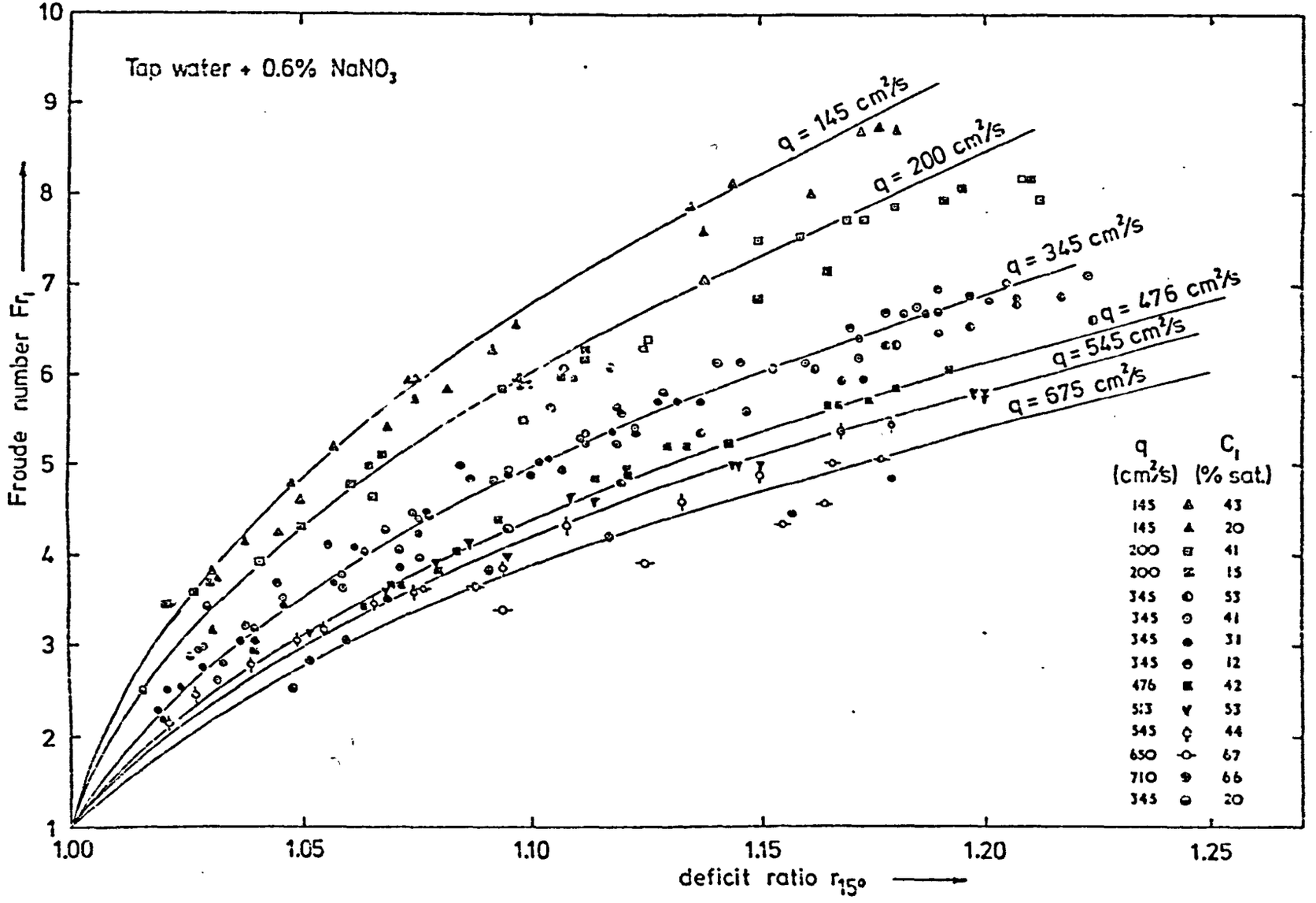

figure 4.6 deficit ratio v Froude No. for various discharges

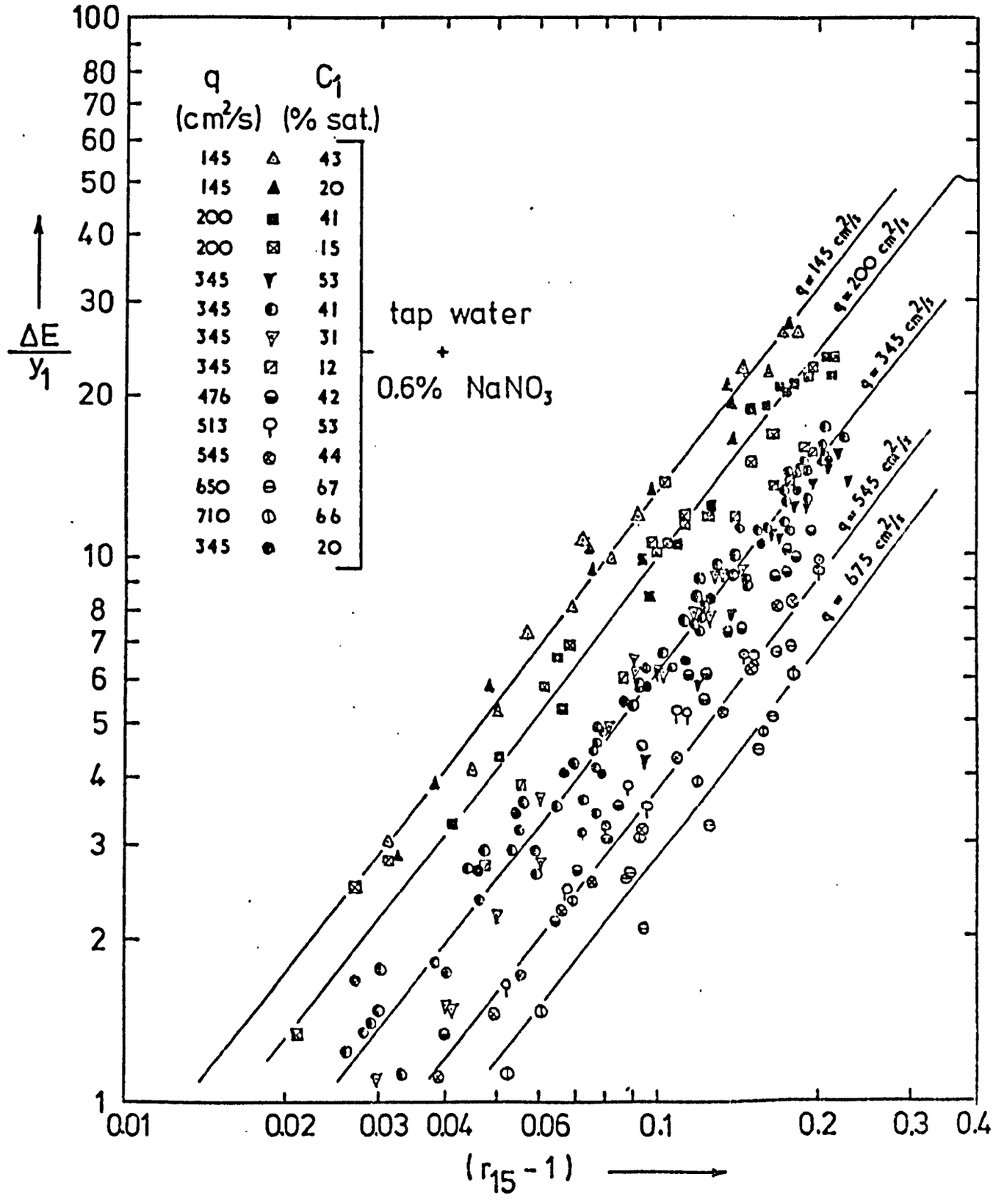

figure 4.7 $(\Delta E/y_1)$ v $(r_{15}-1)$ for various discharges

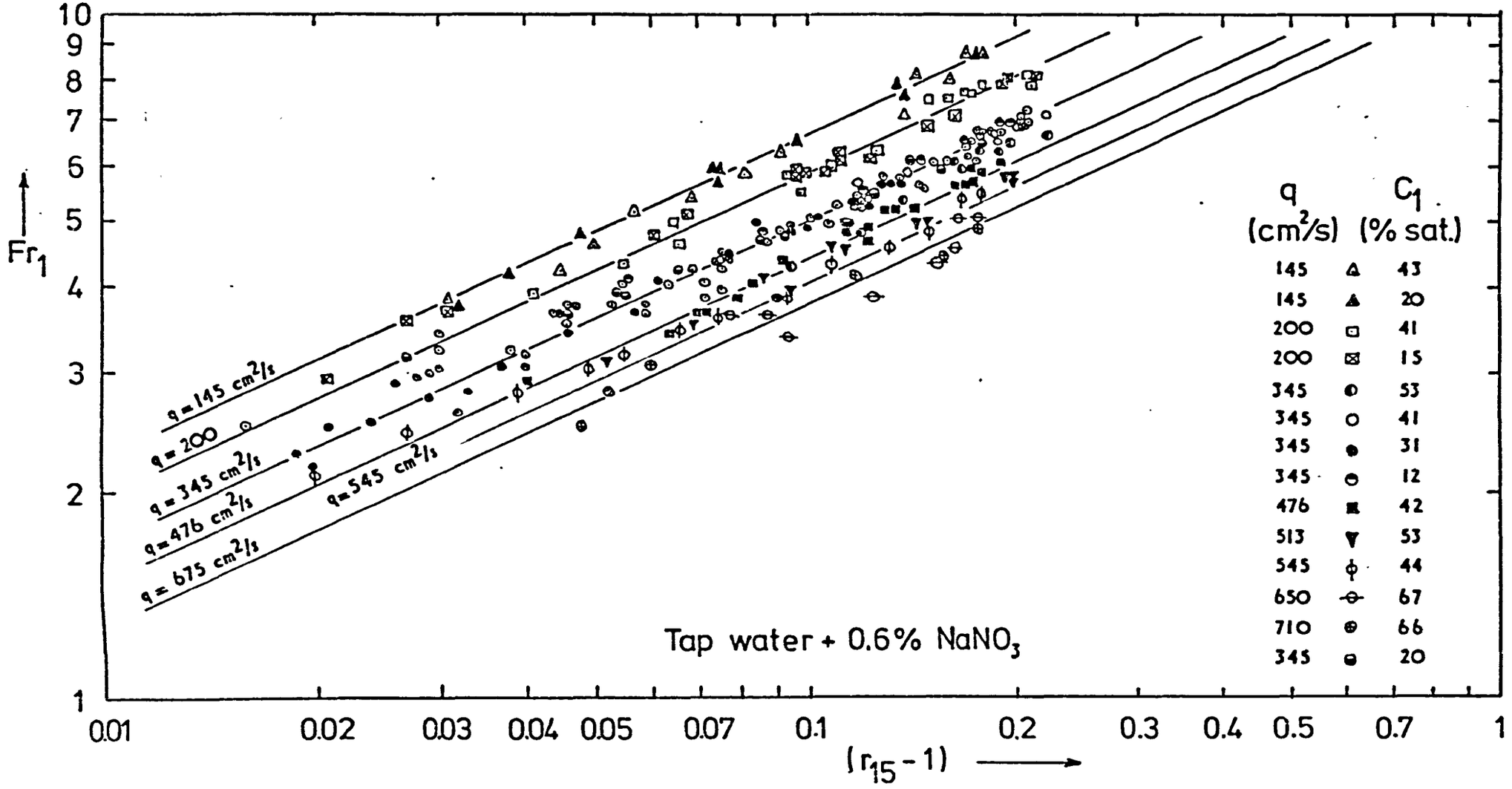

figure 4.8 Fr_1 v $r_{15}-1$ for various discharges

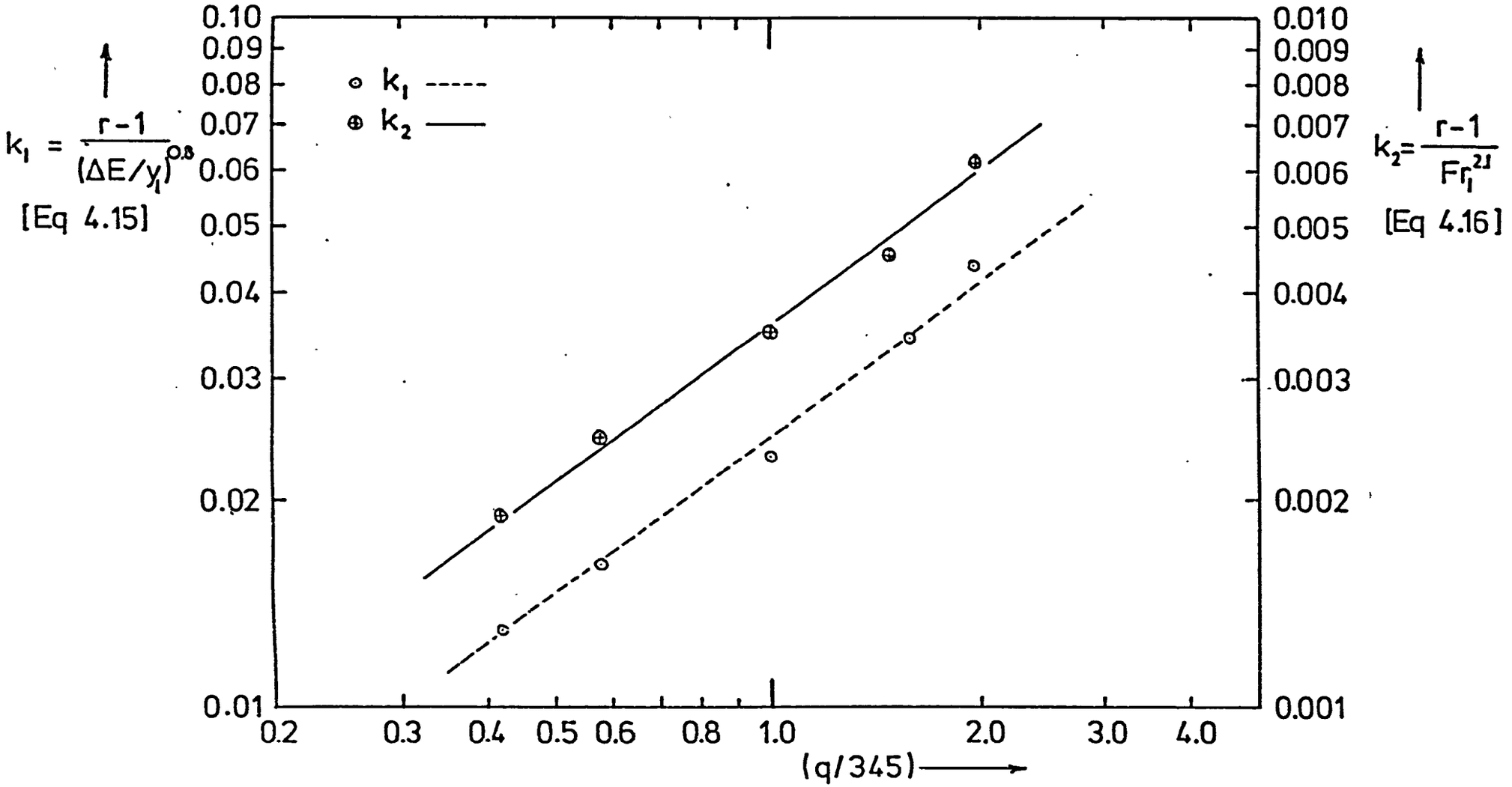

figure 4.9 k_1 & k_2 (Eq 4.15 & 4.16) v q/345 .

$$r_{15} - 1 = 0.023 \left(\frac{\Delta E}{y_1}\right)^{0.8} \left(\frac{q}{345}\right)^{0.75} \quad (q \text{ cm}^2/\text{s}) \tag{4.17}$$

$$r_{15} - 1 = 0.0035 \, (Fr_1)^{2.1} \left(\frac{q}{345}\right)^{0.75} \quad (q \text{ cm}^2/\text{s}) \tag{4.18}$$

Now

$$q = v_1 y_1 = Fr_1 y_1 \sqrt{g y_1} \tag{4.19}$$

Equation 4.18 can therefore be re-expressed:

$$r_{15} - 1 = 0.000044 \, g^{0.375} \, Fr_1^{2.85} \, y_1^{1.125} \tag{4.20}$$

(y_1 in cm, g in cm/sec^2)

which confirms the theoretically derived supposition, Equation 4.12, that r is a function of Fr_1 and y_1.

The energy loss ΔE is also a function of Fr_1 and y_1 and this has been plotted against deficit ratio in Figure 4.10 leading to the relationship:

$$r_{15} = 1 + 0.01 \, \Delta E \quad (\Delta E \text{ cm})$$

or (4.21)

$$r_{15} = 1 + \Delta E \quad (\Delta E \text{ m})$$

The relationship between ΔE, y_1 and Fr_1 is given by Equation 4.3 but in this form it is not easily utilised. From Figure 4.11, derived from Equation 4.3, the following equation is approximately valid for the limits shown:

$$\frac{\Delta E}{y_1} = 0.098 \, Fr_1^{2.6} \quad 10 \geqslant Fr_1 \geqslant 4 \tag{4.22}$$

figure 4.10 energy loss v deficit ratio for various discharges.

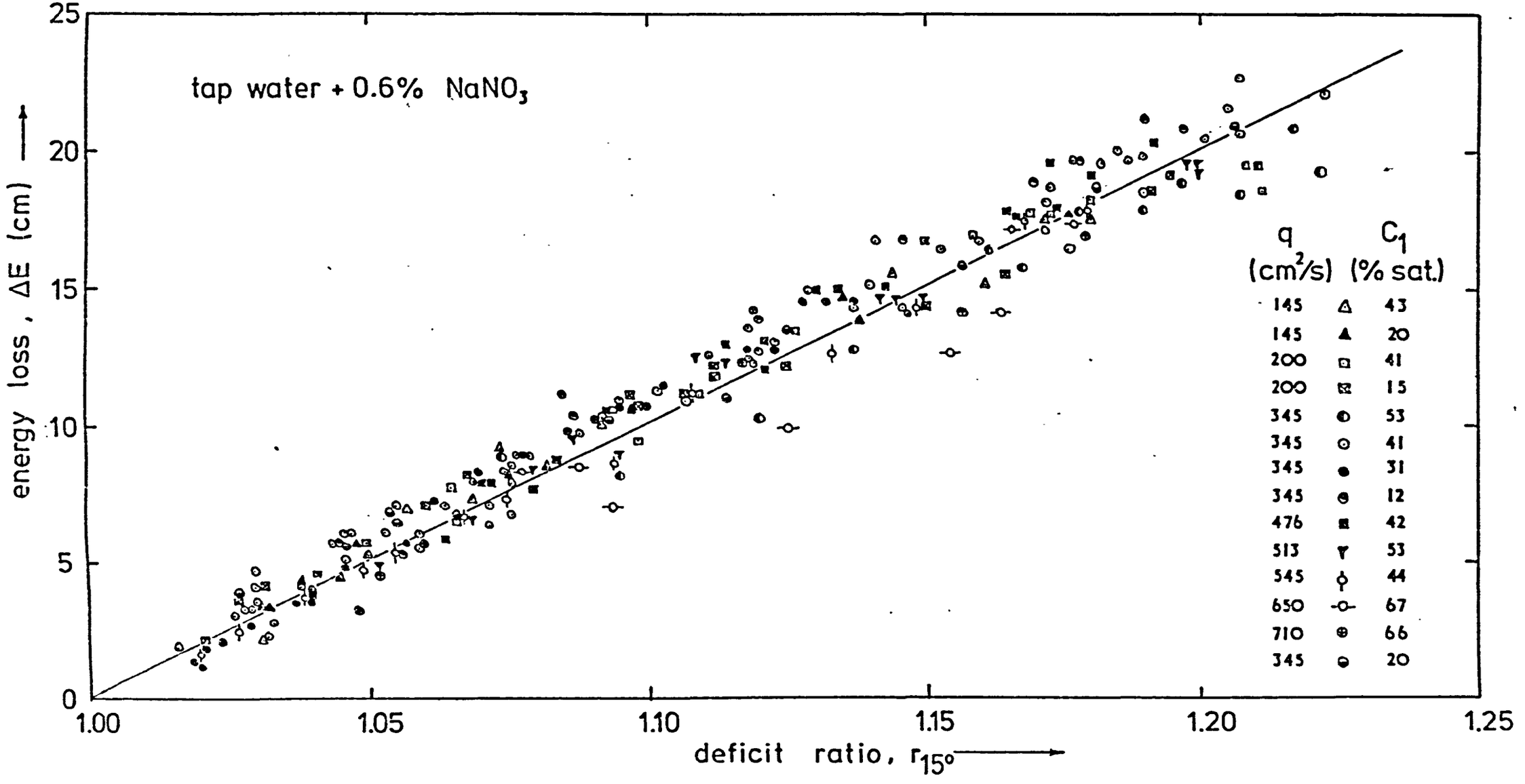

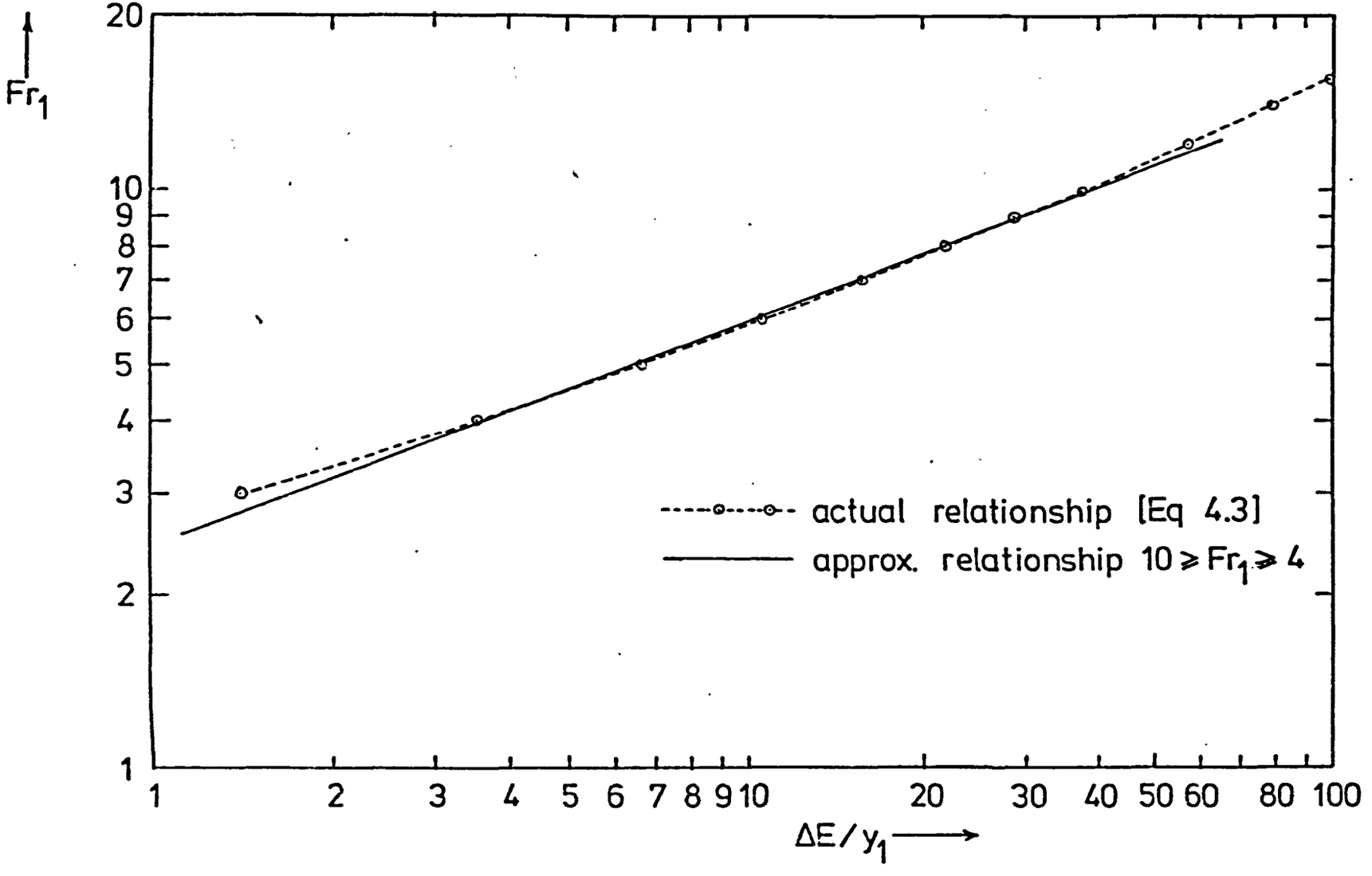

figure 4.11 relationship between Froude No. and $\Delta E/y_1$

This relationship could equally well be derived from Equations 4.17 and 4.18.

Substituting Equation 4.22 into 4.21:

$$r_{15} = 1 + 0.00098\ y_1\ Fr_1^{2.6} \qquad (4.23)$$

which is very similar to Equation 4.20. In view of the small range of ΔE tested, the use of Equation 4.21 is not recommended, either of the two non dimensional expressions, Equations 4.17 and 4.18, being preferable.

4.7 THE EFFECT OF DISSOLVED SALTS

4.7.1 Further Experiments

The experiments reported so far were carried out using the laboratory water which contained approximately 0.6% of sodium nitrite for reasons discussed in Section 4.3.

Two further sets of tests were conducted (a) for laboratory water containing 0.3% $NaNO_3$ and (b) for tap water piped directly from the mains water supply. The range of discharges for (a) was similar to those already presented in Figure 4.5 while for (b) only two discharges were possible, 1.45 and 2.00 l/s.

The experiments were conducted similarly to those already reported except that the tap water was not permitted to enter the laboratory sump. This was necessary to avoid dilution of the laboratory water containing sodium nitrite, therefore the tap water was intercepted at outlet from the flume and pumped directly to the sewers.

4.7.2 Results

The presence of dissolved salts in water is seen in Figure 4.12 to enhance the aeration achieved. The ratio $\Delta E/y_1$, is plotted against deficit ratio for three discharges, 145, 345 and 675 cm^2/s. The curves corresponding to water containing 0.6% sodium nitrite have been reproduced from Figure 4.5. The data in Figure 4.12 have been replotted, together with some additional data, in Figure 4.13. All these results for tap water and water containing 0.3% sodium nitrite have also been plotted against Froude number in Figure 4.14.

A comparison of Figures 4.7 and 4.13, also 4.8 and 4.14, indicates a similar dependence on hydraulic characteristics as indicated previously by Equations 4.17 and 4.18 except that the constants in these latter equations become functions of dissolved salt level. Similar conclusions may be drawn from Figure 4.15 - a plot of deficit ratio against energy loss.

From Figures 4.13, 4.14 and 4.15:

$$r_{15} - 1 = k_{J1} \left(\frac{\Delta E}{y_1}\right)^{0.8} \left(\frac{q}{345}\right)^{0.75} \quad (q \text{ cm}^2/\text{s}) \qquad (4.24)$$

$$r_{15} - 1 = k_{J2} \, Fr_1^{2.1} \left(\frac{q}{345}\right)^{0.75} \quad (q \text{ cm}^2/\text{s}) \qquad (4.25)$$

$$r_{15} - 1 = k_{J3} \cdot \Delta E \quad (\Delta E \text{ m}) \qquad (4.26)$$

with k_{J1}, k_{J2}, k_{J3} constants which varied with dissolved salt level as shown in Table 4.3.

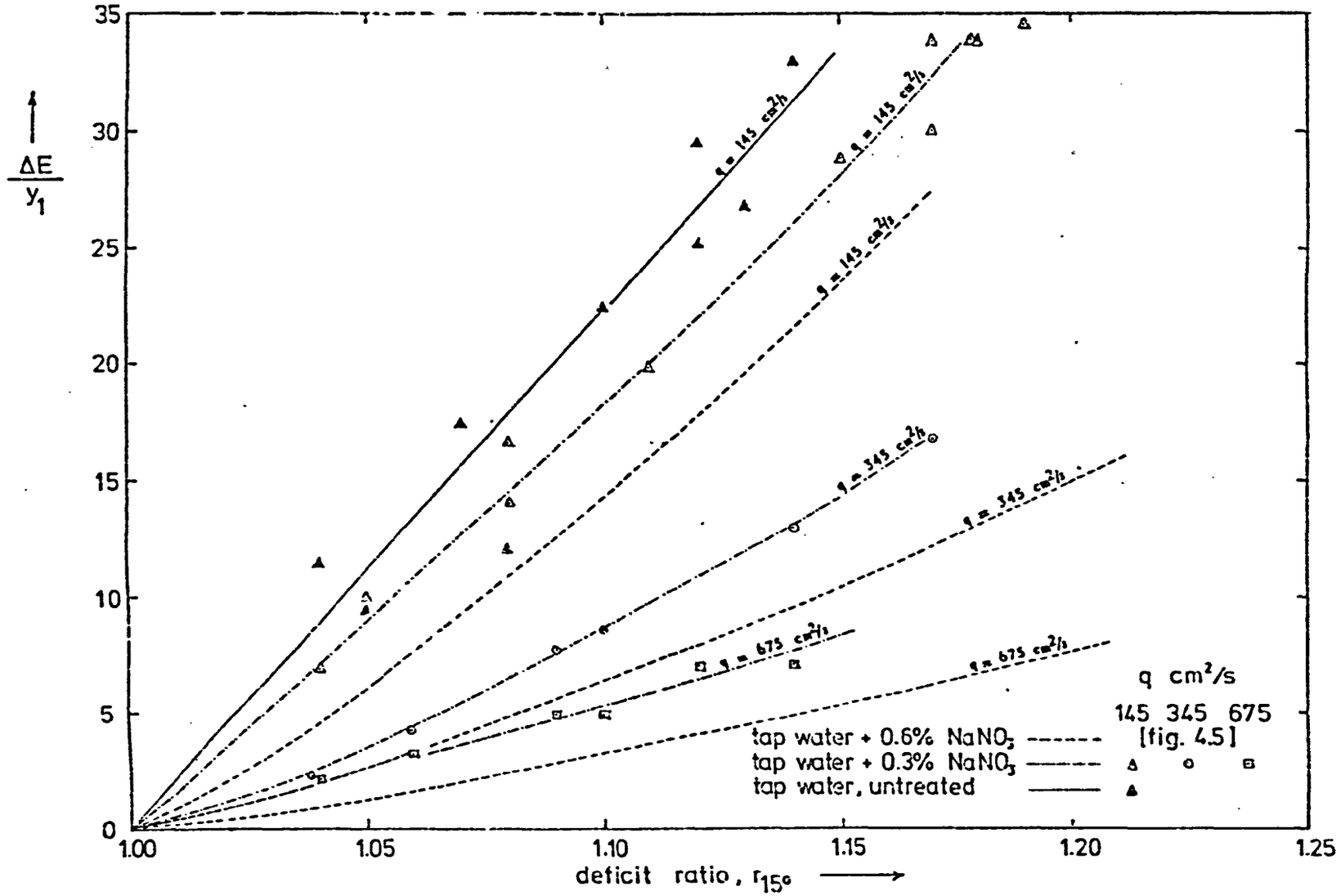

figure 4.12 $\Delta E/y_1$ v deficit ratio for various discharges - the effect of dissolved salts on the oxygen transfer.

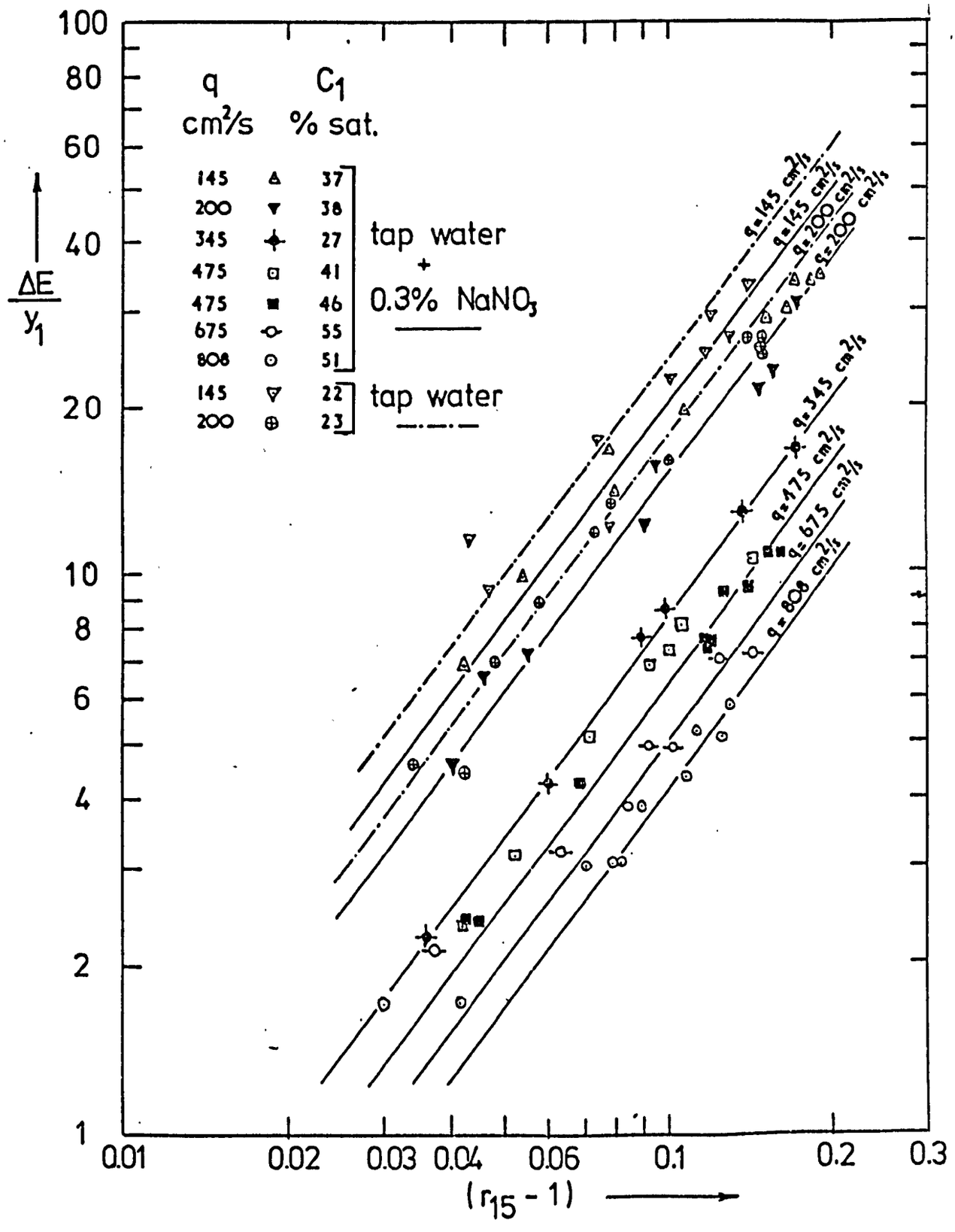

figure 4.13 $\Delta E/y_1$ v $r_{15}-1$ - additional tests

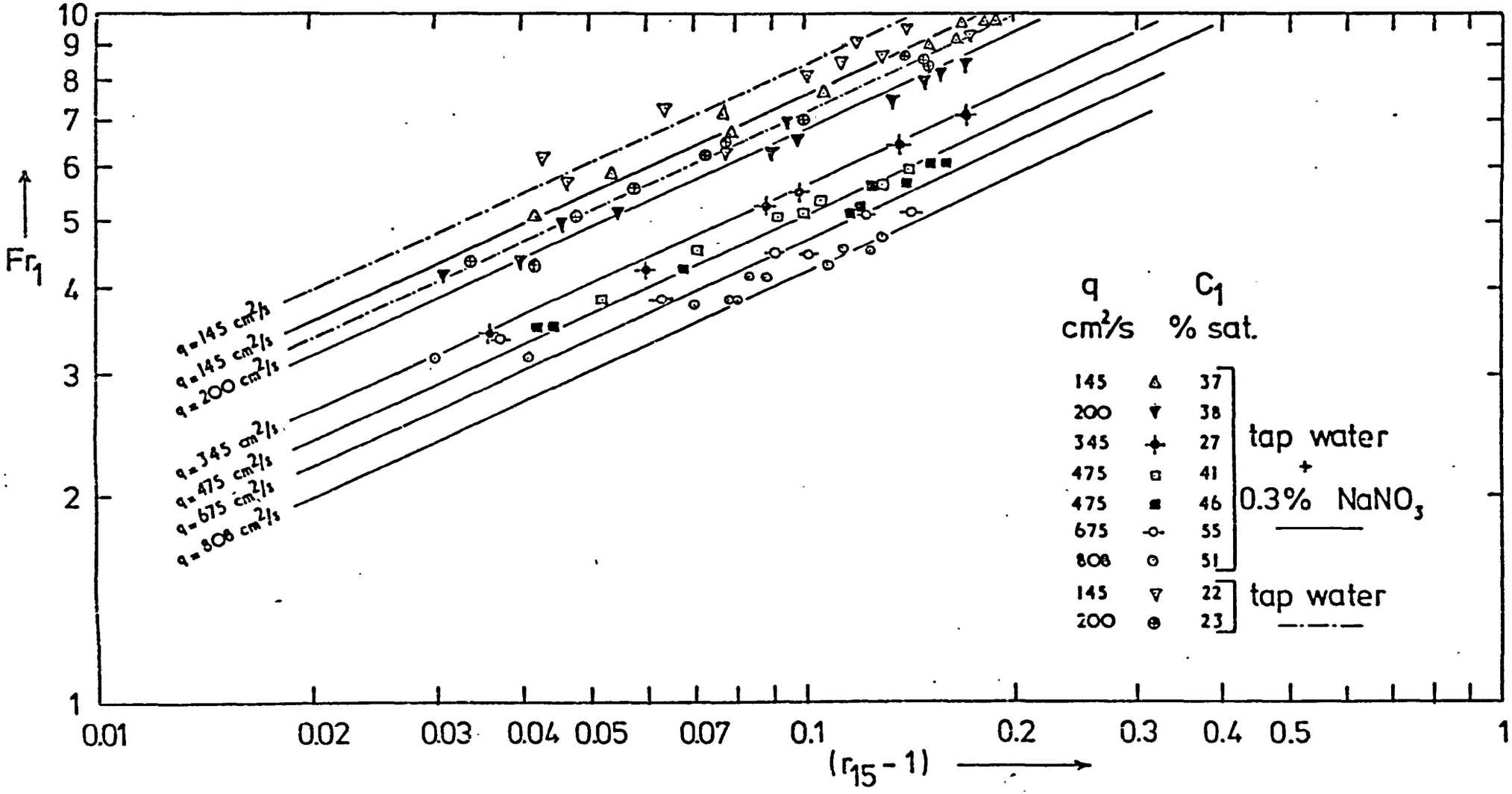

figure 4.14 Fr_1 v $[r_{15}-1]$ - additional tests

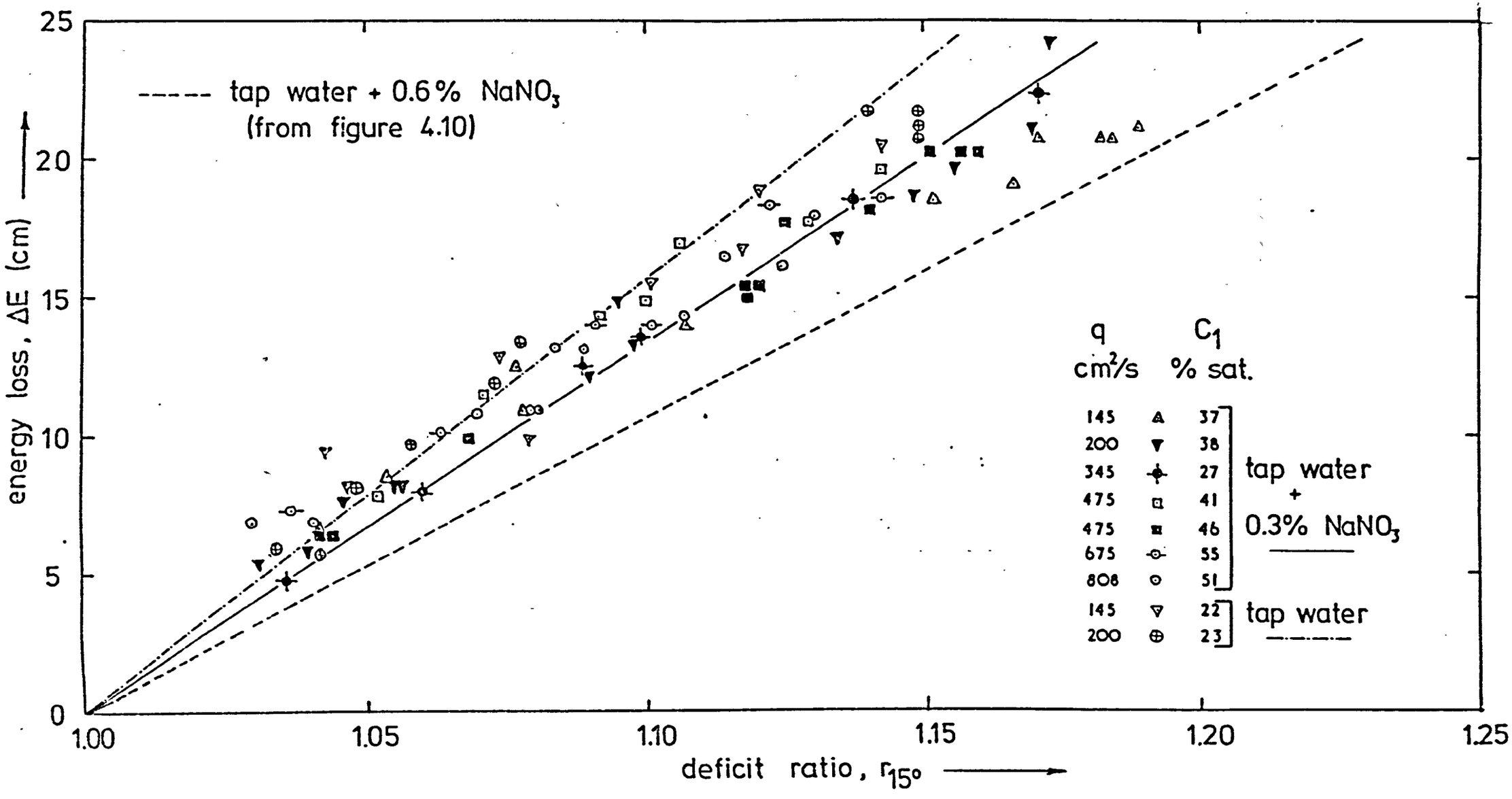

figure 4.15 energy loss v deficit ratio for various discharges - the effect of dissolved salts on the oxygen transfer.

TABLE 4.3

Variation of the Constants k_{J1}, k_{J2} and k_{J3} with Dissolved Sodium Nitrite Concentration

Sodium Nitrite Concentration %	k_{J1} (Eq. 4.24)	k_{J2} Eq. 4.25)	k_{J3} (Eq. 4.26)
0	0.0158	0.00230	0.0064
0.3	0.0186	0.00285	0.0075
0.6	0.0230	0.00355	0.0100

The variation of the constants with sodium nitrite concentration is shown to be approximately linear in Figure 4.16 within the range tested. Extrapolation beyond the limits tested is not recommended for reasons discussed in Section 4.7.4.

The correlation of all the data with Equations 4.24 and 4.25 is demonstrated in Figures 4.17 and 4.18. The results are therefore expressed by Equations 4.24, 4.25 and 4.26 with constants appropriately chosen from Table 4.3 according to the concentration of sodium nitrite present.

4.7.3 An Explanation of the Observed Effect of Sodium Nitrite

The observed increases in aeration with increases in sodium nitrite concentration are at first surprising since it is well established that increases in salinity levels will lead to a decrease in the solubility of oxygen in water as shown by Equation 1.41. Furthermore, experiments by OGDEN, GIBBS and GAMESON (1959) on the surface aeration of water flowing in experimental channels showed that there

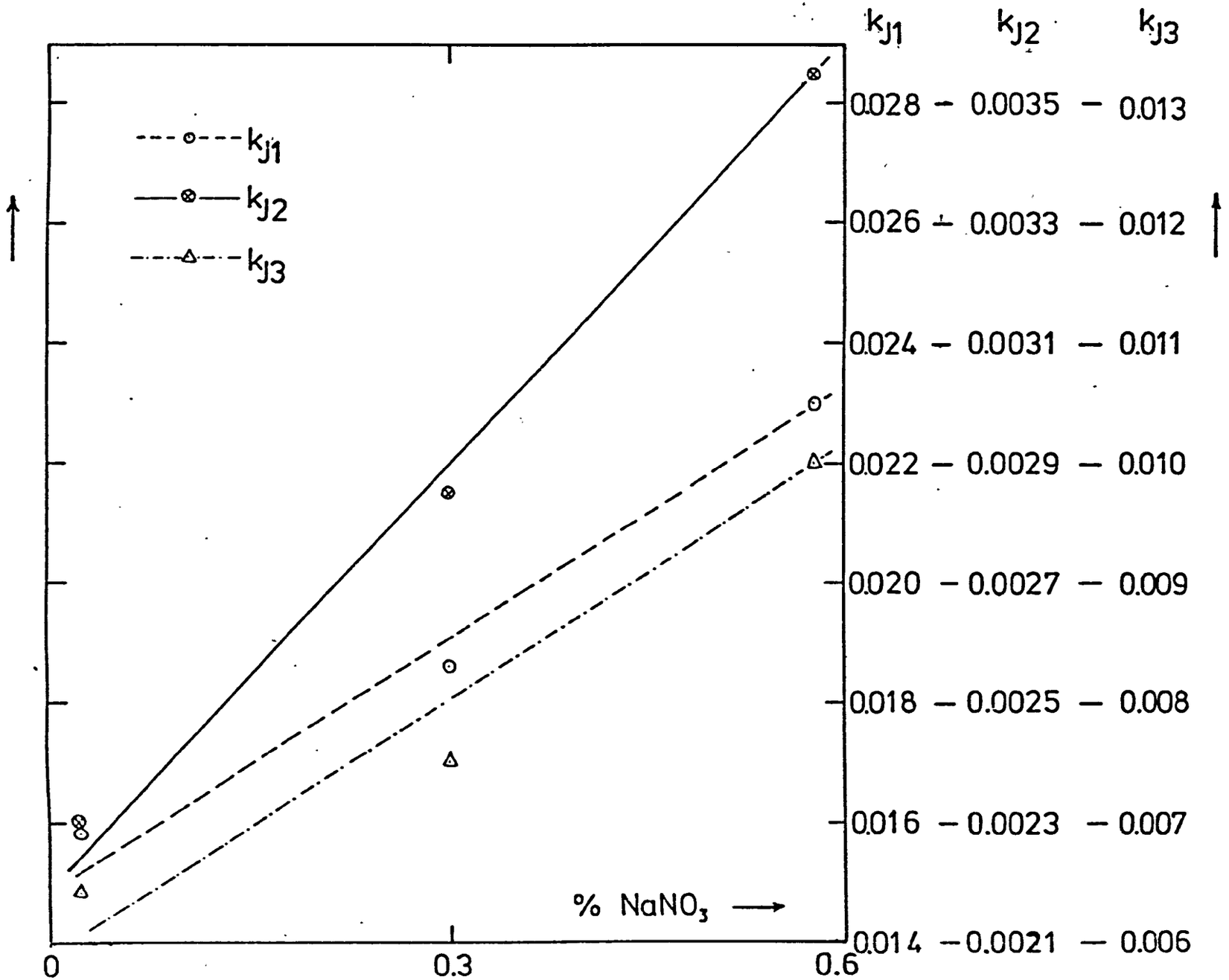

figure 4.16 k_{J1} , k_{J2} , k_{J3} ... (Eq 4.24, 4.25, 4.26) v concentration of sodium nitrite

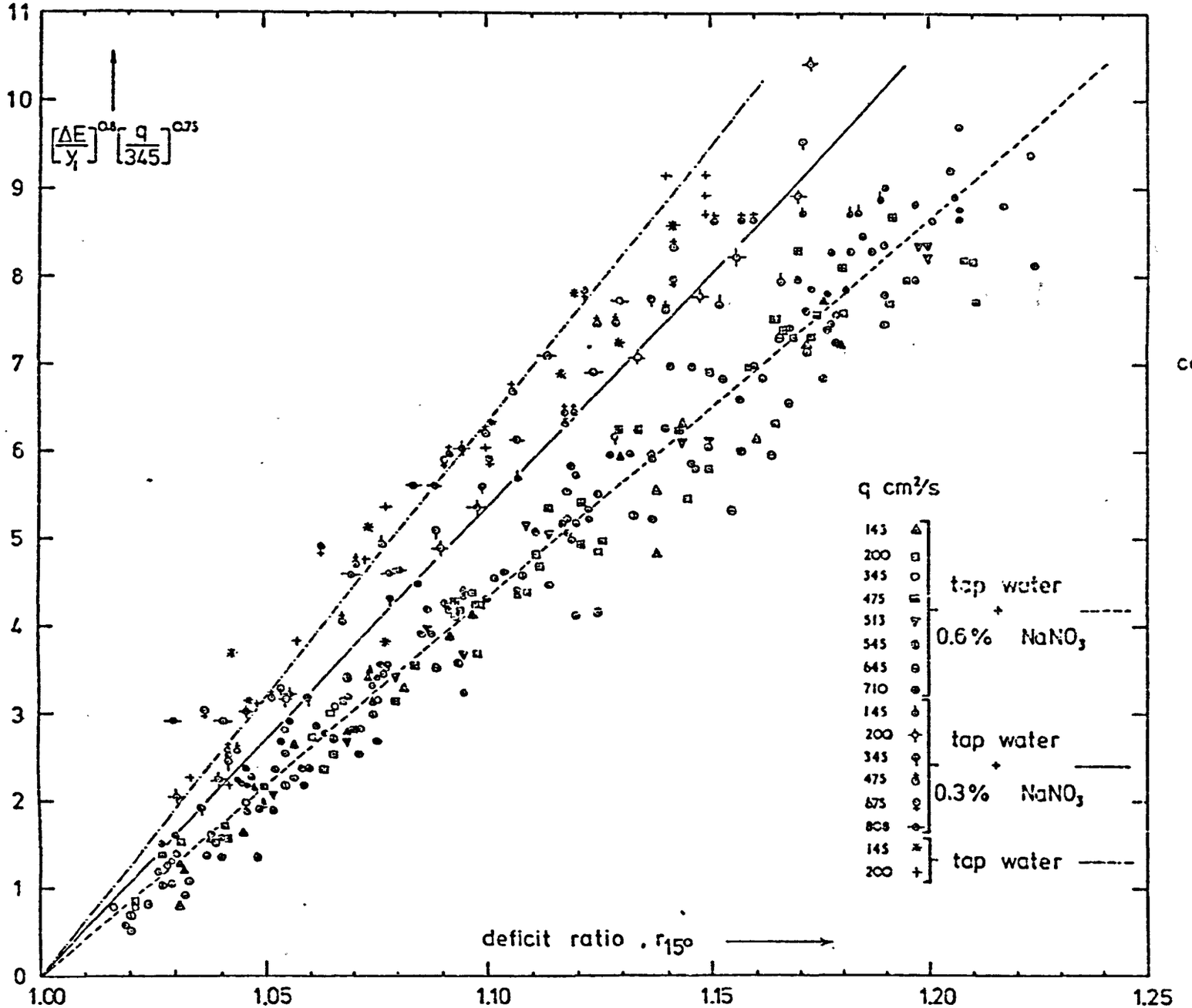

figure 4.17
correlation of data with
Eq. 4.24

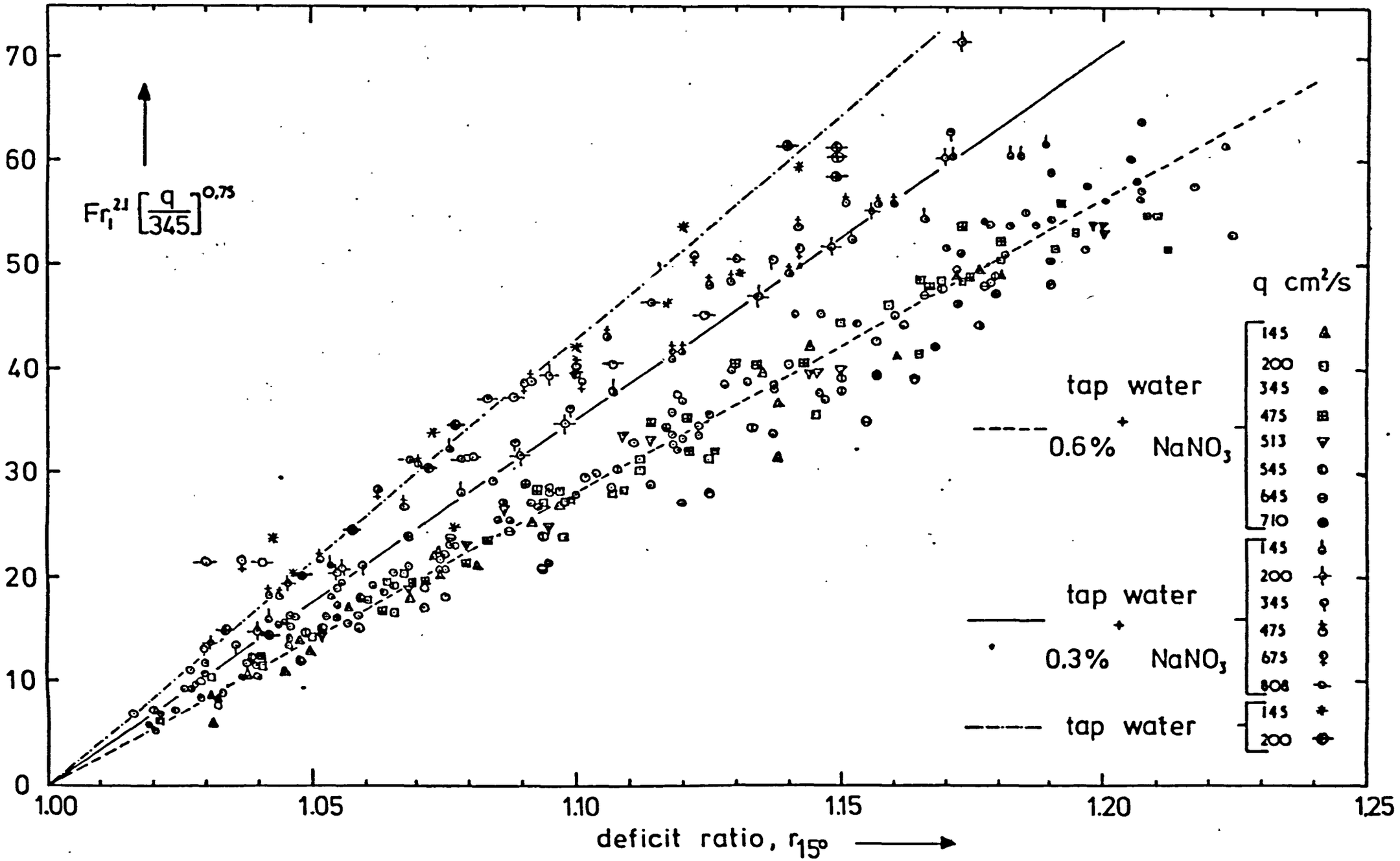

figure 4.18 correlation of data with Eq. 4.25

is a pronounced lowering of the rate of aeration in saline water. A linear relationship was found between the square root of the salinity and the percentage reduction in the aeration exchange coefficient. This reduction is of course consistent with the reduced gas solubility.

Conversely, DOWNING (1958) stated that under conditions of very high turbulence in combination with entrainment of air, the presence of dissolved salts can increase the mass transfer coefficient which agrees with the findings reported in this thesis. Unfortunately neither reasons nor experimental evidence were submitted to support this observation.

The presence of dissolved salts will naturally alter the density and viscosity of the fluid which in turn governs the coefficient of molecular diffusivity, but, these effects will be relatively small. In any case, the liquid film coefficient K_L is unlikely to be a major factor controlling the rate of gas transfer since the degree of turbulence or mixing will generally be high in an air entrainment situation.

The relative quantities of air entrained are unlikely to be affected by the salt content of the water since these are generally acknowledged to be governed by the supercritical Froude number only.

Referring to the general gas transfer equation, Equation 1.36, two possibilities remain, namely, the contact time and the surface area offered by the entrained air. The contact time is unlikely to be affected by the presence of dissolved salts since this is basically dependent on the velocity distribution through the jump, i.e. an hydraulic dependent characteristic. If constant volumes of air are entrained then the only parameter governing the entrained air/water interfacial area will be the mean diameter of air bubble entrained. The size of bubble entrained into hydraulic jumps is a matter which has received much attention (Chapter 5) but no effects due to the presence of dissolved

salts or other contaminants have been noted.

It is interesting at this stage to refer in detail to the work of VERSCHOOR (1950) in which the effect of lowering the liquid phase surface tension was investigated. SEELIGER (1949) found that if the surface tension of water was reduced by adding ethanol, and air was bubbled into the liquid, then the swarm of gas bubbles was found to be composed of very much smaller bubbles. VERSCHOOR noted however that bubbling air through separate volumes of water and methanol resulted in more or less equal bubble sizes in each case despite the fact that the surface tension of the methanol was approximately one third that of the water. The kinematic viscosity of the two liquids was approximately the same. However the reduction of the surface tension of water by the addition of Teepol did result in the formation of smaller bubbles, a similar observation to that by SEELIGER. More recently, ECKENFELDER and BARNHART (1961) observed a reduction in the mean size of bubbles produced by diffusers in the presence of surface active agents.

VERSCHOOR explained the contrasting effects resulting from reduced surface tension by recourse to the work of FOULK and MILLER (1931).

FOULK and MILLER discovered that in liquids containing dissolved matter, a resistance was present which prevented two bubbles from coalescing. This resistance was absent in the case of pure liquids. Furthermore, the presence of certain inorganic salts was observed to result in considerable foaming thus further indicating the presence of a coalescence inhibiting film on the bubbles. This film or resistance exists as a result of a difference between the dissolved salt concentration at the bubble/liquid interface and the concentration in the

main body of the liquid. This concentration difference has been experimentally demonstrated.

SCRIVEN and PIGFORD (1958) came to a similar conclusion from their experiments - the accumulation of contaminants on the liquid film surface was visualised as forming a rigid or semi-rigid surface structure which drastically impedes liquid flow close to the surface. HISE (1975) similarly referred to the concentration of surfactants at the bubble surface thus creating tangential shear stresses resulting from surface tension gradients which in turn are caused by surfactant concentration gradients around the bubble's surface.

HABERMAN and MORTON (1956) observed an increased drag on free rising bubbles (ranging in diameter from 0.6mm to 6mm) in the presence of surface active agents and a certain critical concentration of these surfactants was identified beyond which further concentration increases had no further effect on the bubble drag. HISE likened this critical concentration to a state at which the shear stress equals that of a solid wall and at which the liquid velocity at the bubble surface is effectively zero. Similarly, HOLROYD and PARKER (1949) demonstrated the production of smaller bubbles and reduced velocities in the presence of detergents.

The presence of the inhibiting films as a result of surfactants does of course reduce the liquid film coefficient, but, the production of smaller bubbles for a given air volume results in a significantly larger air/water interface and hence the increased overall transfer coefficient $K_L\frac{A}{V}$ observed by MANCY and OKUN (1960) and also by ECKENFELDER and BARNHART (1961). In an air entrainment situation accompanied by vigorous mixing, the disadvantages of the film formed on the surface of the bubbles become virtually non existent since this

film will be rapidly removed by the turbulent water anyway. The advantage of a reduced bubble rise velocity, i.e. increased contact time, together with the greater air/water interface offered results in a significant increase in the gas transfer as observed with the current experiments.

The relevance of the above reasoning to the results observed here with the hydraulic jump, was validated by the measurement of the size of bubble entrained by an hydraulic jump. These tests are reported in Section 5.2.4. It is clear from these measurements (Figure 5.2) that the mean bubble size was reduced by the presence of sodium nitrite, a reduction in the mean bubble diameter from 2.53mm to 1.57mm being noted from tap water to tap water with 0.6% added sodium nitrite. The tendency for the bubbles to coalesce in the absence of dissolved salts is well illustrated by comparison of Plates 5.1 and 5.2b.

4.7.4 Implications of the Observed Effect of Dissolved Salts

If the enhanced aeration recorded above in the presence of dissolved sodium nitrite could be taken as representative of the effect of dissolved inorganic salts in general then the implication with regard to saline waters is very significant. This is especially so since the maximum salinity of 6 parts per thousand in the above experiments is relatively small in comparison with sea water salinity levels which would be of the order of 30 parts per thousand.

Whilst Table 4.3 illustrates the variation in the constants in Equations 4.24, 4.25 and 4.26 with dissolved sodium nitrite over the range tested, extrapolation is inadvisable since there will be a critical salinity level beyond which there will be no further reduction in bubble size, i.e. the coalescence is fully prevented and the bubble

size will be governed solely by the size at inception. This critical salinity is in accordance with the observations HABERMAN and MORTON and others noted in Section 4.7.3. Furthermore any increases in salinity beyond this critical point may in fact result in a reduction in oxygen transfer due to the reduction in solubility.

4.8 A FURTHER TEST OF THE CORRELATION EQUATIONS

HOLLER (1971) measured the reaeration of a discharge of 33.9 l/s in a 38cm wide open channel.

Summarised in Table 4.4 are some of the data supplied by HOLLER for an initial oxygen deficit of 50%. Deficit ratios have been corrected to 15°C, and energy losses computed from Equation 3.3. The deficit ratios have been predicted from Equations 4.24, 4.25 and 4.26, assuming tap water was used, with constants appropriately selected from Table 4.3.

TABLE 4.4

Some Hydraulic Jump Measurements by HOLLER (private communication 26/11/74)

y_1 (cm)	y_2 (cm)	ΔE (cm) (Eq. 3.3)	Fr_1	DEFICIT RATIO r_{15}			
				Measured	Predicted		
					(Eq. 4.24)	(Eq. 4.25)	(Eq. 4.26)
3.14	19.38	23.74	6.12	1.223	1.162	1.21	1.152
3.38	17.37	20.05	4.58	1.117	1.134	1.114	1.128
3.42	16.79	6.95	3.06	1.056	1.057	1.049	1.044

The predictions are remarkably good, particularly with Equation 4.25. The assumption of tap water is therefore validated. Note: The different results given by Equations 4.24, 4.25 and 4.26 result from the fact that HOLLER's conjugate depth measurements do not satisfy the equation of Bélanger. This has already been demonstrated in Figure 3.5 and discussed in Section 3.7.

A wider range of validity of the prediction Equations 4.24 and 4.25 is therefore suggested with constants chosen appropriately according to Table 4.3. The further application of Equation 4.26 was discussed in Section 4.6.

4.9 RELATIONSHIP BETWEEN AIR UPTAKE AND OXYGEN TRANSFER

The ratio of air to water discharge is known to be dependent solely on the supercritical Froude number - Equations 2.1, 2.2, 2.3, whilst the oxygen transfer expressed as the deficit ratio was shown to be a function of Froude number, discharge and mean bubble size - Equation 4.25.

Equation 2.1 was expressed in terms of (Fr_1-1) simply because an hydraulic jump does not form if $Fr_1=1$. The ratio β could equally well have been expressed in terms of Fr_1 as follows:

$$\beta = \frac{Q_a}{Q} = 0.0037\ Fr_1^{1.57}, Fr_1 \geqslant 1 \qquad (4.27)$$

This form is as valid as the original, Equation 2.1.

From Equations 4.27 and 4.25:

$$r_{15} - 1 = k_{J2} \left(\frac{\beta}{0.0037}\right)^{1.34} \left(\frac{q}{345}\right)^{0.75} \qquad (4.28)$$

Equation 4.28 may be simplified:

$$r_{15} - 1 = 22.66\, k_{J2} \frac{q_a^{1.34}}{q^{0.59}} \qquad (4.29)$$

q_a being the air discharge per unit channel width (cm^2/s) and with q in cm^2/s.

Equation 4.29 shows the deficit ratio dependence on air discharge for the hydraulic jump studied assuming the air discharge ratio to be as given by the equation of KALINSKE and ROBERTSON, Equation 2.1.

4.10 SIMILARITY CONSIDERATIONS

In Section 4.4 it was suggested that for a constant Froude number, $\frac{A}{V}$ is constant and the time of contact varies as the square root of the scale.

$$\text{i.e. } M_t = M_L^{\frac{1}{2}} \quad (M_t = \frac{t_1}{t_2})\,(M_L = \frac{\ell_1}{\ell_2}) \qquad (4.30)$$

Also from Equation 4.24 or 4.25:

$$M_{r-1} = \frac{(r-1)_1}{(r-1)_2} = M_L^{9/8} \qquad (4.31)$$

The basic equation of gas transfer (Equation 1.35) states that

$$\frac{1}{r} = e^{-K_{LV}\frac{A}{V}t}$$

which when expanded into a series gives

$$r = 1 + \sum_1^n \frac{(K_{LV}\frac{A}{V}\, t)^n}{n!} \qquad (4.32)$$

i.e. $$r-1 = f\left(K_L \frac{A}{V} t\right) \simeq k\left(K_L \frac{A}{V} t\right) \qquad (4.33)$$

From Equations 4.30, 4.31 and 4.33:

$$M_{r-1} = M_{K_L} \cdot M_t = M_L^{9/8}$$

The scale of the liquid film coefficient is therefore $M_{K_L} \simeq M_L^{5/8}$ subject to confirmation that $M_t = M_L^{\frac{1}{2}}$. Whilst the scale of contact time for the hydraulic jump may be $M_L^{\frac{1}{2}}$, the scale of contact time in the aerated zone downstream of the jump may be bigger than indicated by the length scale since for an unchanged bubble size this zone may extend further beyond the bigger jump than indicated by the length scale. Possibly, therefore, $M_t > M_L^{\frac{1}{2}}$ and $M_{K_L} < M_L^{5/8}$.

The limit of validity of Equations 4.24 and 4.25 in terms of q remains to be seen, but, the contribution to oxygen transfer of the aerated zone downstream of the jump will be relatively small compared to the highly mixed roller regime.

Also, the supposition by WISNER that there is a lower limit ($Fr_1 > 8$) for satisfactory modelling of air entrainment in a prototype hydraulic jump situation (Section 2.4.3) remains to be similarly confirmed for the modelling of gas transfer. Also, for the very low Froude numbers tested here, the energy expenditure per unit volume was not very high (Table 4.2) and therefore the slower diffusion processes may have been more predominant in the model than in a prototype situation of the same Froude number. Again, this remains to be seen.

There will also be some upper limit beyond which the scale of the liquid film coefficient will tend to unity i.e. $M_{K_L} \simeq 1$. This follows,

since there will be some degree of mixing above which any increased mixing will not result in any change in the value of K_L (HIGBIE) and is therefore a waste of time.

4.11 SUMMARY

Some observations of temperature effects on gas transfer by IMHOFF and ALBRECHT have been discussed in relation to work by GAMESON, VANDYKE and OGDEN. The former worker's results were shown to be based on an insensitive measure of oxygen transfer and incompatible with the latter's results. The temperature correction of GAMESON, VANDYKE and OGDEN was considered to be applicable to a variety of model and prototype situations.

The oxygen transfer in an hydraulic jump was shown theoretically to be a function of the Froude number and the scale, and this was confirmed by a series of tests conducted for various discharges. Whilst the ratio of air to water discharge was constant for constant Froude number, an increase in discharge was shown to result in increased energy loss and time of contact and hence a greater oxygen transfer.

An enhanced aeration was observed for water containing quantities of sodium nitrite. This was attributed to the formation of smaller bubbles in the presence of sodium nitrite and thus, for a constant volume of air, the creation of a larger air/water interfacial area. The presence of dissolved salt prevented the coalescence of bubbles, a supposition which was confirmed by measurements of bubble size reported in Chapter 5.

Two general equations expressing the oxygen transfer in terms of the measurable hydraulic characteristics of an hydraulic jump have been recommended, Equations 4.24 and 4.25. A wider range of applicability of

these is suggested although this has only been tentatively confirmed by successful prediction of some measurements by HOLLER (1971). The appropriate choice of the constants for this equation is made by reference to Table 4.3.

A discussion of similarity considerations suggested that the time of contact scale varied as the square root of the length scale, i.e. $M_t = M_L^{\frac{1}{2}}$, also that the liquid film coefficient scale $M_{K_L} \propto M_L^{5/8}$. The experimental results led to the conclusion that the scale of $r_{15}^{-1} = M_L^{9/8}$ for the range tested.

CHAPTER 5

A DETAILED STUDY OF BUBBLE SIZE AND CONTACT TIME IN THE HYDRAULIC JUMP WITH SUBSEQUENT APPLICATION TO THE ESTIMATION OF THE GAS TRANSFER COEFFICIENT

5.1 OBJECTIVES

(a) To confirm that bubble size is independent of scale.

(b) To test the effect of dissolved salts on the size of air bubble entrained.

(c) To attempt to measure the time of contact and thereby confirm that the time of contact can be estimated by an expression of the form Equation 4.10.

(d) To estimate the transfer coefficient and thus test the dependence of K_L on energy loss.

5.2 A PHOTOGRAPHIC STUDY OF THE BUBBLE SIZE DISTRIBUTION IN THE HYDRAULIC JUMP

5.2.1 A Justification for Further Measurements

It has been demonstrated by a number of research workers, notably HAINDL (1958) and WISNER (1965), that the size of entrained air bubble remains constant irrespective of scale.

The mean diameter of bubble has been measured by various workers producing generally similar results - HAINDL (1958) 2 to 3mm, WISNER (1965) 3 to 5mm, whilst bubble diameters ranging from 2 to 5mm were referred to by ALBRECHT (1968). APTED (1975) quoted a median bubble diameter of 1.25mm in an hydraulic jump whilst LEUTHEUSSER, RESCH and ALEMU (1973) referred to an average bubble size of the order of 10mm for their hydraulic jump.

Both HAINDL and APTED photographed the entrained air bubbles whilst LEUTHEUSSER and co-workers employed hot film anemometry using conical probes assuming that (i) all bubbles are intercepted by the probe along their diameters and (ii) that the bubble velocity is equal to the

water velocity at the instant of bubble arrival at the probe.

The measurements of LEUTHEUSSER and co-workers also indicated that the hydraulic jump with fully developed inflow entrained significantly larger bubbles than its counterpart with undeveloped inflow. The contrasting measurements of APTED and LEUTHEUSSER and others merit further investigation.

Furthermore, in Chapter 4 an enhanced aeration has been observed with increasing quantities of dissolved salt. In Section 4.7.3 it was shown that this could only be due to the creation of a larger air/water interface as a result of the formation of smaller air bubbles in the presence of dissolved salts. This hypothesis requires substantiation.

5.2.2 A Means of Measuring the Bubble Size Distribution

Use was made of the apparatus described in Chapters 3 and 4. The hydraulic jump was formed in a glass walled flume thus enabling high speed photography of the air water mixture. The use of 1/1000 sec electronic flash successfully froze the bubbles against a scale thus allowing for accurate measurement of the bubble size distribution. Plate 5.1 is an example of one of the photographs used for analysis. LEUTHEUSSER and co-workers indicated that the bubble size distribution is the same in all regions of the jump, thus it was unimportant which particular grid within the zone of aeration was analysed.

5.2.3 The Effect of Scale

Figure 5.1 summarises results obtained here over a small range of discharges for a relatively constant range of Froude number. Data have been presented as the percentage of the total number of bubbles whose measured diameters fell within $\pm$ 0.25mm of the plotted point. A

PLATE 5.1 Entrained air bubbles in the hydraulic jump (tap water + 0.3% $NaNO_3$)

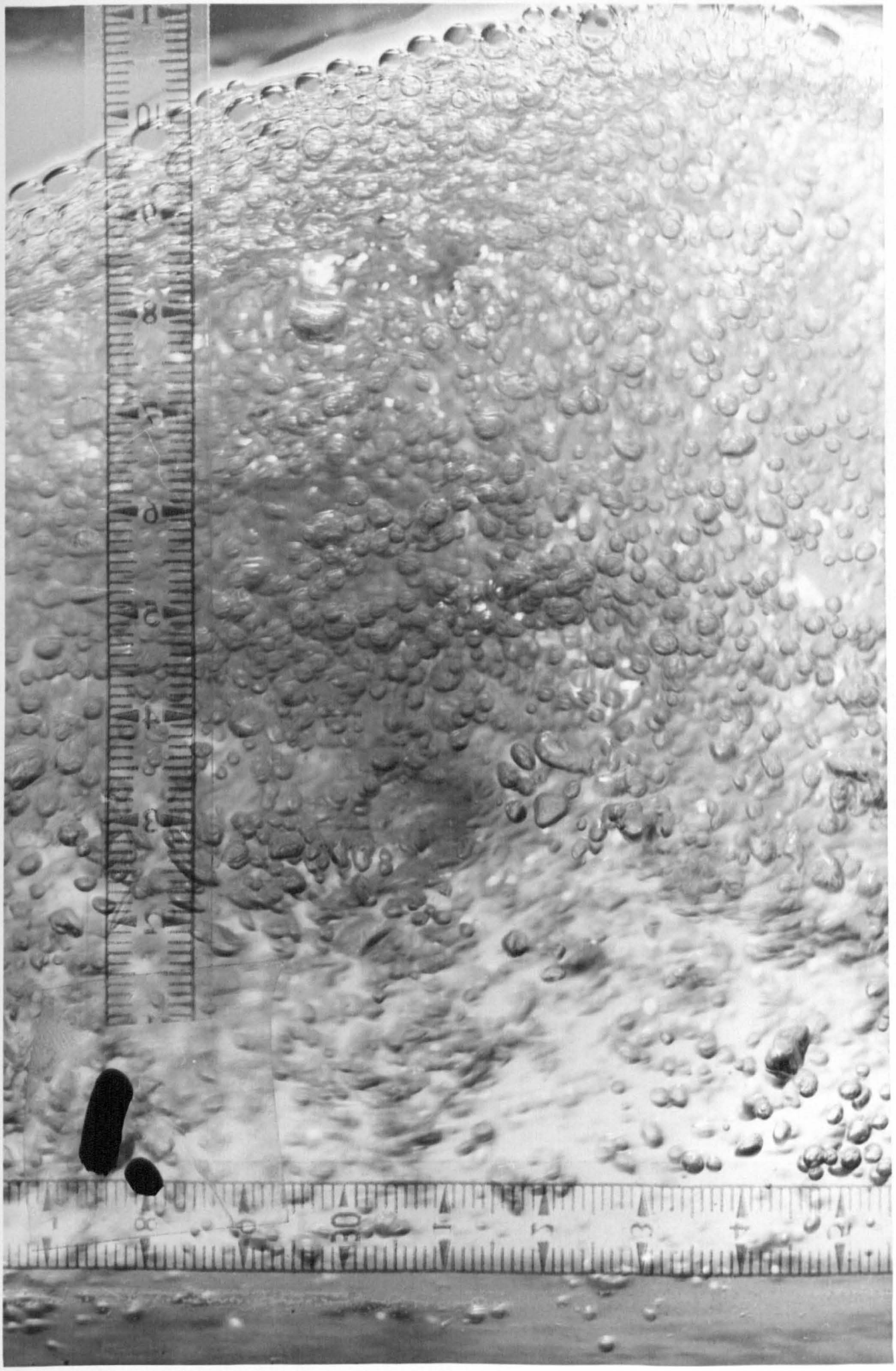

PLATE 5.2a Entrained air bubbles in the hydraulic jump (tap water)

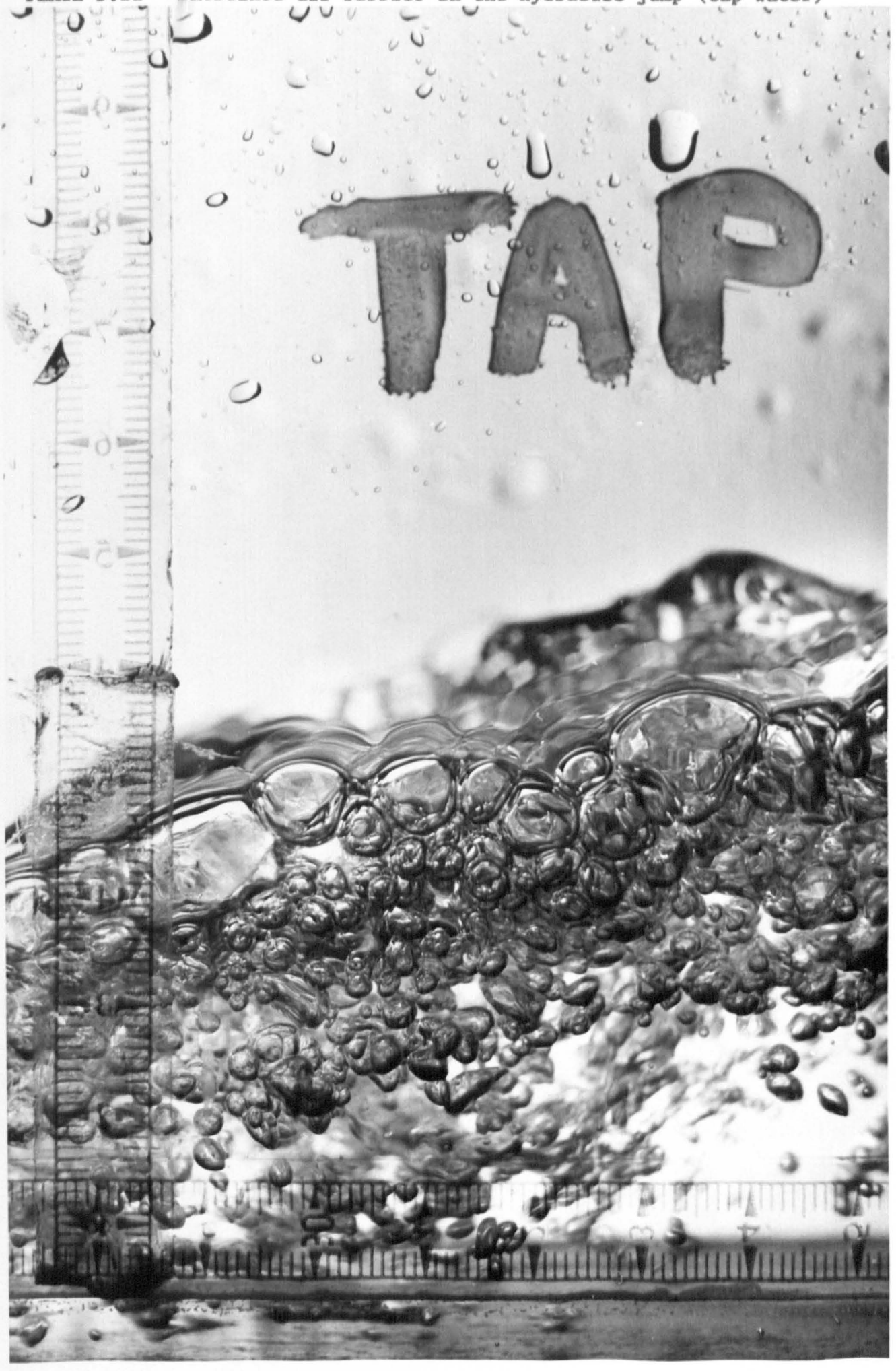

PLATE 5.2b Entrained air bubbles in the hydraulic jump (tap water)

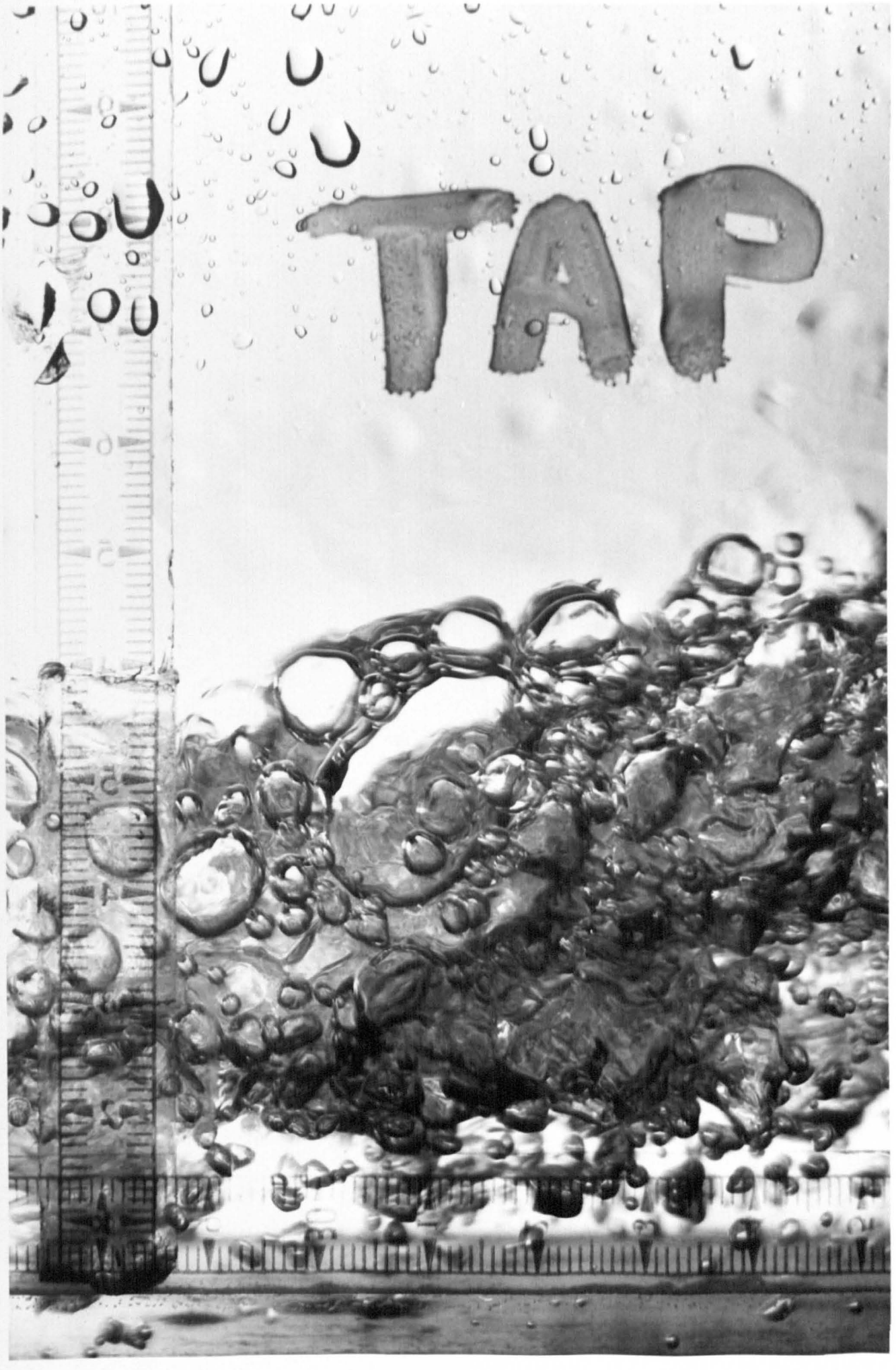

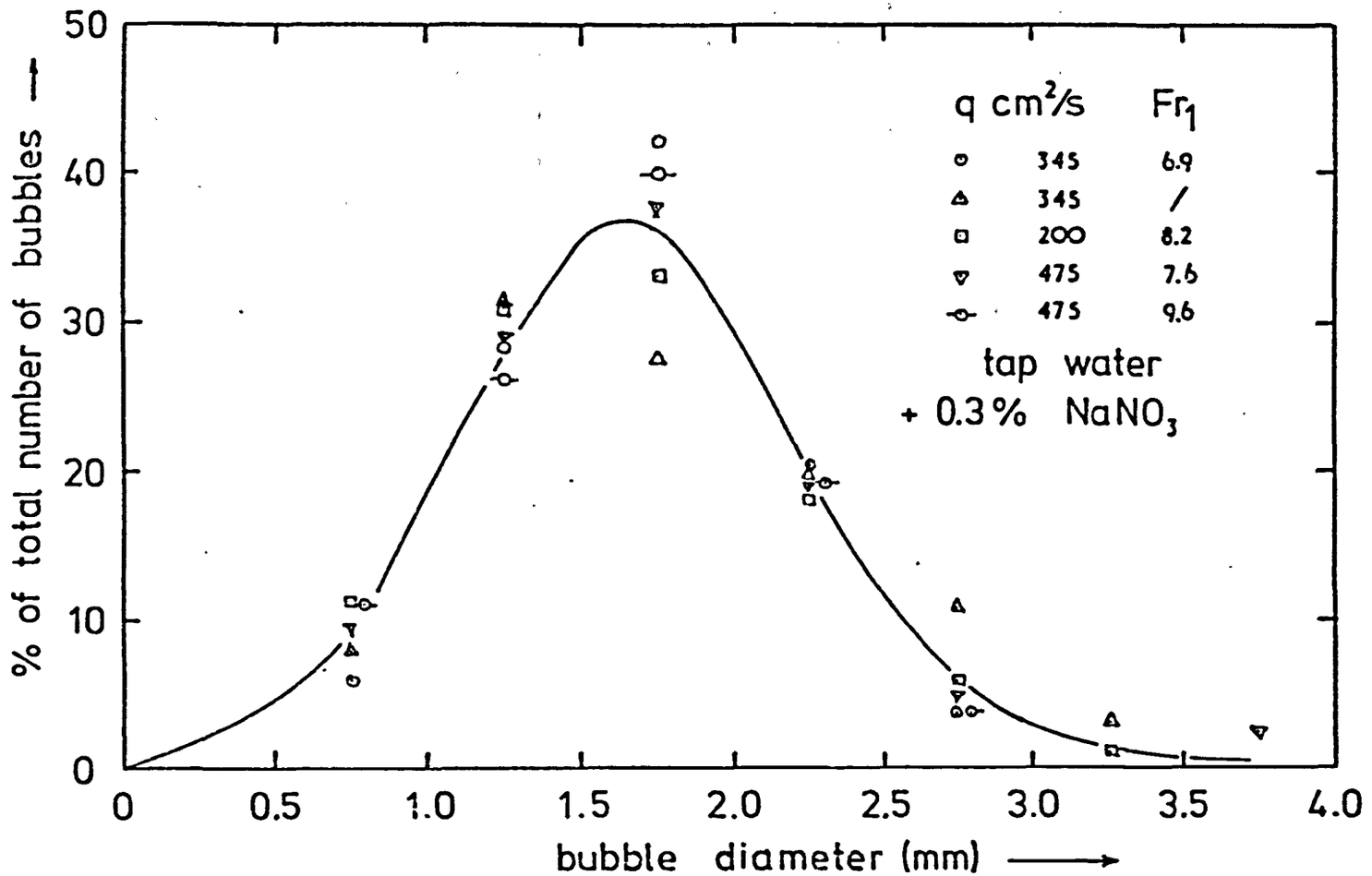

figure 5.1 the effect of model scale on bubble size distribution in an hydraulic jump

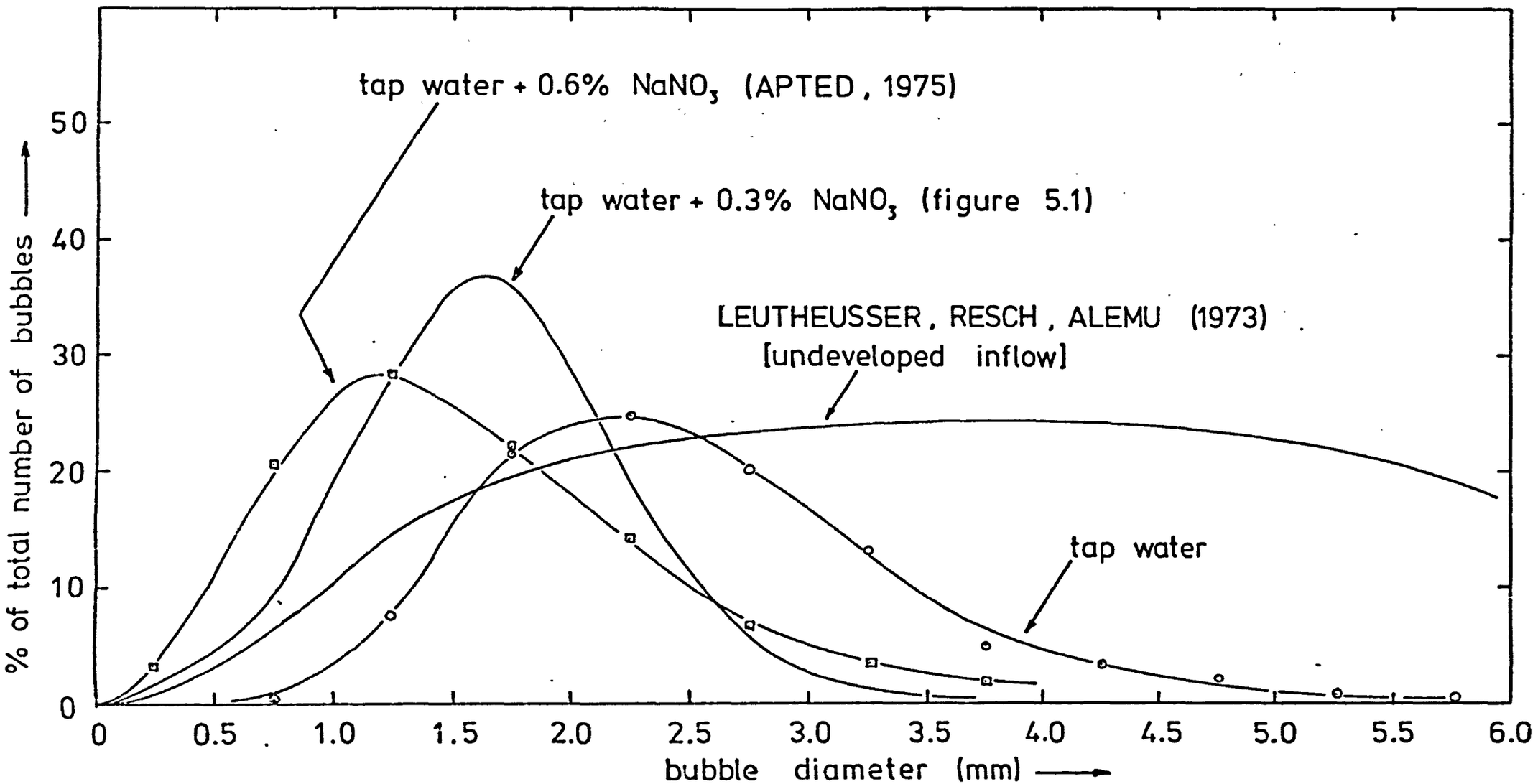

figure 5.2 the effect of dissolved salt (sodium nitrite) on the bubble size distribution in an hydraulic jump.

are to be found in Section 4.7.3. The larger bubbles obtained with tap water can be visually appreciated by comparison of Plate 5.1 (0.3% $NaNO_3$) and Plates 5.2a and 5.2b (tap water).

The range of bubble diameters obtained with tap water is in agreement with those quoted separately by HAINDL, WISNER and ALBRECHT - presumably therefore, these latter researchers obtained their values in waters low in dissolved salt concentration. The predominance of large bubbles suggested by the data of LEUTHEUSSER, RESCH and ALEMU reproduced in Figure 5.2 is inexplicable with regard to water quality. This casts some doubt on their anemometric technique, it is possible that the physical obstruction afforded by the conical probe on intercepting the bubble resulted in a reduction in the bubble velocity relative to the main flow and a consequent overestimate of the size.

5.3 AN ATTEMPT TO MEASURE THE CONTACT TIME

5.3.1 Description of the Technique and Apparatus Utilised

The objective was to measure the time taken by a typical fluid element to pass through the aerated zone and thus give a measure of contact time. This was achieved by timing the passage of a tracer through the hydraulic jump. The tracer usedwas a concentrated solution of sodium nitrite and this was "gulp" injected into the flow upstream of the jump. The progress of the tracer was registered by a Wheatstone Bridge to which two conductivity probes were connected. The probes were suitably positioned in the water upstream of the jump and at the end of the zone of aeration downstream of the jump. The change in conductivity on passage of the tracer pulse was registered by the Wheatstone Bridge and recorded on Ultra Violet paper. The Ultra

Violet recorder was capable of accurately recording time lapses as small as 0.01 secs. The layout of the equipment is shown in Figure 5.3 whilst the conductivity probes and Ultra Violet recorder are illustrated in Plate 5.3.

One of the main difficulties anticipated was the loss of the salt pulse as a result of intense mixing and dispersion by the hydraulic jump. In fact strong pulses were generally recorded with clearly discernible peaks. This is illustrated by a typical trace in Figure 5.4. The pre-selected time intervals of 0.1 sec are marked along the base of the trace thus enabling ready analysis of time elapsed between the recording of the upstream and downstream pulses. This time is taken to be the measure of time of contact for a fluid element.

5.3.2 Length of the Zone of Aeration

The correct positioning of the downstream conductivity probe is of obvious importance. Two definitions of the length of hydraulic jump are indicated in Figure 5.5. The definition of PETERKA (1963) is the conventional length of the roller (see Figure 3.1a) whilst LEUTHEUSSER and KARTHA (1972) defined the length as that measured from the toe of the jump to the point downstream where the influence of the jump has become negligible and the flow characteristics are governed by the channel alone. The length utilised for these tests, i.e. the distance between the conductivity probes, required visual observation of the end of the main zone of aeration. As shown in Figure 5.5 this criterion lies between the two discussed above as is to be expected. The length of the aerated zone is similarly a function of the downstream conjugate depth alone over the range tested, i.e. L_j/y_2 is constant. The scatter displayed in Figure 5.5. is perfectly acceptable in view of the

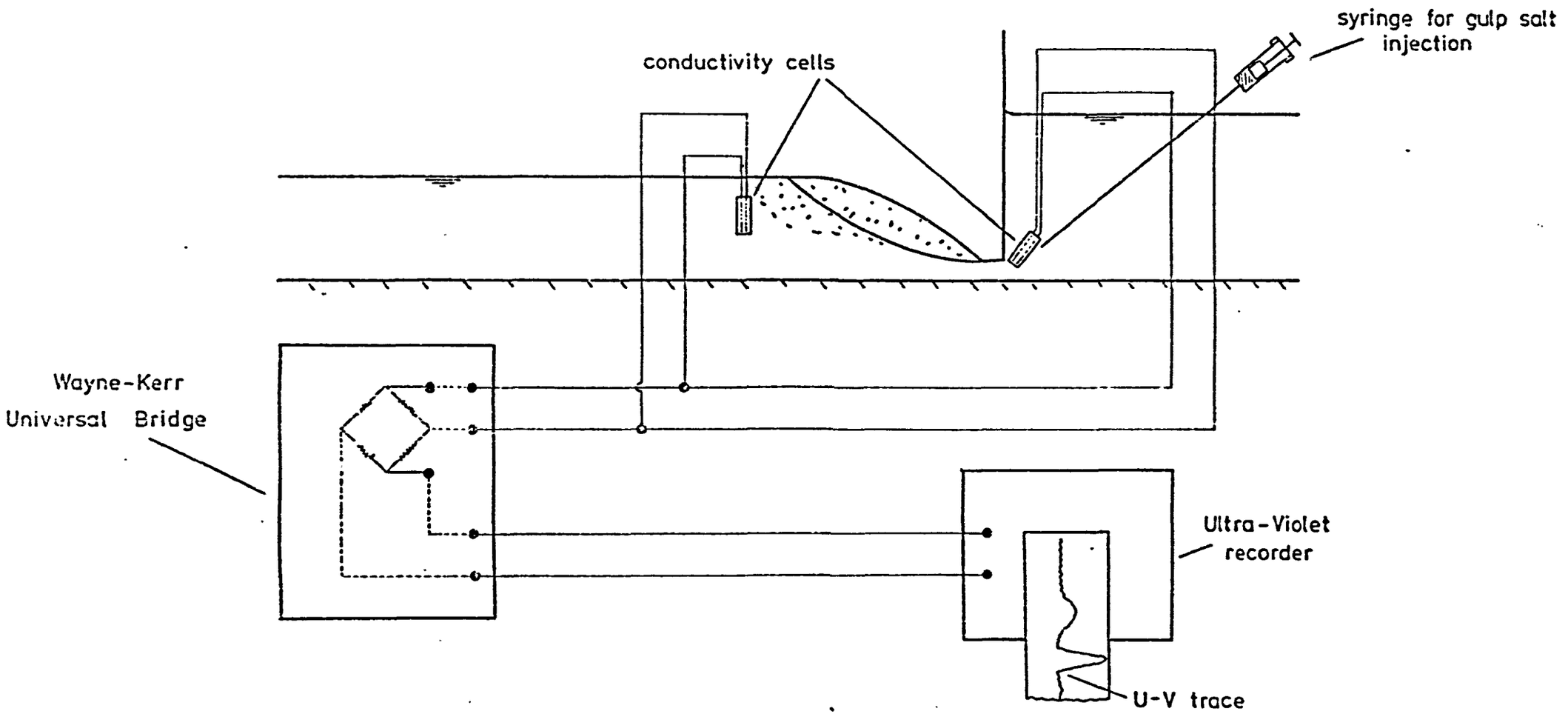

figure 5.3 Schematic - apparatus to determine contact time in an hydraulic jump

PLATE 5.3 Wheatstone Bridge, conductivity probes and Ultra-Violet recorder

figure 5.4

ULTRAVIOLET TRACE

$q = 675\ cm^2/s$

$Fr_1 = 3.54$

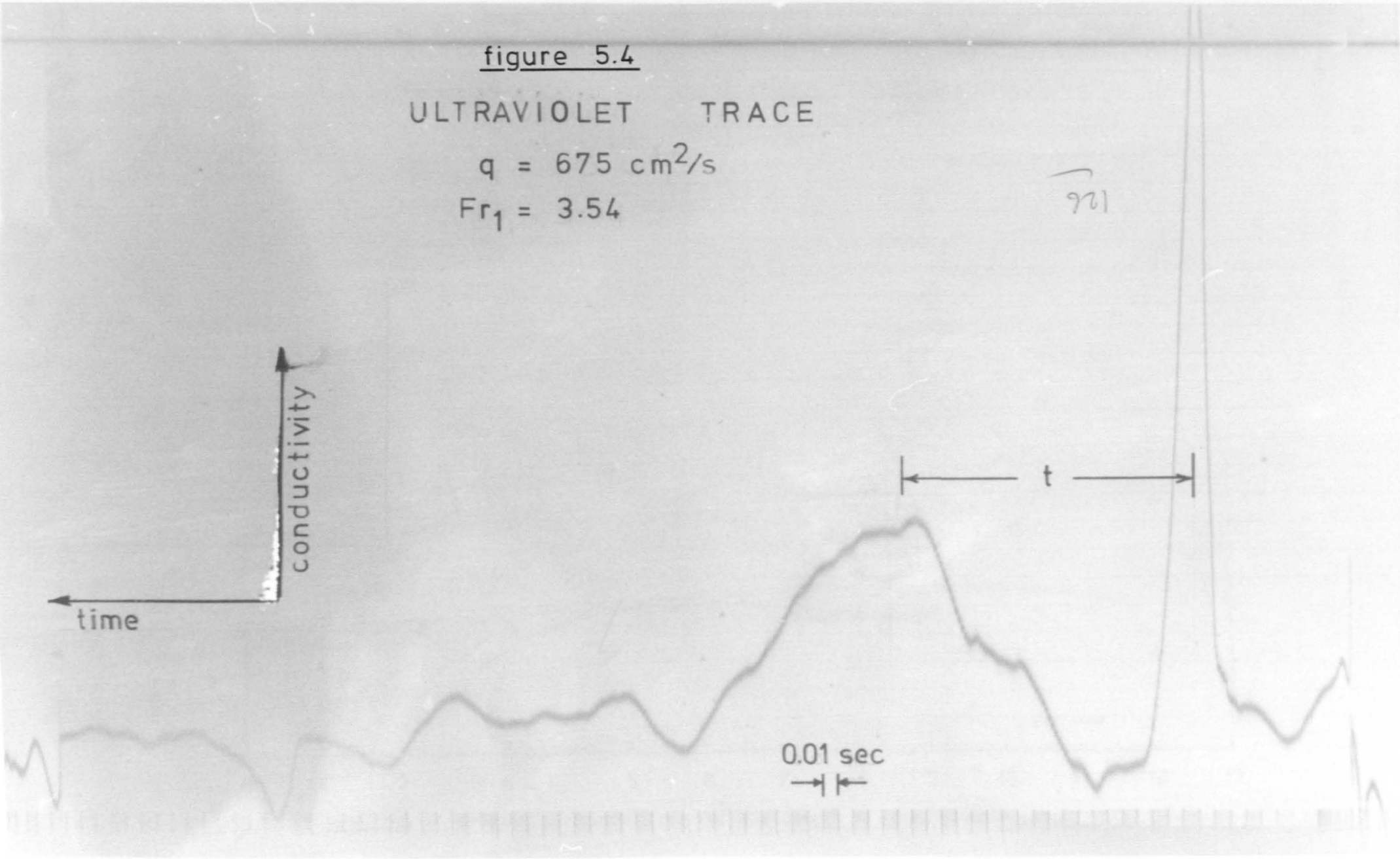

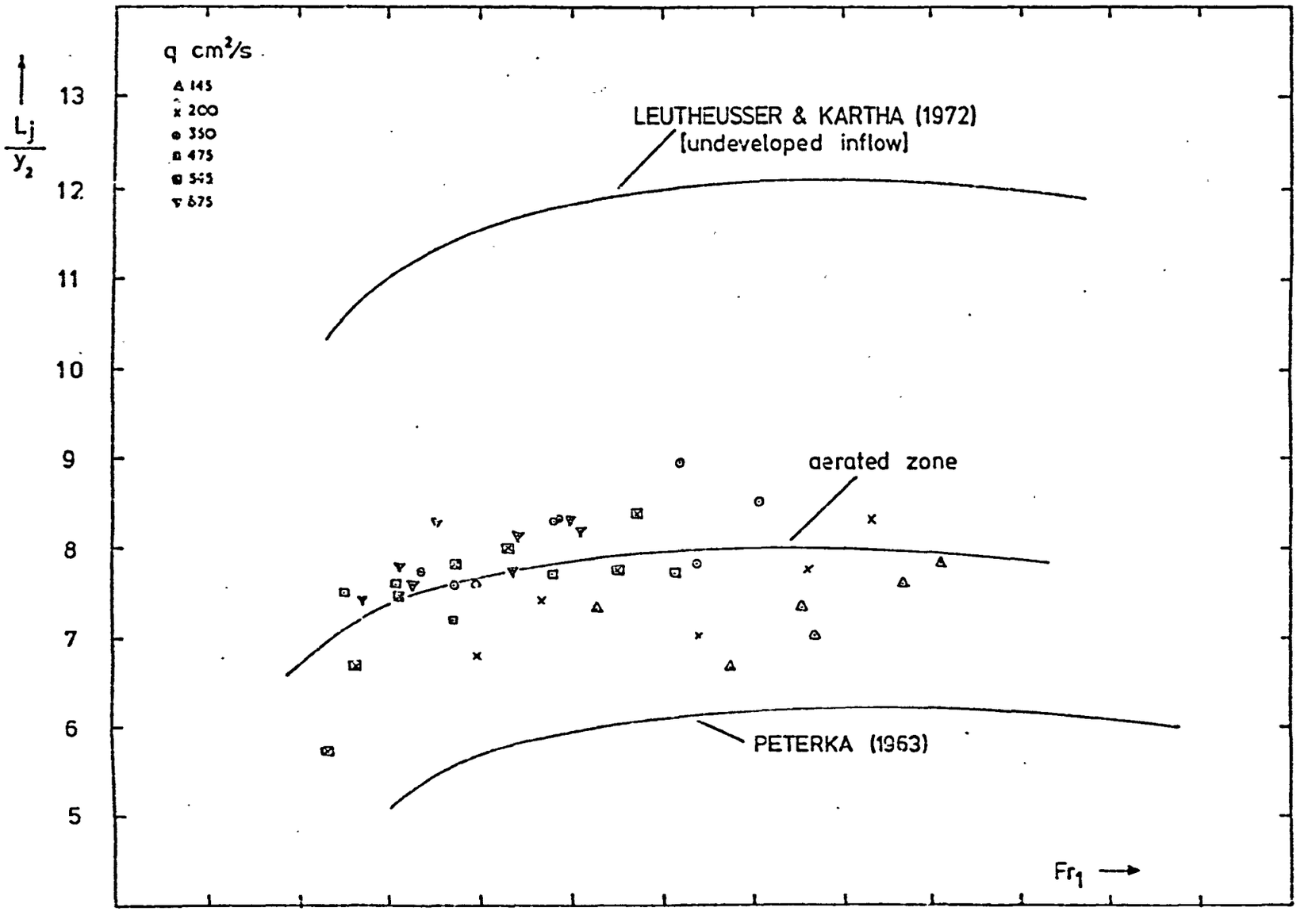

figure 5.5 different interpretations of the length of the hydraulic jump

insensitivity of visually determining the end of the aeration zone. The data of LEUTHEUSSER and KARTHA in Figure 5.5 is for a condition of undeveloped inflow, for developed inflow they showed that $L_j \simeq 16y_2$, i.e. larger for this latter condition.

5.3.3 Results

It was earlier suggested in Section 4.4 from an approximately derived model of contact time in the aerated zone of the hydraulic jump (Equation 4.10), that

$$\frac{t\sqrt{g}}{\sqrt{y_1}} = f(Fr_1)$$

i.e. for a constant Froude number, the contact time varies as the square root of the length scale. The current tests for a variety of discharges are summarised in Figure 5.6, these results are quite consistent with the observations made from the model. Furthermore, the validity of the approximate model is successfully tested in the dimensionless plot Figure 5.7, from which the following expression for the time of contact may be stated:

$$t = 9.26\ Fr_1 \sqrt{\frac{y_1}{g}} \quad \text{(sec)} \qquad (5.1)$$

The variation of contact time scale with the square root of the length scale is validated by the measurements over the range of scale encompassed by the oxygen transfer tests.

The technique just described has proved a most useful means of determining contact times of fluid elements. Furthermore, the nature of the pulse observed downstream indicates the degree of recirculation

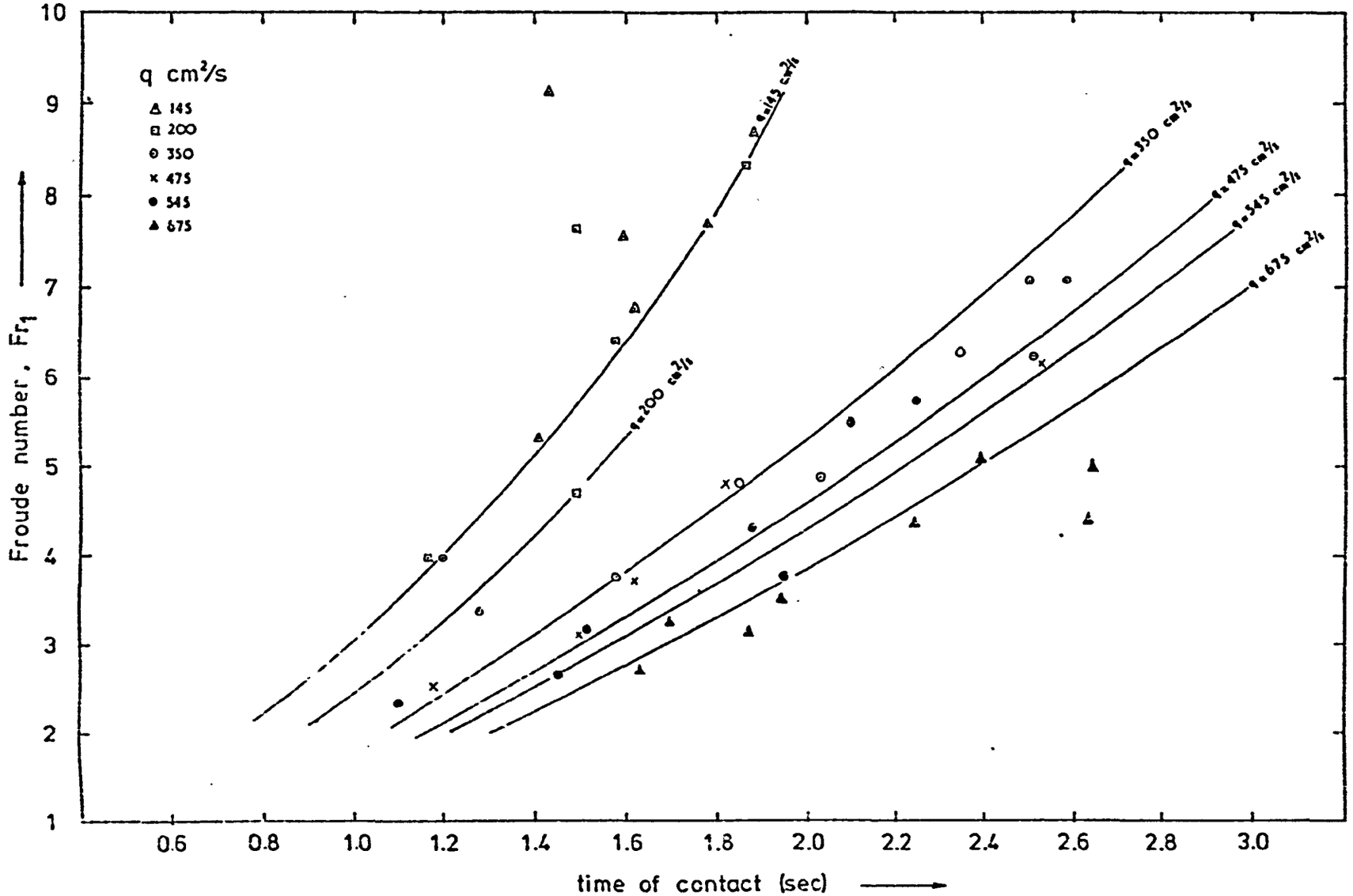

figure 5.6 the variation in contact time with scale of hydraulic jump

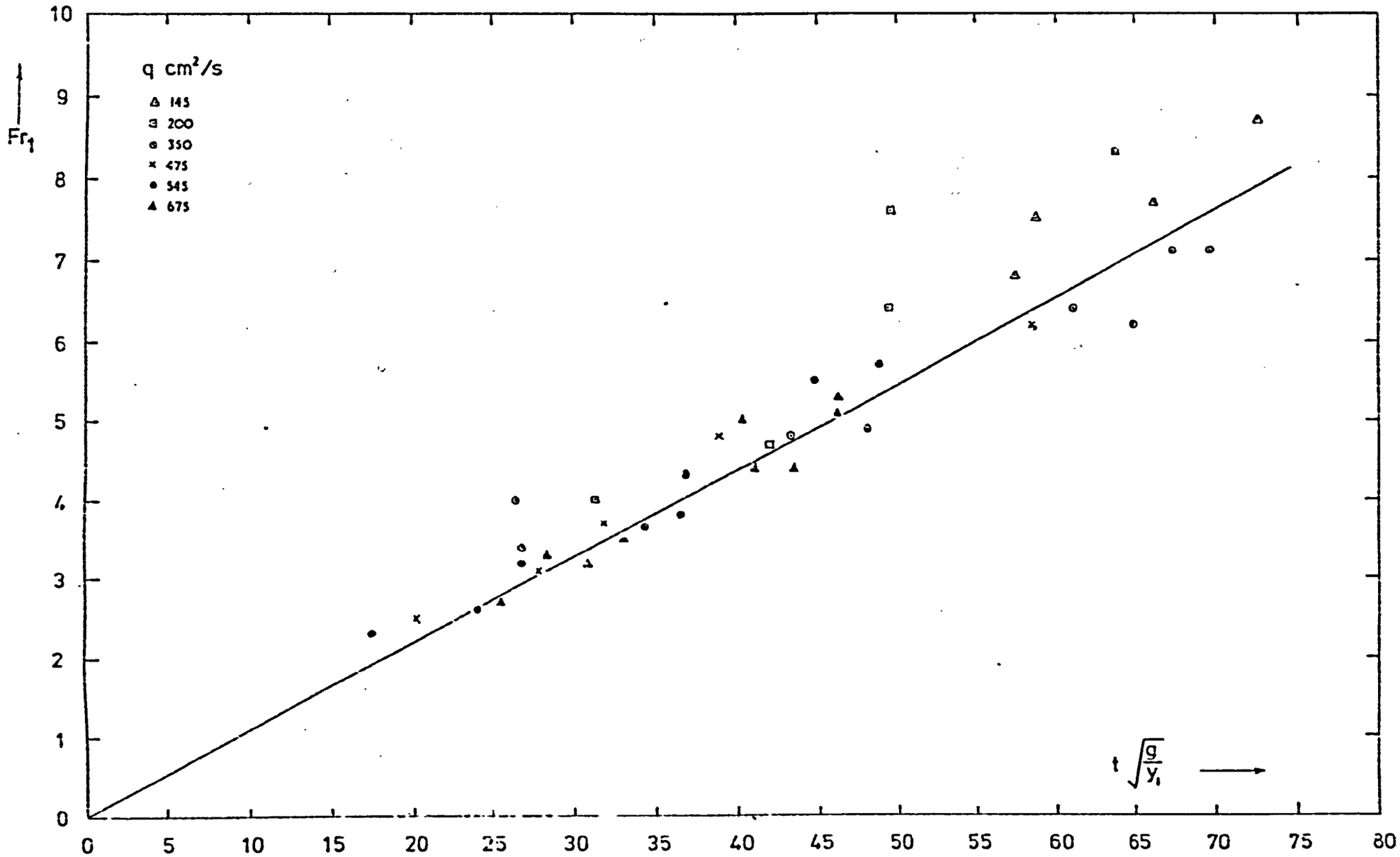

figure 5.7 verification of Eq 4.10

occurring. In the experiments reported above, a rapid rise in conductivity to a peak value was generally followed by rapid re-attainment of background levels (Figure 5.4). The technique is versatile, and could be refined to quantify the degree of dispersion or recirculation occurring.

5.4 AN ESTIMATE OF THE TRANSFER COEFFICIENT

5.4.1 Computation of the Liquid Film Coefficient

From Equation 1.36:

$$K_L = \frac{\text{Log}_e r}{\frac{A}{V} t} \tag{5.2}$$

where

$$\frac{A}{V} = \frac{Q_a}{Q} \times 4\pi \left(\frac{d_b}{2}\right)^2 \Bigg/ \left[\frac{4}{3}\pi \left(\frac{d_b}{2}\right)^3\right] = \frac{Q_a}{Q} \cdot \frac{6}{d_b} \tag{5.3}$$

The ratio Q_a/Q is readily determined from Equation 2.1, t was measured in Section 5.3 (Equation 5.1), d_b was measured in Section 5.2 whilst measurements of deficit ratio were reported in Chapter 4. A realistic estimate of the liquid film coefficient is therefore possible. Table 5.2 contains the liquid film coefficients computed for a range of discharges, for three Froude numbers in each case and for the three different water types tested. The contribution to the surface area of the upper water surface is considered negligible since this is largely occupied by air bubbles (see Plate 5.1).

TABLE 5.2

A Computation of Liquid Film Coefficient for the Hydraulic Jump Studied

Specific Discharge q (cm^2/s)	Upstream Froude No. Fr_1	Energy Loss ΔE (cm)	LIQUID FILM COEFFICIENT K_L cm/hr		
			Water Type A *	Water Type B **	Water Type C ***
145	8.37	17.67	60.1	53.9	68.1
	6.53	10.58	68.8	61.7	77
	3.73	3.29	78.5	70.2	89.3
345	7.10	22.01	90.8	81.9	103.7
	5.59	14.04	101.1	90.9	114.5
	3.22	4.08	118.3	100.8	129.6
710	4.85	16.95	139.6	127.2	158.6
	3.51	8.20	152.9	136.2	172.5
	2.50	3.20	157.9	139.9	173.2

* Water Type A - Tap water + 0.6% $NaNO_3$ d_b = 0.157cm

** Water Type B - Tap water + 0.3% $NaNO_3$ d_b = 0.172cm

*** Water Type C - Tap water d_b = 0.253cm

The values of K_L computed have been plotted in Figure 5.8 together with numerous published data for various bubble sizes reproduced from BARNHART (1969) for freely rising bubbles.

The orders of magnitude of K_L for the hydraulic jump are comparable.

For a constant discharge an increase in Froude number results in greater energy loss, air entrainment and gas transfer but also a reduced liquid film coefficient. This similarly follows from Figure 4.10 where a constant oxygen transfer was recorded for constant energy loss irrespective of discharge. From Equations 4.21 and 4.33 it follows that for constant deficit ratio:

$$K_L = f\left(\Delta E \Big/ \left[\frac{A}{V}\, t\right]\right) \tag{5.4}$$

i.e. K_L is a function of the energy loss per unit time per unit interfacial area to volume ratio. In addition K_L is a function of the molecular diffusivity D_m of oxygen in water, and of the kinematic viscosity of the water. K_L also varies with bubble size. These parameters have all been incorporated in the dimensionless correlation depicted in Figure 5.9 from which

$$K_L \frac{d_b}{D_m} = 0.266 \left(\frac{V.\Delta E}{At\ \nu}\right)^{1.2} = 0.266 \left(\frac{Q}{A}.\ \frac{\Delta E}{\nu}\right)^{1.2} \tag{5.5}$$

where $K_L . \frac{d_b}{D_m}$ is the Sherwood number.

In producing Figure 5.9, the molecular diffusivity of oxygen in water at 15°C was determined from the INTERNATIONAL CRITICAL TABLES to be 0.07 cm^2/h, a figure which is approximately equal to that determined

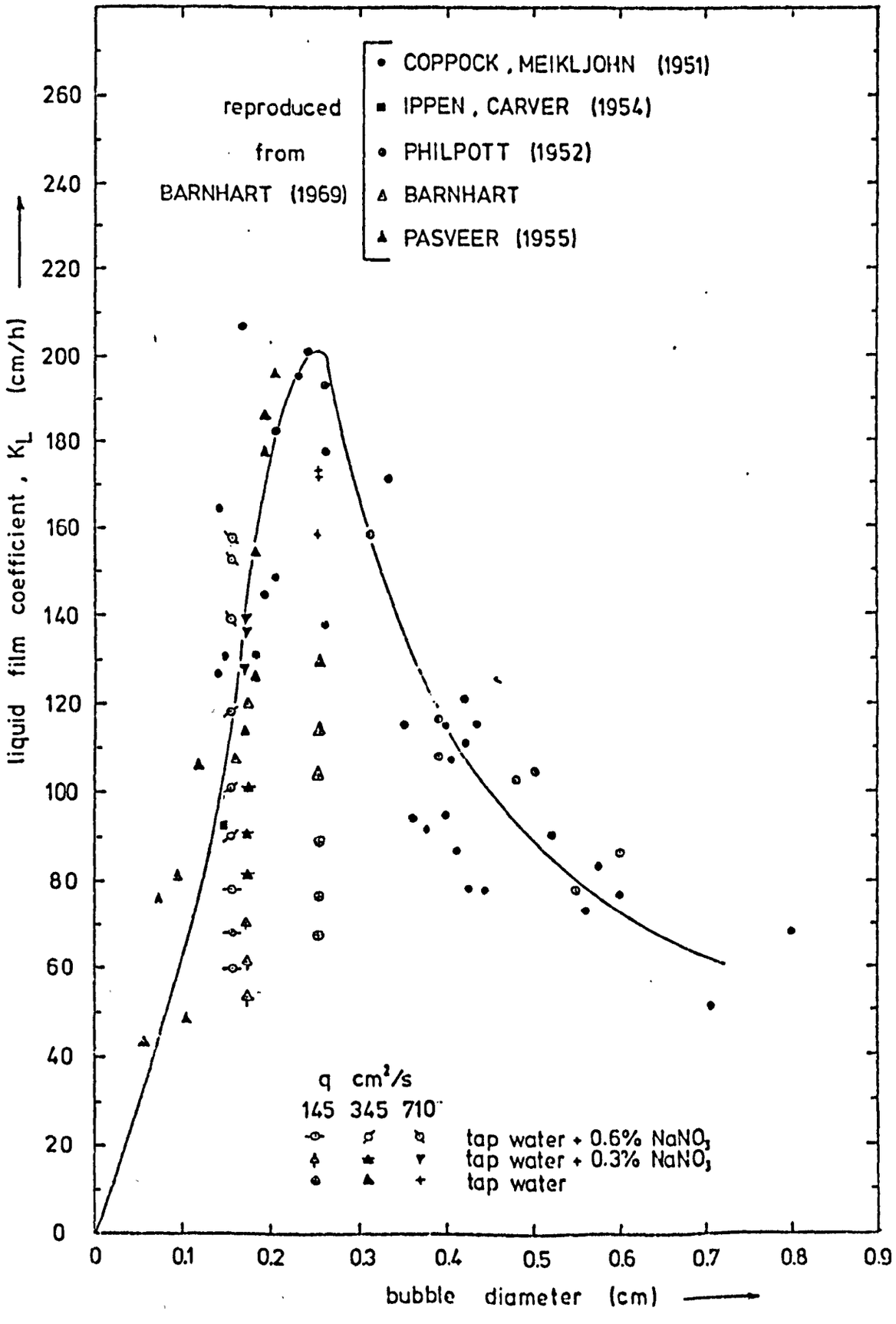

figure 5.8 a comparison of liquid film coefficients for the hydraulic jump and published values for free rising bubbles

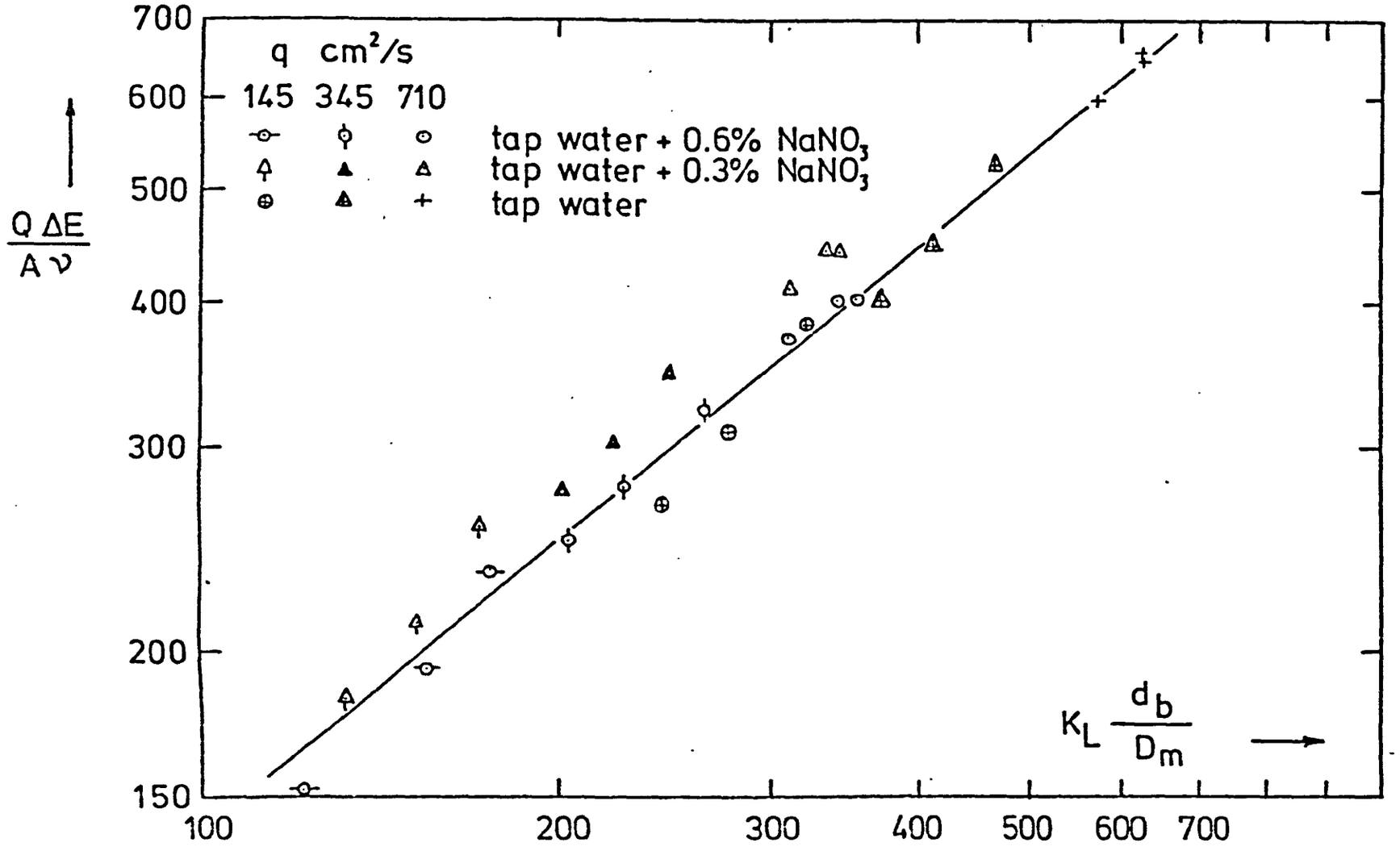

figure 5.9

[Q ΔE / A ν] v Sherwood No.

more recently by BAIRD and DAVIDSON (1962). The kinematic viscosity of water at 15°C was taken to be 0.01143 cm^2/s, the changes in this value due to the presence of dissolved salts being ignored.

5.4.2 Implications for Similarity of K_L

For a constant water quality, d_b is constant, and for a constant temperature D_m and ν are constant.

If the gas transfer situation is modelled according to the Froude law of similarity then $\frac{A}{V}$ is constant and the time scale $M_t = M_L^{\frac{1}{2}}$ from Equation 5.1. Also, according to Equation 4.3 $M_{\Delta E} = M_L$ whence from Equation 5.5:

$$M_{K_L} = \left(\frac{M_L}{M_L^{\frac{1}{2}}}\right)^{1.2} = M_L^{0.6}$$

The liquid film coefficient therefore varies as the 1.67 root of the length scale or $M_L^{0.6}$. This is indicated in Section 4.10 where it was suggested that $M_{K_L} \simeq M_L^{0.625}$. A caution about limits of validity was expressed in Section 4.10.

5.5 SUMMARY

The size of bubble entrained by an hydraulic jump was studied. The results confirmed HAINDL's statement that a constant size of air bubble is entrained irrespective of scale. The distribution of bubble sizes indicated a slight positive skew, i.e. a predominance of bubble sizes larger than the median. The presence of dissolved salts was observed to result in a reduced bubble size thus confirming the reasons expressed in Section 4.7.3 for the enhanced aeration observed

in Section 4.7.2. Some comments were made regarding the extremely large bubble sizes recorded by LEUTHEUSSER, RESCH & ALEMU as these contrasted markedly with the observations of other published measurements.

A technique for estimating the time of passage of a fluid element through the hydraulic jump was reported and the results provided confirmation of an approximately derived time of contact model presented in Section 4.4. The suggestion made in Section 4.10, that the scale of time of contact varied as the square root of the length scale, was validated, i.e. $M_t = M_L^{\frac{1}{2}}$.

An estimate was made of the liquid film coefficient for the hydraulic jump studied. The values calculated were shown to be comparable to others published in the literature. A dimensionless correlation equation (Equation 5.5) was presented which related K_L to the Energy loss per unit time per unit ratio of air interface to volume. The scale of the liquid film coefficient was shown to vary as the 1.67 root of the length scale over the range of the current tests for constant Froude number, a similar conclusion to one reached in Section 4.10, namely that $M_{K_L} \propto M_L^{0.625}$.

CHAPTER 6

THE EFFECT ON OXYGEN UPTAKE OF DOWNSTREAM POOL GEOMETRY AND JET DISCHARGE FOR A PARTICULAR WEIR NOTCH

6.1 INTRODUCTION

Although much useful work has been published on the oxygen uptake at weirs this has largely proved inconclusive. Figure 6.1 serves to summarise much of this work, and, with the exception of NAKASONE, all the workers mentioned have attempted to relate the oxygen uptake solely to the height of fall although VAN DER KROON and SCHRAM did note that discharge variations are also effective. The inconclusiveness of previously published work is further illustrated by the inability of both the WATER POLLUTION RESEARCH LABORATORY (D.O.E. 1973) and HOLLER to relate their laboratory correlations directly to prototype measurements although reasons for this were advanced.

It was intended therefore to exhaustively study the effect of all important variables in the hope of clarifying the different effects displayed in Figure 6.1.

6.2 AIMS

The experiments reported in this chapter represent a continuation of work begun by APTED. The effect of varying the jet discharge and the geometry of the downstream pool for a particular weir crest and a constant water quality is investigated.

6.3 DESCRIPTION AND USE OF APPARATUS

6.3.1 General

The laboratory re-circulatory system has already been discussed (Section 3.4.1) as has the supply of de-oxygenated water from the mixing tank (Appendix B). The weir apparatus was set up immediately

figure 6.1 deficit ratio v height of fall - various published results

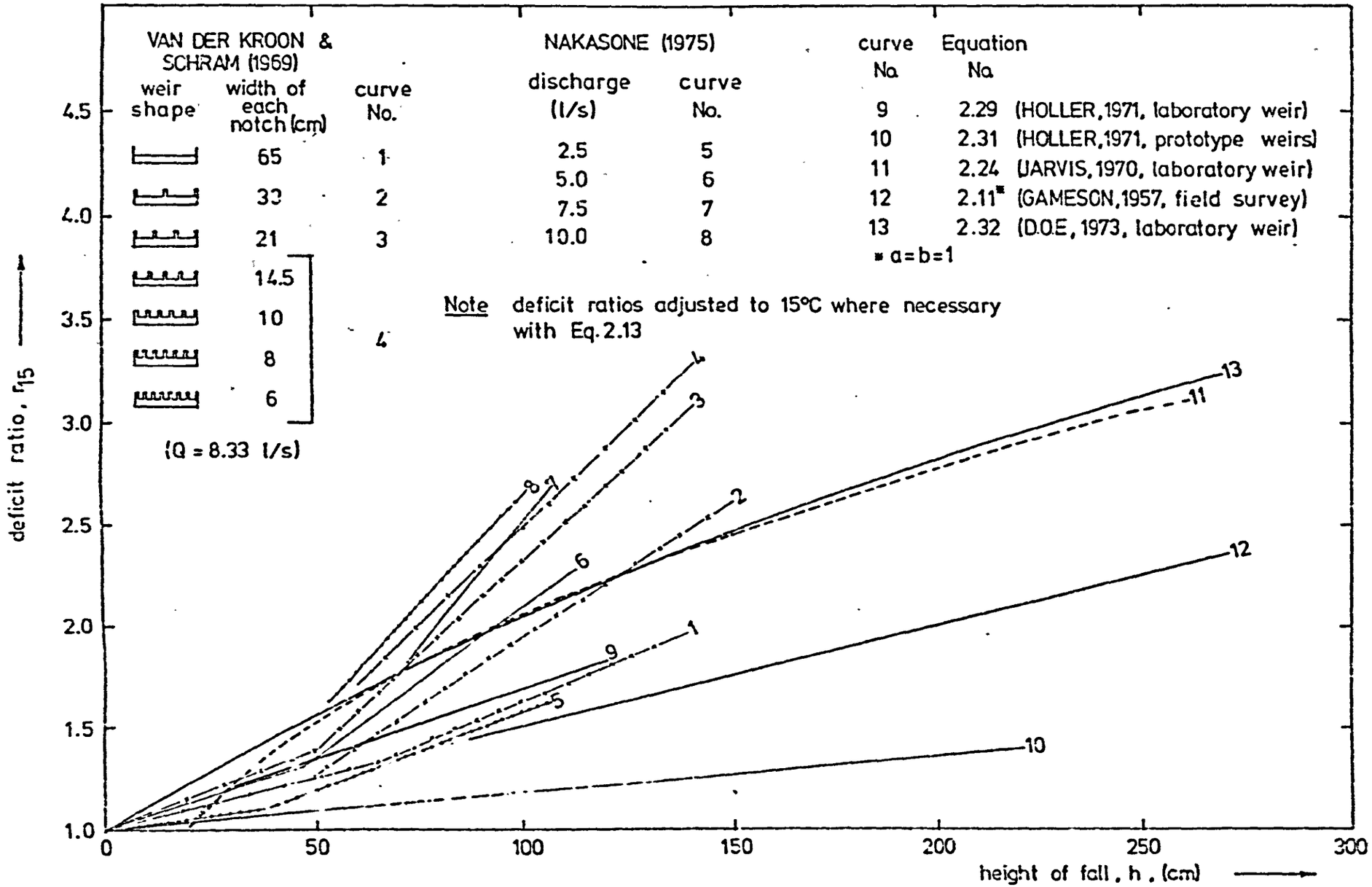

beneath the mixing tank, on the floor below, and connected to the mixing tank as shown in Figure 6.2.

6.3.2 The Weir Apparatus

After deoxygenation in the mixing tank water flowed under gravity to the upper weir pool. This pool consisted of a galvanised mild steel tank 0.92m x 0.65m x 0.60m fitted with a system of baffles to stabilize the flow prior to discharging over a sharp crested weir. The water then fell freely to the pool below. The rate of flow was metered by passage through a pair of rotameters illustrated in Plate 6.1, and placed in parallel in the supply line between the mixing tank and weir stilling pool. Sensitive control of the flow rate was effected by a pair of valves, one placed prior to each rotameter. The weir notch was readily removable thus permitting the substitution of alternative notches as required.

The downstream pool was constructed of timber and was fitted with a wicket-type outflow gate which enabled the depth in the pool to be varied up to the maximum of 0.5m. The length of the pool remained constant at 1.5m while the width of the pool could be reduced at will from 1.0mby the insertion of a pair of timber baffles placed appropriately but parallel to the sides of the tank. With the baffles in position it was necessary to line the pool with a plastic sheet to prevent water from escaping under the baffles.

For all the tests conducted at the maximum pool width it was possible to observe the behaviour of the jet underwater through a glass inspection window built into one side of the lower pool.

The water discharging from the lower weir pool was returned down a shute to the laboratory sump whence it was again available for re-circulation to the header tank.

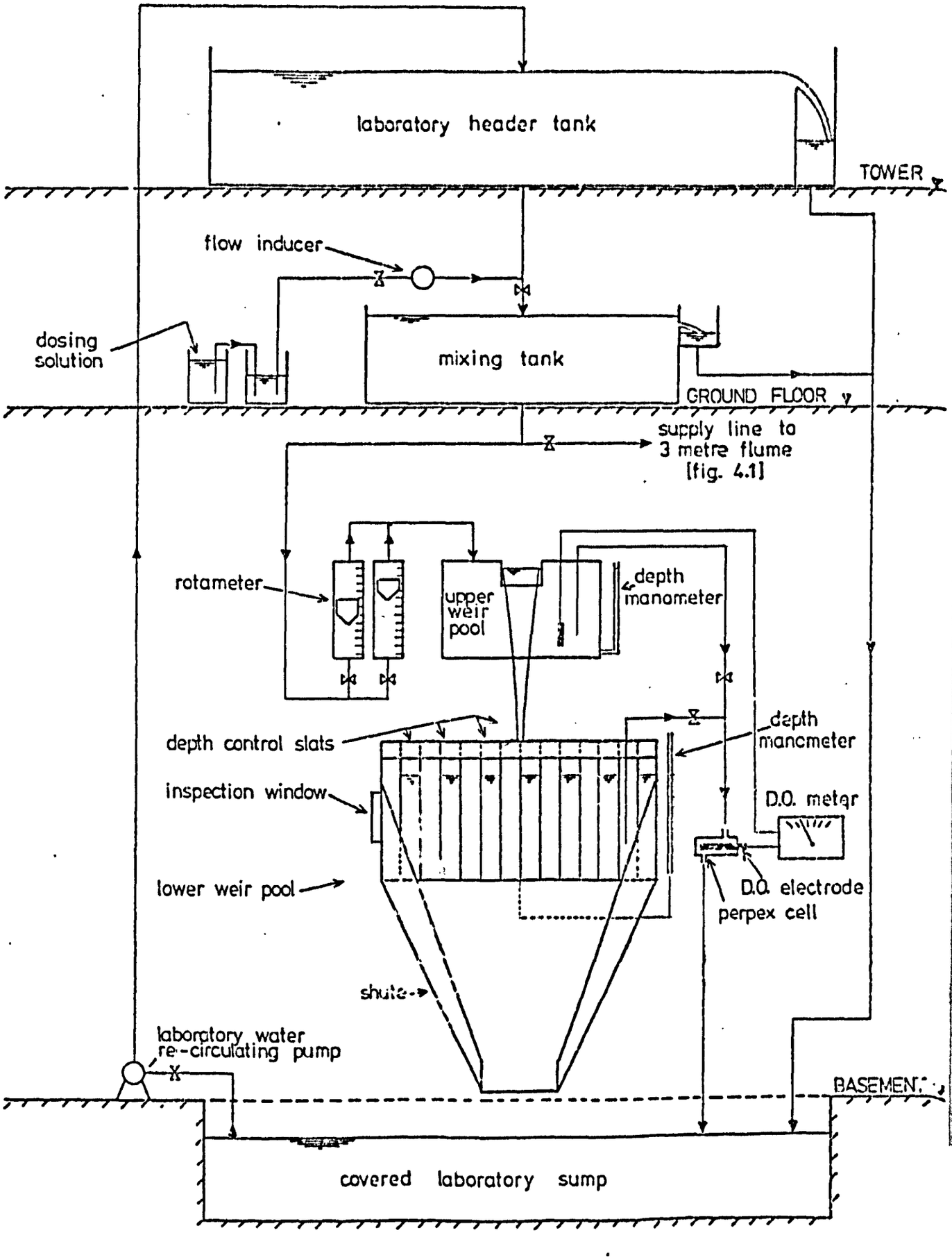

-⧖ signifies a flow control valve

figure 6.2 LABORATORY CIRCUIT - FREE OVERFALL EXPERIMENTS

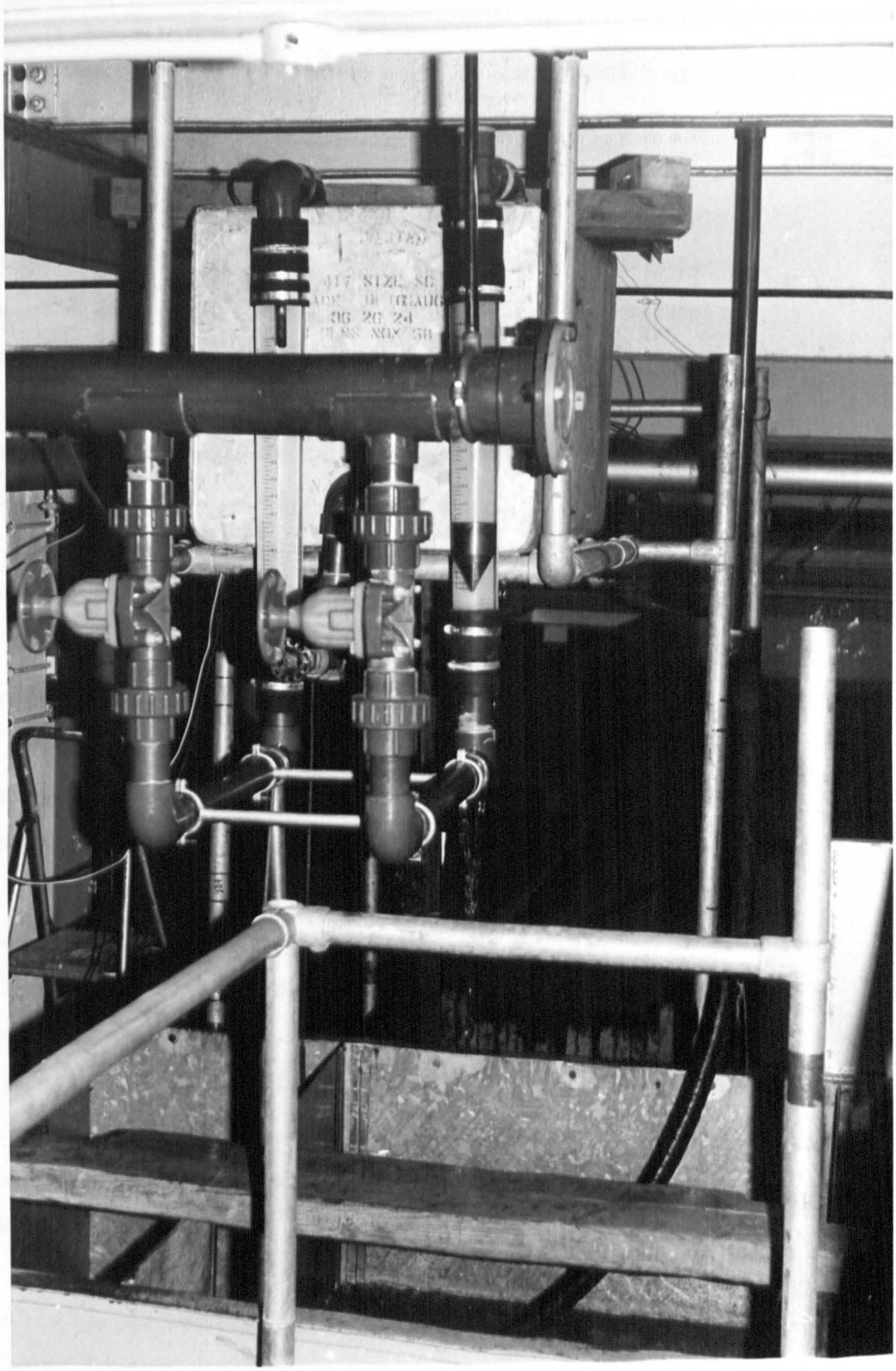

PLATE 6.1 Weir stilling pool and rotameters

The measurement of water levels in both the stilling pool and downstream pool was effected by a calibrated single limb manometer in each case tapped into the bed of each pool.

The height through which the jet fell was varied simply by either raising or lowering the downstream pool. At all times the upper weir pool was fixed in position and the whole apparatus was rigidly supported by scaffolding tubes.

The layout described above is illustrated by the flow diagram set out in Figure 6.2 and the weir apparatus is depicted under operating conditions in Plate 6.2.

6.3.3 Test Procedure

This set of experiments was conducted with a sharp crested rectangular notch of width 100mm for a variety of discharges.

For various positions of the lower pool and for various discharges over the weir the depth of water in the lower pool was varied. Tests were similarly conducted for reduced widths of the lower pool.

After any adjustment to any of the variables discharge, pool depth, pool width, height of fall, etc., it was essential to allow sufficient time for the attainment of both stable hydraulic conditions and steady oxygen levels. These were continuously monitored and were recorded only when equilibrium was judged to have been achieved.

The sequence of operations discussed below was arrived at through experience and although somewhat wasteful in chemicals it was most efficient with regard to time.

With the pool position and width fixed, the discharge was set to 2.5 l/s and the downstream pool wicket gate adjusted to provide the maximum depth in the pool. A series of tests was now conducted altering

PLATE 6.2 Operational weir apparatus

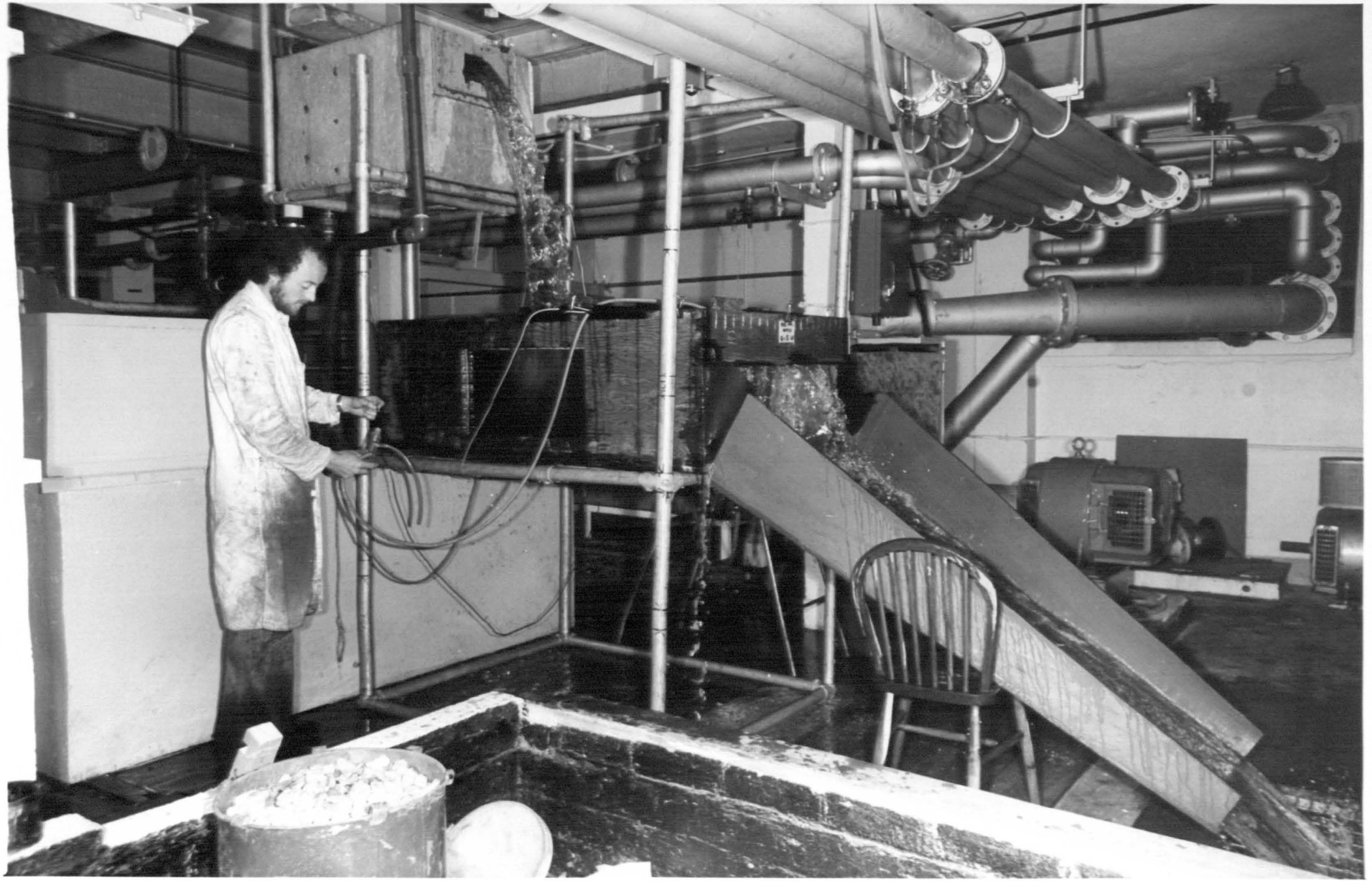

only the discharge. As with the previously reported hydraulic jump tests, the inflow to the mixing tank was fixed, in this case at $\hat{Q}$ = 2.5 l/s, with the result that as the discharge through the weir apparatus was reduced, then the excess flow was removed by the overflow weir in the mixing tank. It was found that to alter the inflow to the mixing tank each time a new discharge was selected, and thus the chemical dosing as well, was far too time consuming because of the large retention time of the mixing tank and the consequent length of time to re-attain stability.

Thus, with all other variables constant, the discharge in the weir apparatus was gradually reduced. On completing recordings at the minimum discharge 0.6 l/s, the discharge was again set at 2.5 l/s, the depth in the downstream pool set to a new level and the procedure repeated.

The tests were conducted over a range of the variables as limited by the physical size of the apparatus. In addition to the discharge range 0.6 to 2.5 l/s, an extra experiment was conducted for one higher discharge 5.0 l/s.

Throughout these experiments the levels of sodium nitrite in the water were monitored and remained constant at a concentration of 0.3%.

6.3.4 The Measurement of Oxygen Uptake

As discussed in Appendix A.3, oxygen levels recorded were expressed as percentage saturation.

The measure of oxygen uptake selected was the deficit ratio (Equation 1.35) and all deficit ratios were corrected to a standard value at 15°C by means of the temperature correction of GAMESON, VANDYKE & OGDEN (Equation 2.13).

In contrast to the hydraulic jump tests the dissolved oxygen electrode was placed in a perspex cell and not suspended freely in the water. The reasons for this are discussed more fully in Appendix A. Suffice to mention here that this was designed to avoid the dangers of oxygen depletion in the vicinity of the electrode. The validity of this technique is also discussed in detail in Appendix A.

6.4 EFFECTS OF VARYING DISCHARGE-RESULTS

6.4.1 Variations in Optimum Depth

The results of the experiments for various discharges are plotted in Figures C2.1 to C2.7 (See Appendix C). A typical sample of the data collected is given in Table 6.1 together with the deficit ratios computed. This data is reproduced in Figure 6.3 in the typical form of presentation of Appendix C. For a particular discharge, water quality and notch type, the deficit ratio adjusted to 15^{o}C has been plotted against the lower pool depth for the various elevations of the lower pool tested.

The behaviour displayed in Figure 6.3 confirms the observations of JARVIS, the D.O.E., and also APTED, in that for any fixed pool position, an increase in deficit ratio is observed for an increase in pool depth up to a critical value of depth beyond which a decrease in the deficit ratio becomes apparent. This critical depth, being the depth at which optimum aeration is achieved, is henceforth referred to as the optimum depth, d'. It has already been established (see Section 2.4.6) that this is the depth to which the jet or bubble plume would penetrate into the pool if unimpeded. For lesser depths the bubble plume would strike and be deflected off the bed of the pool and this reduced contact time is reflected by the reduced oxygen uptake observed

TABLE 6.1

A Typical Sample of the Data Collected for one Notch and Constant Discharge

Notch Type = Rectangular, sharp crested, 100mm wide

Discharge = 2.0 1/s

Pool width = 1.00m

Water = Tap water treated with 0.3% sodium nitrite

DISTANCE OF POOL BED BELOW NOTCH (CM)	LOWER POOL DEPTH (CM)	WATER TEMP. (^{o}C)	DISSOLVED OXYGEN % SATURATION		DEFICIT RATIO	
			ABOVE WEIR	BELOW WEIR	r	r_{15}
80.5	31.0	14.8	40.1	62.1	1.58	1.58
	37.4	15.0	39.8	60.1	1.51	1.51
	24.3	15.1	37.8	61.2	1.60	1.60
	17.3	15.2	38.2	60.0	1.55	1.54
126	45.8	17.1	36.3	68.4	2.02	1.96
	37.0	17.2	39.0	71.0	2.10	2.04
	28.6	17.0	35.7	69.0	2.07	2.02
	19.2	16.9	42.5	70.2	1.93	1.88
	24.0	16.8	40.6	70.4	2.01	1.96
	31.6	13.8	47.0	72.4	1.92	1.95
	27.4	16.6	41.6	70.8	2.00	1.96
	33.8	16.7	38.2	69.7	2.04	1.99
	40.2	16.8	39.5	69.8	2.00	1.96
	23.1	16.9	39.0	68.7	1.95	1.90
	14.3	17.0	38.8	65.0	1.75	1.71
157	45.7	16.7	36.0	72.3	2.31	2.25
	35.6	16.9	34.6	73.0	2.42	2.35
	30.5	17.1	34.5	73.0	2.43	2.35
	24.5	17.1	34.8	71.6	2.30	2.23
	17.3	17.2	34.7	69.0	2.11	2.04
200	45.6	19.0	43.0	79.9	2.84	2.66
	32.0	19.0	43.5	80.5	2.90	2.71
	25.8	19.1	43.3	79.6	2.78	2.60
	26.8	19.2	42.6	80.0	2.87	2.68
	11.1	19.3	43.2	74.7	2.25	2.12
245	42.7	20.2	42.0	83.7	3.56	3.24
	33.7	20.3	39.9	83.5	3.64	3.31
	27.0	20.4	40.5	82.8	3.46	3.15
	15.1	20.4	38.4	77.7	2.76	2.54
	38.0	20.5	40.9	83.9	3.67	3.33

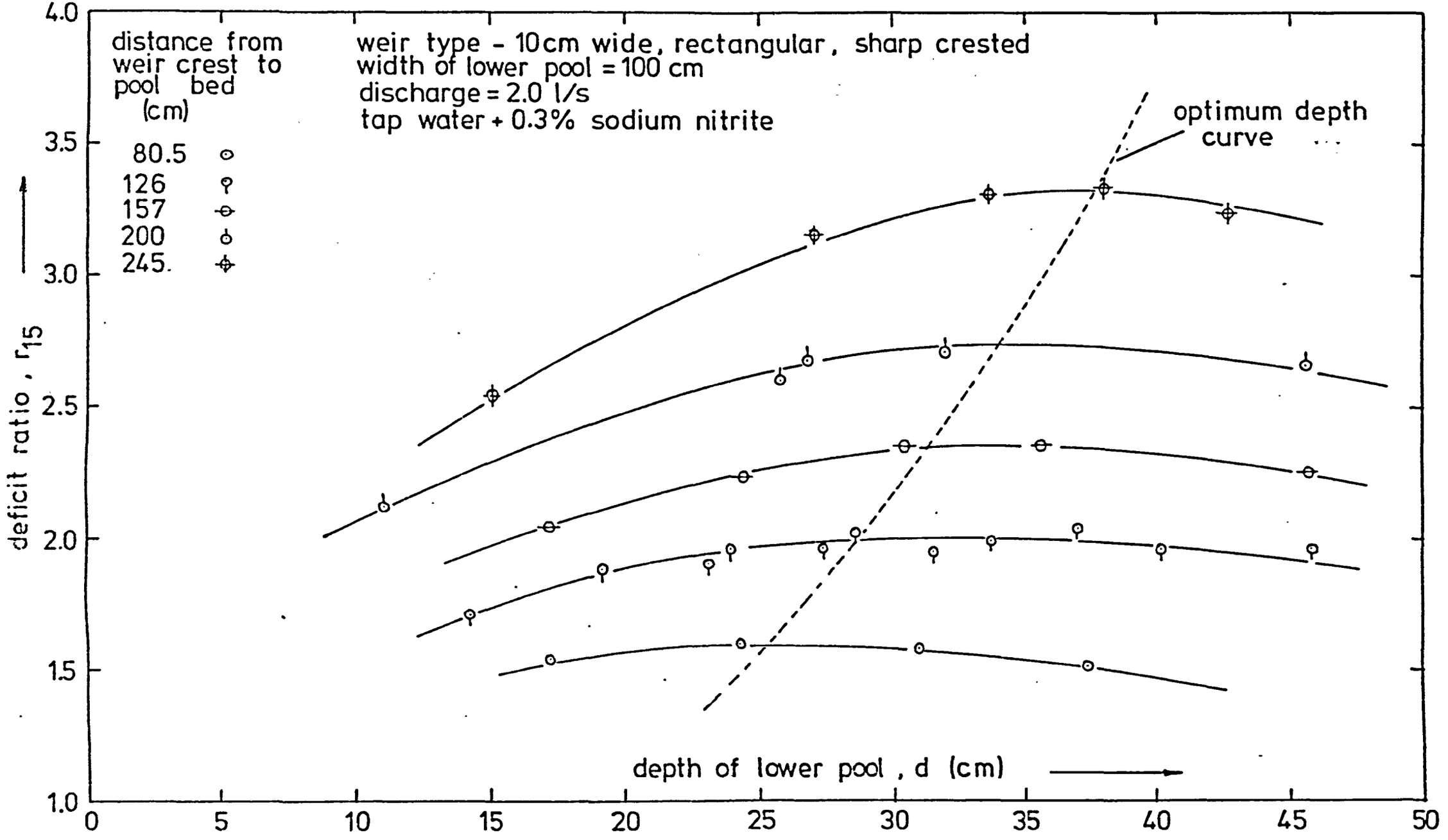

figure 6.3 effect of varying the pool depth on the deficit ratio for various elevations of the lower weir pool

for the lower pool fixed in position; an increase in depth beyond the optimum depth provides no further increase in bubble contact time and the reduced aeration experienced is as a result of the reduction in the available height of fall. For depths leading up to the optimum depth, the increase in aeration due to increasing contact time clearly outweighs the drop in aeration due to the reduction in height of fall.

For a particular weir situation the maintenance of optimum depth conditions is desirable for both reasons of oxygen uptake and in order to avoid excessive scour on the river or stilling pool bed.

The optimum depths observed in Figures C2.1 to C2.7 (Appendix C) have been plotted in Figure 6.4 against the height of fall. The general trend for a constant height of fall is an increase in d' for an increase in discharge. The plunging jet can be visualised as losing part of its energy at impact with the water surface and the rest through the process of entraining large quantities of air into the pool. The higher the discharge then the larger the cross sectional area presented at impact, but, the observations in Figure 6.4 show the lower discharge jets requiring a smaller entrainment depth due, possibly, to their capacity to entrain relatively larger quantities of air. The ratio of surface area to volume of the jet is clearly a controlling factor in the air entraining process.

This discussion is confined to the jets tending to a circular cross section ($0.6 < Q < 2.5$ l/s) - the contrasting behaviour shown by the jet $Q = 5$ l/s in Figure 6.4 illustrates the effect of jet shape. This jet was essentially a broad flat jet and these are treated in more detail in Chapter 7.

The attainment of a constant value of d' at high heights of fall noted with the lower discharges ($Q < 2.0$ l/s) is undoubtedly due to the

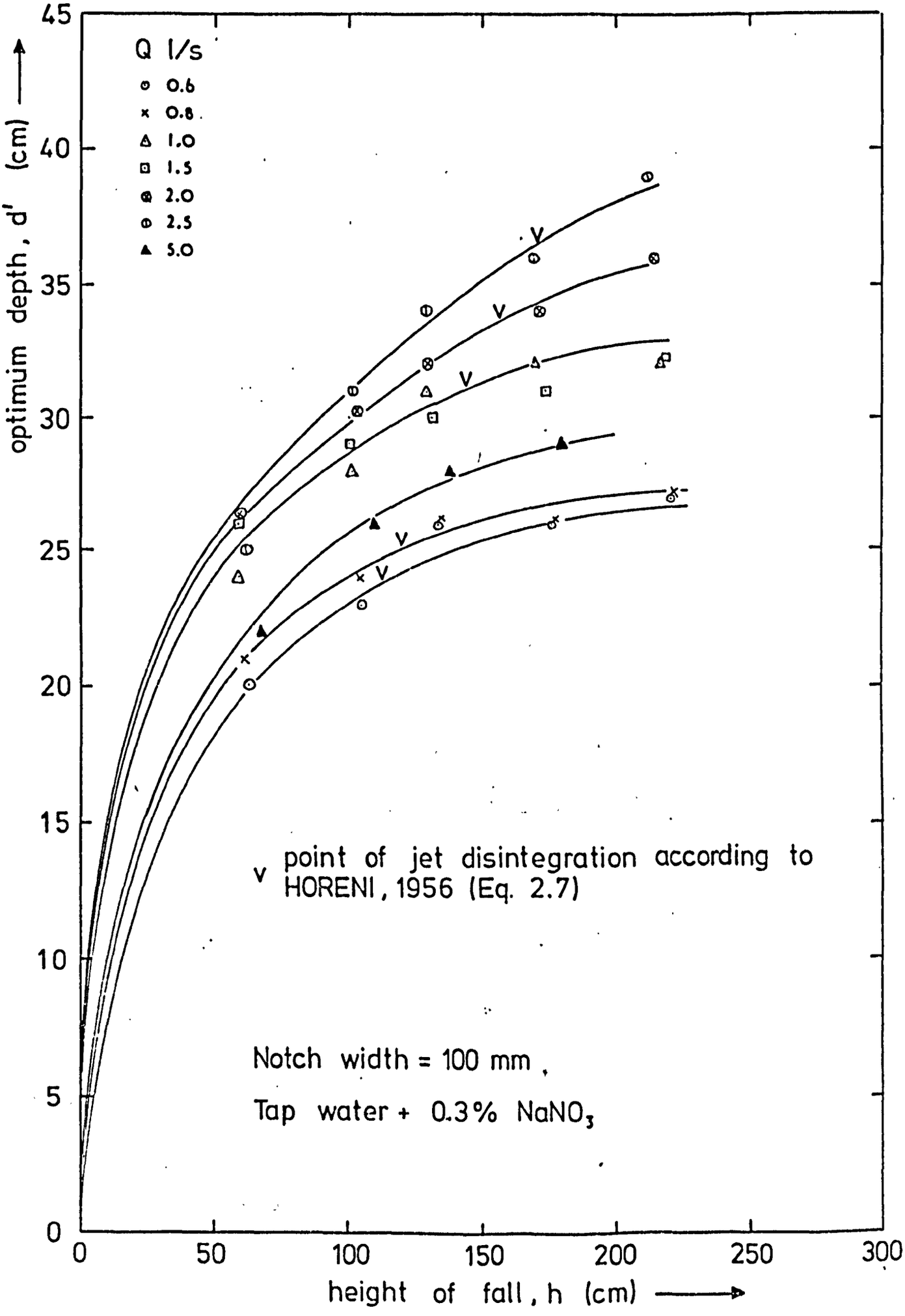

figure 6.4 the effect on optimum depth of varying discharge for a particular rectangular notch

disintegration of these jets. The point of disintegration of the various jets as determined from the equation of HORENI (Equation 2.7) has been marked in Figure 6.4. The application of this equation was generally validated by visual observation of these jets. The point of disintegration was identified as the point at which the jets were seen to have expanded in cross sectional area and broken up across the width of the jet - an observation which is quite consistent with those of HORENI. The disintegration of the jets will be accompanied by a loss of jet energy which is reflected by no significant increase in penetration depth for falls in excess of that at which disintegration occurs. The process of disintegration is progressive and therefore not instantaneous and the height of fall at which the optimum depth ceases to increase with height of fall will not necessarily be specifically described by HORENI's equation. This is illustrated by the higher discharges 2.0 and 2.5 l/s in Figure 6.4.

The disintegration of a jet is illustrated in Plate 6.3 (facing the weir) and also in Plate 6.4 (the jet viewed from the side). The development of oscillation and subsequent break up of the jet is plain to see and can be further appreciated if Plate 6.3 is compared with Plate 7.1. This latter plate shows a different but solid jet photographed shortly after discharge from the notch.

6.4.2 Variations in Oxygen Uptake

For all the discharges studied and for pool depths greater than or equal to the optimum, the deficit ratio has been plotted against the height of fall, h (difference between water levels), in Figure 6.5.

The data for each discharge fall clearly on separate curves with a reduction in oxygen uptake apparent for any increase in discharge

PLATE 6.3 A disintegrating jet viewed head-on

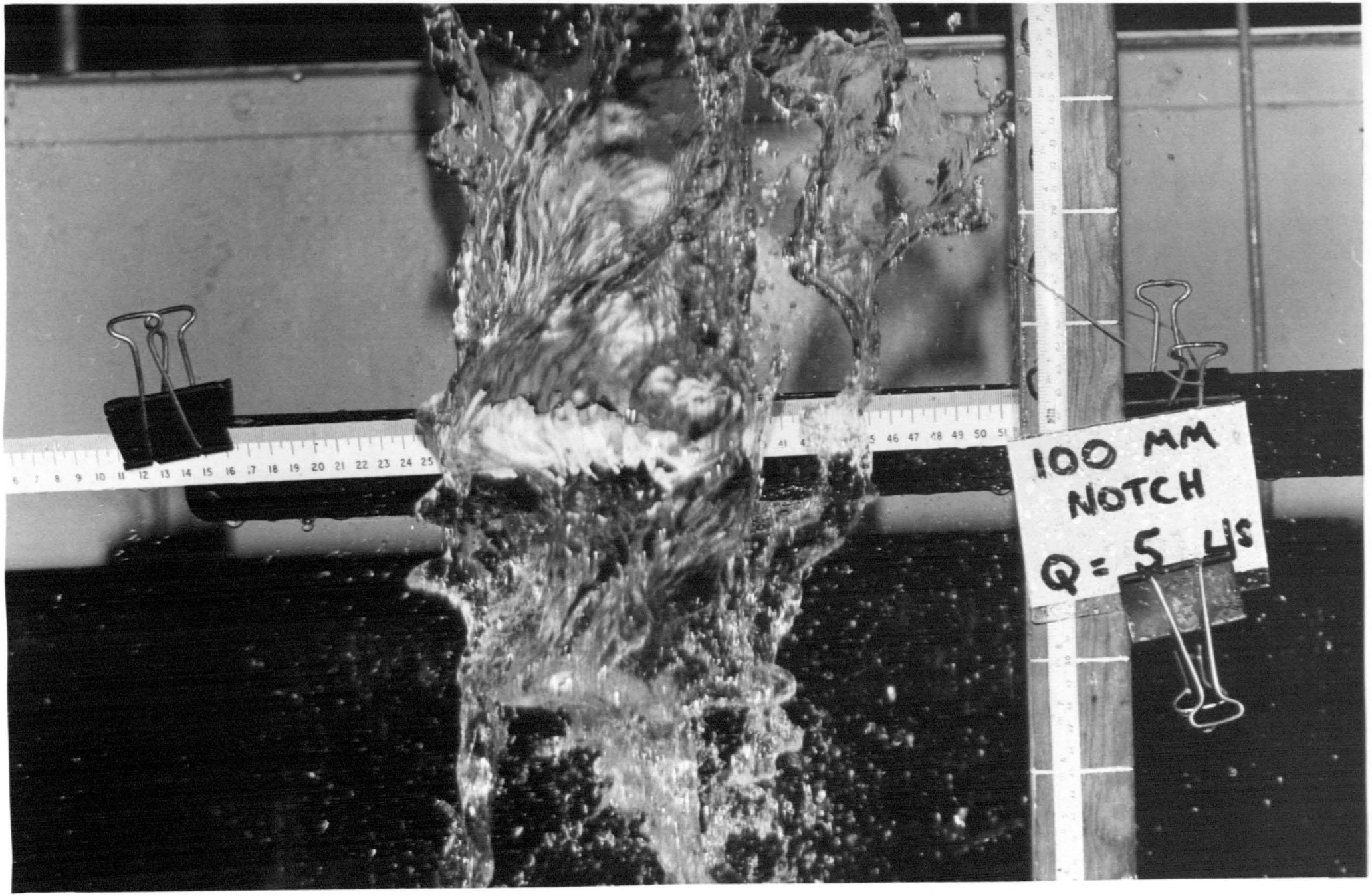

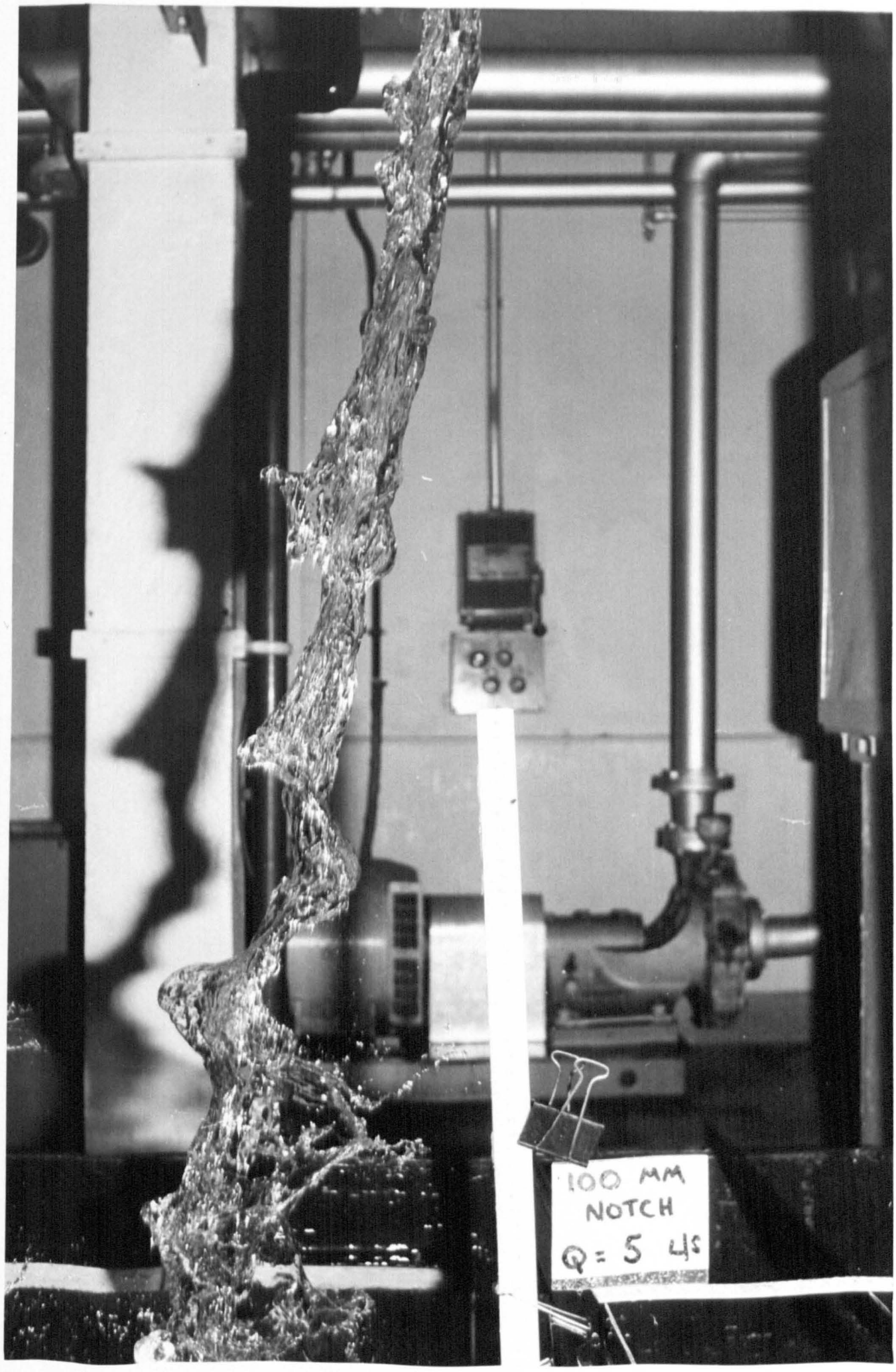

PLATE 6.4 A disintegrating jet viewed from the side

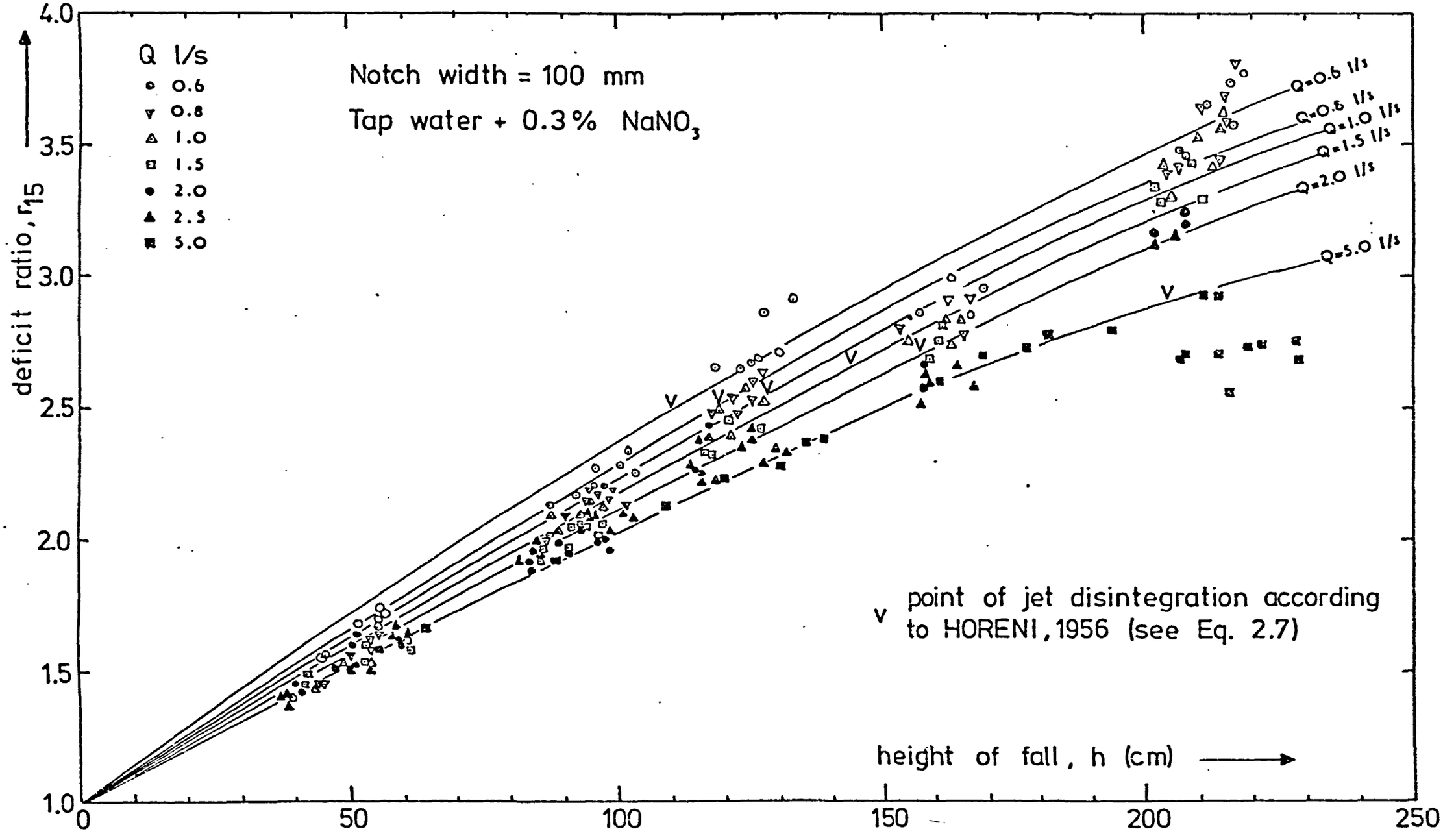

figure 6.5 the effect of discharge on oxygen transfer for a particular rectangular notch discharging into a pool of width=1.0 m and depth ≥ the optimum depth.

between 0.6 and 2.5 1/s. This agrees with the findings of VAN DER KROON and SCHRAM although NAKASONE recorded a completely opposite effect. For an increase in discharge from 2.5 to 5.0 1/s there is no further reduction in oxygen transfer, in fact, the curves for these two discharges are practically coincident. This is attributed to the shape of the free falling jet. For discharges 0.6 to 2.5 1/s the jet was observed to contract during the free fall showing a tendency towards a circular cross section. VAN DER KROON and SCHRAM recorded a similar tendency. However, the jet for discharge 5.0 1/s was observed to expand in width after passing through the notch and thereafter showed no tendency to contract. In fact this jet proved very unstable, oscillating markedly during its free fall. In view of the high specific discharges tested by NAKASONE it is possible that his jets behaved similarly to this jet. The specific discharge 500 cm^2/s tested here might indicate a turning point in the oxygen uptake variation with specific discharge towards a similar trend to that observed by NAKASONE. It would have been interesting to test this by further experiments with higher specific discharges. Unfortunately it was not feasible to pass a higher discharge through the apparatus though a separate set of tests with an even narrower notch might have been considered.

The points of disintegration of the various jets have been marked in Figure 6.5 (according to equation of HORENI, Equation 2.7) but there is no apparent change in the rates of aeration thereafter.

The disintegration of the jet will result in a more significant oxygen absorption by the jet prior to impact with the pool due to the larger air/water interface created. Plate 6.3 illustrates the disintegration of a jet into water droplets. However, as seen in

Figure 6.4, the depth of jet penetration will be adversely affected, although from the results in Figure 6.5 it is clear that the disintegrated jets continue to entrain large volumes of air.

The varying effects of discharge are apparent from the results in Figures 6.5 and 6.1 but are also somewhat confusing. Apart from the effects of changing the discharge itself they serve to illustrate the importance of the jet shape and the effects of changing it. The influence of the jet shape is not surprising since this determines the perimeter of the jet and thus will regulate the quantities of air entrained into the pool. The depth to which air will be entrained into the pool will also be affected by the jet shape as was pointed out with Figure 6.4.

Effects of varying jet shape for constant discharge are discussed in detail in Chapter 7.

The variation in deficit ratio with height of fall displayed in Figure 6.5 follows the same pattern as the experiments of the D.O.E. (1973). The magnitude of the values of deficit ratio obtained in the current studies is generally higher than the curve produced by the D.O.E., although the curve for the highest discharges studied is only slightly above the D.O.E. curve. The D.O.E. experiments were conducted using a 220mm wide notch passing a discharge of 1.82 l/s. (Details by private communication.) This jet similarly contracted rapidly during its free fall, but, the downstream pool being only 30cm square, the retention time was substantially lower than in the current experiments. The effect of retention time is tested and discussed fully in Section 6.5.

6.4.3 The Contrasting Results of APTED (1975)

APTED reported on similar experiments to test the effect of discharge for a single height of fall. Although the tests reported in this chapter were obtained from the same apparatus with only minor modifications, the contrasting results obtained were unexpected.

Figure 6.6 contains the results of APTED for the bed of the downstream pool 1.15m below the weir crest together with those obtained during these studies for the pool bed 1.26m below the notch. First, it is noticeable that the optimum depths are similar in both graphs but that the peak deficit ratios for APTED's lower discharges are in fact lower than those for the highest discharges. The experience of the current studies contradicts this. Whereas at shallow pool depths the variation displayed by APTED's data with discharge is similar to that shown by these current studies it is clear that as the pool depth increases, APTED's data begins to show a reversal of this trend - a trend which is in no way apparent from the current studies.

The reasons for this became certain during early tests for which the dissolved oxygen electrode was placed directly in the weir pools and as close to the outflow sections as possible. This technique was the same as employed by APTED and also JARVIS, and indeed similar results to those of APTED were initially collected until it was noticed that agitation of the electrodes resulted in a rise in the indicated oxygen level. Despite attempts to place the electrodes in regions of highest velocity, these were apparently insufficient to eliminate the oxygen depletion which was occurring in the electrode vicinity. This source of error was eliminated by the enclosure of the electrode in a perspex cell (See Appendix A.8, also Plate A.1) and

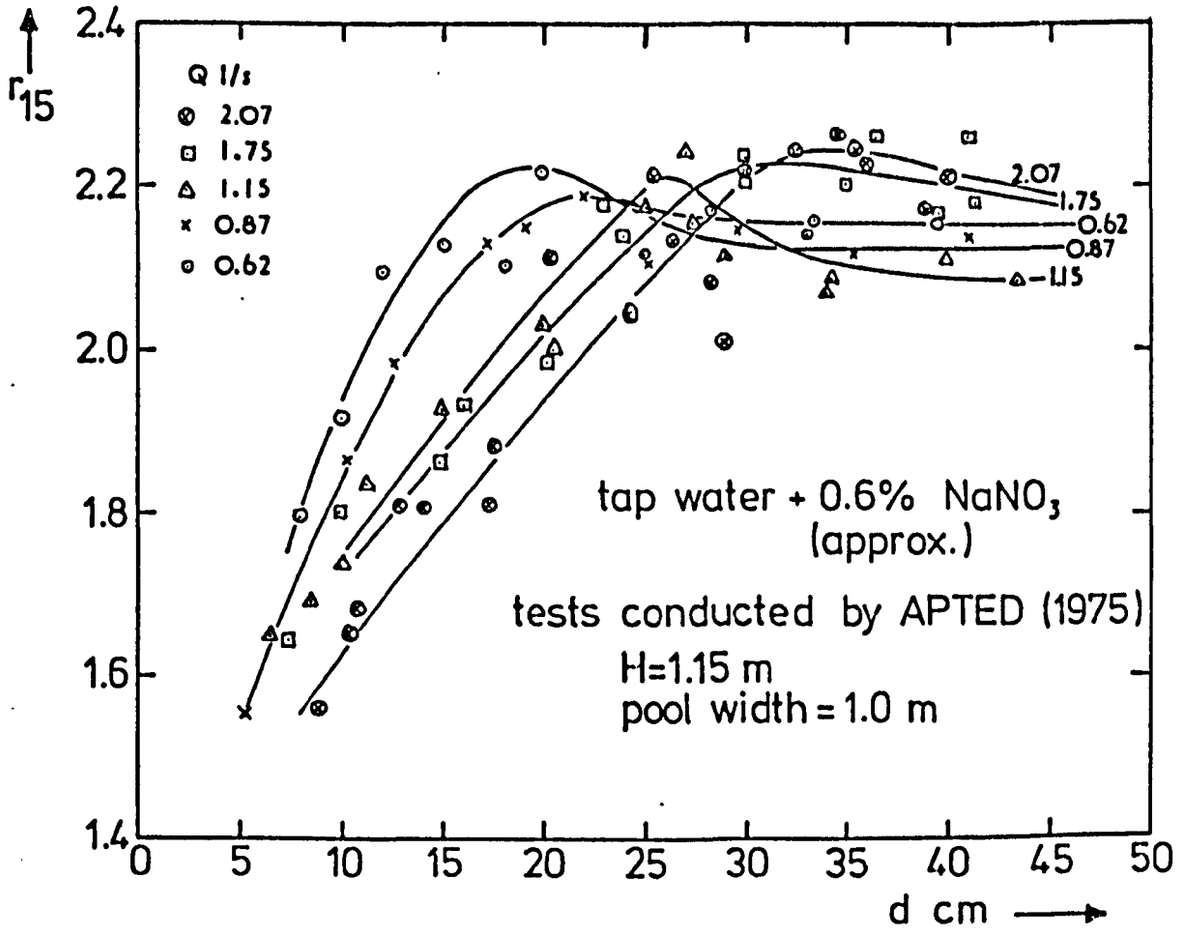

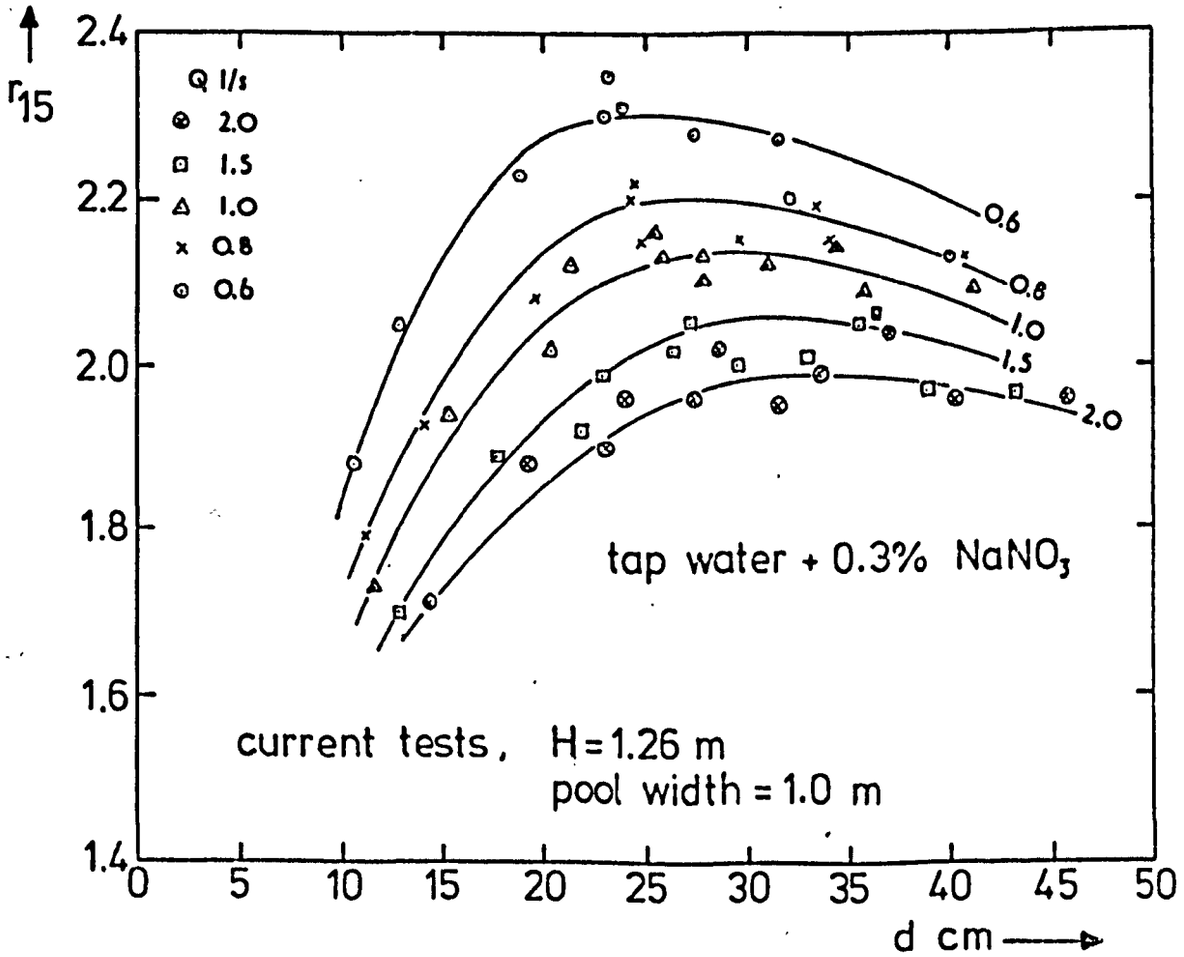

figure 6.6 discharge effects observed during current experiments compared with the observations of APTED for an identical notch of width 100 mm.

the subsequent passage of siphoned sample water through the cell.

The belief that APTED's data was affected by inadequate flow velocities passing his measuring electrodes is consistent with the trends displayed by his data in Figure 6.6. For shallower depths of pool (i.e. higher flow velocities) APTED's data does not contrast with the currently reported experiments. However, for a deeper pool and low discharges (i.e. low flow velocities) the deficit ratios indicated by APTED are depressed compared to the data for his higher discharge. Again, this is considered to be indicative of the occurrence of oxygen depletion. It is also believed that JARVIS's data is equally suspect and further evidence to support this argument is presented in Section 6.5.

The deficit ratios for the current studies are generally not significantly different from those of APTED portrayed in Figure 6.6 - this does not invalidate the above argument. The laboratory water contained approximately 0.6% sodium nitrite at the time of APTED's experiments, which is double that in the current studies. It is demonstrated in Chapter 4 that increasing the concentration of sodium nitrite results in a significant increase in deficit ratio - this is not apparent when APTED's data are compared to the current studies and is further evidence of the dissolved oxygen starvation discussed above.

In the light of the above findings, it was clearly necessary to repeat all APTED's experimental work as well as to expand on it.

6.5 THE EFFECT OF REDUCING THE DOWNSTREAM POOL WIDTH

6.5.1 Introduction

The experiments reported so far were carried out for the maximum pool width of 1.00m. In this case the sides of the pool were judged to

exert no influence on the behaviour of the bubbles. It might be argued that this was an unrealistic model since the width of pool beneath a prototype weir will generally be the same as the width of weir above it. Indeed, the experiments of VAN DER KROON, NAKASONE, and the DEPARTMENT OF THE ENVIRONMENT (Water Pollution Research Laboratory) all employed a downstream channel of similar width to the weir crest, but, it was felt that if the walls of the channel did exert an influence then in a prototype situation the influence would probably not extend far from the boundaries, whereas in the very much smaller model situation such side influences, if indeed they did exist, would probably then be felt across the full width of the channel.

The influence of the sides of the channel will certainly affect hydraulic conditions in the pool but should not alter the quantities of air being entrained by the jet.

A significant reduction in the width of the pool will restrict the sideways spread of the bubbles *thus* perhaps adversely affecting the bubble contact time. On the other hand, this reduction will increase the velocity of flow along the length of the channel thus perhaps increasing the contact time by increasing the path length travelled by the bubbles in their rise to the surface. Again, the reduced pool width results in the more rapid removal of water from the pool. The water is therefore available for further contact with entrained air for a shorter length of time. This will apply also to the contribution to aeration through the pool water surface.

Recourse was made, therefore, to experiment to investigate what effect, if any, there was on the oxygen transfer. For all previously investigated elevations of the lower pool, the width was reduced successively from 1.00 to 0.44m and finally to 0.15m. The

experimental technique was as earlier described in this chapter.

6.5.2 Results of Experimental Work

Reference is made again to Figures C2.1 to C2.6 which also contain the data for the additional two pool widths studied. A typical representation of this data is provided in Figure 6.7 - the deficit ratio variation with pool depth for various elevations of the pool and a constant discharge of 0.8 l/s.

It is clear from Figure 6.7 that for the two highest pool bed elevations, namely 0.80 and 1.26m below the weir crest, that there is no apparent effect from reducing the pool width.

As the pool is dropped further, however, an effect becomes apparent, becoming more noticeable the further the lower pool is lowered. This is not surprising in view of the greater energy losses occurring in the pool for the greater heights of fall. It is at these greater heights that the side influences should be greatest.

The results for the channel reduced to width 0.44m show a slightly reduced deficit ratio but otherwise follow closely the pattern displayed at the maximum width 1.00m. There is no significant change in the depth at which optimum aeration is achieved. For the channel reduced further to 0.15m there is a further reduction in the values of deficit ratio achieved and the optimum deficit ratio is reached at substantially the same depth as in the two wider pools. For depths greater than the optimum, however, there is no indication of any fall off in the values of deficit ratio attained such that for depths in excess of the optimum the deficit ratio recorded is substantially the same whatever the pool width.

It would seem that comments made in Section 6.5.1, concerning a loss of contact time when the pool width is significantly reduced

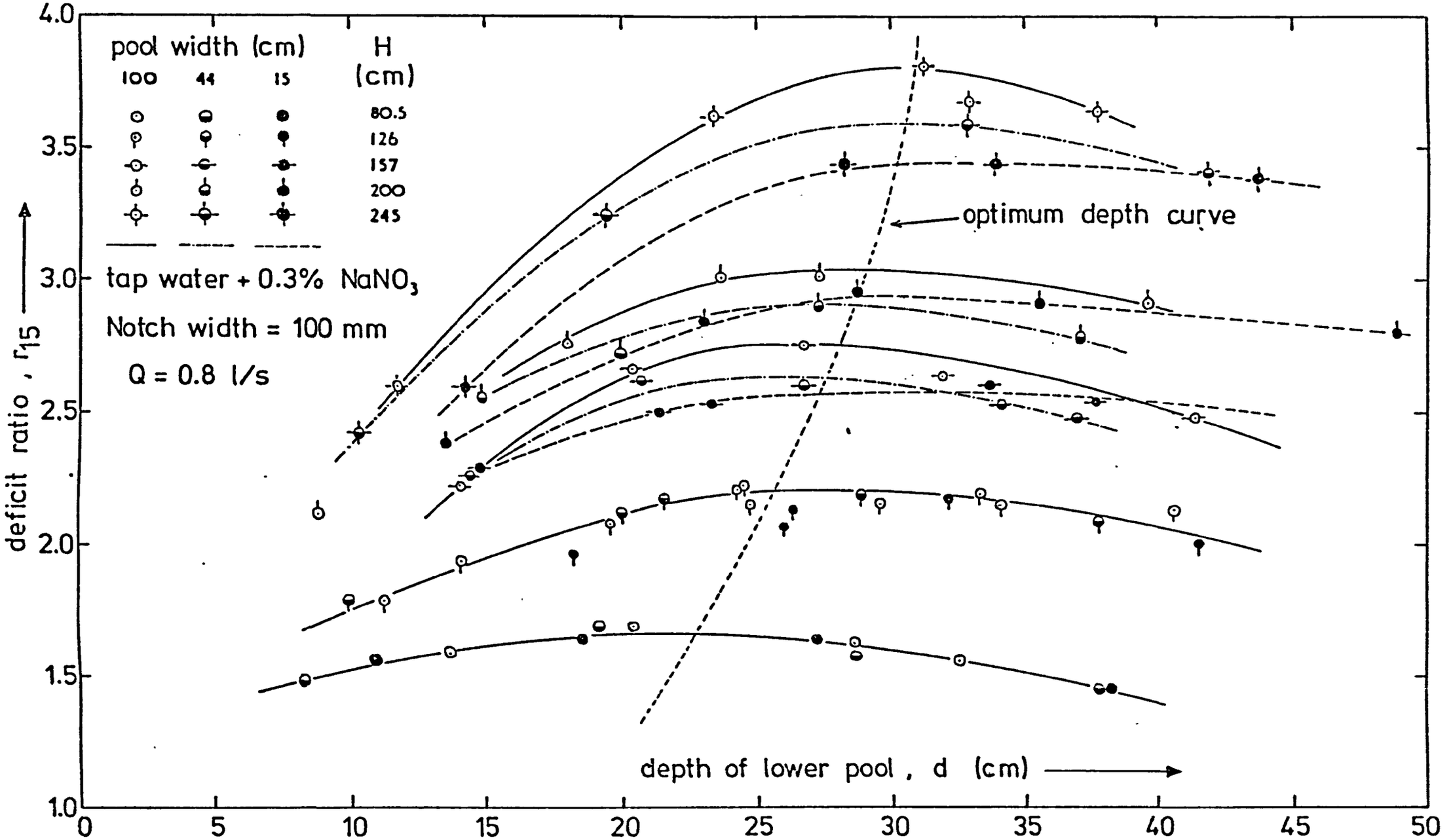

figure 6.7 the effect of reducing the pool width for a fixed discharge and various elevations of the lower weir pool.

were correct, though, for practical purposes the reductions in deficit ratio recorded are not very significant. Also, the fact that such effects were noticeable only at the greater heights of fall indicates that the retention time of water in the pool is not a significant factor and that surface aeration is negligible. Undoubtedly this is because the water jet is substantially saturated with oxygen immediately after entry into the pool with the effect that any subsequent exposure to air, either entrained or at the surface, contributes negligibly to the oxygen transfer.

6.5.3 Results Contrasted with those of JARVIS and APTED

The conclusion from the experiment above is that a reduction in the pool width will result in a reduction in deficit ratio. In contrast JARVIS reduced his pool width from 0.600 to 0.305m for one height of fall and recorded an increase in the deficit ratio at all depths of pool. APTED's results similarly indicated a general tendency for the deficit ratio to increase with reduction in pool width. JARVIS's data, together with some of APTED's (for optimum depth of pool) are reproduced in Figure 6.8 and contrasted with some results reproduced from Figure 6.7.

These contrasting results confirm the suggestions in Section 6.4.3 concerning the occurrence of oxygen depletion in the water in the immediate vicinity of the oxygen measuring electrodes. This condition occurs when these electrodes are placed in flows of insufficient velocities and as a result the indicated oxygen levels are too low. The effect of reducing the pool width during the experiments of both APTED and JARVIS was to increase the flow velocities and this probably led to a reduction in the condition of oxygen depletion in the water in contact with their electrodes, and, hence the higher oxygen readings they obtained on reduction of pool width. Coupled with the

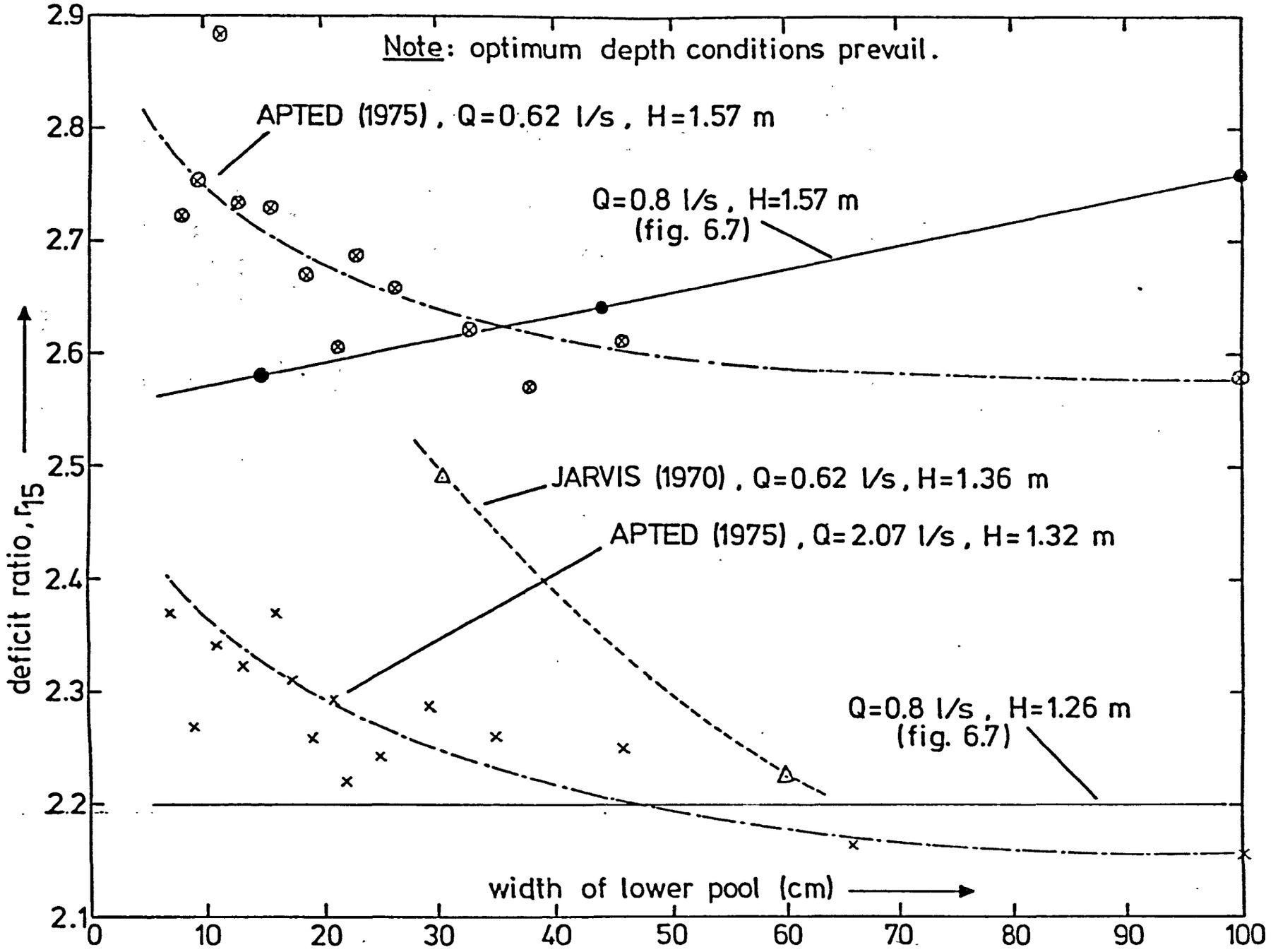

figure 6.8 the effect of varying pool width reported by JARVIS and APTED contrasted with current tests

evidence in Section 6.4.3, serious doubts must be expressed about the accuracy of the oxygen measurements of both APTED and JARVIS.

6.6 SUMMARY

The experiments have confirmed the existence of an optimum depth - the depth at which, for a constant stilling pool bed elevation, optimal aeration is achieved. This depth corresponds to the depth to which the entrained air will penetrate if unimpeded (D.S.I.R., 1958). For depths less than this optimum there was a loss of contact time and thus of aeration also. For depths greater than this optimum (for fixed pool bed) there was no further gain in contact time and thus a loss in aeration as a result of the associated reduction in height of fall. These results are consistent with those of the D.O.E. and JARVIS. The optimum depth was shown to increase with increasing height of fall although the disintegration of the jet was shown to affect this increase. For the jets which contracted and tended to a circular cross section, an increase in the optimum depth for constant height of fall was observed with increasing discharge. This was similarly demonstrated by APTED for one height of fall. The effect of jet shape has been recognised and is dealt with in Chapter 7.

An increasing discharge has been shown to result in a reduction in oxygen uptake which is consistent with the findings of VAN DER KROON and SCHRAM. These results have emphasised the importance of the jet perimeter since this affects the quantities of air entrained. The disintegration of the jets did not appear to result in any noticeable change in the rate of oxygen transfer.

The reduction in the downstream pool width resulted in small but practically insignificant reductions in the aeration achieved. This

contrasted with the observations of JARVIS and APTED. However, doubts have been expressed as to the accuracy of oxygen measurement during both the latter researcher's experimental work and evidence has been presented to support these doubts.

The studies in this section have been confined to a series of jets which contracted rapidly during their free fall thus tending to a circular cross section and which were discharged from a sharp crested rectangular notch of width 100mm. The water during these tests contained 0.3% sodium nitrite for reasons already discussed in Section 4.3.

CHAPTER 7

THE EFFECTS OF JET SHAPE AND DISSOLVED SALTS ON THE OXYGEN UPTAKE - NEW CORRELATIONS INTRODUCING A JET FROUDE NUMBER

7.1 THE EFFECT OF JET SHAPE - AIMS AND TEST PROCEDURE

The importance of the ratio of jet perimeter to cross sectional area was demonstrated in Chapter 6. By reducing the discharge of a circular jet, a greater ratio of the jet interfacial area to volume was produced, thus greater relative quantities of air were entrained as reflected by the larger oxygen uptake recorded.

The aim of the following tests was to encourage the formation of a broad flat jet, i.e. to vary the hydraulic radius of the jet for any particular discharge. Two similar sharp crested rectangular notches were selected, with 220mm and 300mm crest lengths, and a similar set of tests to those reported in Chapter 6 was carried out with each notch. As in Chapter 6, the laboratory water contained 0.3% sodium nitrite during these tests.

The range of discharges tested was 1.0, 1.82, 2,5, 5.0 l/s for the 220mm notch and 1.0, 1.5, 2.0, 2.5, 5.0 l/s for the 300mm notch.

7.1.1 Results

7.1.1.1 The Effect of Jet Shape on Optimum Depth

This data was initially treated in the same fashion as that reported in Chapter 6. The deficit ratio was plotted for the two notches against the downstream pool depth - Appendices D1 and E1. The general observations made in Section 6.4.1 apply to this data also. In Section 6.4.1 the flat jet for Q = 5.0 l/s was shown (in Figure 6.4) to contrast with the trend set by the other rapidly contrasting jets.

The effect of this jet shape is confirmed by the optimum depth data collected from Appendices D1 and E1. For one discharge, Q = 2.5 l/s, the optimum depths have been plotted against the height of fall in Figure 7.1. Also shown are the data for this discharge from Figure 6.4.

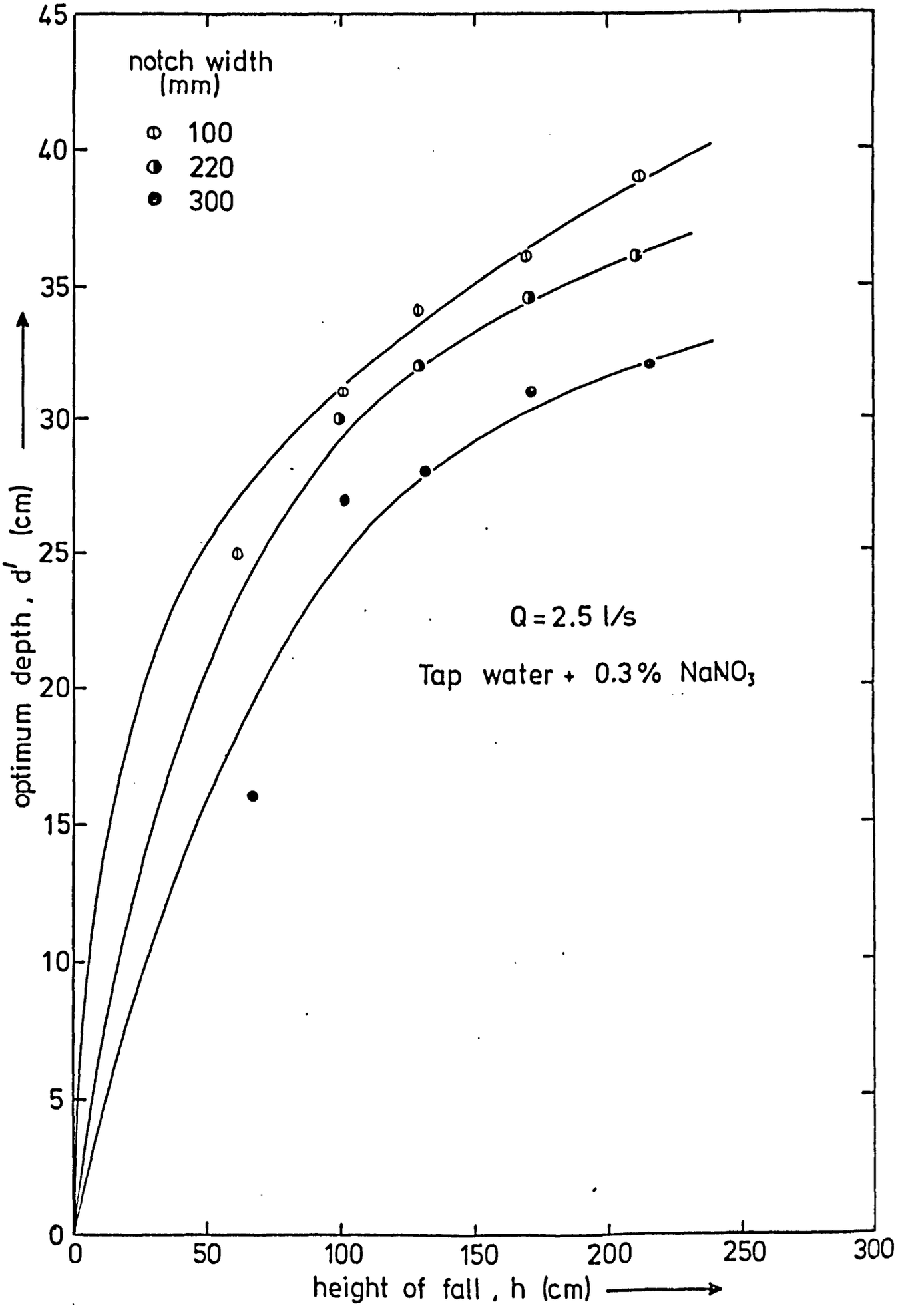

figure 7.1 the effect of jet shape on optimum depth for constant discharge.

The conclusion to be drawn is that for constant discharge and height of fall, the effect of altering the jet shape from one of circular cross section to one which is broadly rectangular is to reduce the depth to which air is entrained. This is possibly as a result of greater energy losses due to larger quantities of air being drawn into the pool. This is obviously desirable but the reduced contact time resulting might offset this advantage.

It should be borne in mind that changes in the depth of penetration affect the contact time during two phases, namely, during the forced descent of the bubbles and during the subsequent buoyant rise of the bubbles.

7.1.1.2 The Effect of Jet Shape on the Aeration Achieved

To illustrate the effects of a change in jet shape on the oxygen uptake, the deficit ratio for depths of pool greater than or equal to the optimum have been plotted against height of fall for the two notches along with data for the same discharge (2.5 l/s) from Figure 6.5. See Figure 7.2.

Despite the apparent reduction in contact time for the broader jets (noted in Section 7.1.1.1), there was a noticeable increase in the oxygen uptake recorded.

This implies that there are indeed greater quantities of air entrained by the wider flat jets and that this advantage offsets the disadvantage of a possibly reduced contact time. This greater air entrainment is consistent with the larger air/water interface offered by this type of jet.

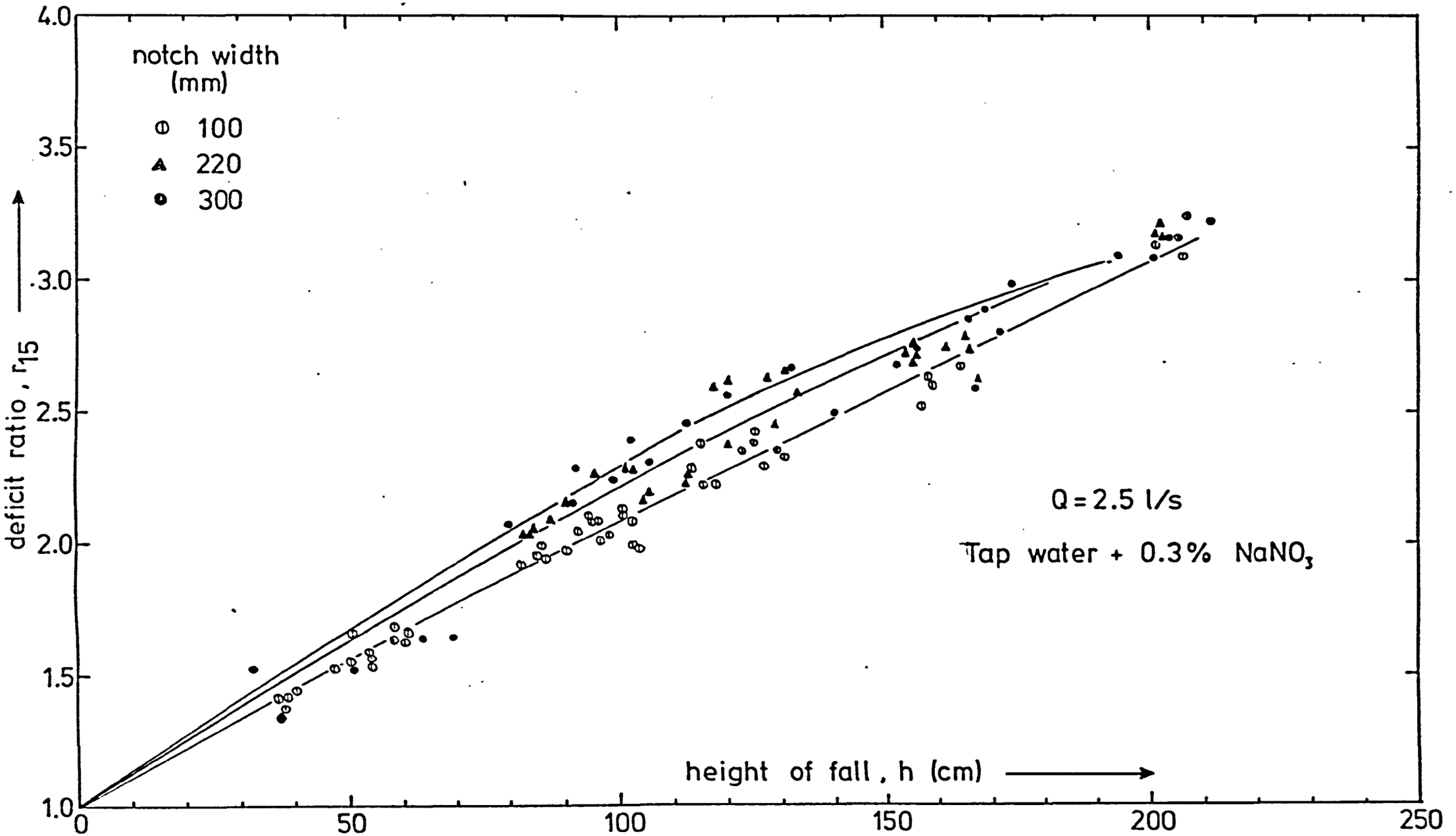

figure 7.2 the effect of jet shape on oxygen transfer for constant discharge and optimum pool depth conditions.

7.1.2 The Concept of a Jet Froude Number

7.1.2.1 General Approach

Because of the conflicting effects of bubble contact time and the quantities of air entrained, a need was felt to separate these two components and to attempt to quantify their separate effects.

To do this, it was decided to attempt to correlate the oxygen uptake with some form of jet Froude number. It was earlier (Section 2.4.2) noted that modelling air entrainment on the Froude number criterion was indeed possible and that this has been validated by a number of workers (RENNER, WISNER). The general concept shown to be true was that for a constant Froude number the ratio of air discharge to water discharge will be constant. One advantage for analysis purposes, is that this immediately fixes one of the two conflicting factors (noted earlier) contributing to the oxygen transfer, and, further, it offers the possibility of correlating oxygen transfer in some non-dimensional form. In fact this has yet to be achieved, being a major drawback with most work published to date.

7.1.2.2 The Definition of a Jet Froude Number

For a circular jet of diameter D and velocity U, the jet Froude number is defined here as :

$$Fr_J = \frac{U}{\sqrt{gD}} \qquad (7.1)$$

Further, for a circular jet and assuming a unit coefficient of velocity of the jet, we can write:

$$Q = q_J \pi D \text{ and } U = \sqrt{2gh} \qquad (7.2)$$

whence

$$Q = \frac{\pi}{4} D^2 \sqrt{2gh} \tag{7.3}$$

where Q, q_J are respectively the discharge, specific discharge of the jet, h is the height fallen.

Equation 7.1 may now be re-expressed:

$$Fr_J = \left[\frac{(2gh)^{3/2}}{4q_J g}\right]^{\frac{1}{2}} \tag{7.4}$$

For non circular jets, Equation 7.4 is also applicable:

$$q_J = R \sqrt{2gh} \tag{7.5}$$

where R is the hydraulic radius of the jet. D = 4R is an equivalent jet diameter and for q_J in Equation 7.4, $q_J = Q/P$ must be substituted where P is the perimeter of the jet at impact.

Equation 7.4 is therefore a general expression of Froude number for any solid jet for which the vertical height of fall and the discharge per unit jet perimeter, q_J, are known.

7.1.3 A Correlation of Results with Jet Froude Number

7.1.3.1 The Measurement of Jet Perimeters

The application of Equation 7.4 to the data requires a knowledge of the geometry of the various jets at various heights of fall.

The direct measurement of the widths or diameters of the jets generally proved difficult and inaccurate on account of their oscillatory

nature. Therefore it was decided to employ high speed photography to freeze each jet against a fixed calibrated scale and by taking several photographs at each position a sensible mean jet width was arrived at. A typical photograph is shown in Plate 7.1.

This photographic technique was used for all the jets studied with the 220 and 300mm notches, but the jets formed by the 100mm notch for discharges 0.6 to 2.5 1/s inclusive and 5.8 1/s were directly observed without recourse to photographs. For $Q \leqslant 2.5$ 1/s these jets were seen to rapidly tend to a circular cross section. The point at which each jet became circular was judged as the point at which the measured jet width equalled the diameter satisfying Equation 7.3.

$$\text{i.e.} \quad D = \left(\frac{4Q}{\pi (2gh)^{\frac{1}{2}}} \right)^{\frac{1}{2}} \tag{7.6}$$

Thereafter the observed jet diameters were found to be described by Equation 7.6.

The resultant jet width variations with height are summarised in Figures 7.3, 7.4 and 7.5. The behaviour of the jets for $Q \geqslant 5.0$ 1/s formed by the 100mm notch was exceptional. On passing through the notch these jets were seen to expand into a curved cross section, the upper surface of the jet being convex and the lower edge concave. As the jet fell progressively further this cross section tended to flatten with the consequent increase in jet width displayed in Figure 7.4. For these two jets it was difficult to obtain a good estimate of jer perimeter. All the other jets were broadly flat and permitted accurate measurement.

The perimeter of the jets was calculated assuming the flat jets to be rectangular.

PLATE 7.1 A solid jet viewed head-on

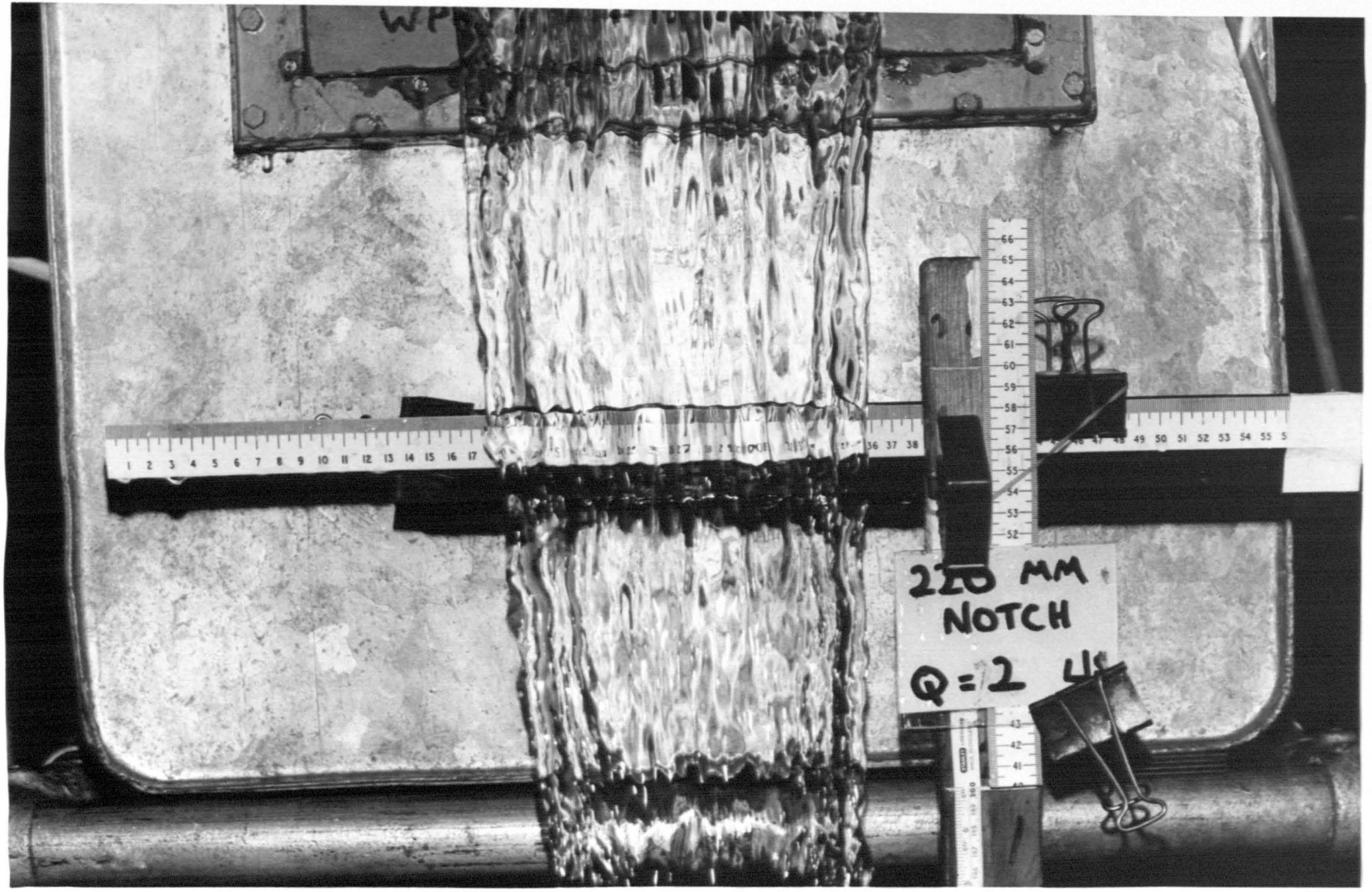

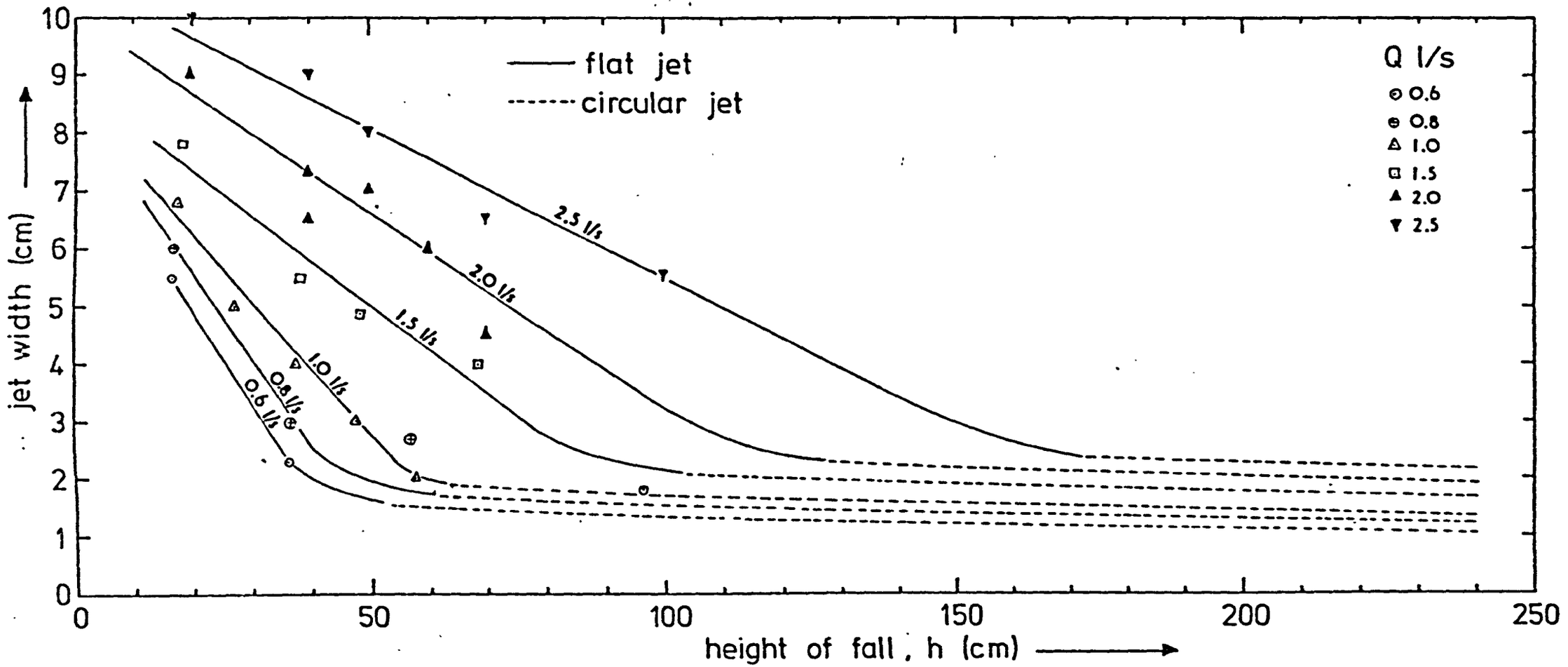

figure 7.3 variation in jet width with height of fall -100 mm notch.

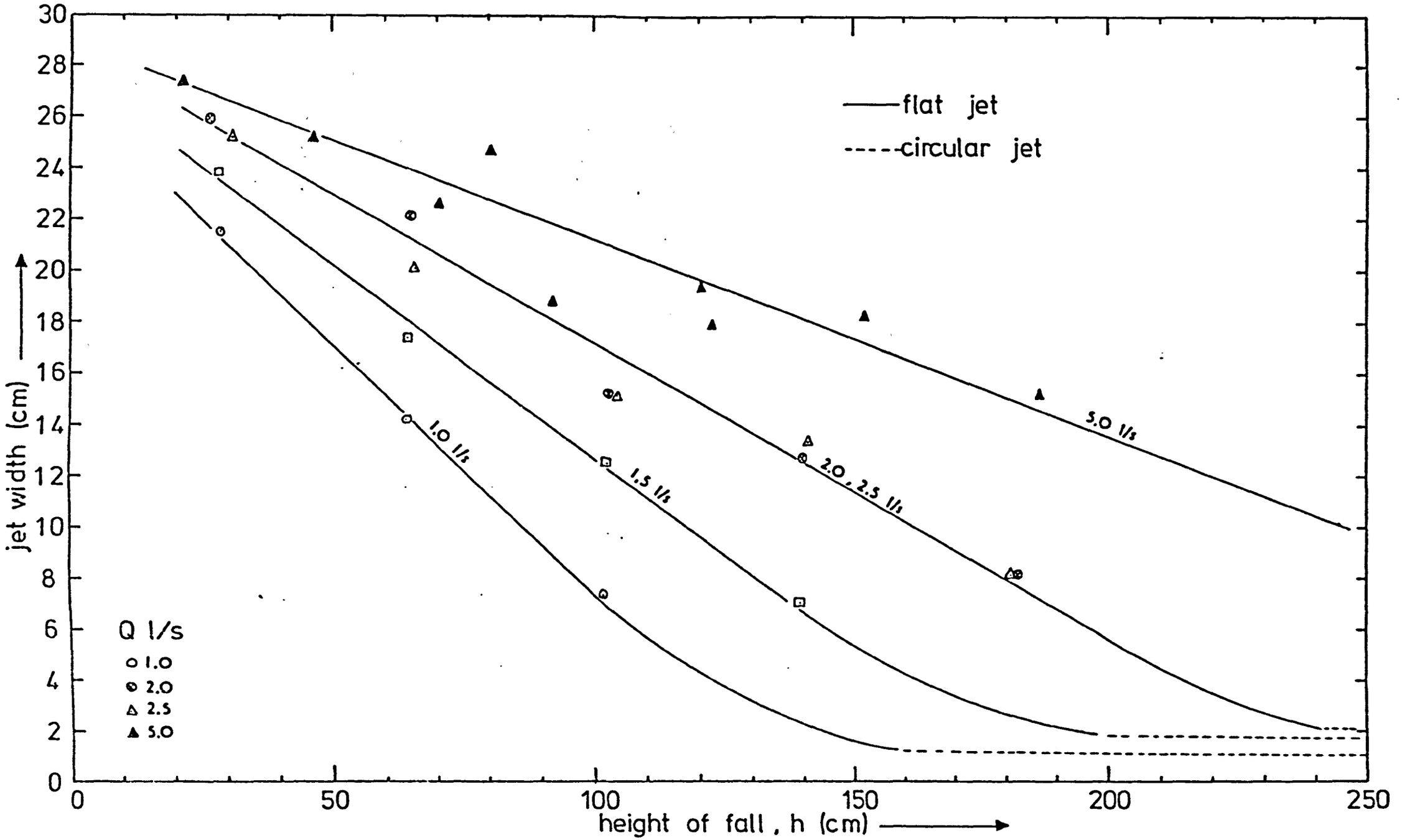

figure 7.5 variation in jet width with height of fall - 300 mm notch.

Thus

$$P = 2(B_J + t_J) \qquad (7.7)$$

where B_J and t_J are the width and thickness of the jet. t_J was estimated by using measured values of B_J and by assuming the velocity of the jet after falling through a height h to be $\sqrt{2gh}$.

whence $$Q = B_J t_J \sqrt{2gh} \quad \text{and} \quad t_J = \frac{Q}{B_J \sqrt{2gh}} \qquad (7.8)$$

Similarly, for jets of assumed circular cross section and diameter D:

$$P = \pi D$$

where D is estimated from Equation 7.6.

7.1.3.2 Application to Test Results

The calculation of the jet Froude number will of course be restricted to solid jets only. An analysis for disintegrated jets lies beyond the scope of this thesis.

For the data with depths $\geq$ the optimum depth for all three notches the Froude number has been determined from Equation 7.4 with perimeters determined as detailed in Section 7.1.3.1. The Froude numbers thus calculated are plotted against the deficit ratio in Figure 7.6. Also plotted against the Froude number, in Figure 7.7, are the optimum depths for solid jets. In Figure 7.6 no attempt has been made to separate the individual curves for all the discharges between 0.6 and 2.5 l/s for the 100mm notch. For a constant Froude

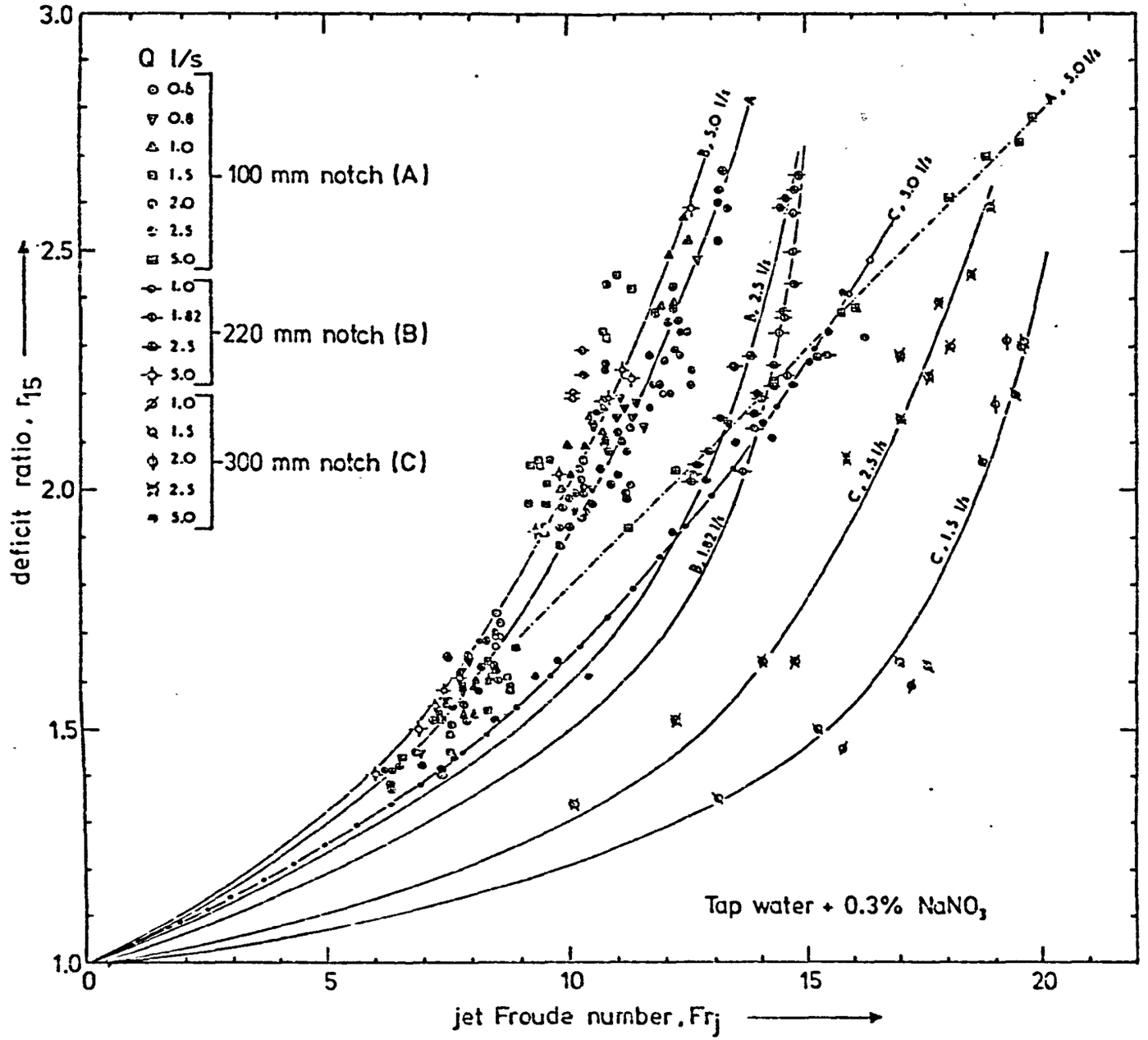

figure 7.6 deficit ratio v jet Froude number for solid jets and optimum pool depth conditions

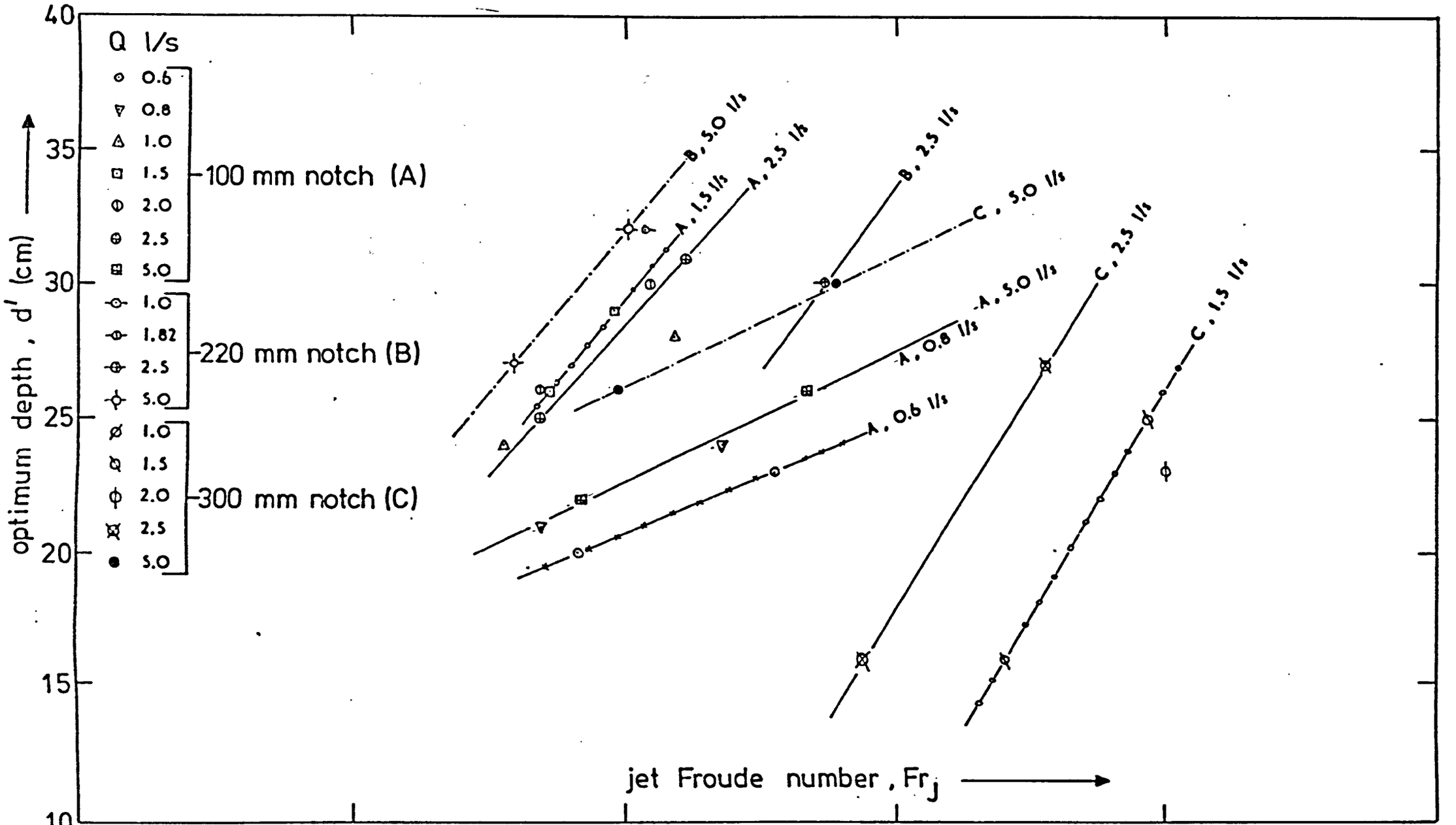

figure 7.7 optimum depth v jet Froude number (solid jets only)

number, the relative quantities of air entrained are assumed the same but a very significant variation in amount of oxygen transferred is indicated in Figure 7.6. This is in part due to the differing depths of jet penetration associated with the different jet shapes. This is well illustrated in Figure 7.7. For a constant discharge and Froude number the penetration depth associated with the flat jet formed by the 300mm notch is much less than that with the equivalent jet formed by the 100mm notch and this is reflected by the reduced oxygen levels observed in Figure 7.6 for the former notch. However the different oxygen levels recorded for constant Fr_J are due not only to different contact times but also to different heights of fall and thus different energy losses in the downstream pool. This follows from Equation 7.4. In order to keep Fr_J constant for a change in discharge or jet perimeter, a change in h is required. A practical example is provided by discharges 0.8 l/s and 5.0 l/s for the 100mm notch. In Figure 7.7 the depth of penetration for these jets is the same for constant Froude number but as seen in Figure 7.6 the oxygen transfer is lower for the higher discharge. The importance of the relative heights of fall lies in the relative levels of pool turbulence. The more vigorous the mixing in the pool the more rapidly is the film of oxygen saturated water in contact with bubbles replaced by unsaturated water with consequent more efficient oxygenation.

To summarise, for a constant Froude number, but for a variety of jets of differing perimeter and discharge, the oxygen transfer will differ according to differences in the height of fall, jet shape, and therefore depth of penetration.

7.1.3.3 A Correlation of Optimum Depth with Height of Fall and Jet Froude Number

The optimum depths presented in Figure 7.7 have been rendered non dimensional by division by the height of fall and this ratio has been plotted against Fr_J in Figures 7.8 and 7.9. The available data for solid jets is limited, but, from Figure 7.9 it is reasonable to suppose that

$$\frac{d'}{h} = K_d \, Fr_J^{-1.2} \tag{7.9}$$

and that K_d will be some function of the height of fall or scale. To test this, the height of fall for each jet has been expressed as a ratio of the height of fall for a circular jet with the same Froude number and discharge 0.6 l/s, i.e. as a scale ratio, $h/h_{0.6}$. The choice of this 0.6 l/s jet was largely a matter of convenience since this jet was circular over the whole height of fall with the diameter being conveniently calculated from Equation 7.6.

In Figure 7.10, K_d has been shown to be a function of this scale ratio, i.e. that

$$K_d = f \left(\frac{h}{h_{0.6}}\right)^{-0.42} \tag{7.10}$$

From Equations 7.4 and 7.6

$$h_{0.6} = 1.794 \, Fr_J^{1.6} \quad (h \text{ cm}) \tag{7.11}$$

The resulting correlation may be expressed as

$$\frac{d'}{h} = \frac{5.9}{Fr_J^{1.2}} \left(\frac{h}{h_{0.6}}\right)^{-0.42} \tag{7.12}$$

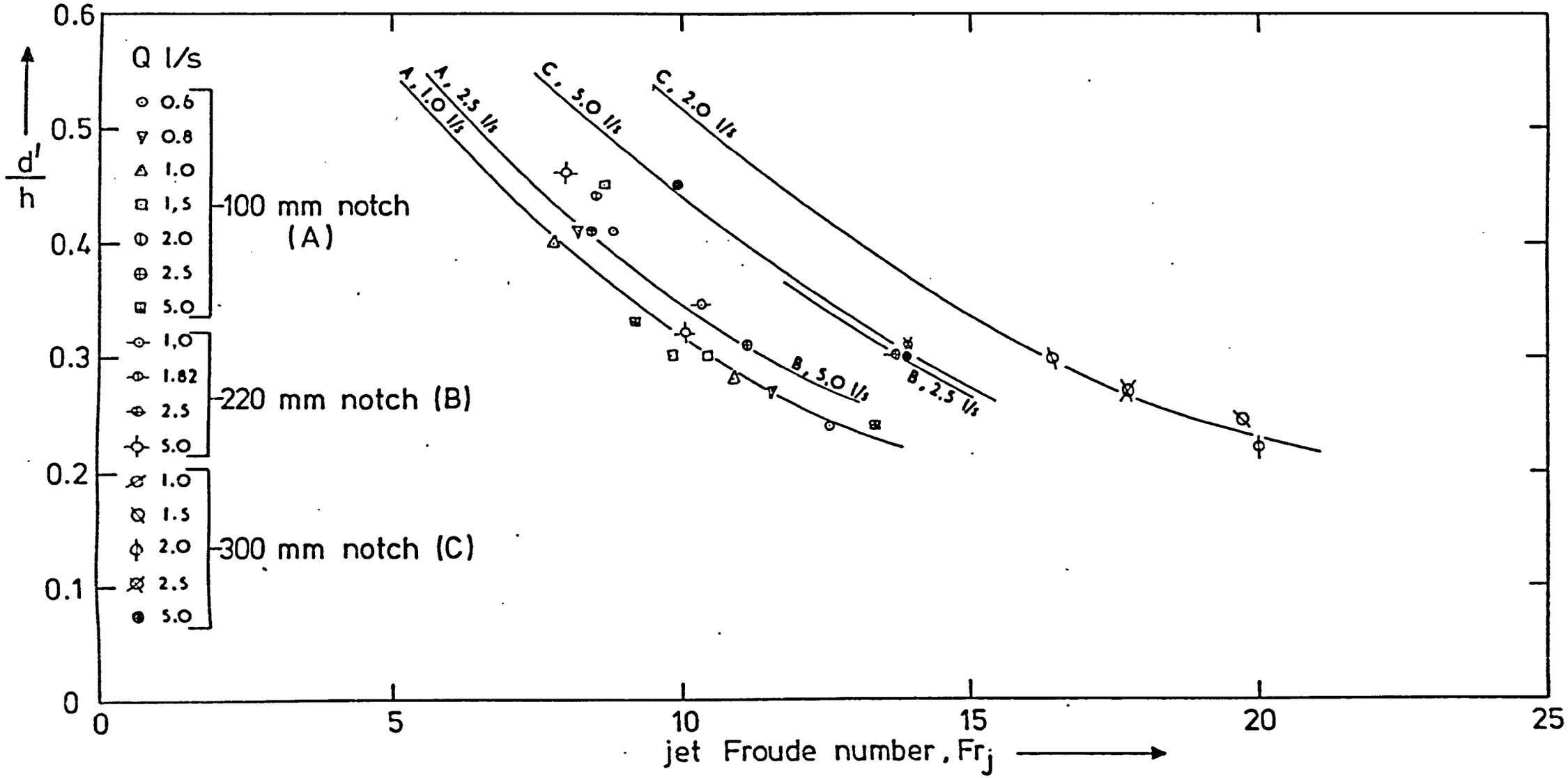

figure 7.8 ratio d'/h v jet Froude number.

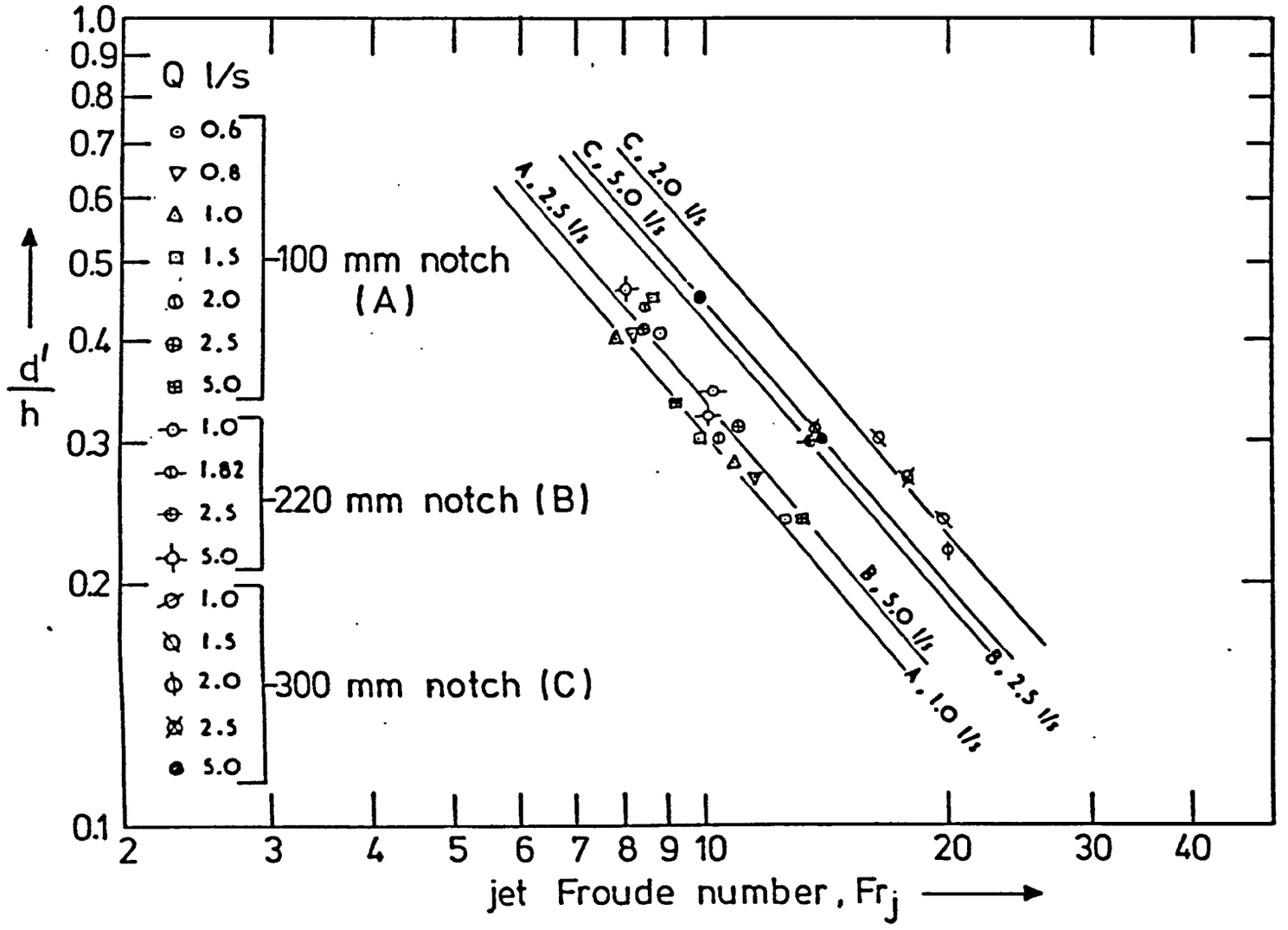

figure 7.9 d'/h v jet Froude number

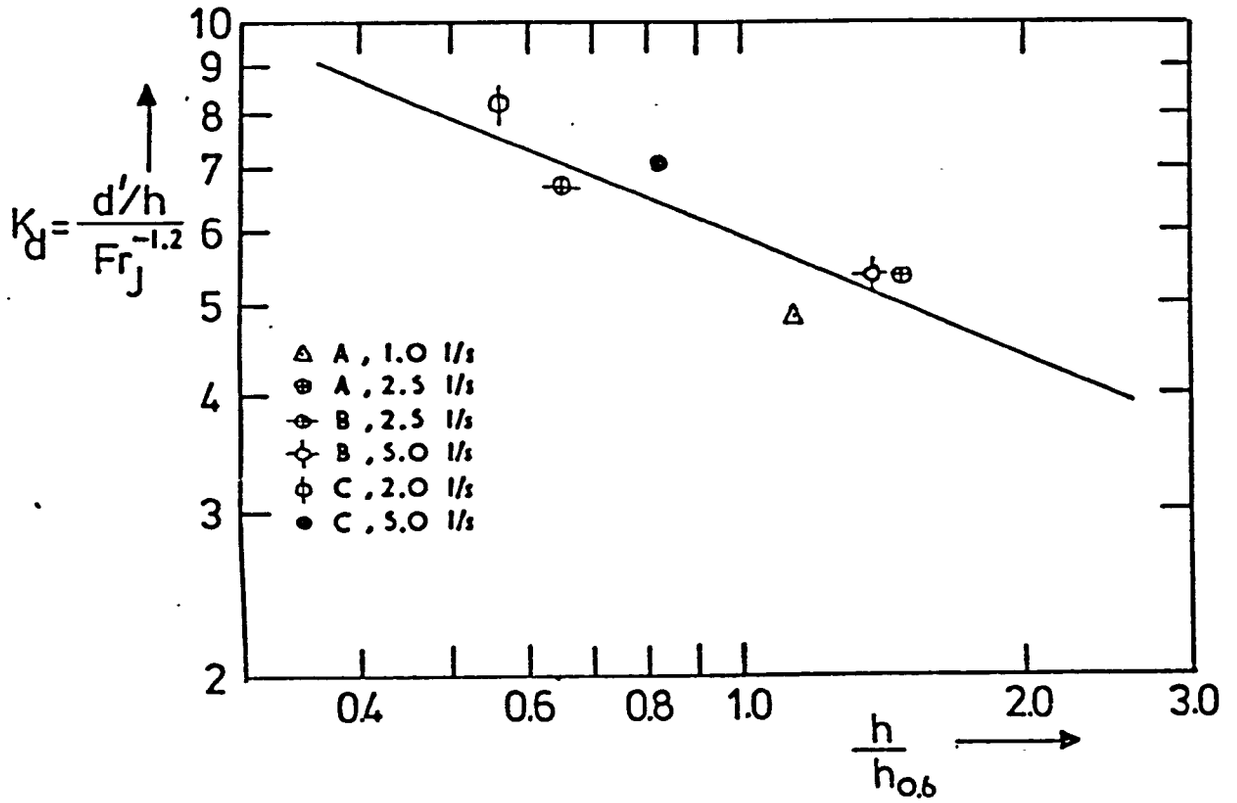

figure 7.10 K_d v $h/h_{0.6}$

Thus

$$\frac{d'}{h} = \frac{7.5}{Fr_J^{0.53}\, h^{0.42}} \quad (h \text{ cm}) \tag{7.13}$$

or

$$d' = \frac{7.5\, h^{0.58}}{Fr_J^{0.53}} \quad (h \text{ cm}) \tag{7.14}$$

This correlation has been tested against the data in Figure 7.11 where good agreement has been exhibited. Also plotted is the data collected by the D.O.E. (1973) together with that of APTED (1975). For these latter data, the jet perimeters have been determined from measurements tabulated in Figures 7.3 and 7.4 and only solid jets as determined by the equation of HORENI (Equation 2.7) have been considered.

A wider range of validity of Equations 7.13 and 7.14 is therefore suggested though it has not yet proved possible to test this in a prototype situation.

7.1.3.4 A Correlation of Oxygen Uptake with Height of Fall and Jet Froude Number

The data in Figure 7.6 have been re-plotted in logarithmic form in Figure 7.12.

From Figure 7.12 it appears that for a particular jet:

$$r_{15}^{-1} = K_J\, Fr_J^{2} \tag{7.15}$$

As already discussed in Section 7.1.3.2, for a constant Froude number, the oxygen uptake will vary according to the contact time and energy loss in the pool. It is therefore probable that K_J in

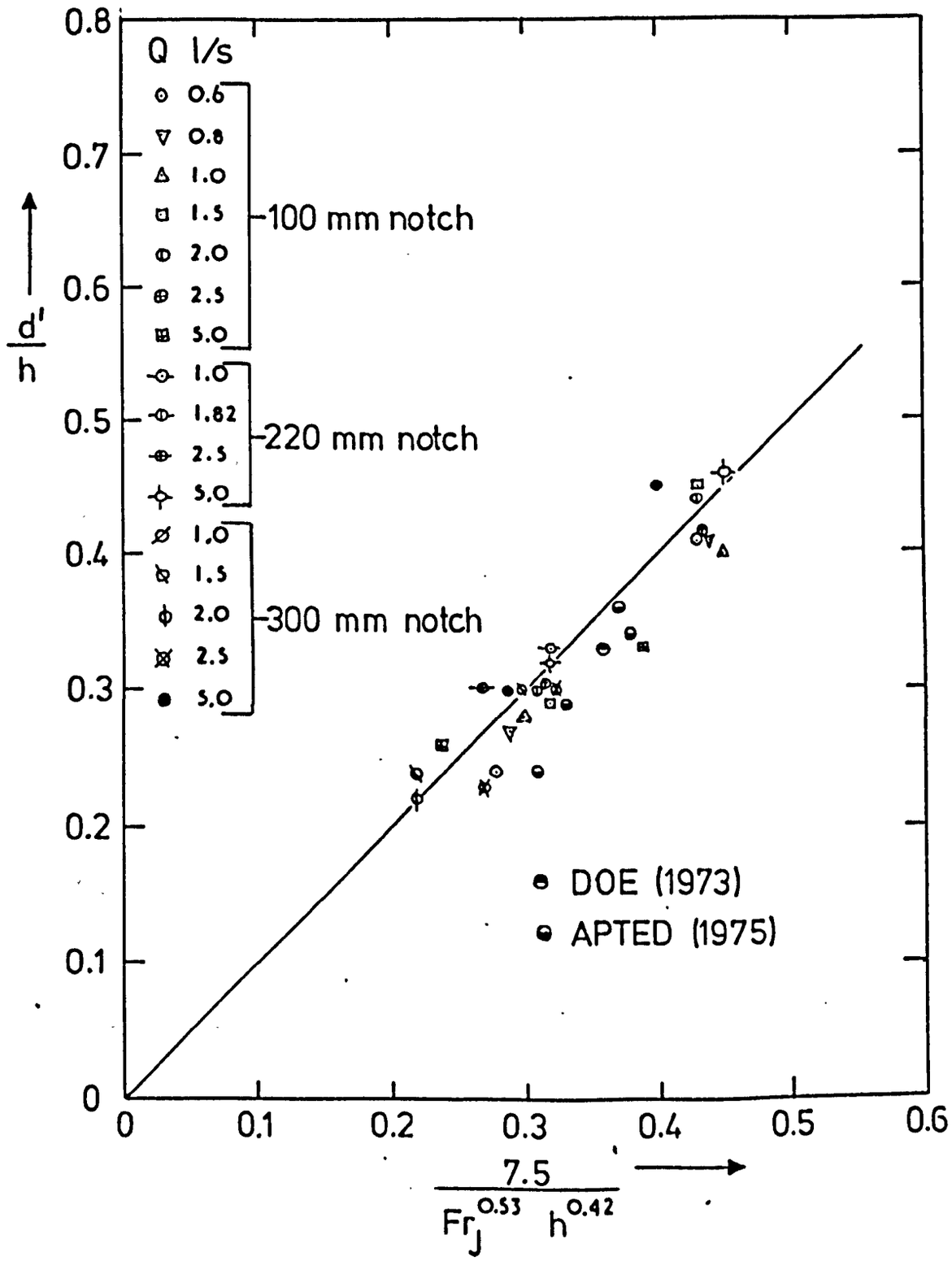

figure 7.11

correlation of data with Eq. 7.13

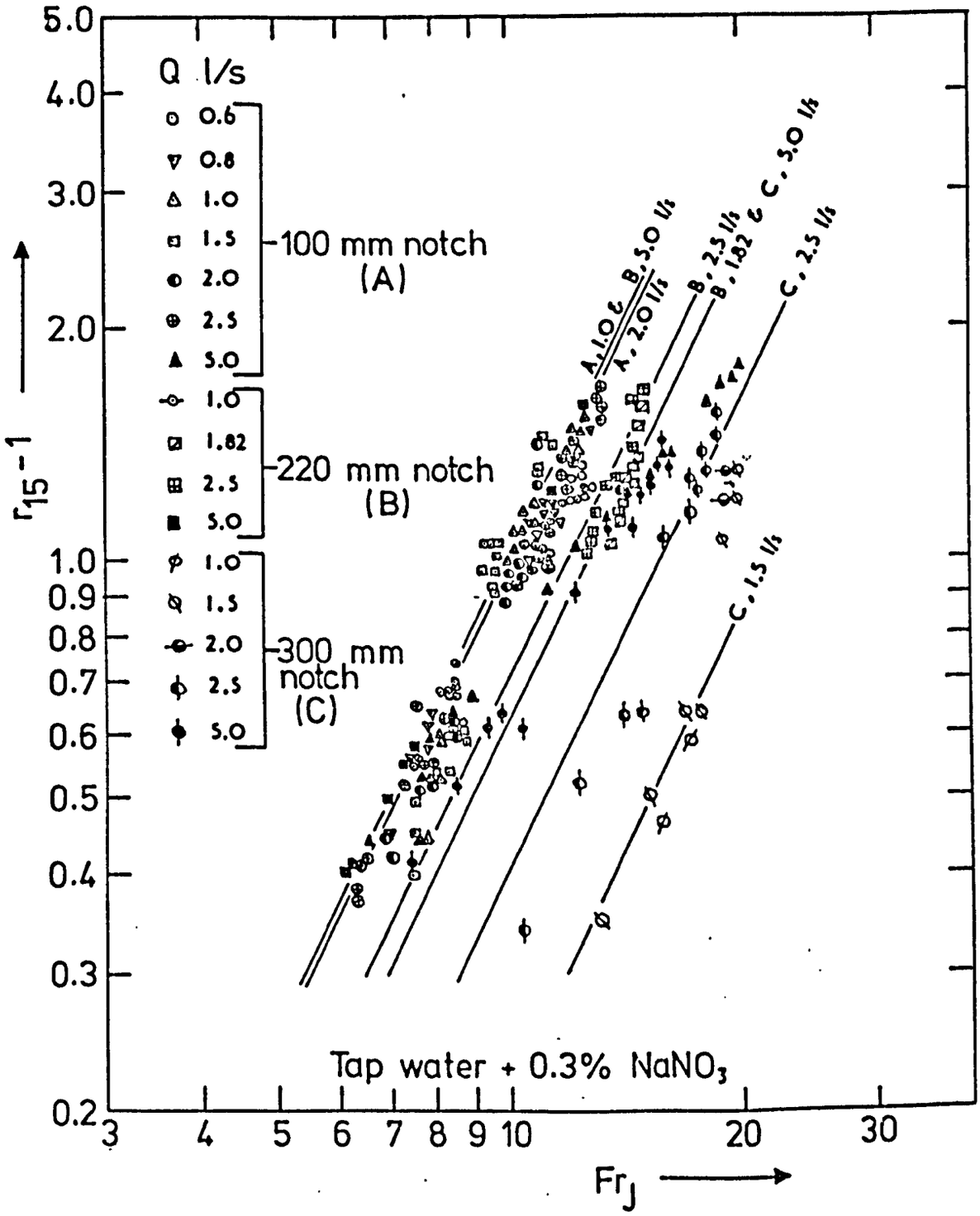

figure 7.12 $r_{15}-1$ v jet Froude number
(solid jets and optimum pool depth conditions)

Equation 7.15 will be some function of the scale. This is shown to be possible in Figure 7.13 from which:

$$K_J = 0.008 \left(\frac{h}{h_{0.6}}\right)^{0.8} \qquad (7.16)$$

As in Section 7.1.3.3, scale comparisons have been made as a scale ratio relative to a 0.6 l/s circular jet.

∴ From Equations 7.11, 7.15 and 7.16:

$$r_{15}-1 = 0.008 \left(\frac{h}{1.794\ Fr_J^{1.6}}\right)^{0.8} Fr_J^2 \quad (h \text{ cm}) \qquad (7.17)$$

or

$$r_{15}-1 = 0.008\ (0.63\ Fr_J^{0.72}\ h^{0.8}) \qquad (h \text{ cm}) \qquad (7.18)$$

The correlation given in Equation 7.15 with K_J given by Equation 7.16 is the first non dimensional correlation describing oxygen uptake at a free overfall, but, the form given in Equation 7.18 is not quite complete as will be discussed in Section 7.3. A comparison of observed to predicted (Equation 7.18) values of $r_{15}-1$ is presented in Figure 7.14 and on the whole, good agreement is displayed. The biggest divergences occur for the thinnest jets and high values of Froude number. This is close to the points of total disintegration described by the Equation of HORENI, i.e. the divergences noted are attributed to partial disintegration of the jets.

Also a factor which has not been considered is the energy loss by a jet during its free fall. This will be greater for the jet

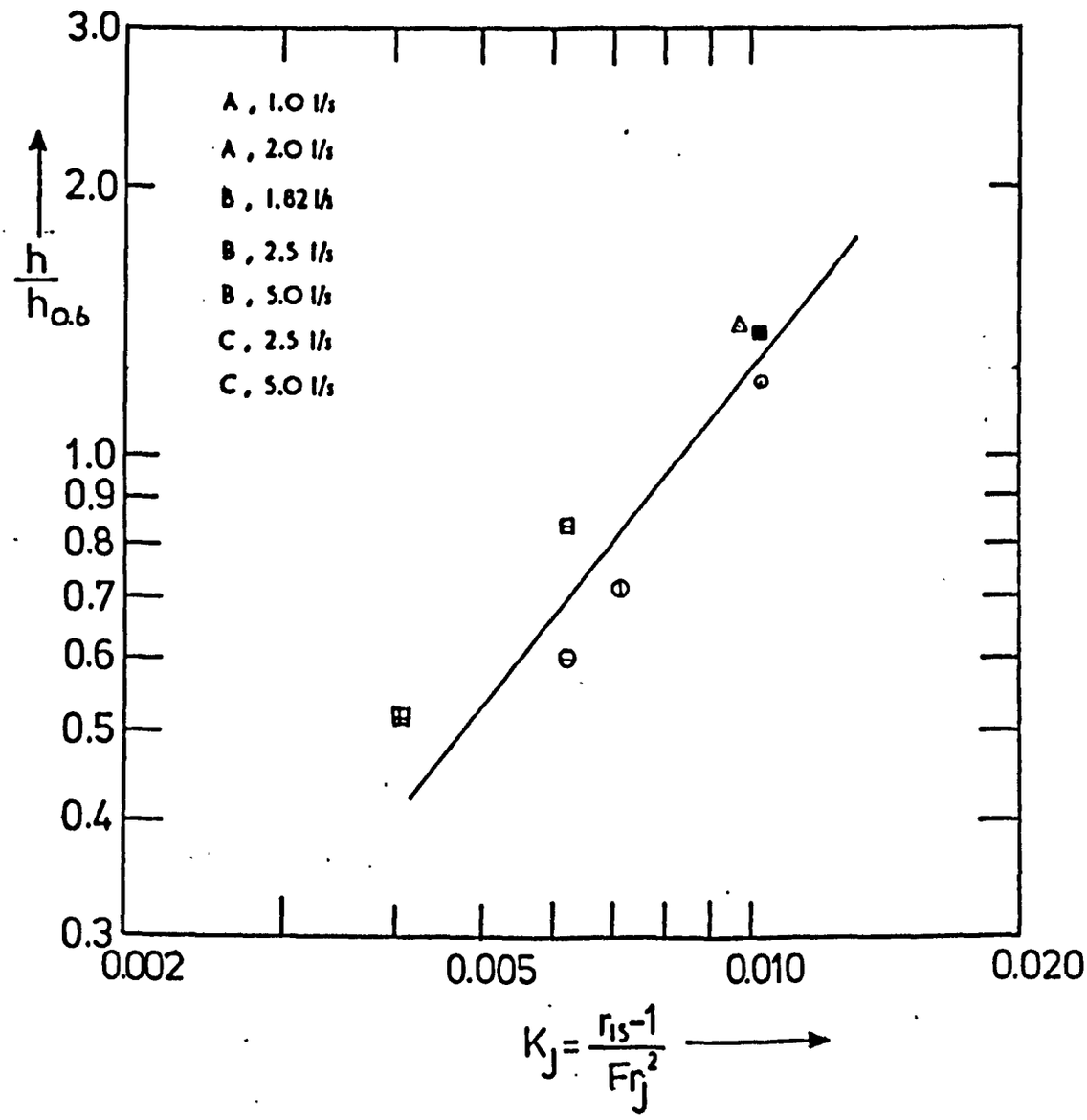

figure 7.13

K_J (Eq. 7.15) as a function of scale

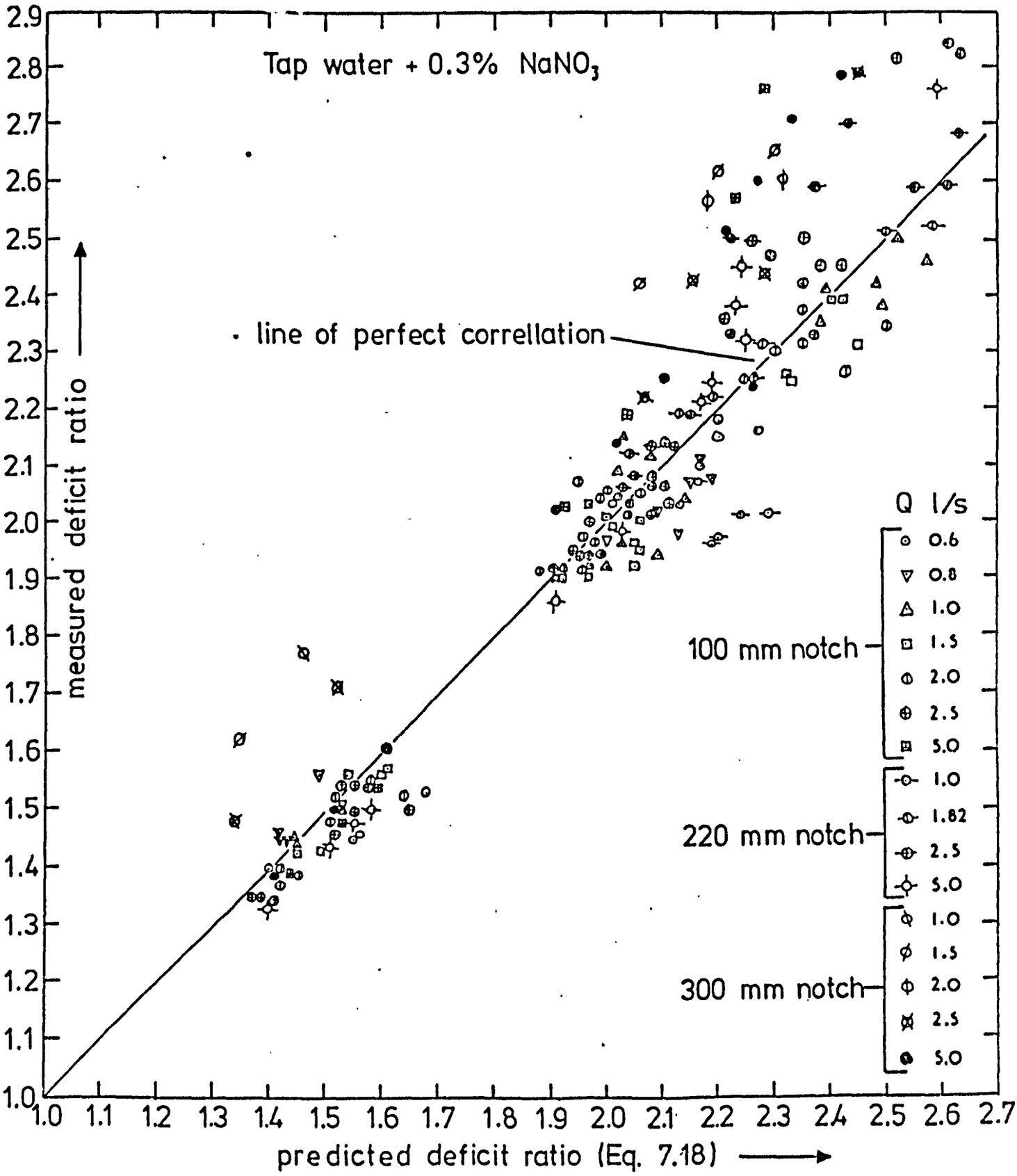

figure 7.14 Equation 7.18 tested against measured results (optimum depth conditions)

presenting the largest air water interface and for a constant height of fall this jet would then have less energy available during the air entraining process. The significance of this is difficult to gauge, but this reasoning would be consistent with the divergence of the broadest and thinnest jets as displayed in Figure 7.14.

However for practical purposes, Equation 7.18 provides a good correlation for the data with optimum lower pool depths.

7.2 THE EFFECT OF DISSOLVED SALTS

7.2.1 Further Tests

The addition of sodium nitrite to the laboratory re-circulatory water system has already been discussed in Section 4.3.

The experimental work reported in Chapter 6 and Section 7.1 of the current chapter refers to tests with sodium nitrite levels of 0.3%. Additional tests are shortly reported:

(a) Experiments with the 100mm wide rectangular notch, for a range of discharges 0.6 to 5.8 1/s over the same range of heights of fall and depths of pool already reported but with a single pool width of 100mm. This set of experiments was carried out prior to those already reported and with sodium nitrite levels in the water estimated to be 0.6%. This data has already been published (AVERY and NOVAK, 1975).

(b) Experiments with sharp crested rectangular notches, 100, 220 and 300mm wide respectively, for a range of discharges up to 2.5 1/s over the same range of heights of fall and depths of pool already reported, but with a single pool width of 0.44m. For these, the laboratory water supply to the mixing tank was substituted by a supply taken directly from the tap water mains. A discharge of 2.5 1/s

was the maximum possible from the available mains supply. The only other modification to the apparatus, in these tests only, was to intercept the water discharging from the lower weir pool and thence to pump this water directly into the main sewers. This was wasteful but necessary to avoid dilution of the laboratory water treated with sodium nitrite.

7.2.2 Results for Different Salt Concentrations

The data for the tests with tap water and the laboratory water containing 0.6% sodium nitrite are presented in Appendices C1, C3, D2 and E2 as the deficit ratio adjusted to 15°C plotted against the depth in the lower pool for various elevations of the latter pool.

A typical example of the effect of sodium nitrite on oxygen transfer is shown in Figure 7.15.

This figure shows the deficit ratio plotted against the pool depth for a discharge of 2.0 1/s over the 100mm wide notch and for the downstream pool fixed in position with the bed 1.57m below the weir crest.

The presence of sodium nitrite does not appear to alter the pattern of deficit ratio change with pool depth and the optimum depth is not significantly altered. There is, however, a very significant effect on the oxygen transfer as previously noted with tests on the hydraulic jump. This is further illustrated in Table 7.1 which has been constructed by reading from Figure 7.15 the respective values of deficit ratio for a pool depth of 32cm. A 60% initial oxygen deficit has been presumed.

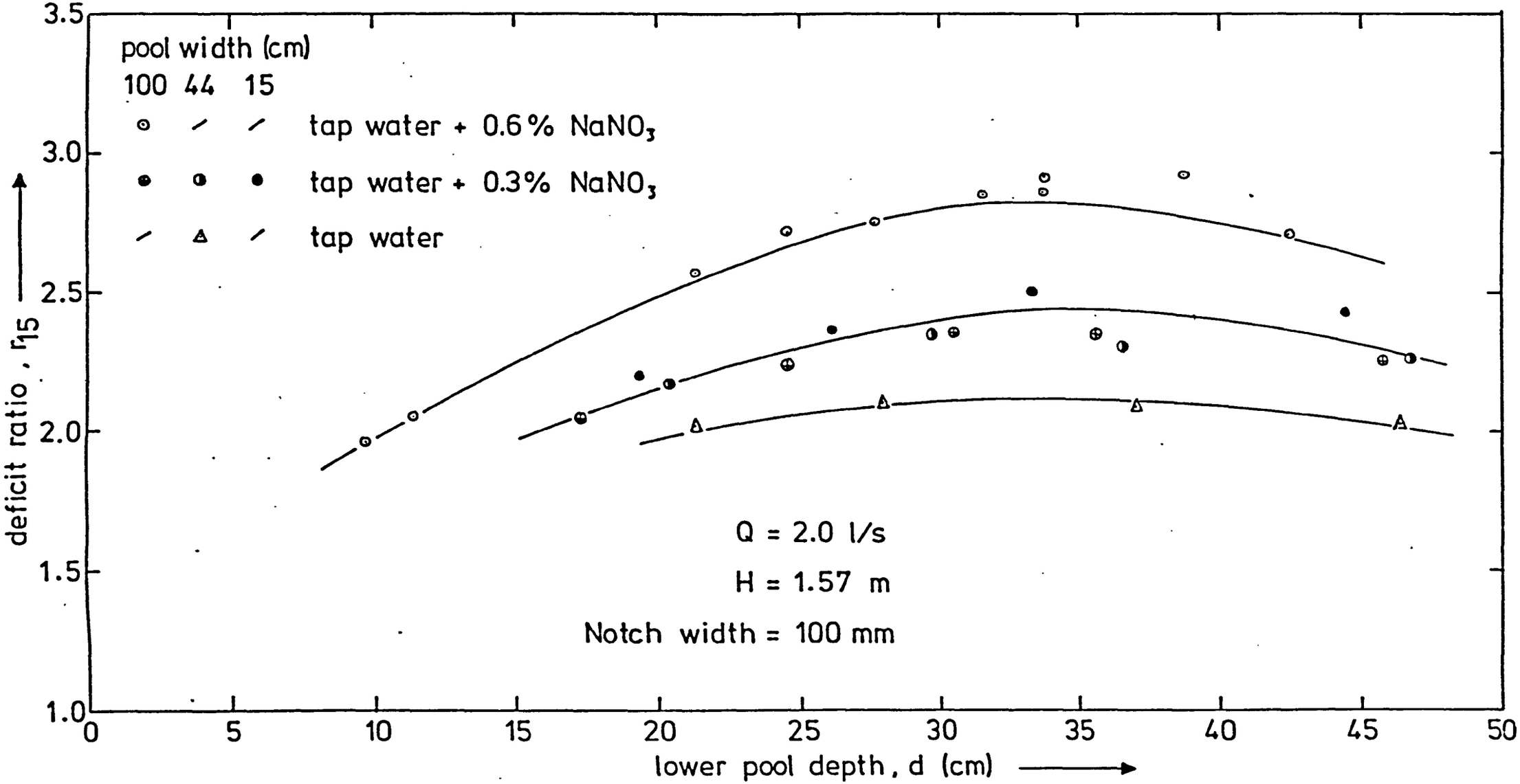

figure 7.15 the effect of dissolved salt ($NaNO_3$) on the oxygen transfer for fixed specific discharge and pool bed elevation but varying pool depth.

TABLE 7.1

THE EFFECT OF DISSOLVED SALT ON AERATION FOR CONSTANT HYDRAULIC CONDITIONS

Sodium Nitrite content %	Deficit Ratio r_{15}^{o}	Dissolved Oxygen % Saturation		$\frac{C_2 - C_1}{C_S}$ %
		C_1	C_2	
0	2.12	40	72	32
0.3	2.42	40	75	35
0.6	2.82	40	79	39

The addition of sodium nitrite to a concentration of 0.6% results in a 7% increase in the relative oxygen transfer and a 33% increase in the deficit ratio. This represents a very significant change.

The effect noted in Figure 7.15 is similarly described by the data for the other discharges and notches tested. The results of deficit ratio, for the 100mm notch and a discharge of 0.6 l/s with pool depths in excess of or equal to the optimum depth, are plotted against the height of fall in Figure 7.16. This figure is similarly typical in displaying the effect of sodium nitrite on the oxygen transfer.

In conclusion it would seem that the general comments made in Chapter 6 and earlier in this chapter in Section 7.1 apply irrespective of salinity levels but that the relative levels of aeration achieved are very significantly affected by the relative salinity levels present.

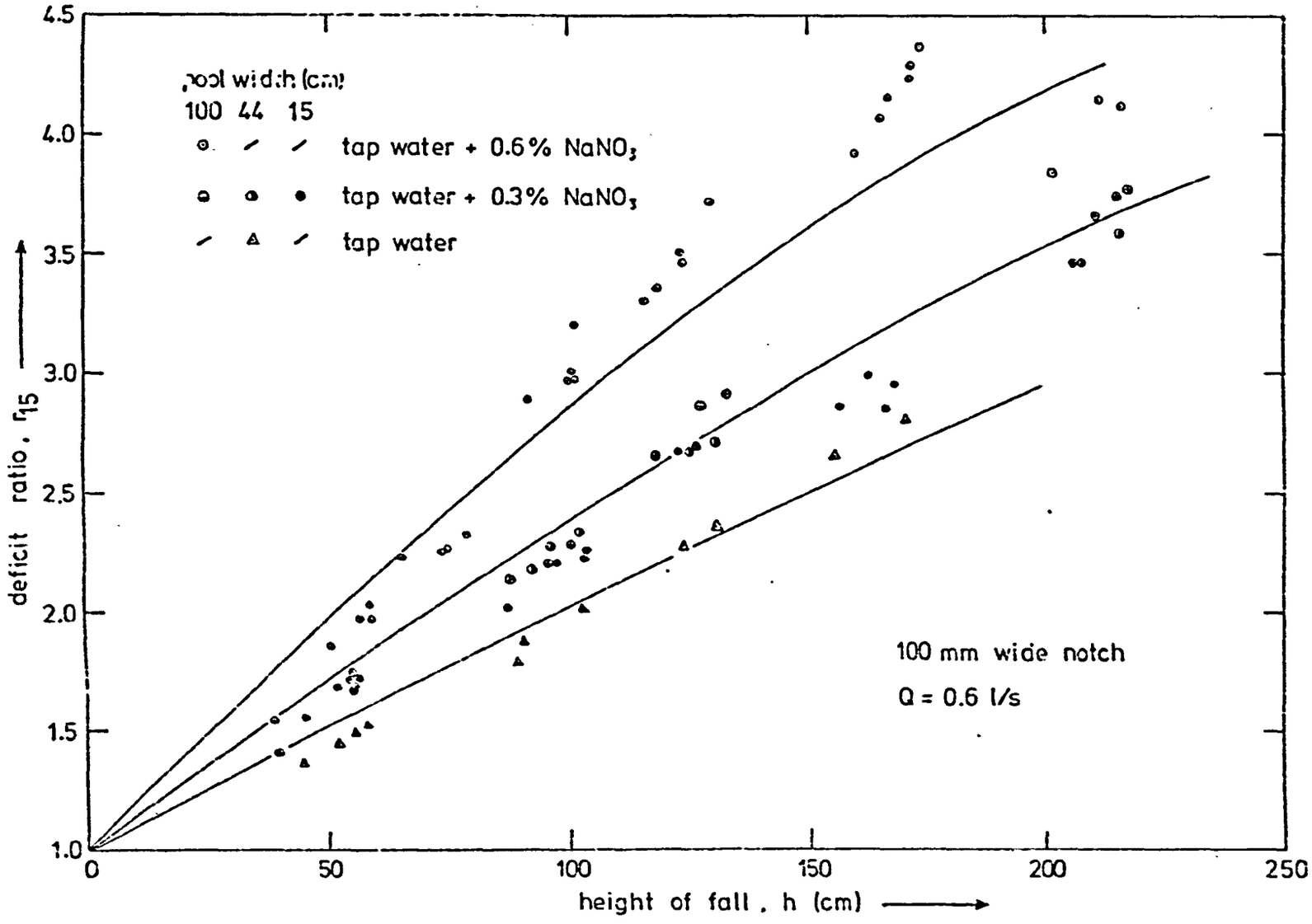

figure 7.16 effect of dissolved salt ($NaNO_3$) on oxygen transfer for fixed specific discharge, varying height of fall and optimum pool depth conditions

7.2.3 Reasons for the Observed Effects of Sodium Nitrite

These have already been discussed in detail in Section 4.7.3

It was suggested that the quantities of air entrained by an hydraulic jump are unlikely to be affected by the presence of dissolved salts. This is similarly true here since the quantity of air entrained by a jet is a function of the jet velocity and the air/water interface of the jet. It was also suggested that the contact time is also unlikely to be significantly affected. This is consistent with observations in Section 7.2.2 that the optimum depth remained constant irrespective of dissolved salt level.

The observations in this chapter are therefore consistent with the argument presented in Section 4.7.3. The enhanced aeration recorded in the presence of sodium nitrite is due to the formation of smaller bubbles and thus the creation of a larger air/water interfacial area for a given volume of air. As previously noted in Section 4.7.3, this was confirmed by measurements of bubble size reported in Section 5.2.4.

7.3 FINAL CORRELATIONS WITH JET FROUDE NUMBER

The presence of dissolved sodium nitrite in water has been shown to enhance the quantities of oxygen transferred at a free overfall, the degree of enhancement depending on the quantities of salt dissolved.

The data collected with tap water and for laboratory water with 0.6% sodium nitrite concentration have been similarly treated as detailed in Section 7.1.3. The resultant relationships between deficit

ratio and jet Froude number for optimum pool depth conditions are illustrated in Figure 7.17 with linear scales and Figure 7.18 with logarithmic scales. Comparison with Figures 7.6 and 7.12 for sodium nitrite levels of 0.3%, indicates that the dependence of the deficit ratio on the jet Froude number is similar irrespective of the dissolved salt levels in the water, i.e. for a particular jet:

$$r-1 = f\ (Fr_J^{\,2}) \quad \text{as shown in Section 7.1.3.4.}$$

This in fact follows from the argument presented in Section 4.7.3 which suggested that the only factor to change markedly as a result of the presence of dissolved salts was the bubble diameter and hence the ratio air/water interfacial area. It is possible to conceive that the dependence on the various controlling parameters is similarly the same here irrespective of dissolved salt concentrations, i.e. that the transfer rate per unit air/water interface is the same (governed solely by hydraulic conditions) and therefore that the total oxygen transfer occurring differs solely according to the different air/water interfacial areas offered.

If this were so, then Equation 7.18 would apply, but with a different constant K_S, K_S being dependent on the quantities of dissolved salt present,

$$\text{i.e. } r_{15}-1 = K_s \left[Fr_J \left(\frac{h}{1.794\ Fr_J^{\,1.6}} \right)^{0.4} \right]^2 \quad (h \text{ cm}) \qquad (7.19)$$

or

$$r_{15}-1 = K_s\ (0.63\ Fr_J^{\,0.72}\ h^{0.8}) \qquad (h \text{ cm}) \qquad (7.20)$$

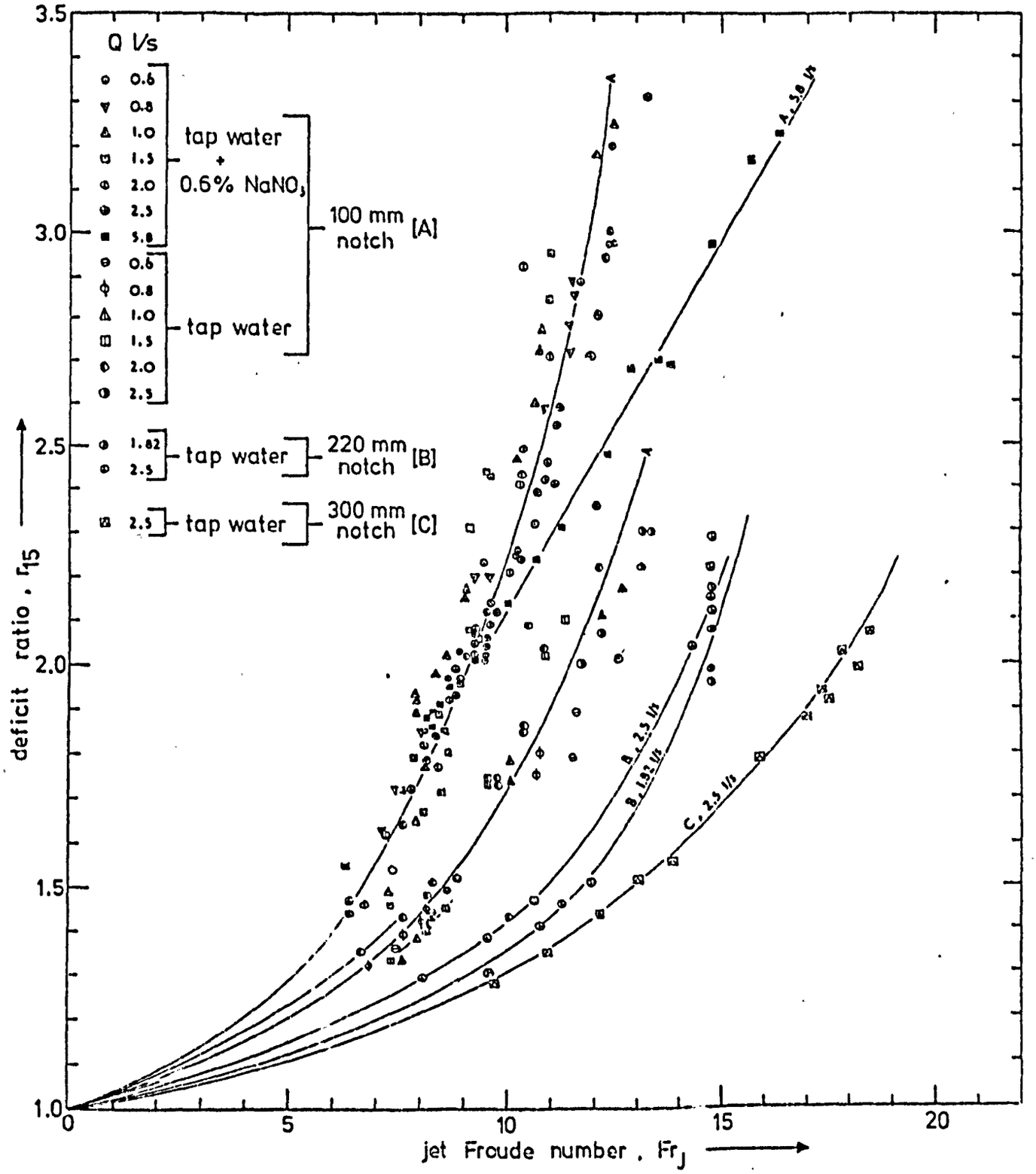

figure 7.17 deficit ratio v jet Froude number for solid jets and optimum pool depth conditions - additional tests with tap water, also tap water + 0.6% sodium nitrite.

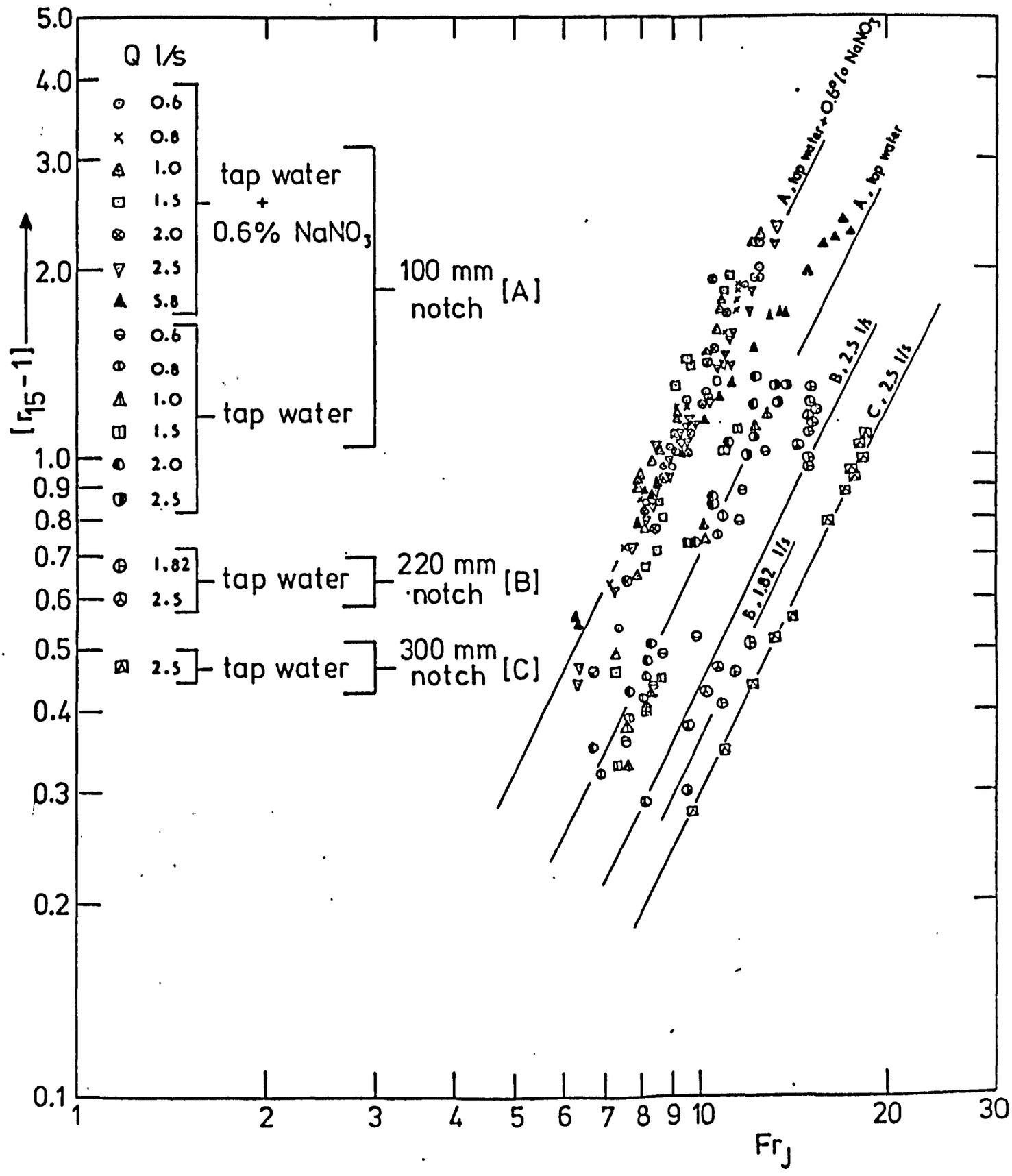

figure 7.18 $r_{15}-1$ v jet Froude number - additional tests with tap water, also tap water + 0.6% $NaNO_3$ (solid jets and optimum pool depth conditions)

Equation 7.20 is tested with all the data in Figure 7.19. Also plotted is the best straight line for the data collected for sodium nitrite levels of 0.3% (from Equation 7.18).

Equation 7.20 is seen to accurately describe the aeration due to a jet plunging into a pool whose depth exceeds or equals the optimum (described by Equation 7.14), with constants K_s as tabulated in Table 7.2 below.

TABLE 7.2

The Variation in K_s (Equation 7.20) with Change in Sodium Nitrite Concentration

$NaNO_3$ concentration in tap water %	K_s (Eq. 7.20)
0	0.0057
0.3	0.0079
0.6	0.0113

The variation of K_s with % sodium nitrite is also displayed in Figure 7.20, an approximately linear variation exists over the range of these experiments as given by the equation:

$$K_s = 0.0054 + 0.009\ S_a \quad (S_a\ \%) \tag{7.21}$$

It must be emphasised that Equation 7.21 is only applicable over the range tested and that extrapolation to higher salinity levels will probably result in an over estimate in the value of K_s. Reasons for this have been discussed in Section 4.7.4.

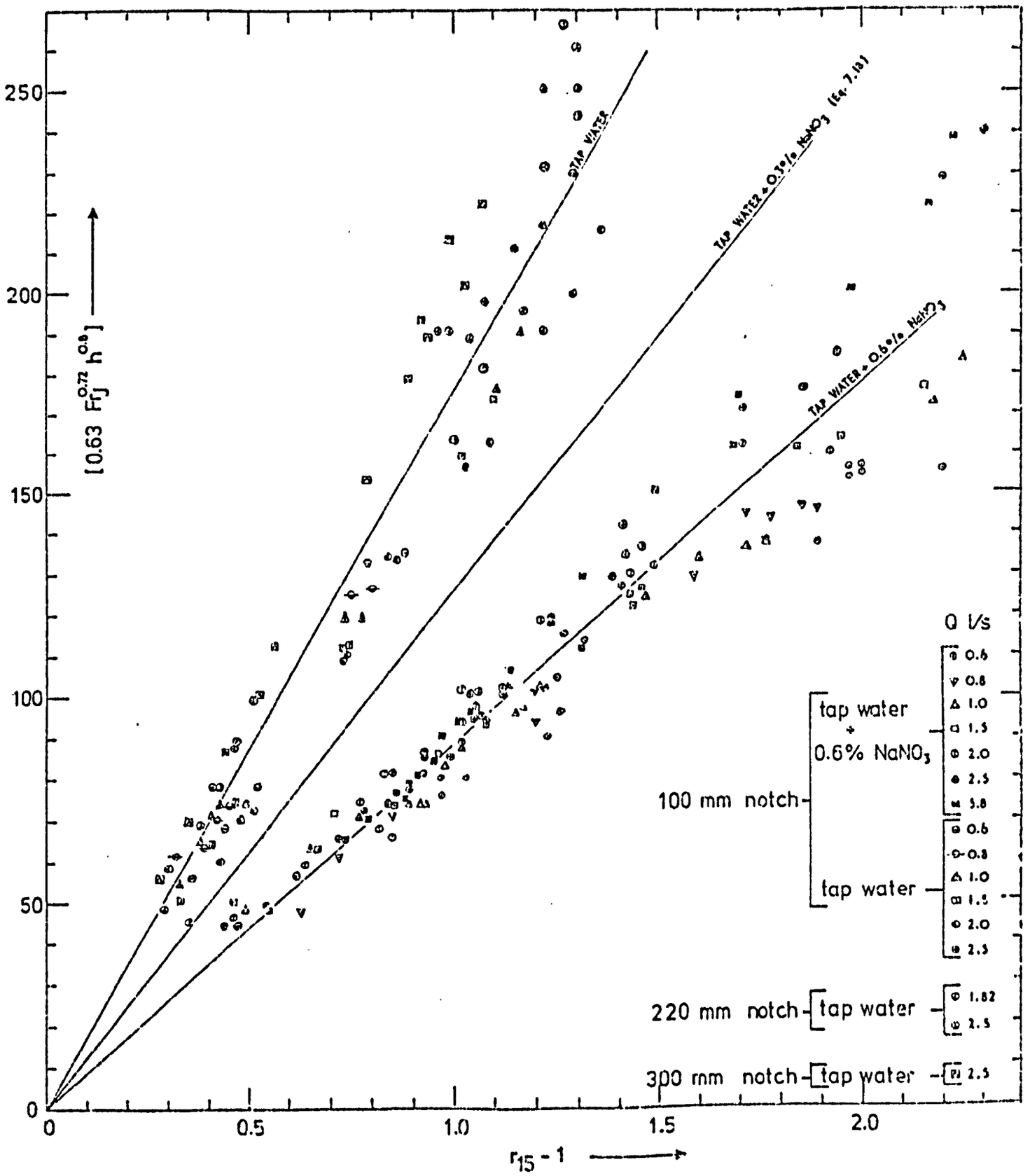

figure 7.19 correlation of data with Equation 7.20.

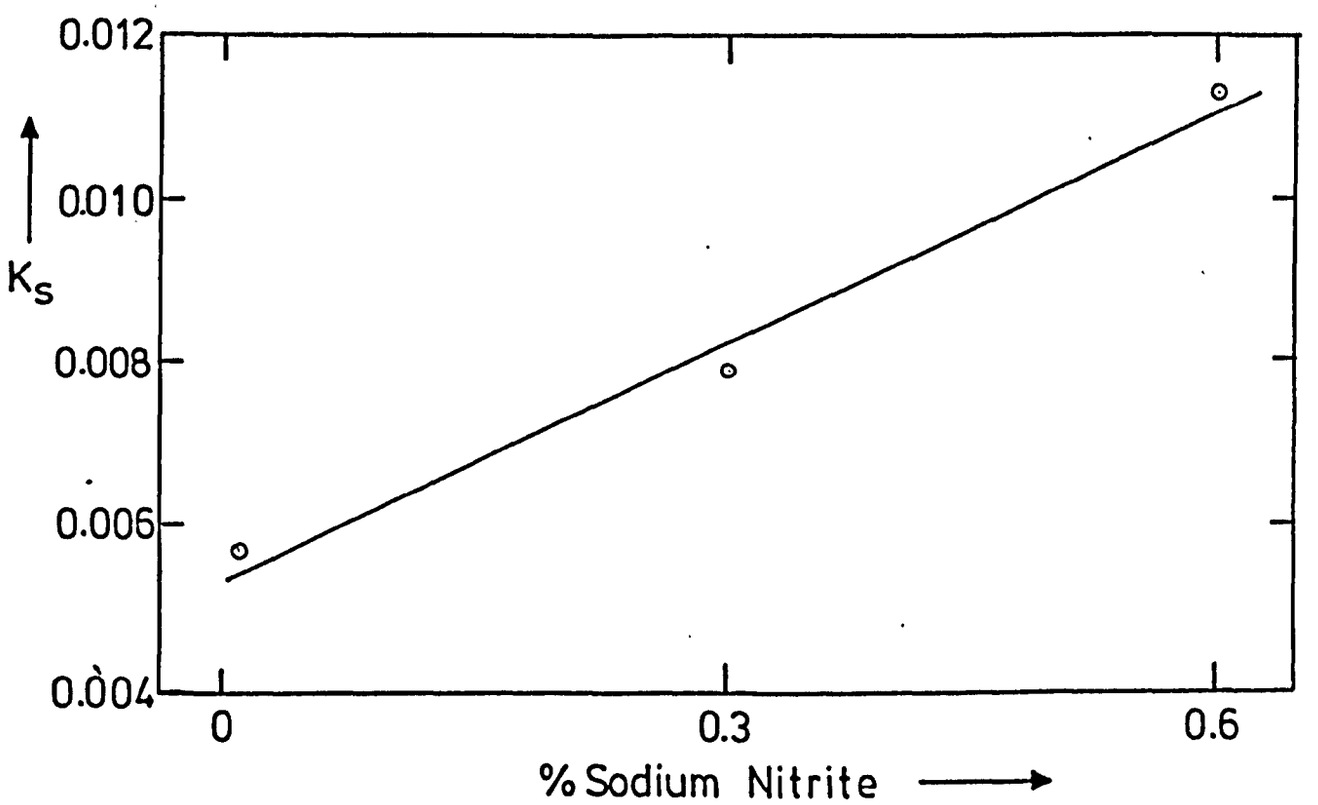

figure 7.20 variation of K_S in Eq.7.20 with dissolved salt ($NaNO_3$) concentration

7.4 APPLICATION TO MULTI-CRESTED WEIRS

7.4.1 General

Consider a single circular jet of diameter D, and discharge Q falling through a height h.

The Froude number of this jet will be as given by Equation 7.4 with $(q_J)_1 = Q/\pi D$.

This jet is divided into N circular jets of equal discharge by partitioning the notch. The diameter of each jet will be $D/\sqrt{N}$ and the Froude number of these jets will still be given by Equation 7.4 except that

$$(q_J)_N = \frac{Q/N}{\pi D/\sqrt{N}} = \frac{(q_J)_1}{\sqrt{N}} \qquad (7.22)$$

Thus if one jet of Froude number Fr_J is split into N jets of equal diameter, the resultant Froude number will be $\sqrt{N}.Fr_J$.

The advantage afforded is obvious, a higher Froude number can be achieved for the same discharge and height of fall by splitting the jet and therefore greater aeration is anticipated. The more the jet is split, the greater the advantage offered. This is in fact confirmed by the experiments of VAN DER KROON & SCHRAM (1969).

It is proposed therefore that the aeration achieved by multiple crested weirs would be described by Equation 7.20 subject to two conditions: 1. that the jets did not interact during their free fall, and 2. that the air entrainment and mixing process due to any jet was not unduly influenced by that of any neighbouring jets. Any interaction between the jets is likely to result in a greater aeration than indicated by Equation 7.20.

7.4.2 Some Tests with a Twin-Crested Weir

To test the suggestions made in Section 7.4.1 some experiments were conducted with a weir crest consisting of a pair of notches each of width 100mm. Three discharges were selected, 1.2, 2.0 and 2.5 l/s and a range of tests, identical to those for the previously discussed notches, is summarised in Appendix F.

The advantageous effects of splitting the flow demonstrated by VAN DER KROON have been similarly shown here, Figure 7.21 illustrates the increased aeration achieved for a constant flow by partitioning the flow. This confirms comments made in Section 7.4.1, i.e. the splitting of the jet results in a larger air entraining jet perimeter, a larger Froude number and thus greater aeration. The lower optimum depths required for the twin jets (see Figure 7.21) are consistent with the smaller diameter jet entraining larger relative quantities of air. Interaction between the jets in the pool may also be contributing to reduced optimum depths.

The validity of application of Equation 7.20 to describe the aeration achieved by a multiple crested weir is confirmed in Figure 7.22. The twin notch is discharging 1.2 l/s, i.e. 0.6 l/s per crest, and comparison has been made with the discharge of 0.6 l/s from the single notch. Therefore, for a constant height of fall, the Froude number will be the same for both notches. Figure 7.22 shows that constant aeration has been achieved for constant Froude number.

A similar comparison for a higher discharge of 1.0 l/s per crest, (see Appendices C2.3 and F2), indicates a slightly higher aeration achieved for constant Froude number with the twin notch than with the single notch - clearly, there was interference between the jets in the pool.

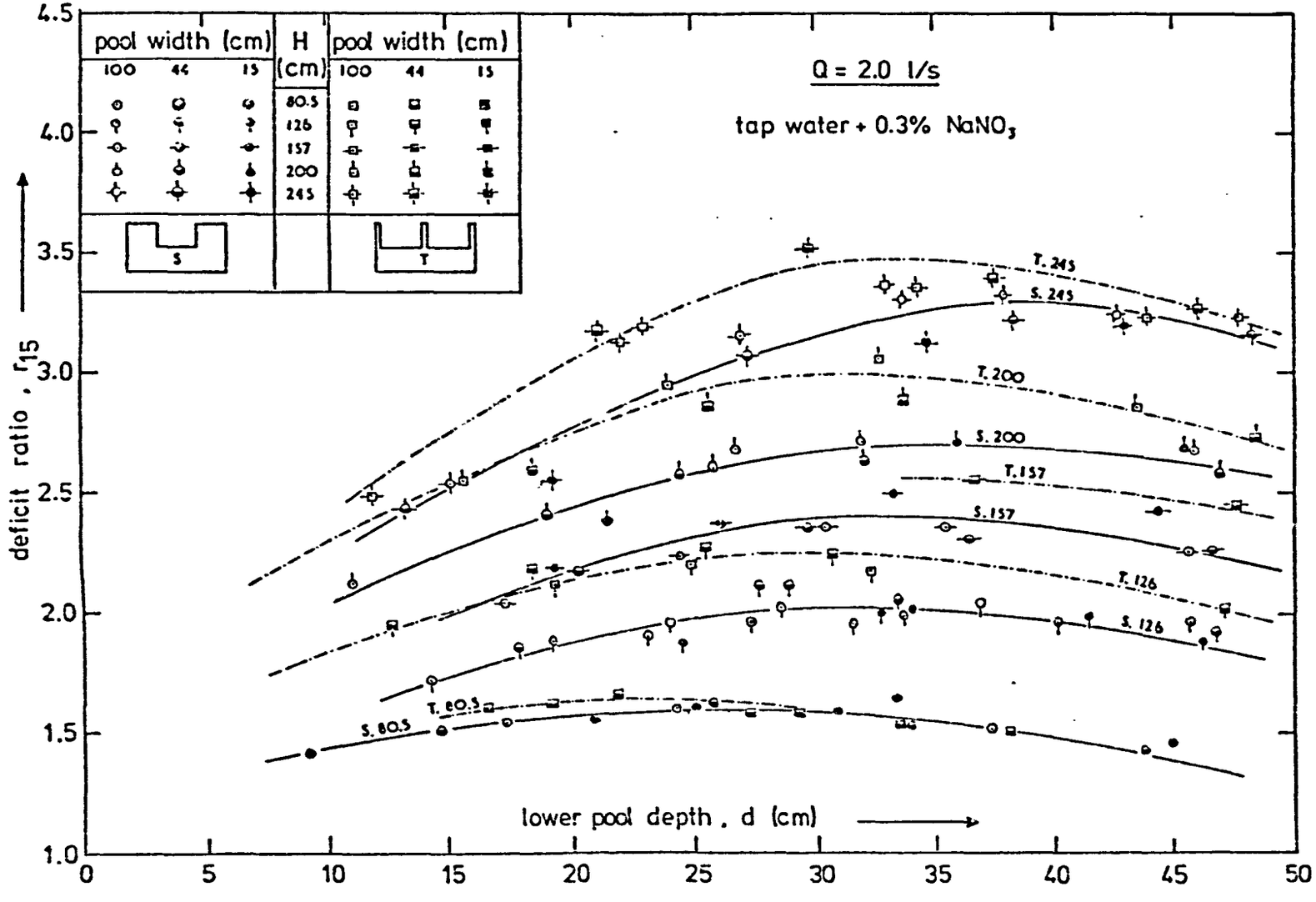

figure 7.21 the effect of splitting the flow over a weir for a constant total discharge

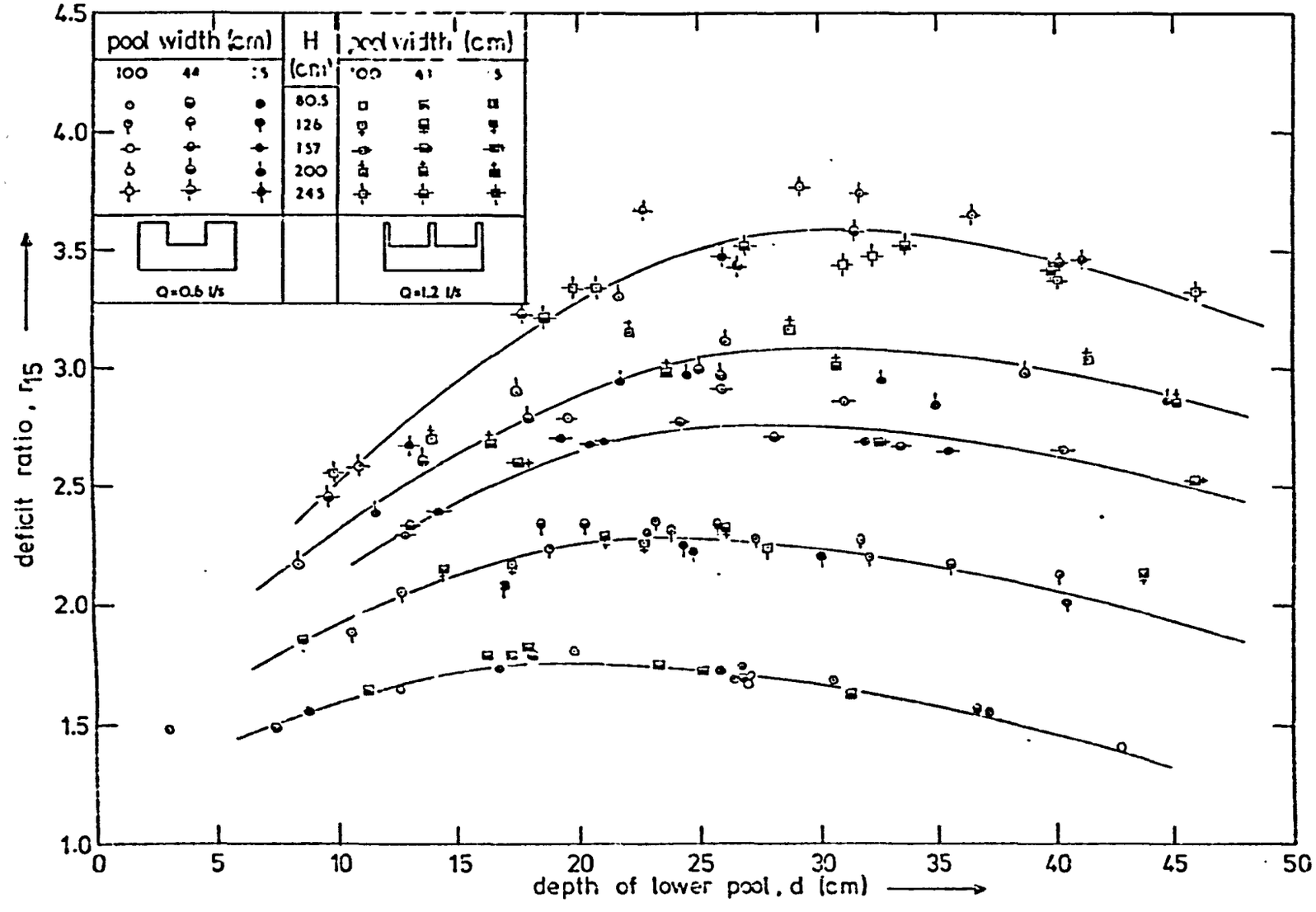

figure 7.22 the effect of splitting the flow over a weir for constant specific discharge

VAN DER KROON & SCHRAM reported that at their lowest height of fall (0.25m) optimal aeration was achieved by partition to the maximum number of jets studied whereas for greater heights of fall the optimal result was attained by progressively fewer jets. They observed that having attained an optimal aeration result, further partitioning did not result in any change in the aeration. This may indicate a stage at which advantages due to increases in air entrainment become offset by detrimental interference of the jets. This detrimental interference of jets is similar to the slight detrimental effects observed in Section 6.5 as a result of reduced pool widths.

7.5 APPLICATION TO A CASCADE WEIR

Since a cascade weir consists basically of a series of free overfalls strung together, then use can of course be made of Equation 7.20 provided the jet does not cling to the face of each step and also that the depth of water on each step is greater than or equal to the optimum. The calculation would be slightly tedious since it would be necessary to calculate the deficit ratio for each step from Equation 7.20. Then, from these deficit ratios and knowing the initial dissolved oxygen level above the cascade, it would be possible to trace the dissolved oxygen profile through the cascade. Hence the dissolved oxygen level at the end of the cascade and hence the overall deficit ratio may be computed.

The process would be simplified, however, if the cascade consisted of a series of equal steps. If the deficit ratio r for one step was determined, then for a cascade of n equal steps, the overall deficit ratio would be r^n (demonstrated in Section 8.4.4).

7.6 SIMILARITY CONSIDERATIONS

Reference is made to the gas transfer equation, Equation 1.35, which is reproduced here:

$$r = e^{K_{LV}\frac{A}{V}t}$$

and which when expanded into a series becomes:

$$r = 1 + \sum_{1}^{n} \frac{(K_{LV}\frac{A}{V}t)^{n}}{n!}$$

$$\therefore \quad r - 1 = f\ (K_{LV}\frac{A}{V}t) \tag{7.23}$$

For a constant Froude number, the ratio air to water discharge is assumed constant. It is an acknowledged fact that whatever the model scale, the mean entrained air bubble size remains unaltered. Therefore $\frac{A}{V}$ is constant for constant Froude number.

The time of contact in a jet air entrainment situation is best considered in two phases, namely plunging bubbles and free rising bubbles. Unfortunately, analysis is complicated since unless the jet is markedly inclined then the plunging bubbles will interfere with the rising bubbles and vice versa. An analysis will be attempted by ignoring this.

The depth of penetration is assumed to be the optimum depth d' as given by Equation 7.14. The velocity of free rise of a bubble in water of a particular quality depends on the bubble size only (HABERMAN & MORTON) and is therefore constant irrespective of scale.

For bubbles rising freely from the optimum depth:

$$\frac{t_1'}{t_2'} = \frac{d_1'}{d_2'} = \left(\frac{h_1}{h_2}\right)^{0.6} = M_L^{0.6} \tag{7.24}$$

M_L is the length scale more conveniently expressed.

For plunging bubbles, initial velocity $v_o = \sqrt{2gh}$ at the water surface and $v_t = 0$ at the optimum depth:

$$d' = \sqrt{2gh}\, t'' - \frac{1}{2} a t''^2$$

$$v_t = v_0 - at''$$

for $v_t = 0$, $a = \frac{\sqrt{2gh}}{t''}$ and $d' = \frac{1}{2} t'' \sqrt{2gh}$

$$\frac{t_1''}{t_2''} = \frac{d_1'}{d_2'} M_L^{-\frac{1}{2}} = M_L^{0.6} . M_L^{-0.5} = M_L^{0.1} \qquad (7.25)$$

Comparing overall contact times for two situations:

$$\frac{t_2}{t_1} = \frac{t_2' + t_2''}{t_1' + t_1''} = \frac{t_1' M_L^{-0.6} + t_1'' M_L^{-0.1}}{t_1' + t_1''} = \frac{1}{M_t} \qquad (7.26)$$

M_t being the time scale.

The limits of the time scale are (from Equations 7.24 and 7.25):

$$M_L^{0.1} < M_t < M_L^{0.6} \qquad (7.27)$$

From Equation 7.20:

$$\frac{(r_{15}^{-1})_1}{(r_{15}^{-1})_2} = M_L^{0.8} \qquad (7.28)$$

From the statement made in Equation 7.23, it is possible to estimate the scale of the liquid film coefficient M_{K_L} for the limits given by Equation 7.27 above:

Assuming that $r-1 = K\ (K_L \frac{A}{V} t)$ (7.29)

then

$$M_L^{0.2} < M_{K_L} < M_L^{0.7} \quad (7.30)$$

The limits are broad but are the best attainable in the circumstances. It is interesting to note that the scale K_L determined from hydraulic jump measurements falls between the limits given by Equation 7.30.

7.7 SUMMARY

The importance of jet shape has been demonstrated. Whilst the substitution of a flat jet for a round jet at the same discharge and height of fall resulted in a reduction in optimum depth, an increased aeration was observed which was consistent with the flat jet presenting a larger air/water interface and thus entraining larger quantities of air.

On the assumption that a similarity of air entrainment is possible according to the Froude criterion (Section 2.4.2), it was considered logical to define a jet Froude number (Equation 7.4) which incorporated the parameters jet velocity and discharge per unit jet perimeter at impact with the downstream pool.

Correlations between this Froude number and the optimum depth and also the oxygen uptake have been demonstrated. In both cases, for a constant Froude number, the optimum depth and oxygen transfer were shown to vary according to simplified functions of the scale.

A significant enhancement in the oxygen transfer in the presence of dissolved sodium nitrite was recorded. Similar observations were made in Chapter 4 and explanations for this effect have already been presented in Section 4.7.3.

A general equation (Equation 7.14) has been presented which enables estimates to be made of the minimum depth required for optimum oxygen transfer in the pool below a weir. A similarly general equation has been presented describing the oxygen uptake (Equation 7.20) as a result of a free falling jet entering a pool with optimum depth conditions. Equation 7.20 incorporates a constant whose value depends on the concentration of dissolved salts present as shown in Table 7.2. Equation 7.20 has also been shown to be applicable to a cascade and also to a multi-crested weir subject to certain conditions.

Tentative suggestions have been made with regard to similarity considerations with limits being suggested for the scales of the time of contact (Equation 7.27) and liquid film coefficient (Equation 7.30) at a free overfall situation.

CHAPTER 8

CORRELATION WITH PUBLISHED LABORATORY AND PROTOTYPE FREE OVERFALL MEASUREMENTS AND AN ASSESSMENT OF AERATION EFFICIENCIES

8.1 INTRODUCTION

A final equation, Equation 7.20, was presented in Chapter 7 which successfully correlated all the experimental results reported in this thesis for a free falling jet entering a free water recipient with depth equal to or in excess of the depth required for optimal oxygen transfer.

While successful correlation was exhibited in Figure 7.19, the general applicability of Equation 7.20 can only be ascertained by application to a variety of model and prototype situations. The collection of the necessary prototype data was beyond the scope of these studies, therefore recourse was made to published work. In most cases the hydraulic measurements required were not published, but, in a number of cases these were kindly supplied as a result of private correspondence.

Since no mention has been found in all the published work of the presence of dissolved salts in the water used, it has been assumed here that the waters were non-saline.

8.2 CORRELATION WITH PUBLISHED LABORATORY RESULTS

8.2.1 Department of Environment (1973)

Direct comparison is possible with the tap water experiments carried out at the Water Pollution Research Laboratory (D.O.E., 1973) since an identical jet was tested during the current studies. The equation describing the aeration measured by the D.O.E. has already been presented (See Equation 2.32 and Figure 6.1). The line describing the D.O.E. deficit ratio measurements is plotted in Figure 8.1

against the height of fall alongside the experimental points for the equivalent tap water jet studied here (Appendix D, Figure D2.2). All data refer to optimum depth conditions. Similarly, Figure 8.2 shows the deficit ratio/Froude number relationship. The agreement indicated in Figure 8.1 is gratifying since it provides independent confirmation of the accuracy of the polarographic oxygen measuring technique employed for the current studies. The D.O.E. used the more precise and well proven WINKLER chemical titration method.

It follows from Figures 8.1 and 8.2 that the D.O.E. measurements could be predicted accurately by means of Equation 7.20 with the appropriate value of K_s for tap water (Table 7.2). To illustrate this, three points in the solid jet region as determined by the equation of HORENI, Equation 2.7, have been selected at random, the jet Froude numbers determined from Equation 7.4 with the aid of the jet widths given in Figure 7.4, and the deficit ratio calculated from Equation 2.32. The results are tabulated in Table 8.1 together with the deficit ratio predicted by Equation 7.20 (K_s = 0.0057). Further comparison with the predicted deficit ratio is afforded by the D.O.E. deficit ratios plotted in Figure 8.3.

TABLE 8.1

The Prediction of the D.O.E. (1973) Measurements by Equation 7.20

Height of fall h (m)	Jet Froude No. Fr_J (Eq. 7.4)	DEFICIT RATIO r_{15}	
		D.O.E. (Eq. 2.32)	Predicted (Eq. 7.20)
0.54	11.27	1.59	1.50
0.89	14.06	1.94	1.88
1.17	14.72	2.19	2.12

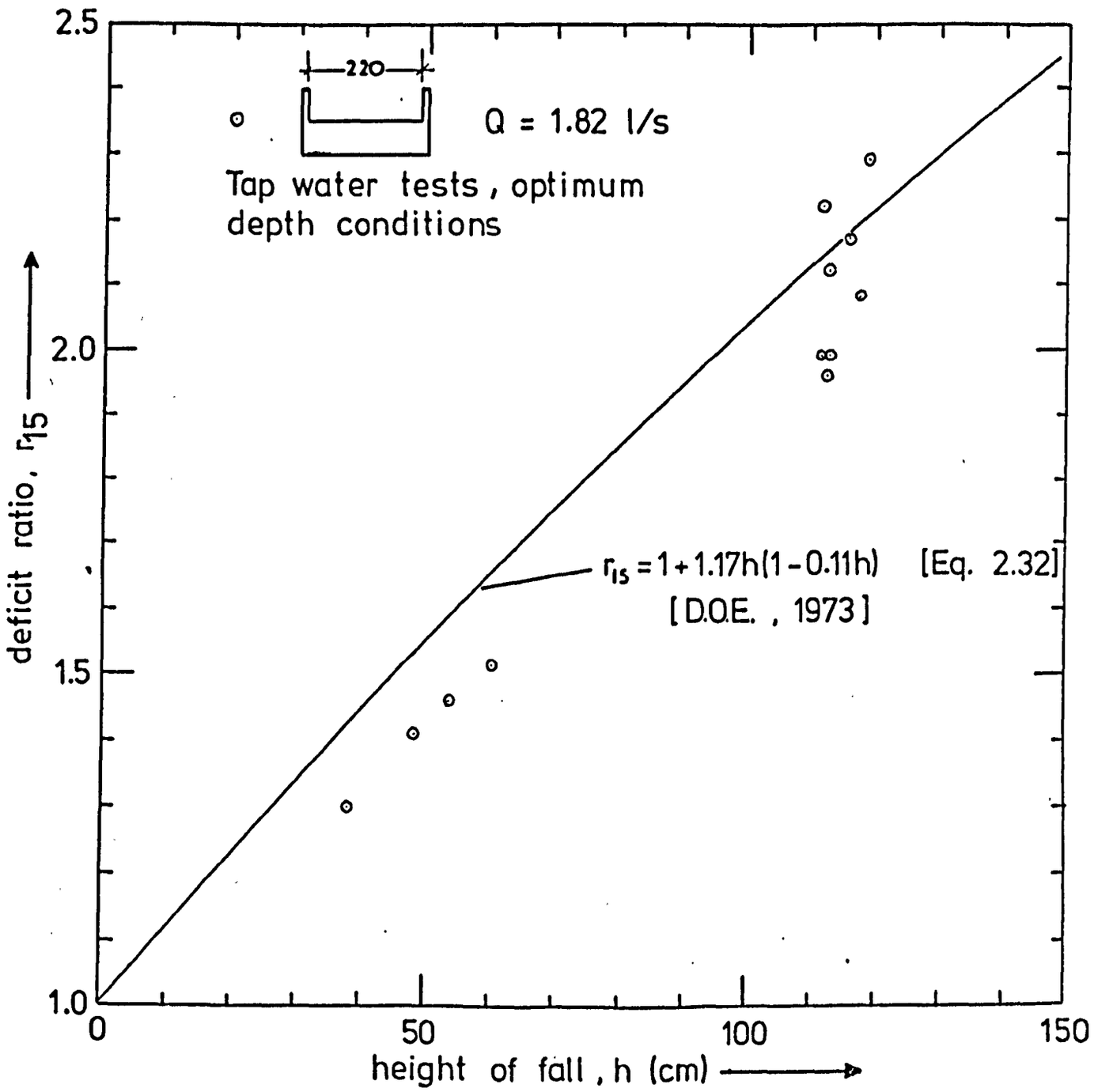

figure 8.1 r_{15} v h , a comparison of D.O.E. (1973) results with current tests for an identical notch

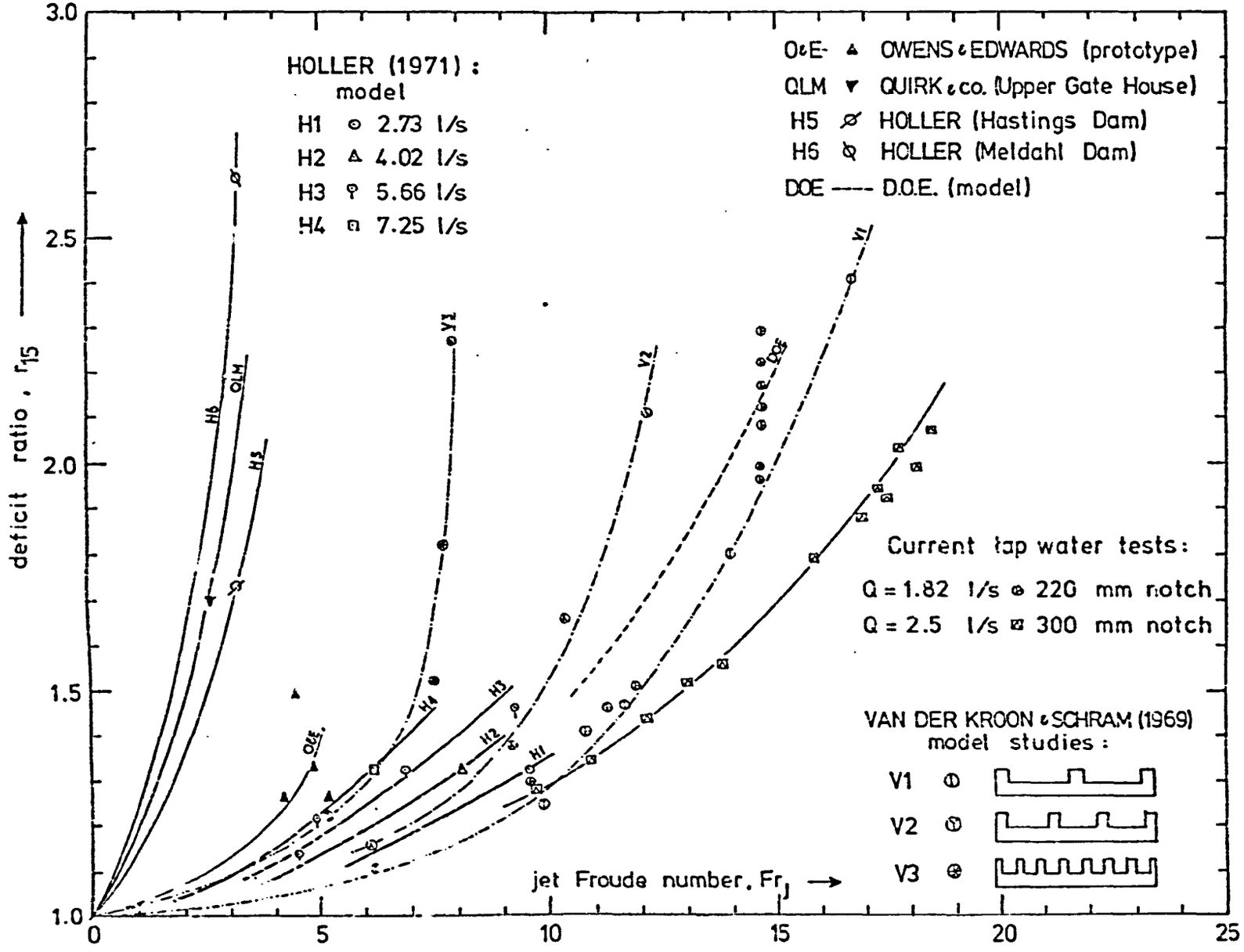

figure 8.2 deficit ratio / jet Froude number correlation for various published results

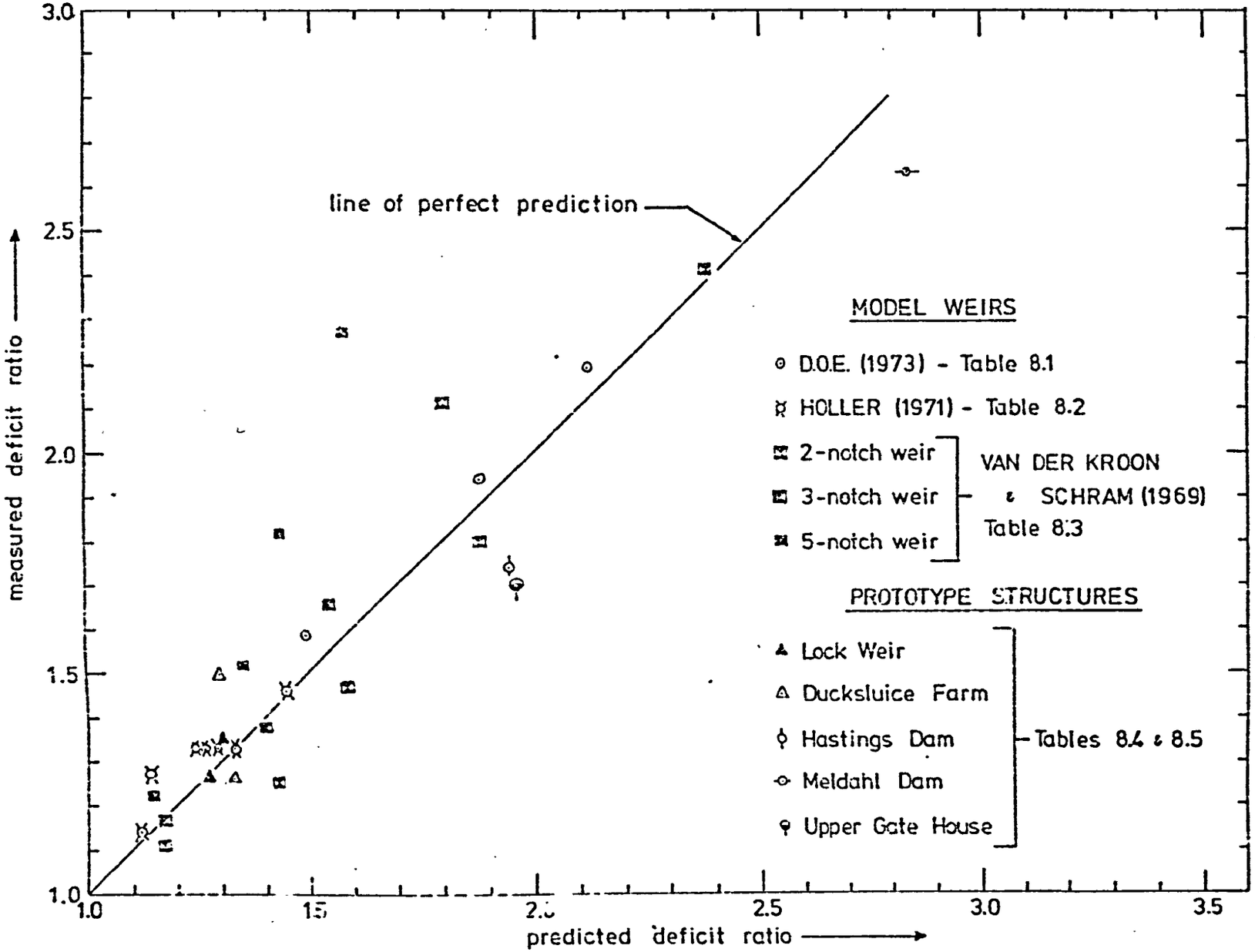

figure 8.3 a comparison of deficit ratios predicted by Equation 7.20 and measured values

8.2.2 HOLLER (1971)

HOLLER (1971) published the results of aeration experiments and precise details of these tests were subsequently received (private communication, 1974). HOLLER conducted experiments with a sharp crested weir placed in a 12 inch (30.48 cm) wide open channel. The jets did not fall to a pool of water but were made to impact on the bed of the downstream channel.

However, similar work by the D.O.E. (1973) revealed, for heights of fall up to 0.61m, that their jet provided the same aeration (for constant h) whether it splashed on to the pool bed or whether it fell to a pool with optimum depth conditions prevailing. On the basis of these results, it has been considered valid to compare the experiments of HOLLER with the current studies for optimum depth conditions.

A very similar weir was studied in the current studies (300mm wide rectangular notch). Thus, with the aid of Figure 7.5, it has been possible to accurately assess the width of HOLLER's jets at impact. The resultant Froude numbers together with data supplied by HOLLER are tabulated in Table 8.2. Deficit ratios have been adjusted to 15°C, and compared with the values predicted by Equation 7.20 assuming tap water, (K_s = 0.0057).

TABLE 8.2

HOLLER (1971) - Laboratory Data for 30.5cm Wide Rectangular Notch

Discharge Q 1/s	Height of fall cm	Froude No. Fr_J (Eq. 7.4)	Deficit Ratio	
			Measured r_{15}	Predicted r_{15} (Eq. 7.20)
2.73	36.8	9.52	1.33	1.33
4.02	36.8	8.02	1.33	1.29
7.25	36.8	6.18	1.33	1.24
5.66	20.3	4.53	1.14	1.12
5.66	22.8	4.90	1.27	1.14
5.66	36.8	6.87	1.33	1.26
5.66	57.1	9.26	1.46	1.45

The variation of deficit ratio with Froude number is shown in Figure 8.2, the behaviour displayed being similar to that shown for the current studies by Figure 7.17. The tap water results of the current studies for the 300mm notch and discharge 2.5 1/s are reproduced in Figure 8.2 and these are seen to extrapolate approximately from the similar jet studied by HOLLER (Q = 2.73 1/s).

The excellent correlation between HOLLER's experiments and the current studies is further illustrated in Figure 8.3 and tends to confirm the assumption of clean water $K_s = 0.0057$ used in calculating the predicted deficit ratios in Table 8.2 from Equation 7.20.

The independence of the deficit ratio on discharge, displayed by HOLLER's results for constant height of fall, is interesting. This might have occurred simply because the height of fall involved was so small, alternatively, it raises the question whether the effects of discharge observed in the current studies for optimum pool depth conditions would similarly have been noted if the jet was allowed to splash directly on to the pool bed.

8.2.3 VAN DER KROON and SCHRAM (1969)

VAN DER KROON and SCHRAM investigated the aeration due to various weir configurations. They devoted much attention to the effect of splitting the weir nappe to produce several jets and increases in oxygen uptake were demonstrated. This is consistent with the increased Froude number demonstrated in Section 7.4.1. For the purposes of comparison with the current studies, three weir configurations have been selected with individual notch widths comparable to those investigated in the current studies. It should thus be possible to assess the individual jet width from Figures 7.3, 7.4 and 7.5. VAN DER KROON and SCHRAM expressed the oxygen uptake as the "aeration capacity" (Equation 1.34) and this they determined to be relatively insensitive to temperature within the range of temperature for their experiments ($18^{o} > T > 12^{o}C$). Table 8.3 summarises the data for the three notches, the deficit ratio was determined from measured aeration capacity by Equation 1.34 and assuming C_s = 10ppm, and, the predicted deficit ratio assumes tap water was used, i.e. K_s = 0.0057 in Equation 7.20.

The variation of deficit ratio with Froude number is graphically presented in Figure 8.2. The twin-jet weir displays similar characteristics to all the other jets discussed so far and good agreement between measured and predicted deficit ratio is indicated in Figure 8.3. The assumption of tap water is therefore validated.

The two other notches, producing 3 and 5 jets respectively, are seen in Figure 8.2 (for heights of fall > 0.5) to display dramatic increases in deficit ratio for small changes in the Froude number. This is more pronounced in the case of the notch producing 5 jets, and is indicative of interference between the jets either during the free

TABLE 8.3

VAN DER KROON & SCHRAM (1969) - Laboratory Data for Three Multi-crested Rectangular Notches

Total Discharge = 8.33 l/s, pool depth = 0.6m, temperature range = 12-18°C.

NUMBER OF NOTCHES	WIDTH OF EACH NOTCH (m)	HEIGHT OF FALL h (m)	FROUDE NO. Fr_J (Eq. 7.4)	DEFICIT RATIO	
				Measured r	Predicted (Eq. 7.20) r_{15}
2	0.33	0.25	6.17	1.11	1.17
		0.50	9.85	1.25	1.43
		0.65	11.65	1.47	1.59
		0.90	14.00	1.80	1.88
		1.35	16.73	2.41	2.38
3	0.21	0.25	6.09	1.16	1.17
		0.50	9.19	1.38	1.40
		0.65	10.42	1.66	1.55
		0.90	12.23	2.11	1.80
		1.35	13.96	2.99	2.21
5	0.10	0.25	5.15	1.22	1.15
		0.50	7.50	1.52	1.35
		0.65	7.73	1.82	1.44
		0.90	7.96	2.27	1.58

fall or more probably in the pool itself. This interference in the pool will lead to more intense mixing with consequent higher degrees of aeration. As mentioned in Section 7.4, it is not possible to predict the aeration occurring under these conditions, the use of Equation 7.20 of course leading to an underestimate of the aeration occurring as illustrated in Figure 8.3. Further research is required in order to specify the limiting jet spacing required for successful application of Equation 7.20.

8.2.4 JARVIS (1970)

In view of the doubts expressed in Sections 6.4.3 and 6.5.3 with regard to the accuracy of the oxygen measurements of JARVIS, no attempts have been made at predictions from Equation 7.20.

It must also be recorded that the similarity between the results of JARVIS and the D.O.E. (Figure 6.1) is believed to have been pure coincidence. The discharge used by JARVIS, 0.62 l/s, was approximately one third that used by the D.O.E., and, from findings reported in Section 6.4.2, JARVIS's aeration results might be expected to be higher. This of course ignores effective factors such as jet shape, however, the dissolved sodium nitrite level during JARVIS's experiments was high, approximately 0.6%. Therefore it is to be expected from findings in this thesis with regard to dissolved salts (Sections 4.7, 7.2), that the aeration recorded by JARVIS should have been considerably higher than those obtained by the D.O.E. with tap water.

8.3 CORRELATION WITH PROTOTYPE DATA

Although many research workers have measured the oxygen transfer at prototype weir systems, very few chose to record the discharge flowing at the time or the geometry of the weirs studied.

Wherever possible, supplementary data for free falling jets has been accumulated by private correspondence.

In all the prototype situations discussed shortly, it has been necessary to assume the width of the jet at impact to be approximately equal to the length of the weir crest. To allow for any contraction in the jet, the jet perimeter at impact has been taken to be twice the weir crest length only. Table 8.4 summarises the prototype structures studied together with the various sources of information.

TABLE 8.4

Identification and Source of the Prototype Data Collected

WEIR REFERENCE LETTER	WEIR OR DAM NAME	RIVER	SOURCE OF INFORMATION
A	Lock	Lark (U.K.)	OWENS & EDWARDS (1963) * Anglian Water Authority
B	Ducksluice Farm	Lark (U.K.)	OWENS & EDWARDS (1963) * Anglian Water Authority
C	Hastings	Mississippi (USA)	HOLLER (1971)
D	Meldahl	Ohio (USA)	HOLLER (1971)
E	Marklands	Ohio (USA)	HOLLER (1971)
F	Upper Gate House	St. Louis (USA)	QUIRK, LAWLER, MATUSKY + Minnesota Power & Light Co.

* weir geometry

\+ weir geometry and discharge data

The data collected have been summarised in Table 8.5. The jet Froude number is calculated according to Equation 7.4 and the measured values of deficit ratio have been adjusted to 15°C. This adjusted deficit ratio has been compared with the predicted deficit ratio obtained from Equation 7.20. A value of K_s = 0.0057 (non-saline water) has been taken when using Equation 7.20.

TABLE 8.5

Aeration Measurements at Six Prototype Weir Systems (See Table 8.6)

WEIR REFERENCE LETTER	CREST LENGTH (m)	HEIGHT OF FALL h (m)	LOWER POOL DEPTH (m)	DISCHARGE Q (m^3/s)	FROUDE NO. Fr_J (Eq. 7.4)	WATER TEMP. T (^oC)	DEFICIT RATIO		
							Measured		Predicted
							r	r_{15}	(Eq.7.20) r_{15}
A	3.5	0.61	-	0.42	4.18	14	1.25	1.26	1.27
A	3.5	0.61	-	0.31	4.89	14	1.33	1.34	1.30
B	3.5	0.66	-	0.42	4.44	14	1.49	1.50	1.30
B	3.5	0.66	-	0.31	5.19	14	1.25	1.26	1.33
C	18.3	3.72	1.83	56.30	3.21	0	1.44	1.74	1.95
D	30.5	8.41	4.57	308.60	3.27	20	2.72	2.63	2.84
E	33.5	10.67	4.57	9.43	*	25	4.04	3.39	*
F	7.3	4.57	3.23	45.90	2.62	20	1.80	1.70	1.96

*indicates disintegrated jet

The correction of the deficit ratios to a standard value at 15^oC by use of Equation 2.13 was justified since the mixing levels or degree of turbulence in the model used by GAMESON, VANDYKE & OGDEN to derive Equation 2.13 were comparable to those estimated for the various prototypes. Energy losses per unit volume of stilling pool were calculated in Section 4.5 for the experiments of GAMESON & Co-workers - Table 4.1. These have been similarly calculated for the prototype structures in Table 8.6. The data in Table 8.5 was utilised and the stilling basin width was assumed to equal the crest width. The length of stilling pool over which the jet power is dissipated was assumed to be equal to approximately six times (6 x) the tailwater depth.

TABLE 8.6

The Energy Expenditure per Unit Volume of Tailwater for the Prototype Structures

WEIR REFERENCE LETTER	POWER AVAILABLE Kw	TAILWATER VOLUME (m^3)	POWER EXPENDED IN TAILWATER (w/m^3)
A		*	*
B		*	*
C	2054	368	5581
D	25460	3763	6766
E	+	+	+
F	2048	457	4481

*Insufficient data available

+Disintegrated jet

The raw data supplied for weirs C and F consisted of a large number of measurements over a range of discharges. The resultant variations in the jet Froude number calculated were small so the data presented in Table 8.5 represents a mean of all the data. The stilling pool depths, where given in Table 8.5, were assumed to be sufficient to ensure optimum oxygen transfer. For weirs A and B, the height of fall was small so the assumption of optimum depth conditions was considered valid.

The deficit ratio variation with Froude number indicated in Figure 8.2 is consistent with the observations made with regard to scale in Chapter 7.

The correlation of the prototype data with predicted deficit ratios illustrated in Figure 8.3 is remarkable, especially in view of the vast range of heights of fall and discharge encompassed. The assumption of K_s = 0.0057 (non-saline water) appears to be validated.

The pollution load of the water flowing over the various prototype systems is not known. However, the data supplied for Hastings dam indicated initial oxygen levels as low as 0ppm. At Lock and Ducksluice Farm Weirs initial oxygen levels as low as 3ppm were present, and, similarly, zero initial oxygen levels were frequently recorded at the Upper Gate House. It would be reasonable to suggest that a spectrum of pollution loads is described by the prototype data. The fact that despite this pollution, good correlation is obtained with the laboratory clean water experiments, is confirmation of observations made in Section 1.7 suggesting no effect of pollutants on the transfer coefficient because of the high turbulence prevailing. This would also invalidate the use of arbitrary water quality constants as suggested by the D.O.E. (1973) (Equation 2.34).

The original introduction of these constants by GAMESON (1957) was not based on an assessment of pollution loads as a result of chemical analysis, but was a broad classification based "mainly on local knowledge and general appearance". In only one case was an undiluted sewage effluent encountered. Furthermore, this field survey did not consider such characteristics as jet shape, discharge etc. These are all factors which will contribute to causing the scatter of points which was originally attributed to various pollution loads.

Distinction must be made between the depressive effects suggested by the D.O.E. water quality constant and the enhanced aeration observed in the current studies in the presence of dissolved salts. The suggestion by the D.O.E. is a reduced transfer coefficient whilst the dissolved salts increased the air/water interfacial area.

If the correlation of the form given by Equation 7.20 is further validated by other prototype measurements, then the non dimensional correlation Equation 7.20 will represent the first successful model/prototype correlation at a free overfall weir. This correlation has already been shown in Figure 8.3 to describe accurately the measurements of all model aeration studies published to date (those for which sufficient information was available), again for the first time.

8.4 A COMPARATIVE EVALUATION OF AERATION EFFICIENCIES

8.4.1 A Measure of Aeration Efficiency

The efficiency of aerators is generally gauged as the quantity of oxygen transferred relative to the power expended (kg O_2 per Kw h).

Consider a situation where C_1 and C_2 mg/l are the oxygen levels before and after aeration. The expression of deficit ratio, $r = C_s-C_1/(C_s-C_2)$, may be re-expressed to give the change in oxygen concentration, thus:

$$C_2-C_1 = C_s-C_1 \left(\frac{r-1}{r}\right) \quad \text{(mg/l)} \tag{8.1}$$

where C_s-C_1 is the initial oxygen deficit (mg/l). If the discharge, Q m^3/s, is known, then the mass of oxygen transferred per hour can be computed:

$$M_o = 3.6\ Q\ (C_s-C_1)\ \left(\frac{r-1}{r}\right) \quad \text{(Kg } O_2\text{/h)} \tag{8.2}$$

and thus the efficiency η for height of fall h:

$$\eta = \frac{3.6\ (C_s - C_1)\ (\frac{r-1}{r})}{gh} \quad (Kg/Kw\ h) \qquad (8.3)$$

Clearly the efficiency is a function of the initial oxygen deficit (as well as Froude number and height of fall) and this should therefore be specified when efficiencies are quoted.

8.4.2 Efficiency of a Number of Supplemental Aerators Compared to Weirs

Table 8.7 summarises the aeration efficiency achieved by a number of aeration systems (See Section 2.3 for discussion of these systems). Wherever possible, the efficiencies are quoted as published whilst the others were calculated from available oxygen data using Equation 8.3 and assumed 50% initial oxygen deficit for a temperature of 15°C.

The potential of a weir as a cheap source of oxygen is confirmed but underestimated by the sample of free overfalls quoted. Significant improvements are possible involving capital costs but no additional operating costs if the single free fall were converted to a series of smaller falls.

In fact, ALBRECHT (1968) quotes ECKOLDT (1962) as referring to the aeration of modern dams with a head of 6 to 7m by a single fall as a "wasteful aeration method", the same effect being obtainable with a lower head.

TABLE 8.7

The Aeration Efficiency Achieved by a Variety of Aerators and Structures

DATA SOURCE	AERATOR	INITIAL DEFICIT	EFFICIENCY $KgO_2/Kw\ h$
IMHOFF & ALBRECHT (1972)	Turbine	50%	0.45-1.41 *
WILEY, LUECK, SCOTT, WISNIEWSKI(1960)	Turbine		0.82-2.46 *
WAGNER (1958)	Turbine		1.50-1.79 *
PADDADINO (1961)	Turbine		0.91 *
WILEY & LUECK (1960)	Air Diffuser	2-3mg/1	0.99 *
PALLADINO (1961)	Air Diffuser		0.23 *
KAPLOVSKY, WALTERS & SOSEWITZ (1964)	Surface Aerator		0.79-2.00 *
MITCHELL (1973)	U-Tube	0	0.30-4.1 *
SPEECE, ADAMS & WOOLDRIDGE (1969)	U-Tube	0.2mg/1 (21°C)	0.61-2.13 *
BRIUZN & TUINZAAD (1958)	U-Tube		1.00-1.50
OWENS & EDWARDS (1963)	Lock Weir +	50%	0.61-0.75
OWENS & EDWARDS (1963)	Ducksluice +	50%	0.56-0.91
HOLLER (1971)	Hastings +	50%	0.21
HOLLER (1971)	Meldahl +	50%	0.13
HOLLER (1971)	Marklands +	50%	0.12
QUIRK, LAWLER & MATUSKY (1966)	Upper Gate House +	50%	0.16
ALBRECHT (1968)	Free Overfall	50%	0.92
ALBRECHT (1968)	Shooting Weir	50%	0.43

+Free overfall weirs (Tables 8.4 and 8.5)

*Values as published

8.4.3 A Comparison of the Aeration Efficiency of the Hydraulic Jump and Free Overfall

Assuming a particular available head loss, an available discharge of approximately 145 cm^2/s and a channel width of 10cm, a comparison has been made between the aeration efficiencies achieved by a free overfall and an hydraulic jump formed downstream of a sluice gate.

Table 8.8 contains the efficiencies calculated for four different head losses.

TABLE 8.8

A Comparison of the Aeration Efficiency of a Free Overfall and Hydraulic Jump

ENERGY LOSS (cm)	HYDRAULIC JUMP + $q = 145\ cm^2/s$			FREE OVERFALL + $q = 150\ cm^2/s$		
	Froude No. Fr_1	Efficiency * (Kg/Kwh)	Tailwater Depth (cm)	Froude No. Fr_J (Eq. 7.4)	Efficiency * Kg/Kwh	Tailwater Depth (cm)
21.1	9.72	1.596	8.08	4.64	1.646	18.1
34.3	13.10	1.495	9.02	6.19	1.498	21.3
57.1	18.30	1.317	10.15	7.67	1.252	25.0
107.4	28.20	1.004	11.80	10.35	0.93	29.1

*50% Initial oxygen deficit assumed
+Water containing 0.3% sodium nitrite

Since the range of head losses studied with the hydraulic jump was limited, extrapolation has been necessary and use was made of Equation 4.25 to determine the oxygen transfer. Figure 6.5 is the source of oxygen measurements for the free overfall.

The data in Table 8.8 has been reproduced in Figure 8.4 together with two other specific discharges for the free overfall. The hydraulic jump did not display any significant change in efficiency with discharge over the range tested. As well as being an efficient aerator over the range tested, the hydraulic jump system had the advantage of requiring a smaller tailwater depth as shown in Table 8.8, i.e. the required fall between upstream water surface and the channel bed downstream was significantly less. The tailwater depths quoted for the free overfall are the optimum depths, (Figure 6.4); in practice the depth required to prevent scour might be greater.

The high efficiencies of free overfall noted for small heights of fall indicate why a cascade weir provides better aeration than a single free fall. An increase in head loss, although resulting in an increased oxygen input, resulted in the fall in rate of increase of oxygen input illustrated in Figure 8.4. Similar observations are to be found elsewhere, notably ALBRECHT (1968). The reasons for this differ for the free overfall and hydraulic jump and it is necessary to compare the relative quantities of air entrained by the two structures.

Figure 8.5 summarises the air entrainment characteristics of the hydraulic jump according to KANLINSKE & ROBERTSON (1942) and also RAJARATNAM (1962) with the relative air discharge, $\beta = Q_a/Q$, plotted against (Fr_1-1). Also plotted are the turbulent jet data of SHIRLEY (1950) and the laminar jet data of LIN & DONNELLY (1966), in both cases the original data have been recalculated and presented in terms of the jet Froude number Fr_J (Equation 7.4). The representation of the data of SHIRLEY by a single relationship in Figure 8.5 is an improvement on SHIRLEY's original presentation of separate relationships with velocity for each jet diameter, and is consistent with comments in Section 2.4.2

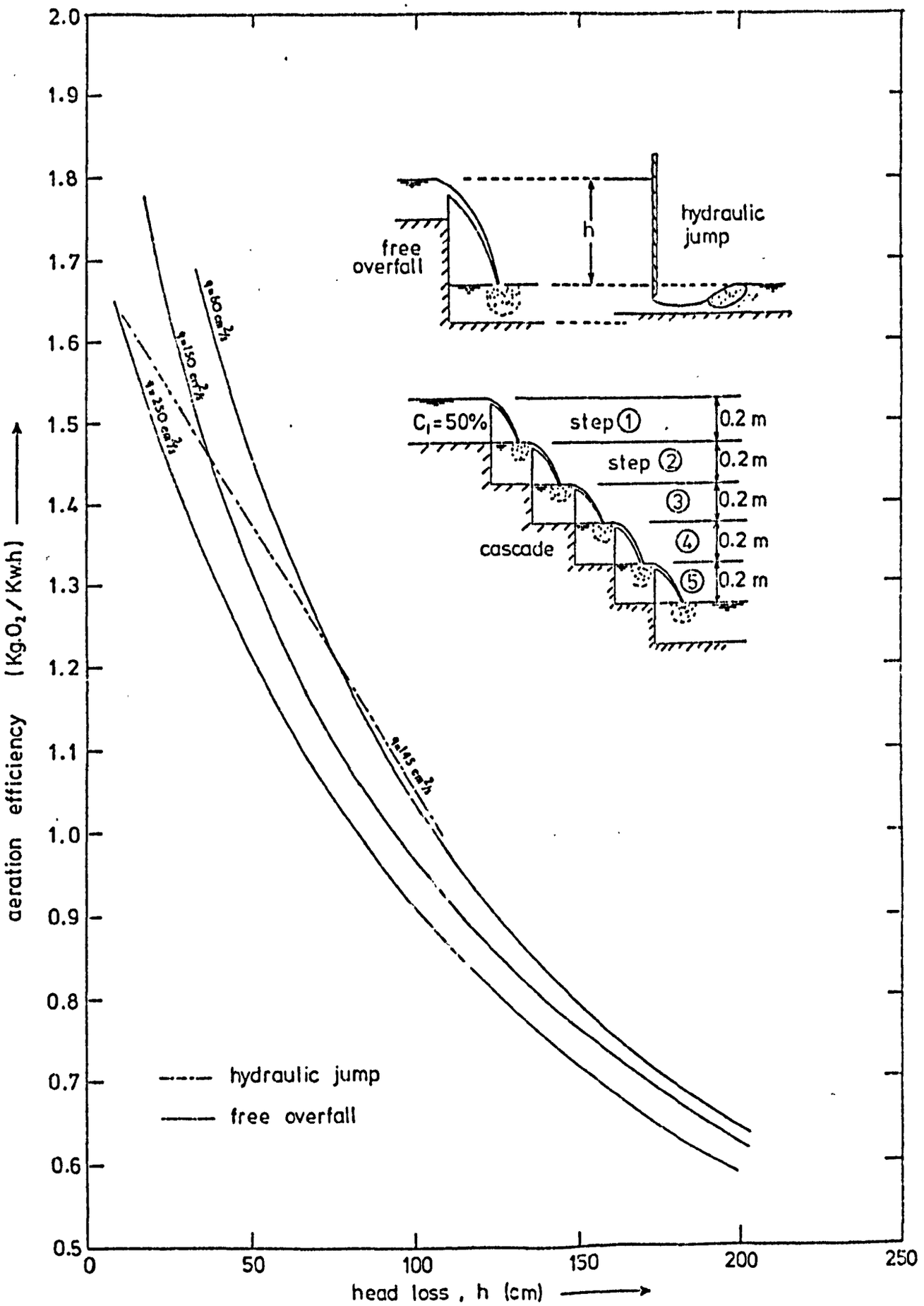

figure 8.4 the aeration efficiency of a free overfall and an hydraulic jump

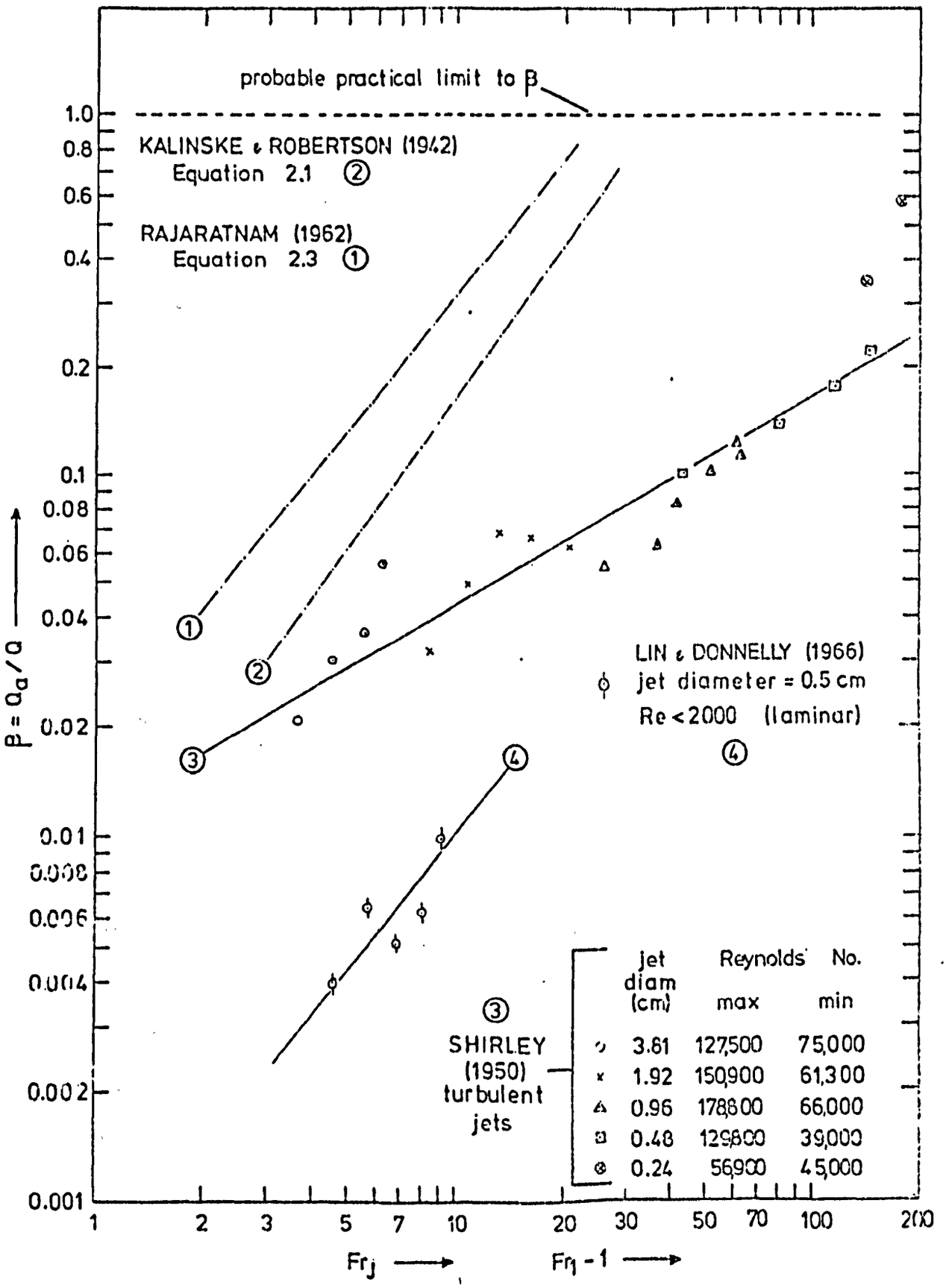

figure 8.5 air entrainment by jets and hydraulic jumps

concerning similarity of air entrainment according to Froude's law. The separate relationship for laminar and turbulent jets is consistent with the different entrainment mechanisms observed by LIN & DONNELLY.

It is apparent from Table 8.8 and Figure 8.5 that the relative quantities of air entrained by the hydraulic jump for a given head loss are far higher and this no doubt explains the greater oxygen transfer efficiency noted with the jump especially as the contact time in an hydraulic jump is likely to be significantly less than for an equivalent jet plunging into a pool with optimum depth conditions prevailing.

MOORE (1941) demonstrated that the ratio of energy loss at the base of a free overfall to available height of fall ($\Delta E/h$) increased as the height of fall increased for constant discharge, i.e. for increasing fall a greater proportion of the available jet energy is lost during free fall and at impact. The proportion of the total head which is lost during the air entrainment process is therefore reduced for increasing fall. This must therefore explain the reduction in aeration efficiency which results for increasing fall despite the greater relative quantities of air entrained. In the case of the hydraulic jump, greater energy losses occur through the sluice gate opening for larger available heads, but, a state of "water saturated with air" is more rapidly reached which will result in losses in the potential air/water interface because of the increased tendency for air bubbles to make contact with each other.

For greater head losses than those tested in Table 8.8 for this specific discharge, the free overfall will probably become the more efficient aerator since the hydraulic jump will have attained the "water saturated with air" condition (RAO & KOBUS, $Q_a/(Q_a + Q) = 50\%$, i.e. $\beta = 1$).

8.4.4 Aeration Efficiency of a Cascade

To enable comparison with the free overfall and hydraulic jump discussed in Section 8.4.3, a cascade has been visualised which fits into a 10cm wide channel and consists of a series of five free overfalls, h = 0.2m each, depth of pool on each step 0.2m (this provides optimum depth conditions, see Figure 6.4) - for illustration of this cascade see Figure 8.4.

The oxygen deficit is traced through this cascade in Table 8.9 below together with the transfer efficiency for each step.

TABLE 8.9

The Efficiency Variation Through a Cascade, $q = 150\ cm^2/s$

STEP	(C_s-C_1) % Saturation	(C_s-C_2) % Saturation	Efficiency Kg/Kwh	Deficit Ratio r_{15} *
1	50	40.65	1.68	1.23
2	40.65	33.05	1.37	1.23
3	33.05	26.87	1.11	1.23
4	26.87	21.84	0.90	1.23
5	21.84	17.76	0.73	1.23

*Figure 6.5 (tap water containing 0.3% sodium nitrite)

OVERALL DEFICIT RATIO = 2.815 = $(1.23)^5$

OVERALL EFFICIENCY = 1.159 Kg/Kwh

The reduction in transfer efficiency through the cascade is to be expected from the reduction in oxygen deficit through the cascade. It is clear from this that an optimal number of steps will exist for a

given height of fall and discharge. Comparison with Table 8.8 shows the improved aeration efficiency attained by this cascade.

8.5 A COMPARISON OF PREVIOUSLY PUBLISHED PREDICTION EQUATIONS WITH EQUATION 7.20

As a final confirmation of the wide range of applicability of Equation 7.20, the measured deficit ratios for the prototype data introduced in Tables 8.4 and 8.5 have been compared in Table 8.10 below with the predicted values using the various prediction equations discussed in Chapter 2 together with Equation 7.20. These results are also plotted in Figure 8.6.

TABLE 8.10

A Comparison of Various Prediction Equations

WEIR REFERENCE LETTER ****	MEASURED r_{15}	PREDICTED DEFICIT RATIO					
		Eq. 2.11 *	Eq. 2.24	Eq. 2.31	Eq. 2.34 **	Eq. 2.43	Eq. 7.20
A	1.26	1.30	1.65	1.11	1.36	-	1.27
A	1.34	1.30	1.65	1.11	1.36	-	1.30
B	1.50	1.33	1.71	1.12	1.39	-	1.30
B	1.26	1.33	1.71	1.12	1.39	-	1.33
C	1.74	2.86	3.62	1.89	2.41	∞	1.95
D	2.63	4.21	5.16	2.56	1.40	∞	2.84
E	3.39	5.33	5.73	2.97	-0.19	∞	***
F	1.70	2.28	3.96	1.85	2.46	∞	1.96

*a = b = 1

**a = b = 1

***disintegrated jet

****for data refer to Tables 8.6 and 8.7

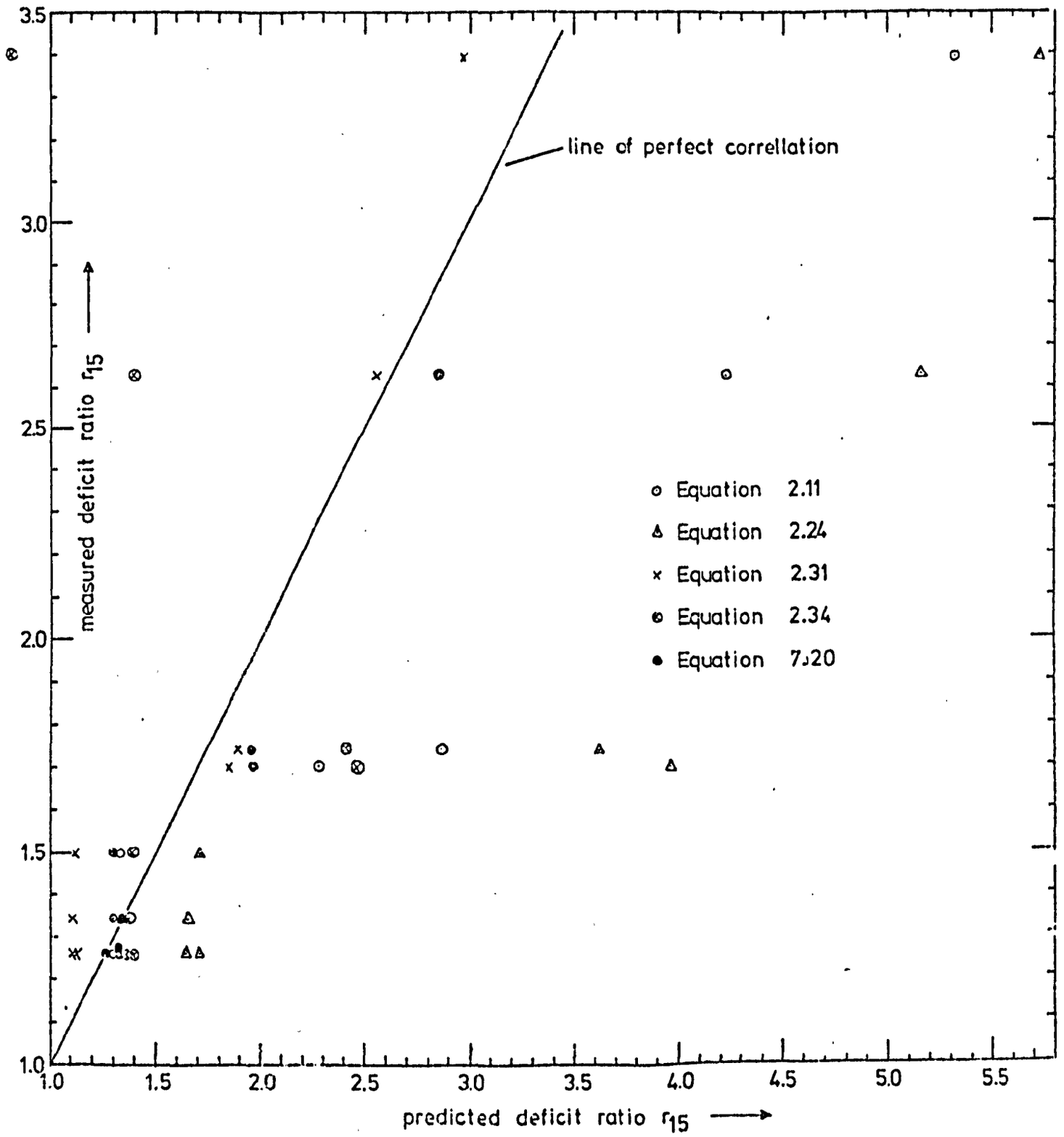

figure 8.6 a comparison of various prediction equations for the determination of oxygen transfer at free overfalls.

When viewing the results in Table 8.10 it should be borne in mind that Equation 2.31 was developed by HOLLER from the data for weirs C, D and E so the prediction of these should be perfect. As expected, Equation 2.43 is inapplicable except to the specific apparatus from which it was derived, and the limitations of the other prediction equations are apparent, particularly for large heights of fall.

Equation 7.20 is the only equation giving consistently reliable predictions.

8.6 SUMMARY

A general equation, describing the oxygen transfer resulting from a jet entering a free water recipient with optimum depth conditions prevailing, was developed from model studies and presented in Chapter 7, Equation 7.20.

This equation has been further validated by successful correlation with laboratory data collected from various publications. Furthermore, satisfactory correlation was achieved without exception with a number of prototype situations encompassing a wide variety of discharges, heights of fall and degrees of pollution (Figure 8.3). A comparison with various other prediction equations has further confirmed the wide range of applicability of Equation 7.20 (Figure 8.6).

If this success can be confirmed by further prototype measurements, then it will establish Equation 7.20 as the first successful correlation of laboratory and prototype data at a free overfall weir.

A comparison of aeration efficiencies of various aerators has been made. While the recently developed U-Tube aerator represents the most efficient and economic aeration system currently available, the

free overfall weir, particularly in the form of a series of falls or cascade, also ranks highly as a cheap efficient means of oxygen transfer. In addition it has the advantage of being a structure which in most cases is not installed for aeration purposes (therefore no capital costs) and which is relatively trouble free being unaffected by floating debris etc.

Similarly, the high efficiency of oxygen transfer in an hydraulic jump has been demonstrated. The efficiency achieved was similar to that with a free overfall for a particular available head, and the hydraulic jump was shown to have an advantage of requiring a smaller tailwater depth than the free overfall.

CHAPTER 9

SUMMARY, SUGGESTIONS FOR FURTHER RESEARCH, AND CONCLUSIONS

9.1 SUMMARY

9.1.1 Background to the Reported Research

1. The processes of gas transfer are generally described by the gas transfer equation, Equation 1.35.

2. Equation 1.35 indicates that the oxygen transfer at a particular aeration system is predictable from a knowledge of the following factors:

(i) the oxygen solubility in the liquid phase which is dependent on the prevailing conditions of temperature and pressure and on the presence of dissolved salts.

(ii) the volume of the liquid phase;

(iii) the air/water interfacial area which may be estimated from a knowledge of gas flow rate, bubble size and contact time;

(iv) the time over which the water volume is aerated;

(v) the liquid film gas transfer coefficient which is dependent on the oxygen diffusion coefficient, the time of exposure or rate of surface renewal, and also in some cases on the presence of surface active agents.

For practical purposes, the application of Equation 1.35 is not possible.

3. Recourse has therefore usually been made to experiment to attempt to relate the oxygen transfer expressed as a deficit ratio (an expression of Equation 1.35) to the measurable hydraulic characteristics of an aeration system.

4. The air entraining capability of many hydraulic features is relatively well understood and successful modelling according the Froude law of similarity has been achieved.

5. Little work has been done to quantify the oxygen transfer in an hydraulic jump.

6. The free overfall weir has been extensively studied, however, the available oxygen transfer prediction equations are generally severely limited in application. Also, attempts at model/prototype correlation have not proved successful and therefore it is clear that all the effective parameters controlling the oxygen transfer at a free overfall weir have yet to be identified.

7. Most research workers have attempted to relate the oxygen transfer at a free overfall weir to the height of fall only, although the importance of the downstream pool conditions and the effect of discharge have been recognised by several workers.

9.1.2 The Reported Research

9.1.2.1 The Hydraulic Jump

1. A study of the velocity coefficients of the flow downstream of an hydraulic jump did not indicate any significant departure of these from unity.

2. Departures in the conjugate depth ratio from the law of Bélanger as indicated by measurements of APTED (and hence the discrepancies between energy losses given by Equation 3.4 and 3.5), and similarly by some measurements of HOLLER, are due to inaccurately measured supercritical depths.

3. The time of contact in an hydraulic jump was both theoretically and experimentally demonstrated to vary as the square root of the length scale over the range tested.

4. The liquid film coefficient was reasoned to be a function of the energy loss and therefore to be a function of Froude number and depth y_1 or y_2 (i.e. the scale).

5. It is established that the relative quantity of air entrained is a function of Froude number only. It was reasoned, and experimentally verified, that the oxygen transfer in an hydraulic jump should therefore be a function of the supercritical Froude number and the scale (and therefore discharge).

6. The presence of dissolved inorganic salts in the form of sodium nitrite was found to significantly enhance the oxygen transfer at this situation of air entrainment.

7. The mean size of air bubble entrained into an hydraulic jump was recorded photographically. Results were in general agreement with the results of a variety of workers, but, it was shown that this size, whilst independent of scale, was substantially reduced in the presence of dissolved sodium nitrite.

8. A positively skewed distribution of bubble sizes was observed. A mean diameter of 2.5mm was observed in tap water, of 1.7mm in tap water containing 0.3% sodium nitrite and of 1.5mm in APTED's measurements in tap water containing 0.6% sodium nitrite.

9. The presence of sodium nitrite is believed to have resulted in the concentration of dissolved matter at the bubble liquid interface, thus creating a resistance which prevented the coalescence of bubbles.

10. The anemometric determination of bubble sizes by LEUTHEUSSER, RESCH and ALEMU was queried as otherwise inexplicably large bubble diameters of the order of 10mm were recorded.

11. For an unchanged quantity of air entrainment, the reduced mean bubble size in the presence of dissolved salt resulted in a larger gas/liquid interface and thus a greatly enhanced aeration.

12. There will be some limiting salinity beyond which no further reduction in bubble size will be observed and a reduction in aeration may follow due to the reduced solubility.

13. Two general equations describing the oxygen transfer in an hydraulic jump have been presented, Equations 4.24 and 4.25 (non dimensional, q/345 is a specific discharge ratio with q in cm^2/s).

14. A non dimensional expression, Equation 5.5, has been presented describing the dependence of the liquid film coefficient on various factors.

.9.1.2.2 The Free Falling Jet

1. The oxygen transfer due to a free falling jet entering a free water recipient has been fully investigated.

2. For a fixed lower pool bed, there was an optimum depth for maximum oxygen transfer as similarly observed by others.

3. The optimum depth, and therefore bubble contact time, was dependent on the jet discharge, and therefore the shape of the jet, also on the height of fall and therefore whether the jet was solid or disintegrated.

4. The reduction of the pool width resulted in slight losses of contact time and thus of oxygen transfer also, but did not alter the optimum depth required.

5. Serious reservations have been expressed concerning the accuracy of oxygen measurements of both JARVIS and APTED.

6. The oxygen transfer as a result of air entrainment by a jet has been shown to depend on the height of fall and discharge as similarly demonstrated by others.

7. For a constant height of fall, an increase in the ratio of jet perimeter to jet cross sectional area (reduced hydraulic radius) resulted in an increased relative air entrainment, a reduced optimum depth requirement and an enhanced oxygen transfer.

8. A reduction in hydraulic radius can be effected for a particular discharge and height of fall by partitioning the flow to produce a series of jets of lesser discharge, or, by inducing the formation of a wider jet.

9. Disintegrated jets may require a lesser optimum depth, however they continue to entrain large quantities of air as evidenced by the fact that no fall off in the rate of aeration was recorded.

10. A jet Froude number, applicable to solid jets only, has been defined (Equation 7.4) in terms of the important factors controlling the air entrainment - the jet velocity (i.e. height of fall) and the discharge per unit jet perimeter.

11. The optimum depth has been shown to vary according to some function of the height of fall (or the length scale of the model) for constant jet Froude number.

12. A correlation equation, Equation 7.13 or 7.14, has been presented which describes the relationship between optimum depth, Froude number and the height of fall (or the model length scale).

13. Equation 7.14 has been shown to provide sensible predictions of the optimum depths observed by the D.O.E. (1973) and also APTED (1975).

14. For pool depths equal to or in excess of the optimum, the oxygen transfer has been shown to vary as a function of the height of fall or scale for constant Froude number. This has been justified since for a constant Froude number, the relative quantities of air entrained are assumed constant whilst the contact time in the pool and also the energy loss in the pool (and hence the liquid film coefficient) will be functions of the height of fall or model length scale.

15. For optimum depth conditions prevailing, a correlation equation, Equation 7.20, has been submitted which describes the relationship between oxygen transfer, jet Froude number and the model length scale.

16. Equation 7.20 accurately correlates all the data from experiments conducted by the author of this thesis for a variety of solid jets of varying discharge and shape as well as for varying heights of fall. The enhancing effects of dissolved salts on aeration have been taken into account with the appropriate value of the constant being selected from Table 7.2.

17. Equation 7.20 correlates well, for the first time, with all available published laboratory measurements at free overfalls.

18. Equation 7.20 has been shown to describe the aeration occurring at a cascade weir and also that due to multi-crested weirs subject to certain conditions.

19. Furthermore, Equation 7.20 has correlated well and without exception with data received for a number of prototype free overfall weirs and dams encompassing a wide variation in heights of fall, jet discharge, and also in degrees of pollution as evidenced by the initial oxygen deficits recorded at these structures.

20. Equation 7.20 therefore represents the first successful correlation of laboratory and prototype oxygen measurements at a free overfall.

21. It has therefore been suggested that the presence of pollutants may influence the size of bubble entrained, but that the effect on the liquid film transfer coefficient will be minimal in a situation of highly turbulent air entrainment, since the degree of mixing will be such as to rapidly replenish liquid films with fresh fluid elements and thus prevent the stifling effects of a congregation of surface active agents surrounding the bubbles.

22. A comparison of predictions by Equation 7.20 and all the previously available equations with measured deficit ratio at a number of prototype structures, confirmed Equation 7.20 as consistently reliable whilst the others displayed alarming discrepancies in several instances. Equation 7.20 therefore takes into account all the important variables.

23. A weir represents an efficient and cheap source of oxygen when compared to various commercial aerators.

24. A free overfall weir and hydraulic jump displayed similar aeration efficiencies at laboratory scale whilst the hydraulic jump had the advantage of requiring a smaller tailwater depth.

25. The efficiency of a weir as an aerator decreases with increasing heights of fall, hence a more efficient use may be made of a large height of fall by constructing a cascade of small falls, thus exploiting the greater efficiency of the smaller falls.

26. The efficiency of a weir as an aerator for a given height of fall may be promoted by ensuring optimum depth conditions in the pool below and by forming a jet with as large a jet Froude number as possible. This may be achieved for a given fall by increasing the crest width or by partitioning of the crest. The increased Froude number also results in a reduced optimum depth requirement (Equation 7.14).

9.2 SUGGESTIONS FOR FURTHER RESEARCH

1. Initially, it is necessary to fully test the prediction equations submitted in this thesis, namely Equations 4.24 and 4.25 for the hydraulic jump and Equations 7.14 and 7.20 for the free falling water jet. From these tests the direction of further research will be more obvious.

2. It is clear that the lower limit ($Fr_1 > 8$) indicated by WISNER for successful modelling of air entrainment in an hydraulic jump, requires investigation with regard to oxygen transfer since the tests reported in this thesis generally fell below this limit. Even with regard to air entrainment, the limit has yet to be fully confirmed.

3. An effect of inflow condition of the hydraulic jump on the air entrainment has been indicated by LEUTHEUSSER, RESCH and ALEMU. There will therefore be a separate relationship describing the oxygen transfer which needs determination.

4. Equation 7.20 could easily be expanded from the data in this thesis to describe the deficit ratio for depths less than the optimum. The deficit ratio may well vary as some function of the ratio of actual depth to optimum depth for constant Froude number and height of fall.

5. Consideration needs also to be given to disintegrated jets since these doubtless display different characteristics of air entrainment whilst creating a large air/water interface during the free fall.

6. The application of Equation 7.20 to multi-crested weirs requires that there be no jet interaction and that the air entrainment processes of one jet should not be unduly altered by those of a neighbouring jet. The effect of jet spacing requires investigation with a view to assessing limits to the application of Equation 7.20.

7. The effects on entrained air bubble size observed with sodium nitrite require to be similarly tested with other inorganic dissolved salts. The range of salinity investigated here requires to be extended with a view to determining the limiting salt concentration anticipated for full prevention of bubble coalescence.

8. The dependence of the oxygen transfer processes on the Froude number and the model length scale as demonstrated with the

hydraulic jump and free overfall weir could similarly be extended to air entraining situations encountered with other hydraulic structures such as morning glory spillways.

9. Further work is required on the effect of temperature to establish the range of applicability of Equation 2.13 in terms of energy levels. The importance of comparable levels of energy expenditure in both model and prototype is obvious in order to equalise the influence of diffusion effects. In this respect, the hydraulic jump tests in this thesis require further substantiation since relatively low energy expenditure levels were encountered in a number of cases.

9.3 CONCLUSIONS

1. If an hydraulic jump is modelled according to the Froude law of similarity, then the oxygen transfer expressed as a deficit ratio will vary as a simplified function of the length scale of the model as described by Equations 4.24 and 4.25.

2. Equations 4.24 and 4.25 may therefore be used to determine the oxygen transferred as a result of air entrainment by an hydraulic jump.

3. Hitherto available prediction equations for application at free overfall weirs are severely limited in application since they do not consider all effective factors governing the oxygen transfer.

4. The oxygen measurements of JARVIS and also APTED were shown to be in error.

5. The importance of maintaining optimum depth conditions in the pool below a weir was confirmed, but the width of the pool did not exert any significant influence on the oxygen transfer from entrained air.

6. A jet Froude number, Equation 7.4, has been defined in terms of the jet velocity and the hydraulic radius of the jet.

7. If a free overfall is modelled according to the Froude law of similarity, then the oxygen transfer, resulting from a solid jet entraining air into a pool with optimum depth conditions prevailing, will vary as a simplified function of the scale as described in Equation 7.20.

8. Equation 7.20 for the first time successfully correlates all hitherto published laboratory data together with the currently reported data at a free overfall for a variety of weir types, discharges and heights of fall.

9. Equation 7.20 successfully correlates the aforementioned model studies with data received for a number of prototype free overfall situations encompassing a very wide range of discharges, crest widths, heights of fall and also pollution levels. This represents the first successful model/prototype correlation for a free overfall.

10. The presence of dissolved inorganic salts in the form of sodium nitrite resulted in a reduction in the mean size of air bubble entrained, an increase in the air/water interface and hence an enhancement of the oxygen transfer resulting.

11. The presence of pollutants or surface active agents in water is not likely to inhibit the oxygen transfer rate per unit area in a highly mixed situation of air entrainment although it may influence the size of bubble entrained and thus the air/water interfacial area.

A P P E N D I X A

THE MEASUREMENT OF OXYGEN DISSOLVED IN WATER

A.1 STANDARD METHODS OF MEASUREMENT

The standard means of determining the quantities of oxygen dissolved in water remains that due to WINKLER (1888).

The method makes use of the fact that under alkaline conditions, oxygen will oxidise Mn++ to a higher state of valence and that on addition of acid, the manganese in a higher state of valence is capable of oxidising I^- to free I_2. The amount of liberated iodine is equivalent to the amount of dissolved oxygen initially present and this amount is measured by titration with a standard sodium thiosulphate solution.

There are a number of modifications of this method designed to cope with various interfering substances. (See SAWYER and McCARTY for details):

(1) Alsterberg (Azide) Method - in the presence of nitrites.

(2) Rideal-Stewart (Permanganate) Method - in the presence of ferrous iron but not in the presence of organic matter.

(3) Pomeroy-Kirshman-Alsterberg Method - in the presence of high organic content or for water supersaturated with oxygen.

The most recent development in dissolved oxygen determination is the Polarographic method. A galvanic cell capable of reducing oxygen is constructed using a basic electrolyte with a lead anode and silver cathode. The electrode is surrounded by a selective semi-permeable membrane which permits the diffusion of oxygen and shields the anode and cathode from contamination. Oxygen diffusing into the electrode is rapidly reduced and a current produced whose magnitude is dependent on

the partial pressure of oxygen in the water. Hence a useful means of measuring dissolved oxygen.

A.2 THE SELECTION OF A SUITABLE MEANS OF MEASURING DISSOLVED OXYGEN

The laboratory water system is treated with quantities of sodium nitrite as a rust inhibitor (Section 4.3).

The concentrations of nitrite ion present unfortunately proved excessive even for the Alsterberg modification of the WINKLER method of dissolved oxygen determination. This factor together with the need for continuous monitoring of dissolved oxygen levels made the choice of the Polarographic technique an obvious one.

A.3 DESCRIPTION OF DISSOLVED OXYGEN METERS AND ELECTRODES

The model 15A Dissolved Oxygen Meter coupled with the Model A15A Mackereth Oxygen Electrode and Model T15A resistance thermometer and temperature compensator as manufactured by Electronic Instruments Ltd., Surrey, is illustrated in Plate A.1. Two such meters were used.

The meters are provided with two scales, the first indicating the partial pressure of oxygen in solution expressed as percentage saturation, with two available scale ranges 0-100% and 0-200%, and the second scale indicating temperature over a range -5 to 30°C. In common with other electrodes which permit gaseous but not liquid or ionic diffusion, the A15A electrode has a high temperature coefficient of approximately 6% per °C change in temperature, compensation for this being provided by the T15A combined resistance thermometer and temperature compensator.

PLATE A.1 Dissolved oxygen meters with probes and perspex cells

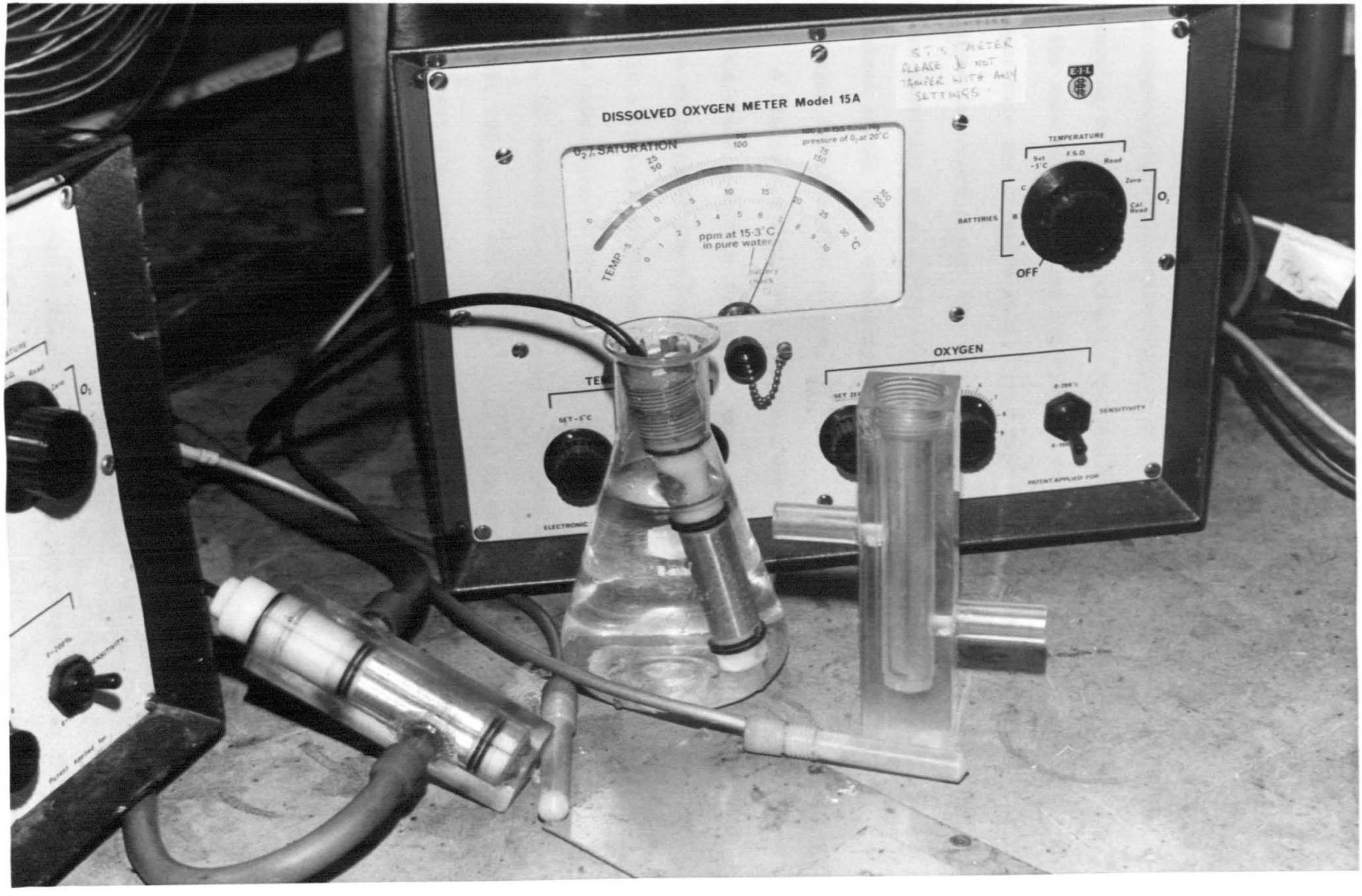

Apart from the obvious convenience of this type of equipment, a major advantage is offered by the measurement of partial pressure. If solutions of varying ionic content are equilibrated with air, then the oxygen saturation concentration in the various solutions will vary according to the ionic content, but the oxygen partial pressure will be the same in the various solutions since this is a function of temperature and pressure only. This type of equipment can therefore be used to record oxygen levels as a percentage of saturation without prior knowledge of salinity levels, the ionic content will only be required should it be necessary to convert from percentage saturation to oxygen concentration in ppm.

A limitation with this equipment was that a minimum flow velocity of 10cm/s was specified to prevent the occurrence of oxygen depletion in the vicinity of the electrode. The relatively sluggish response time is a further limitation. The manufacturers quote the response as the time taken to attain 90% of the final reading: 75 seconds for oxygen, 90 seconds for temperature. However it is worth noting that the last 10%, which was not referred to in the specification, takes a significant time as the rate of approach to the final reading was observed to decrease as the final reading was approached. Hence some difficulty could be encountered in deciding when the final reading had been attained.

A.4 ACCURACY OF OXYGEN MEASUREMENT

The following accuracy limits are quoted by the manufacturers:

Temperature: $\pm$ 1.5°C

Temperature compensation: automatic in the range -5°C to 30°C

Oxygen: $\pm$ 5% of scale reading for temperatures within 10°C of a previously selected temperature.

In fact the equipment performed within the maker's limits as shown by the following example taken from the laboratory log book:

TABLE A.1

Date of Calibration: 9 June 1975				Tap Water
Meter Readings		WINKLER Test oxygen content		Meter error as % of WINKLER determination
Temperature ^{o}C	Oxygen % Saturation	mg/l	% Sat.	
23.7	94.3	8.17	95	-0.7
13.9	88.9	9.62	94	-5.4

A.5 CALIBRATION OF DISSOLVED OXYGEN METERS

The errors indicated in Table A.1 demonstrate inadequate temperature compensation and were not acceptable in view of the accuracy required for these experiments. Thus the meters were always calibrated at the operating temperature in order to reduce the dependence on temperature compensation and under these conditions were observed to perform accurately.

The manufacturers recommend that the meters be calibrated to indicate the ratio (expressed as a percentage) of the partial pressure at prevailing temperature and pressure to partial pressure at prevailing temperature and 760mm pressure. During the current studies it was preferred to calibrate the meters to indicate partial pressure as a percentage of saturation at prevailing conditions of temperature and pressure, since this is a more correct definition.

To calibrate the meters, the electrodes were immersed in a 10 litre vessel of air-equilbrated tap water at the same temperature as the laboratory water - a small air pump with a diffuser stone was used (See Plate A.2). The oxygen electrode was vigorously agitated to prevent the occurrence of oxygen starvation in the vicinity of the electrode, the dissolved oxygen level (mg/l) of the water was determined by the Azide modification of the WINKLER method. Accurate readings of atmospheric pressure were obtained from a mercury barometer (manufactured by Negretti & Zambra, London) and hence the oxygen concentration could be expressed as a percentage of saturation by means of the nomogram of HART (1967) - Figure 1.5. The reading indicated by the meter was set to this value.

It is worth recording here that on a number of occasions the oxygen concentration in the air equilibrated water was some 3 to 4% below saturation. The chemical titration method was very precise, and similarly the determination of pressure and temperature. This occurrence was attributed to differences between air and water temperature, the former generally being higher than the latter.

A.6 A LINEARITY CHECK ON THE DISSOLVED OXYGEN METERS

The daily calibration procedure provided a check on the reading of the Dissolved Oxygen Meter at the top end of its scale and by immersing the oxygen electrode in a 5% solution of sodium sulphite the zero reading was also checked. In addition it was deemed worthwhile to check on the performance at intermediate oxygen levels.

A large vessel of water was de-oxygenated to the required oxygen level by bubbling nitrogen gas into the water. Water was siphoned from this vessel, passed over the oxygen electrode contained in a

PLATE A.2 Dissolved oxygen meter undergoing calibration

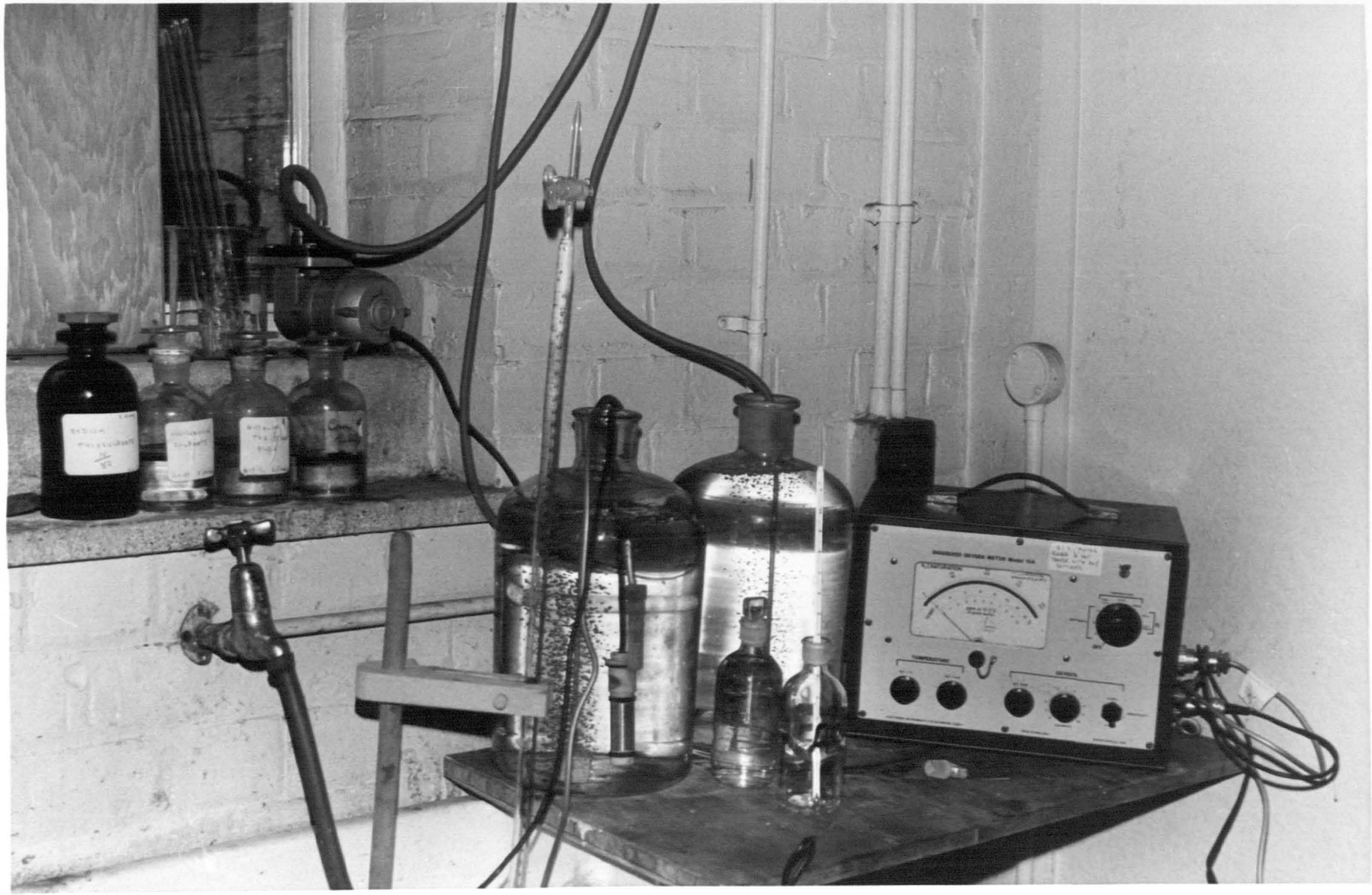

perspex cell (Section A.8) and the indicated reading compared with that obtained from a sample collected and tested by the WINKLER method.

A typical comparison of indicated and chemically analysed dissolved oxygen levels is illustrated in Figure A.1 from which it was clear that the equipment performed accurately over its whole scale range. Also shown in Figure A.1 is a schematic sketch of the test described above.

A.7 THE EFFECT OF FLOW VELOCITY ON READINGS INDICATED BY THE DO METERS

During early experiments with this equipment the dangers of the occurrence of oxygen depletion in the vicinity of the oxygen electrodes and the subsequent underestimate of oxygen levels became apparent. This was particularly so during experiments with the free overfall where relatively low velocities were obviously present at outflow from the lower pool. A detailed examination of the behaviour of the electrode under various flow conditions was considered beneficial.

A series of tests was conducted in the 3 metre flume (Section 4.2.1) to establish the effect of flow velocity on the indicated reading. Various velocities were obtained by appropriately altering the depth of flow in the channel for a range of discharges between 1.0 and 4.0 l/s. The reading of oxygen level indicated with the electrode placed vertically in the flow was compared with the true reading obtained with the electrode in its perspex cell with water siphoning from the channel through the cell. This latter technique is validated in Section A.8.

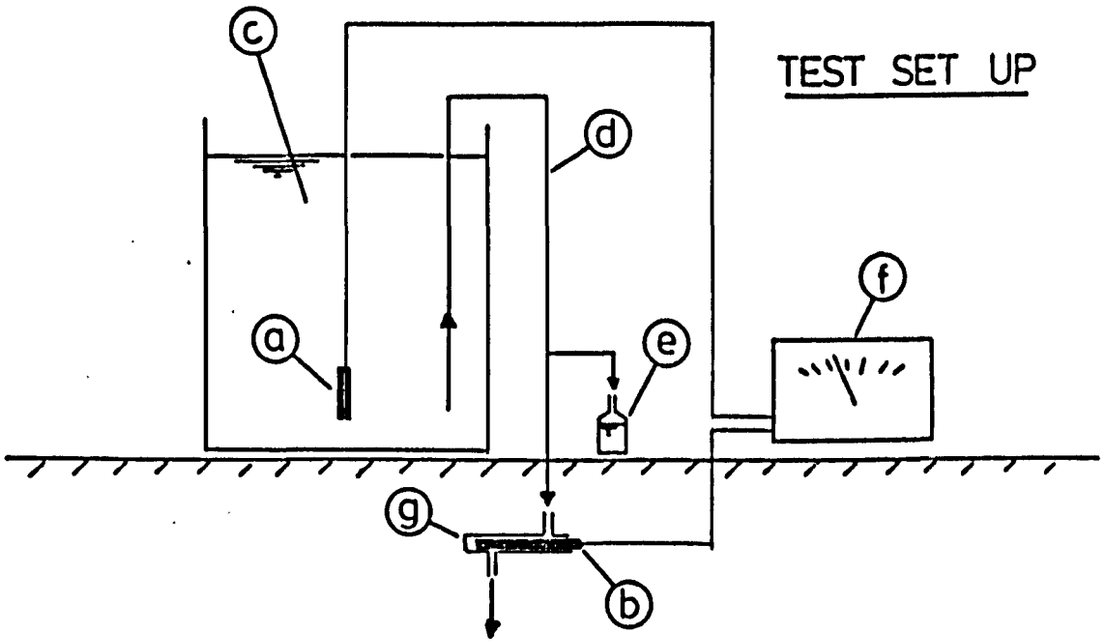

ⓐ temperature probe
ⓑ D.O. electrode
ⓒ deoxygenated water
ⓓ siphon tube
ⓔ sample for WINKLER test
ⓕ D.O. meter
ⓖ perspex cell

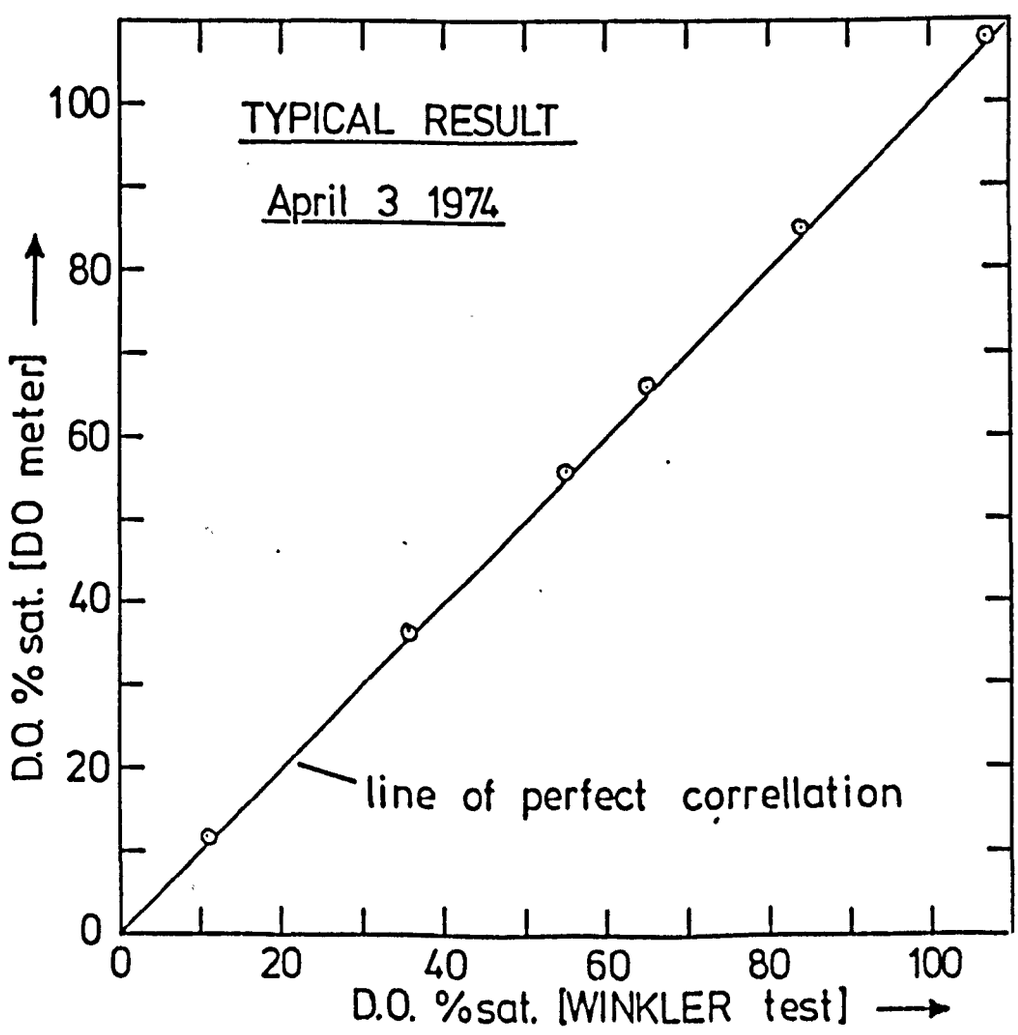

figure A.1 a check on the linearity of a dissolved oxygen (D.O.) meter

The results have been expressed in Figure A.2 where the mean velocity in the channel (Q/A) has been plotted against ΔDO (% saturation), ΔDO being "the oxygen reading indicated by the meter with the electrode in the channel" minus "the true oxygen reading obtained with the same electrode in the perspex cell".

To obtain steady background oxygen levels, the water was allowed to stand overnight in the header tank and thus attain uniform oxygen concentration throughout. This water was then drained from the header tank through the flume. One experiment is reported for which the water was deoxygenated chemically to 44% saturation, however this technique was abandoned since it was impossible to attain the absolute constancy of background oxygen levels required.

From Figure A.2 it can be seen for the minimum flow velocity of 10cm/s recommended by the manufacturers that the electrode is still experiencing an oxygen deficiency in its vicinity. While the 1.7% error is not great in view of the specification accuracy limits of ± 5%, such errors must be eliminated to enable the accuracy of measurement required here. The extent of errors possible for smaller flow velocities is very significant as shown in Figure A.2. Disappearance of oxygen depletion was not apparent until velocities in excess of 30cm/s were flowing.

It is interesting to record that RYDER (1972) quoted a minimum flow velocity of 0.3 m/s (identical to the limit indicated in Figure A.2) in order to prevent inaccuracies due to oxygen depletion at the electrode membrane and electrode polarization.

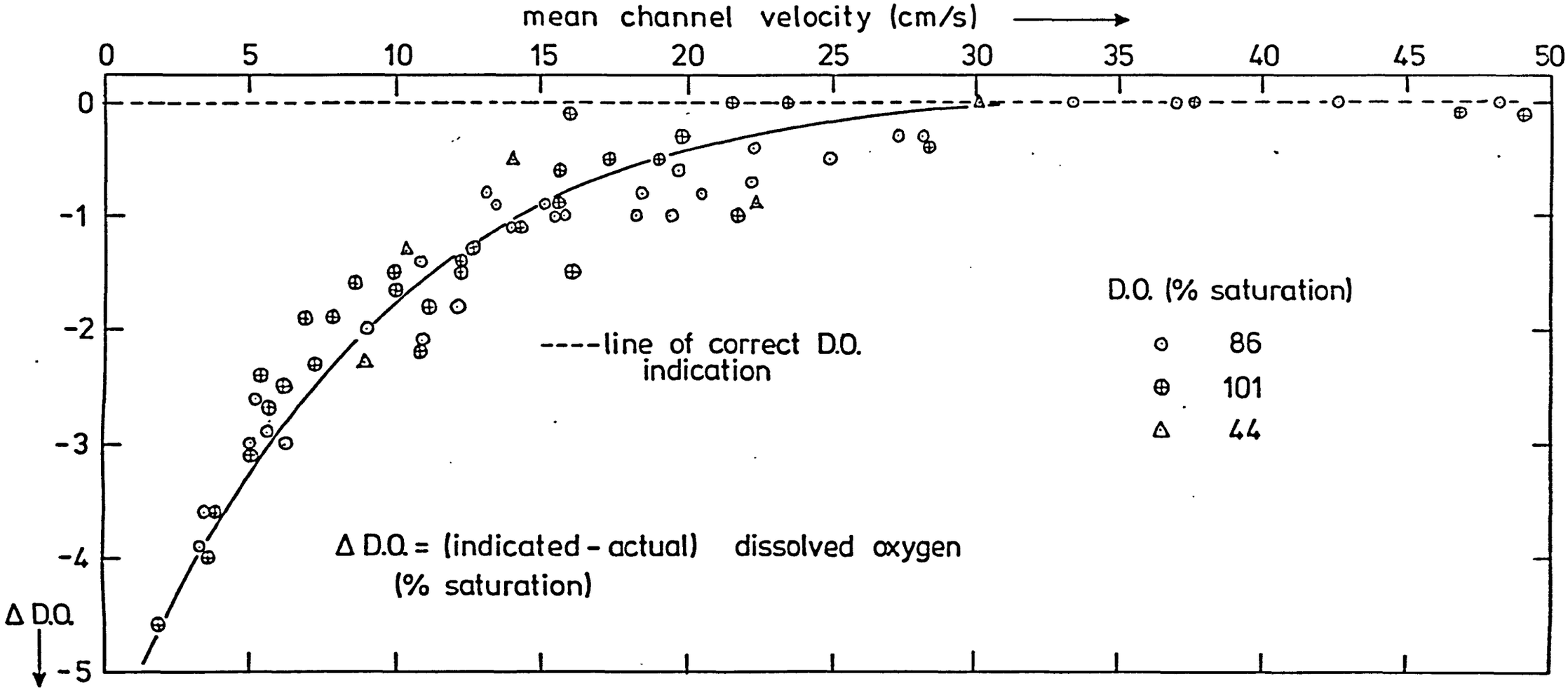

figure A.2 the effect of flow velocity past a dissolved oxygen electrode on the indicated dissolved oxygen level

A.8 A TECHNIQUE TO ELIMINATE OXYGEN DEPLETION

In order to maintain high velocities of flow passing the electrode, a duplicate was made of a perspex cell originally designed by JARVIS (1970) for use when the depth of water was too low to permit complete immersion of the electrode (depths < 5cm). The cell, illustrated in Plate A.1 consists of a block of perspex bored out to snugly accommodate the oxygen electrode. Two tapping points were drilled, one at each end, thus providing the inlet and outlet for the passage of water through the cell. Water could be siphoned through small bore perspex tubing from a selected sampling point and passed along the length of electrode in the perspex cell thus providing an oxygen reading at that sampling point.

The validity of this technique was confirmed over a range of flows from 1.22 to 55cm^3/s passing through the cell. An experimental set up similar to that described in Section A.6 and illustrated in Figure A.1 was utilised, no deviation in indicated oxygen readings was observed from chemically determined levels over the range of flow rates tested. An added advantage of this technique was the protection afforded to the delicate semi-permeable membrane covering the electrode.

A.9 SUMMARY

The standard methods used for the determination of dissolved oxygen have been discussed. The Polarographic technique chosen for the current experiments has been described together with the specifications of accuracy and calibration against the well established WINKLER technique. Some limitations in the automatic temperature compensation of the equipment and also the susceptibility of the oxygen electrodes

to oxygen depletion have been highlighted together with recommendations to overcome these.

A P P E N D I X B

THE DEOXYGENATION OF THE LABORATORY WATER

B.1 INTRODUCTION

Since the laboratory water was generally maintained in an oxygen saturated condition by the recirculatory pump, it was necessary to reduce the oxygen concentration of inflowing water such that even after aeration the dissolved oxygen level was still significantly below saturation.

B.2 VARIOUS MEANS OF REMOVING OXYGEN FROM WATER

The removal of oxygen from water in industrial processes for the prevention of corrosion is usually effected by such processes as vacuum deaeration whereby the water is induced to boil by application of reduced pressures. Oxygen solubility is zero in boiling water, however, absolute oxygen removal is required, and, it is after this stage that chemical scavengers such as hydrazine and sodium sulphite may be employed to remove remaining traces of oxygen. The respective reactions of hydrazine and sodium sulphite with oxygen are as follows:

$$N_2H_4 + O_2 \rightarrow 2H_2O + N_2$$

$$2Na_2SO_3 + O_2 \rightarrow 2Na_2SO_4$$

Hydrazine is generally used in waters of high temperature and has advantages over the sodium sulphite in that it is volatile and does not affect the concentration of dissolved salts. Also it has been claimed to be a corrosion inhibitor (SHREIR, 1963). There is evidence to suggest that the sodium sulphite reaction may have undesirable side effects at high temperature such as production of SO_2 (SHREIR) and thus acidifying the water.

However a side reaction, whereby hydrazine is decomposed, yields ammonia - an undesirable smell to have in any laboratory. Sodium sulphite was therefore used in the current studies.

The reaction between the sulphite ion and oxygen is extremely slow at normal temperatures, but tests by PYE (1947) showed that in the presence of 0.01 ppm cobalt as a catalyst the water was completely deoxygenated from saturation within 15 to 20 seconds. In the absence of a catalyst barely 0.2% of the total oxygen would have been removed.

B.3 THE TECHNIQUE AND EQUIPMENT USED

Contact time between water and sodium sulphite was provided by passage of water through a galvanised steel tank 1.51m x 0.9m x 0.75m whence it flowed under constant head to the free overfall apparatus or 3 metre flume located on the floor below. This tank was fitted with a baffle system to prevent short circuiting of flow between the inlet and outlet sections (Figure B.1). The volume of this mixing tank would therefore enable a total flow of 50 l/s to be satisfactorily deoxygenated according to PYE's findings above.

Both JARVIS and APTED used Mariotte vessels to provide a constant dosing rate of sodium sulphite and cobalt chloride. However this technique was abandoned here due to the inadequate capacity of the vessels and difficulty encountered in maintaining a constant dosing rate.

An efficient system was evolved utilising a 90 litre vessel in which the measured quantities of sodium sulphite and cobalt chloride catalyst were dissolved with water. This solution was pumped by a variable capacity Watson-Marlow Flow-Inducer (See Plate B.1) and

FIG B.1 : MIXING TANK AND DEOXYGENATION SYSTEM

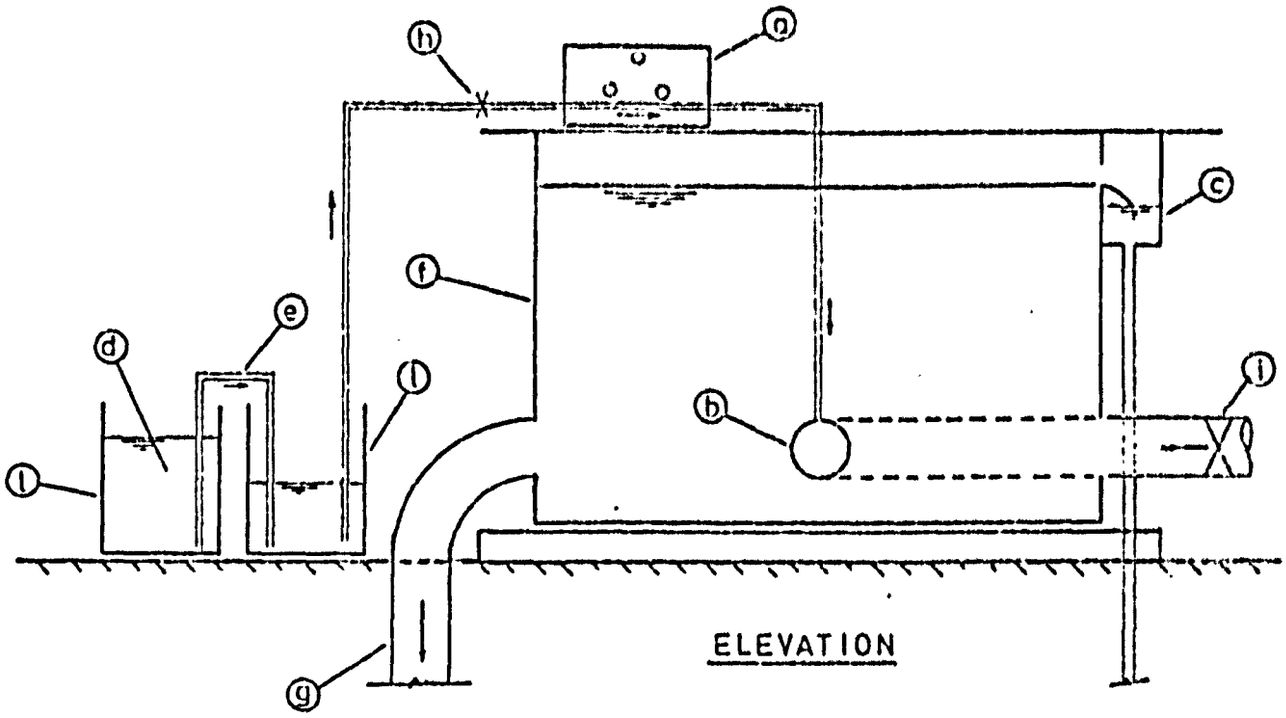

ELEVATION

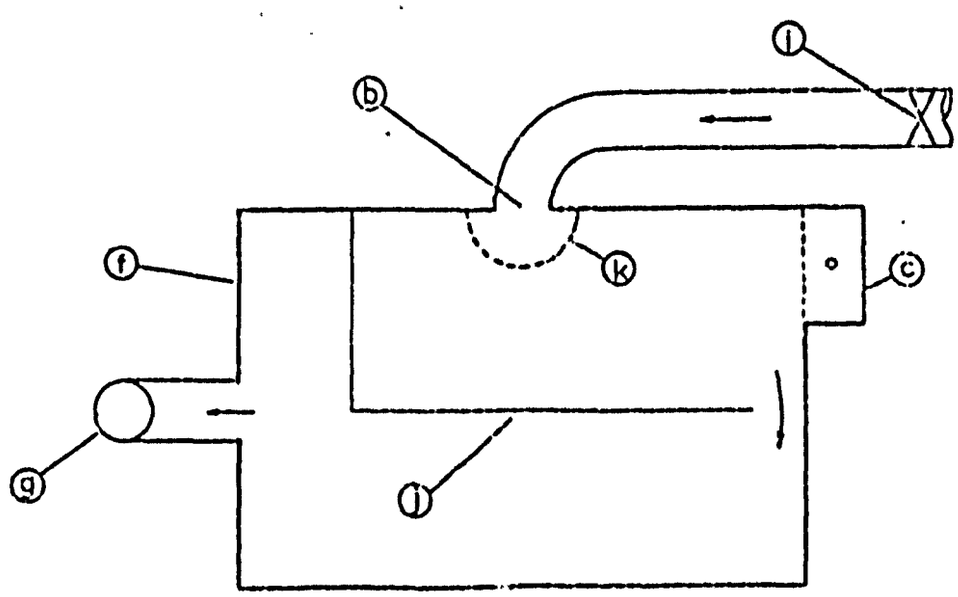

PLAN

ⓐ flow inducer
ⓑ inlet from header tank
ⓒ overflow tank
ⓓ sodium sulphite solution
ⓔ siphon tube
ⓕ mixing tank
ⓖ deoxygenated water supply pipe
ⓗ needle valve
ⓘ gate valve
ⓙ baffle plate
ⓚ wire mesh flow disperser
ⓛ 90 litre vessel

PLATE B.1 Flow-inducer used for dosing sodium sulphite solution

injected into the inlet pipe. Whilst the dosing rate could be regulated by a rheostat control on the pump, a fine control needle valve was installed on the suction side of the pump. The efficient mixing of water and sodium sulphite solution was aided by a wire mesh flow disperser fitted over the inlet to the mixing tank. To maintain a continuous supply of sodium sulphite, a second 90 litre vessel was used for mixing the new solution and this solution was then siphoned into the vessel from which sulphite was already being extracted.

The system described above is illustrated in Figure B.1.

B.4 CALCULATION OF DOSING RATE

The quantities of cobalt chloride added were always in excess of 0.01ppm. The stoichiometric requirement for the fixation of oxygen is 7.88 ppm of sodium sulphite per ppm of oxygen.

Therefore if a discharge of Q l/s is to be deoxygenated from saturation to an oxygen deficit D, then the quantity of sulphite required is:

$$7.88\ Q\frac{D}{100}\ C_s \qquad \text{mg/s of } NaNO_3$$

where the required oxygen deficit D is expressed as a percentage of the saturation concentration C_s (mg/l) of oxygen in water. C_s will depend on the conditions of water temperature and barometric pressure prevailing and also on the dissolved salt level in the water - see Equations 1.38 and 1.41 for estimates of C_s. Various oxygen deficits were used during tests.

B.5 A CHECK FOR SULPHITE RESIDUALS

In view of the rapidity of sulphite reaction and the large contact time provided by the mixing tank, sulphite residuals were not anticipated.

The presence of sulphite is easily identified by iodide in acid solution with a starch indicator. Sulphite present reduces iodide to iodine which gives a blue colour with the starch. In the absence of sulphite no colour is produced when the reagents are added to a sample.

Recourse to this test did not prove necessary. Sulphite residuals were checked for during hydraulic jump tests by measuring dissolved oxygen levels along the length of the flume. If sulphite was present then the dissolved oxygen profile would have indicated a drop in oxygen level along the length of the flume. No such drop was found. Similarly, during a free overfall experiment, the lower pool was maintained at maximum depth. The oxygen levels in the pool were continuously monitored and when steady, the water supply to the weir apparatus was shut off and the outlet from the lower pool was closed. The oxygen level in the water held in the pool was then monitored for several minutes. As with the hydraulic jump tests, no fall in the oxygen level was observed thus confirming the absence of sulphite.

APPENDIX C

FREE OVERFALL DATA - 100MM WIDE RECTANGULAR NOTCH

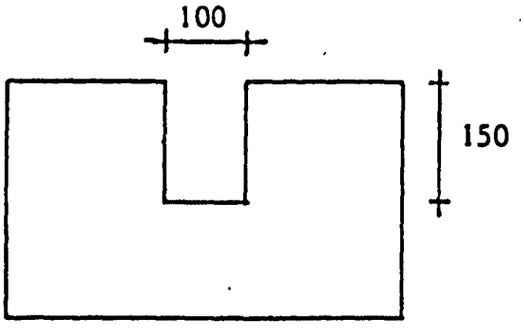

Figures C1.1 to C1.7 Tests with tap water + 0.6% $NaNO_3$

Figures C2.1 to C2.7 Tests with tap water + 0.3% $NaNO_3$

Figures C3.1 to C3.6 Tests with tap water

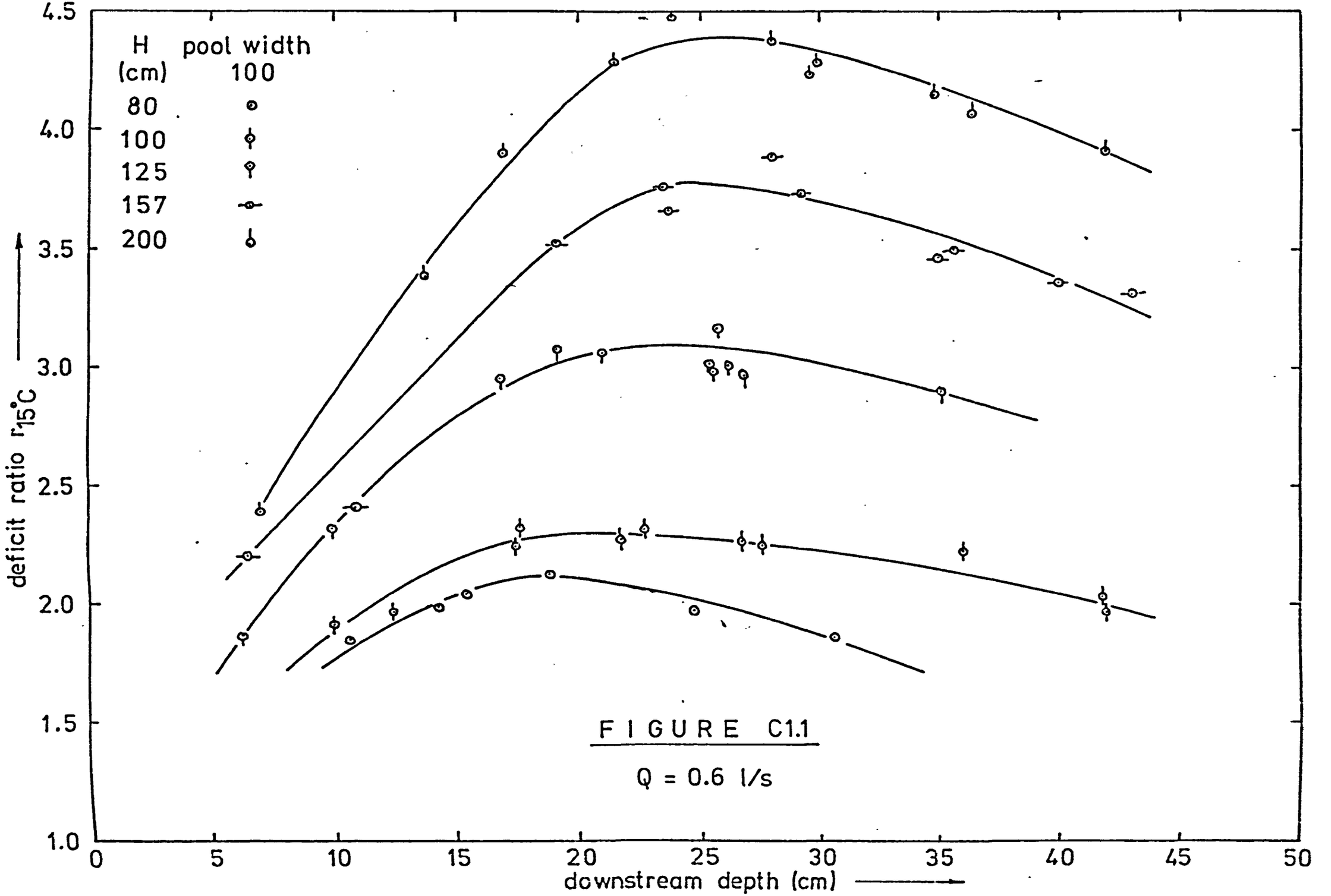

FIGURE C1.1

Q = 0.6 l/s

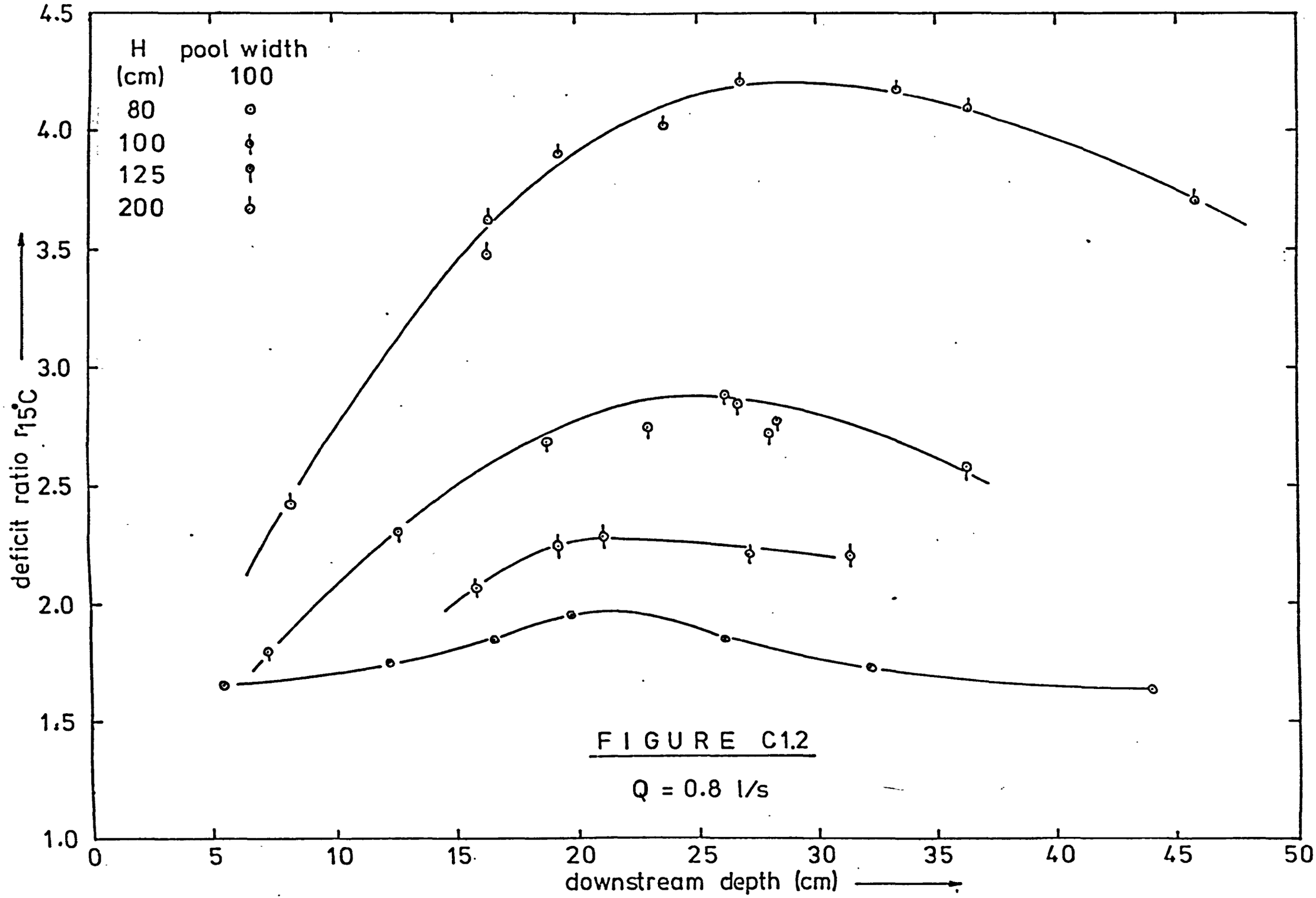

FIGURE C1.2

Q = 0.8 l/s

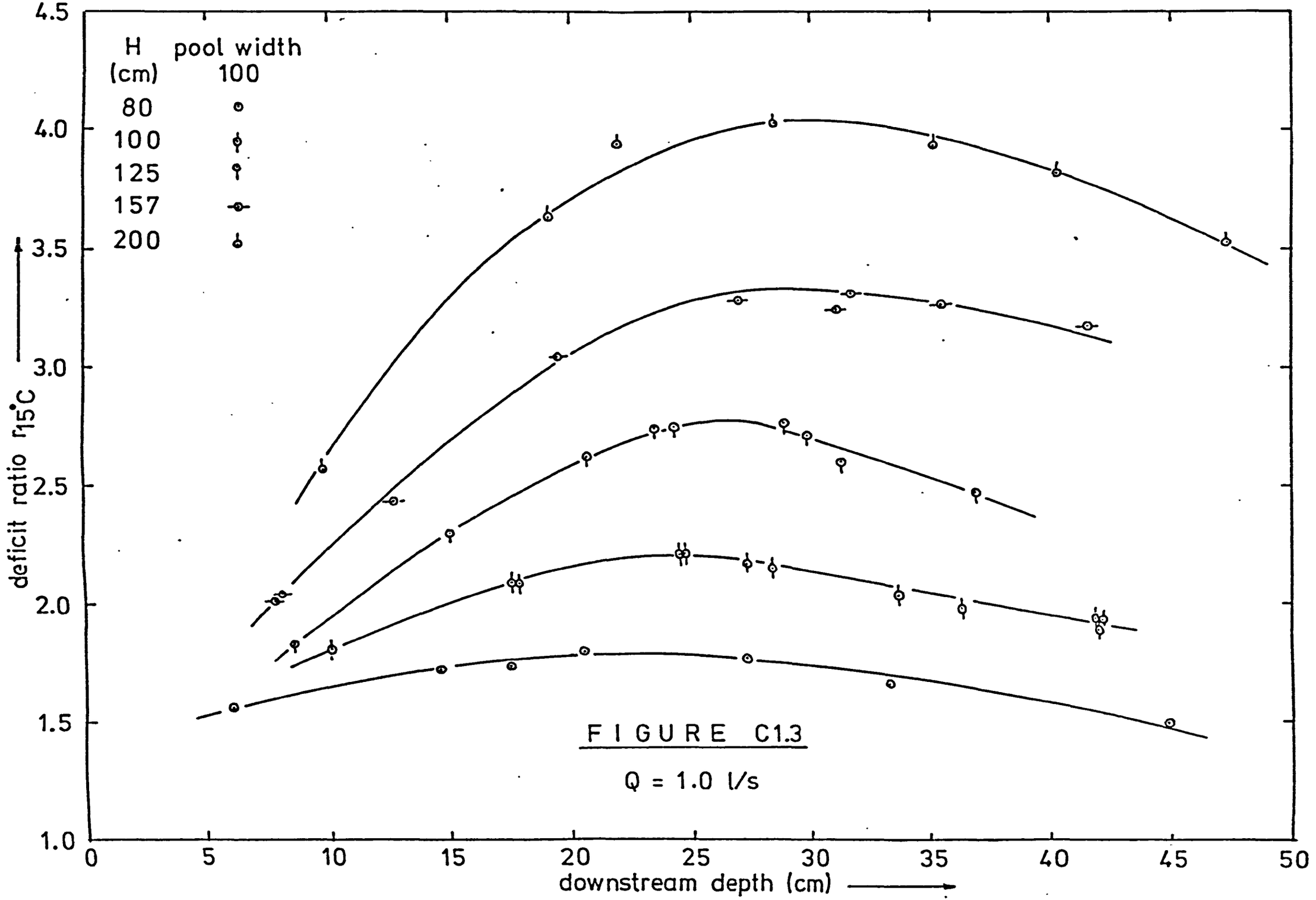

FIGURE C1.3

Q = 1.0 l/s

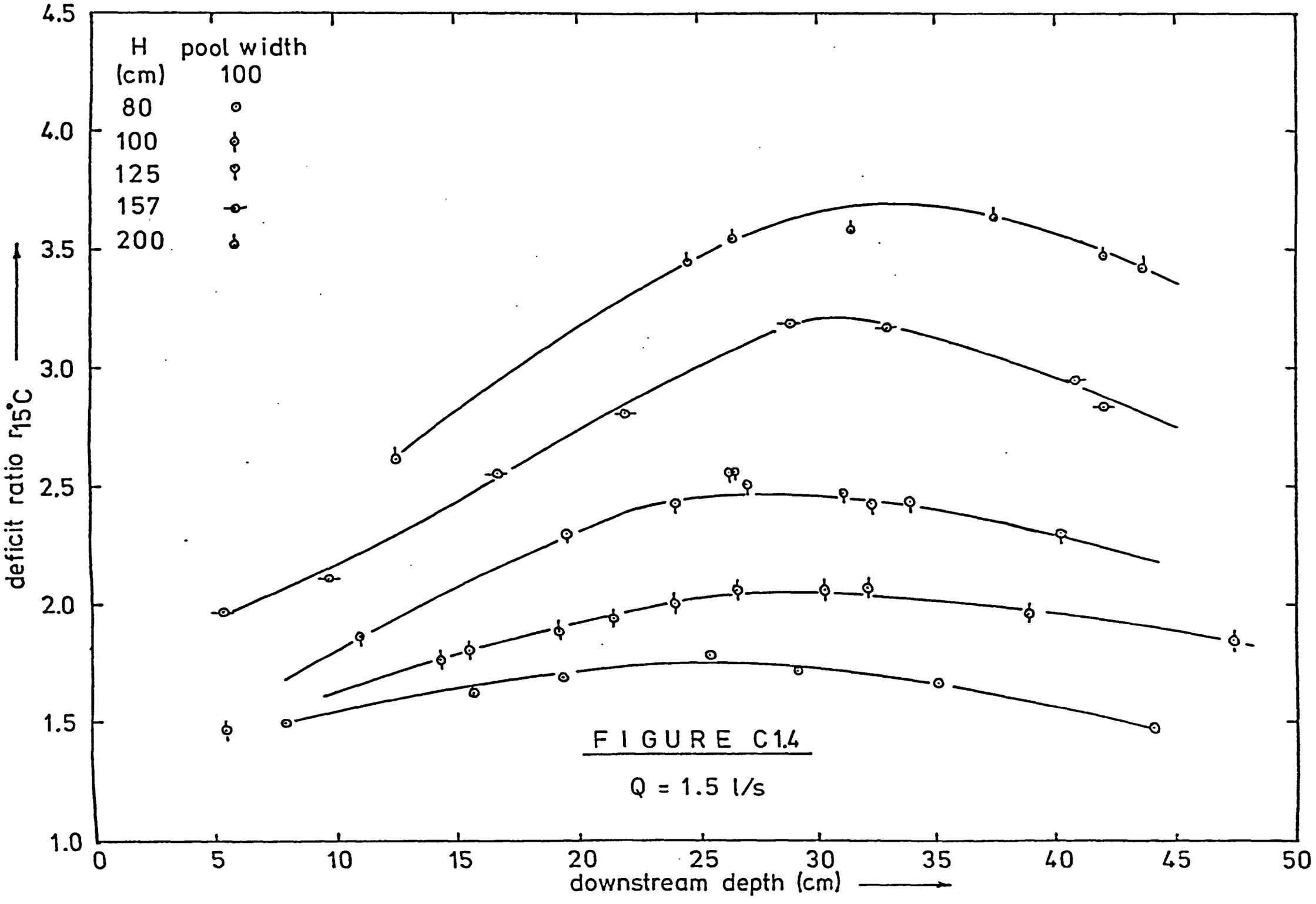

FIGURE C1.4

Q = 1.5 l/s

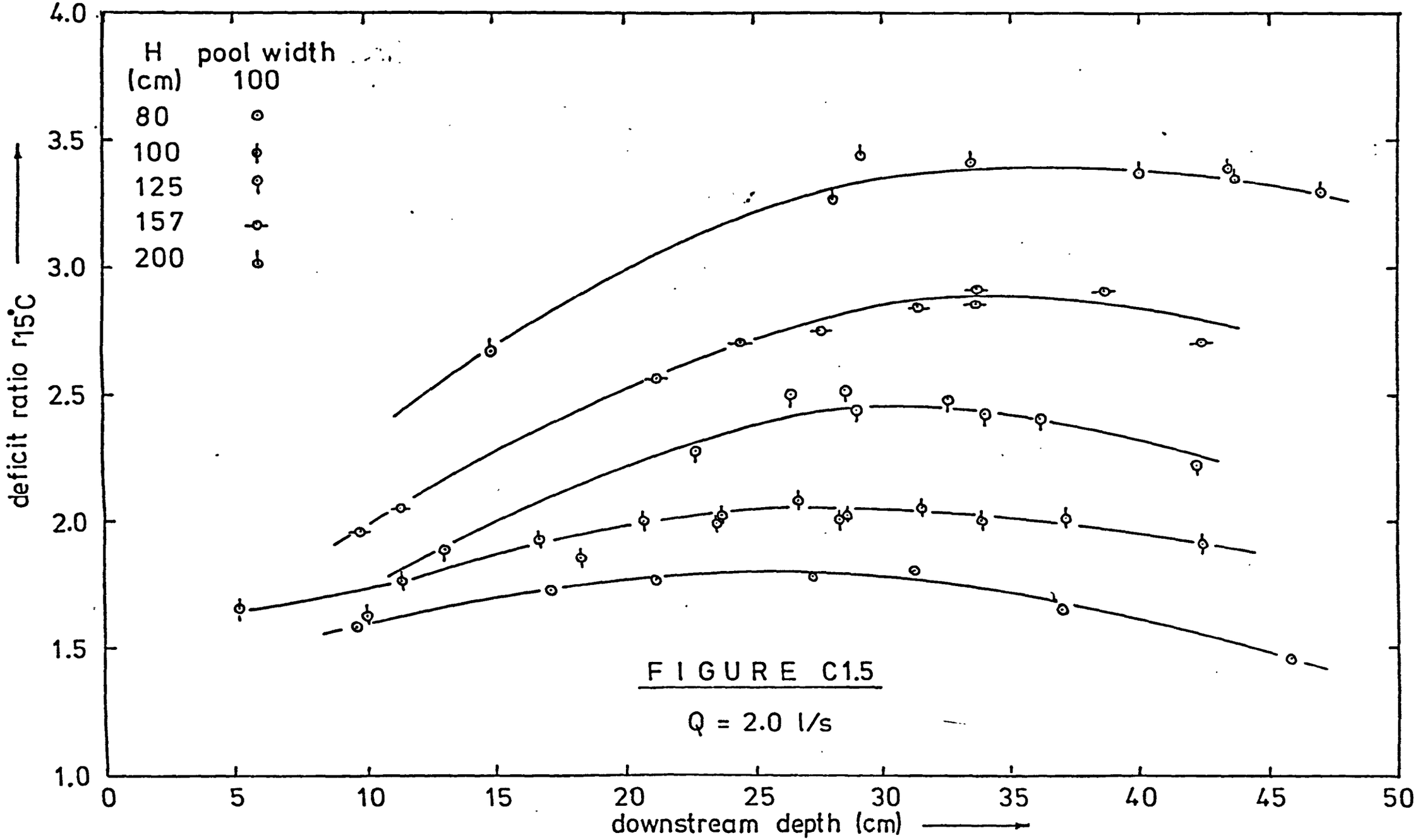

FIGURE C1.5

Q = 2.0 l/s

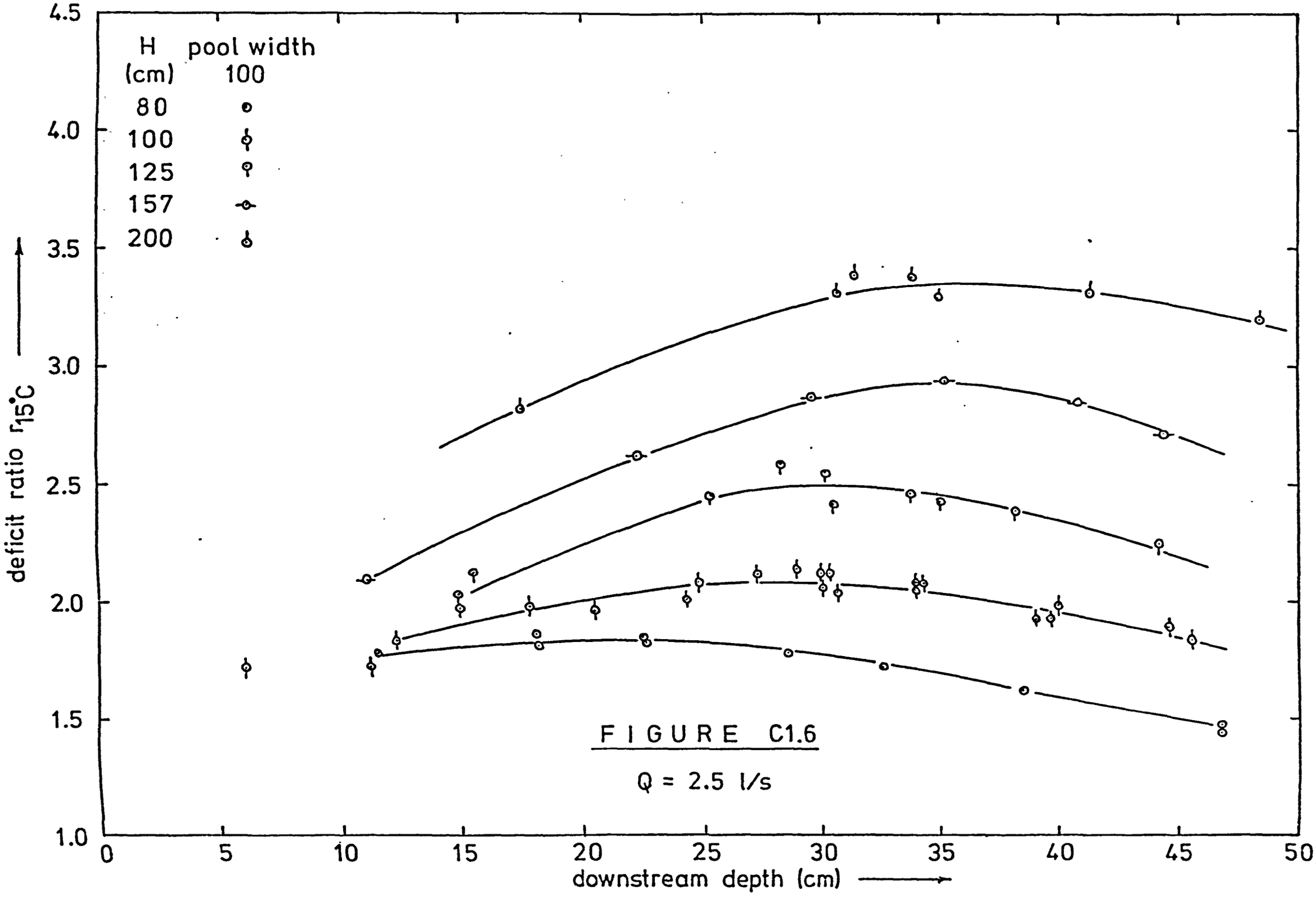

FIGURE C1.6

Q = 2.5 l/s

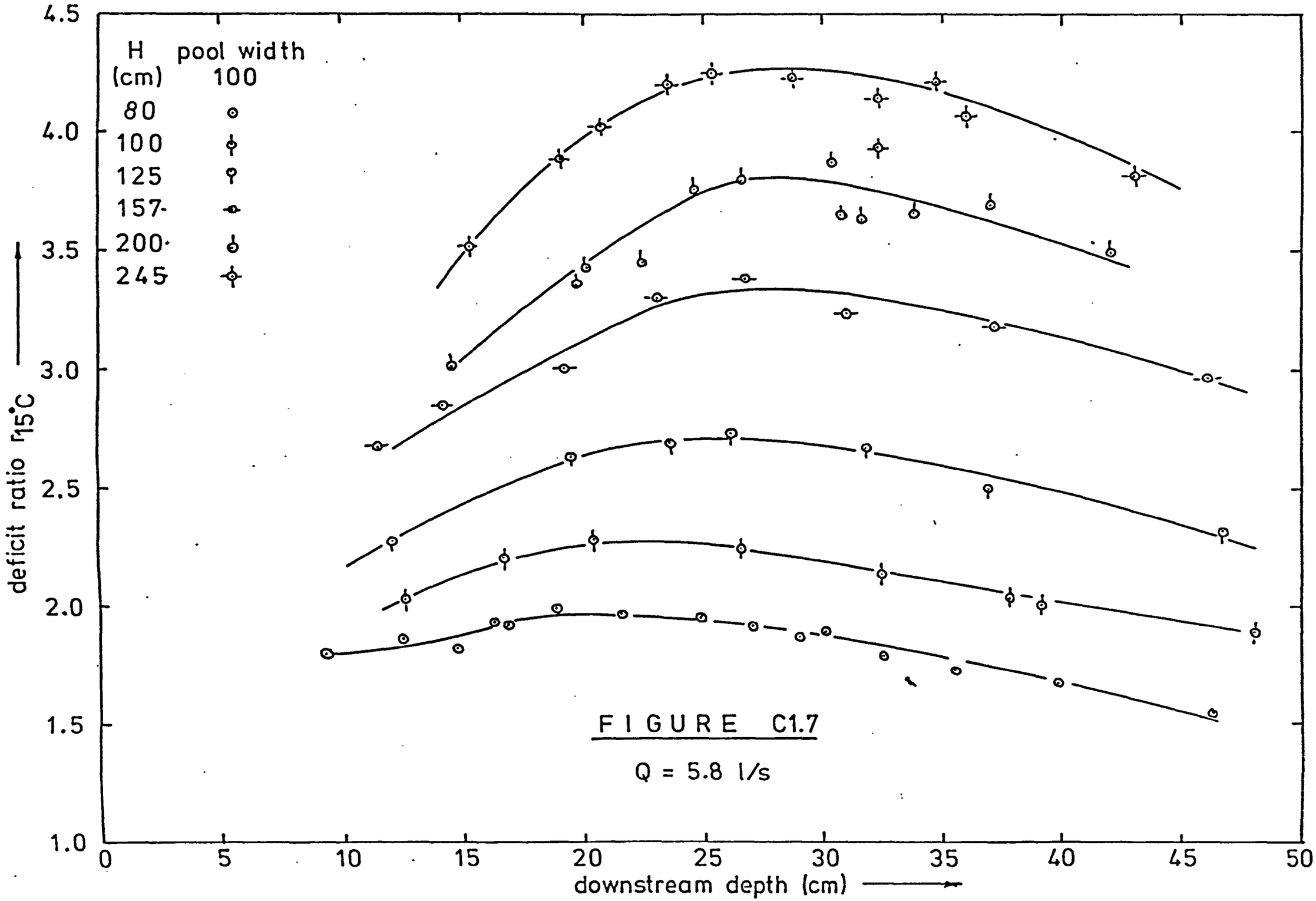

FIGURE C1.7

Q = 5.8 l/s

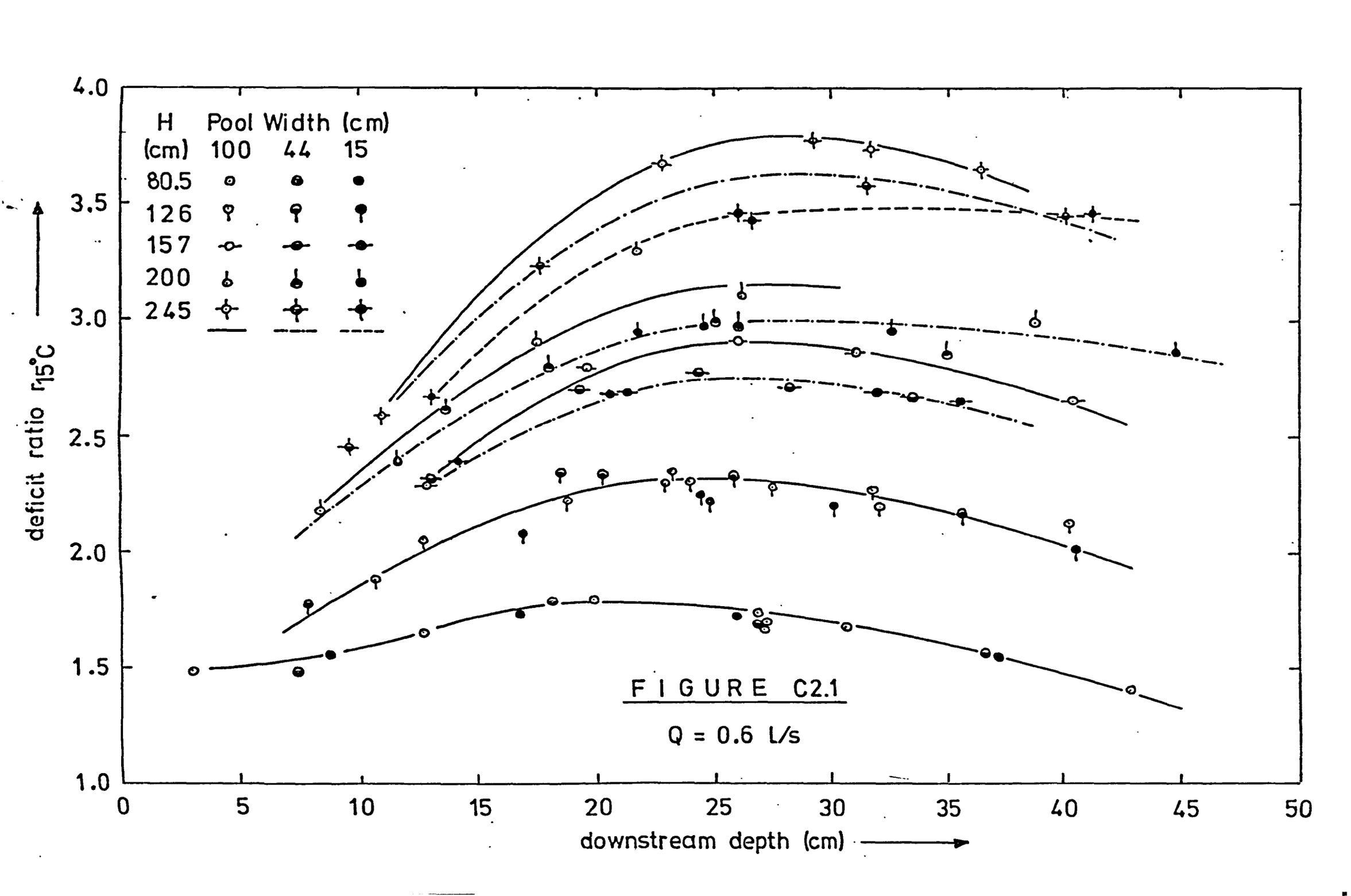

FIGURE C2.1

Q = 0.6 L/s

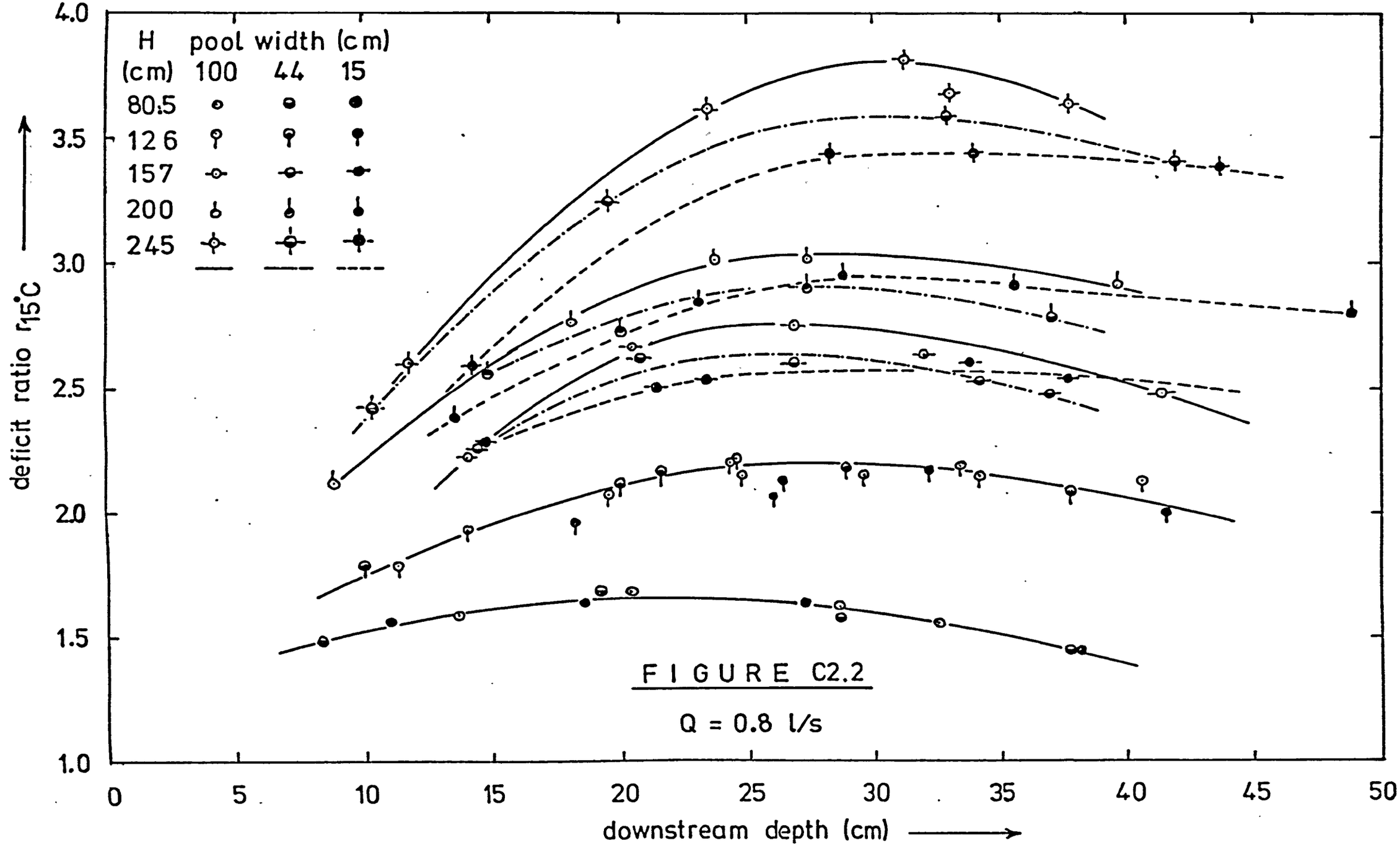

FIGURE C2.2

Q = 0.8 l/s

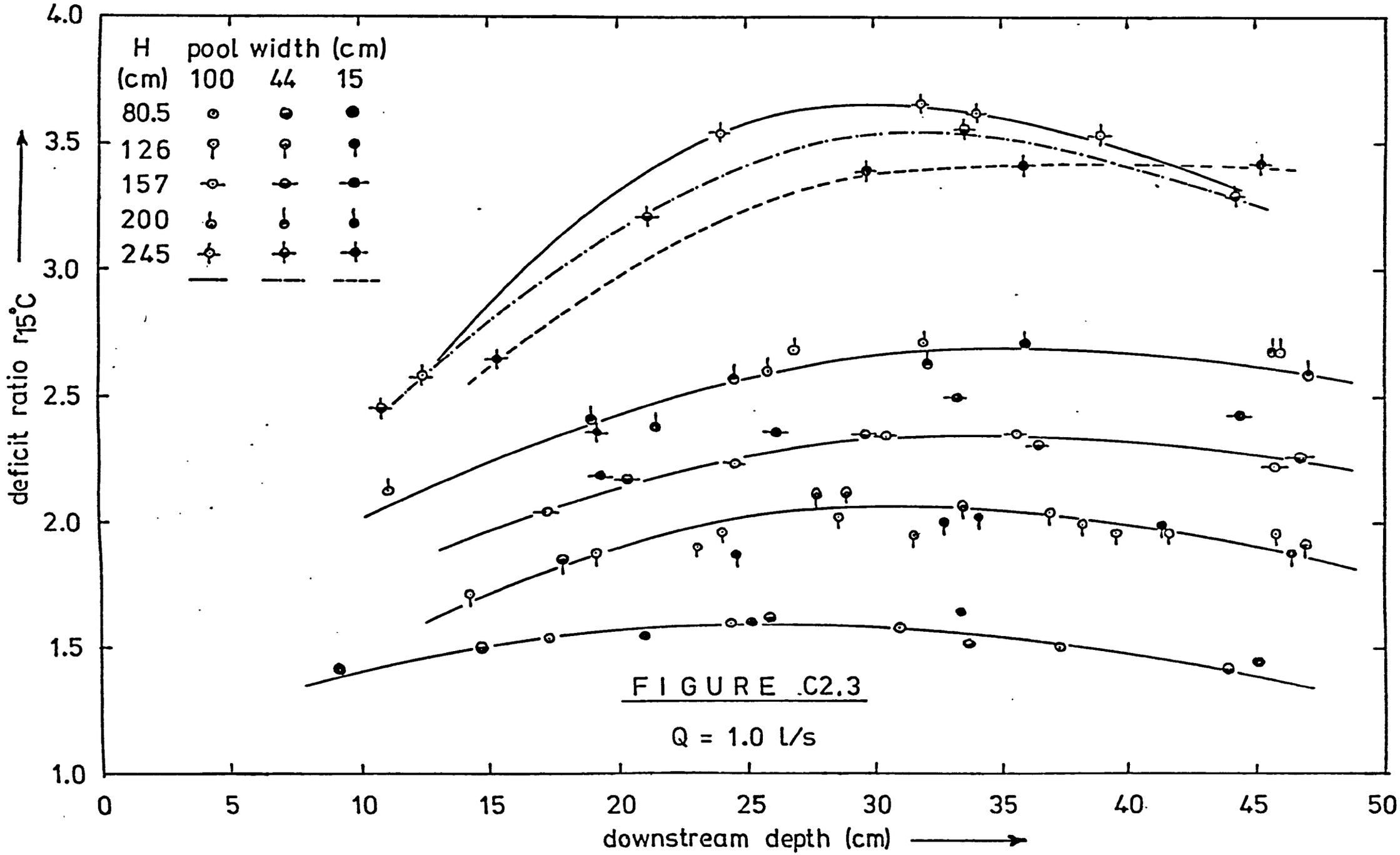

FIGURE C2.3

Q = 1.0 l/s

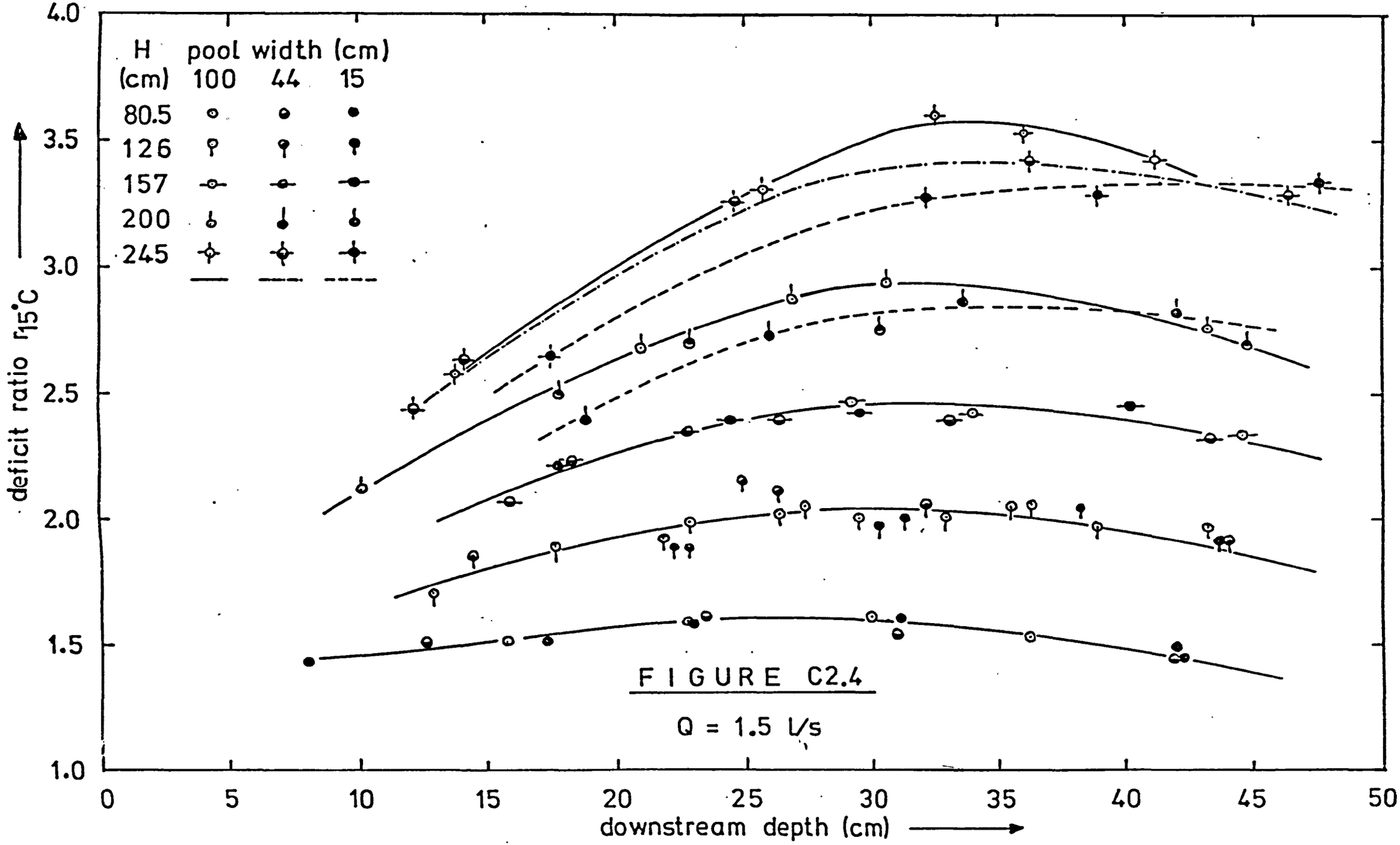

FIGURE C2.4

Q = 1.5 l/s

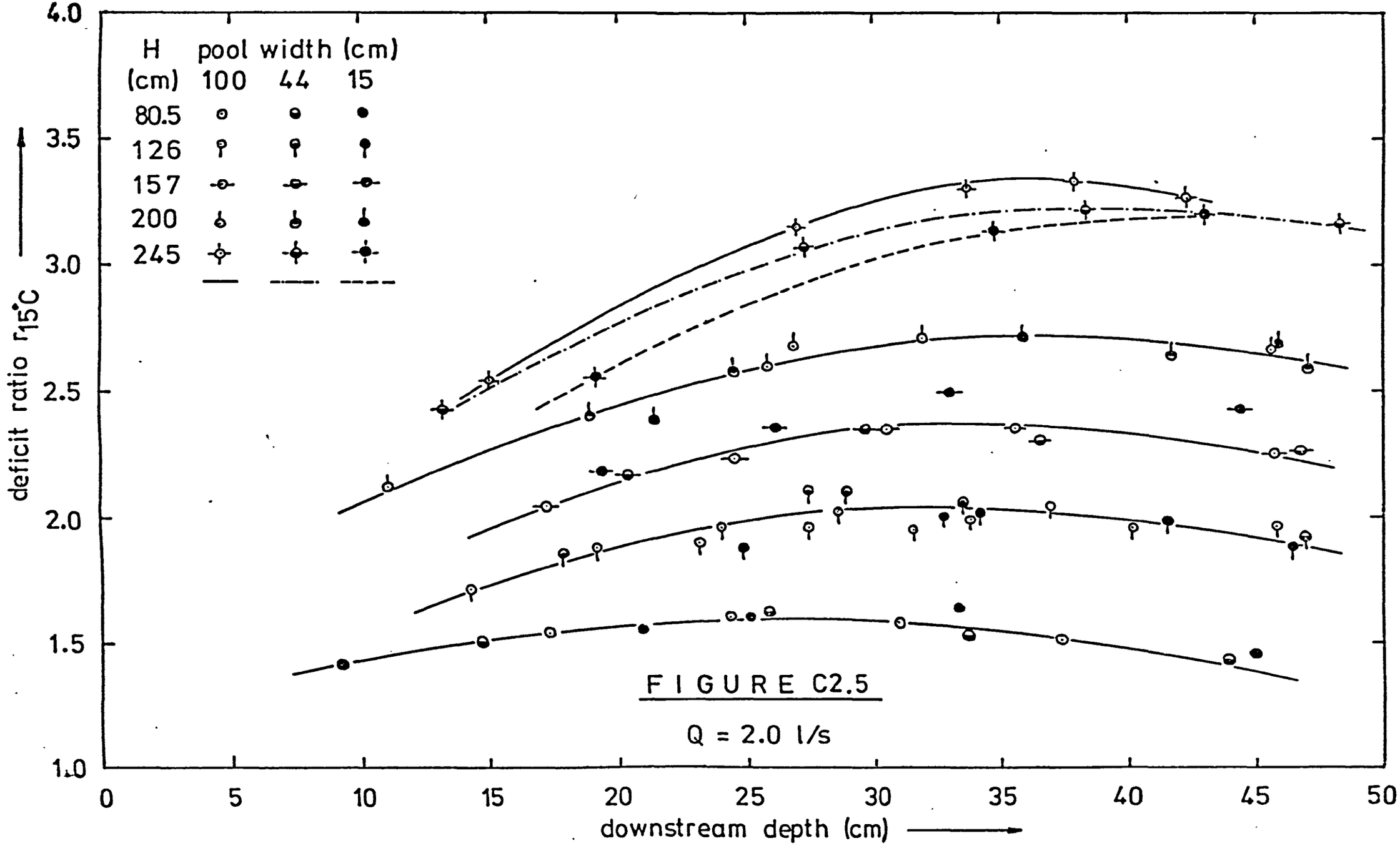

FIGURE C2.5

Q = 2.0 l/s

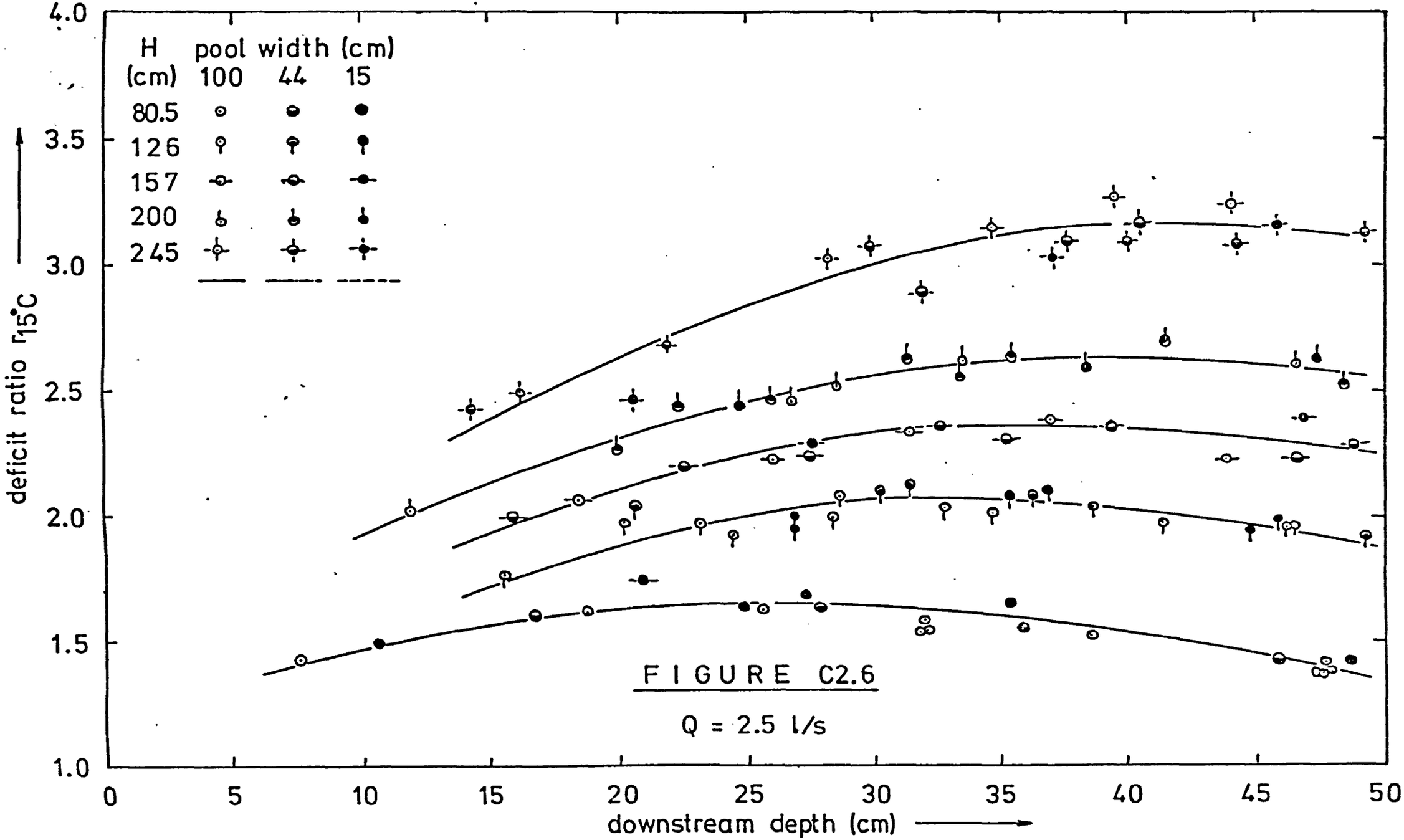

FIGURE C2.6

Q = 2.5 l/s

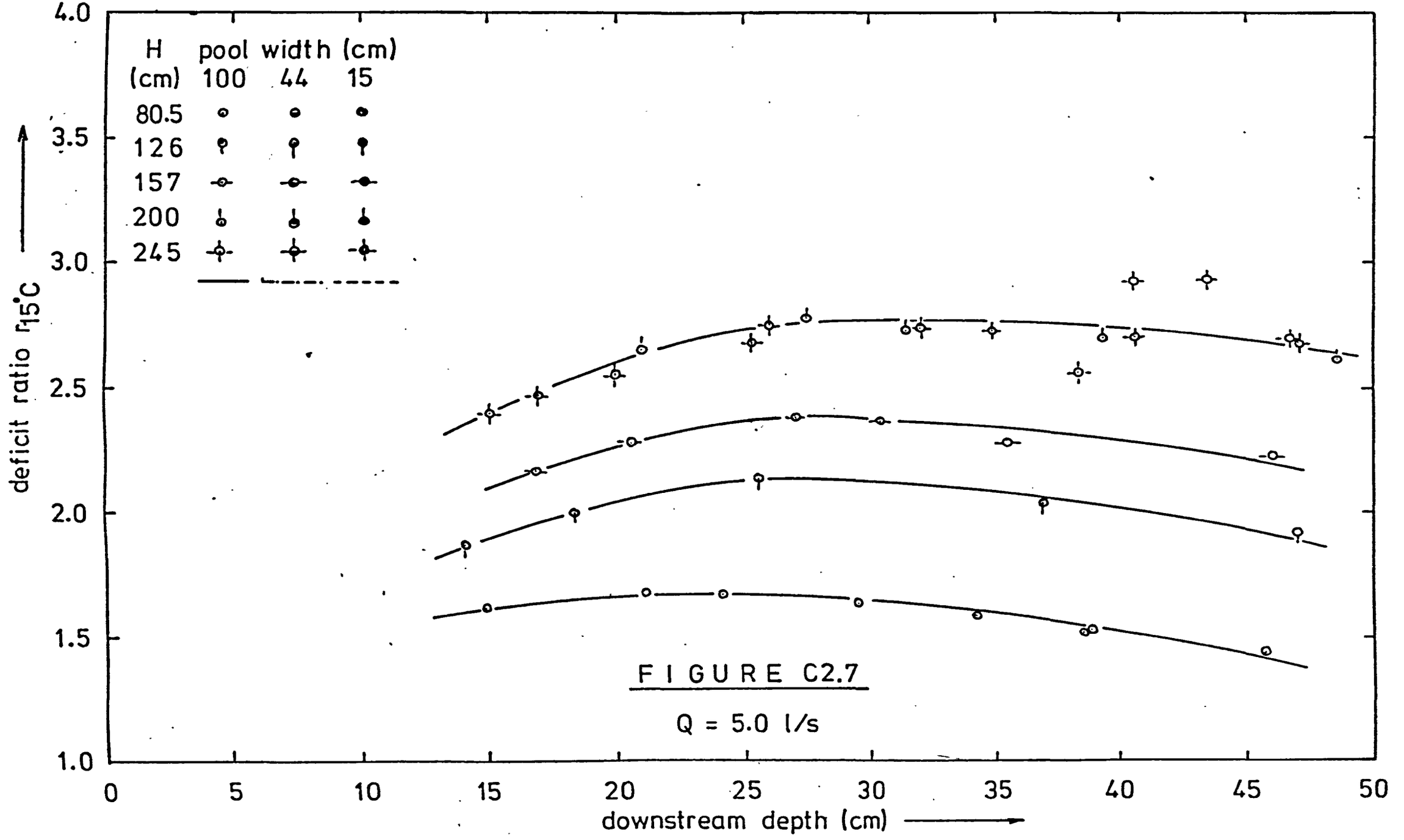

FIGURE C2.7

Q = 5.0 l/s

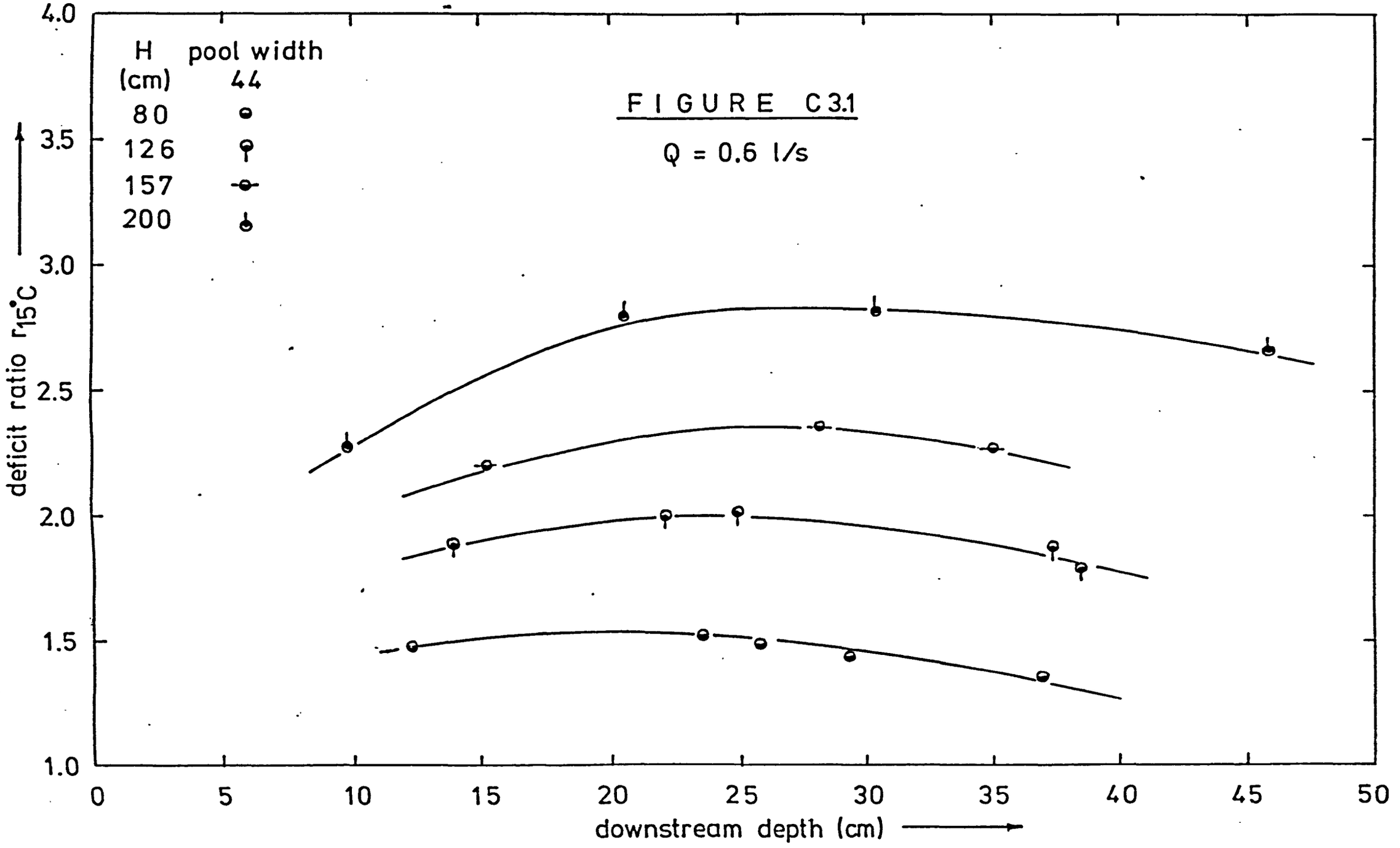
FIGURE C3.1
Q = 0.6 l/s
H (cm)
pool width
44
80
126
157
200
deficit ratio $r_{15°C}$
downstream depth (cm)
4.0
3.5
3.0
2.5
2.0
1.5
1.0
0
5
10
15
20
25
30
35
40
45
50

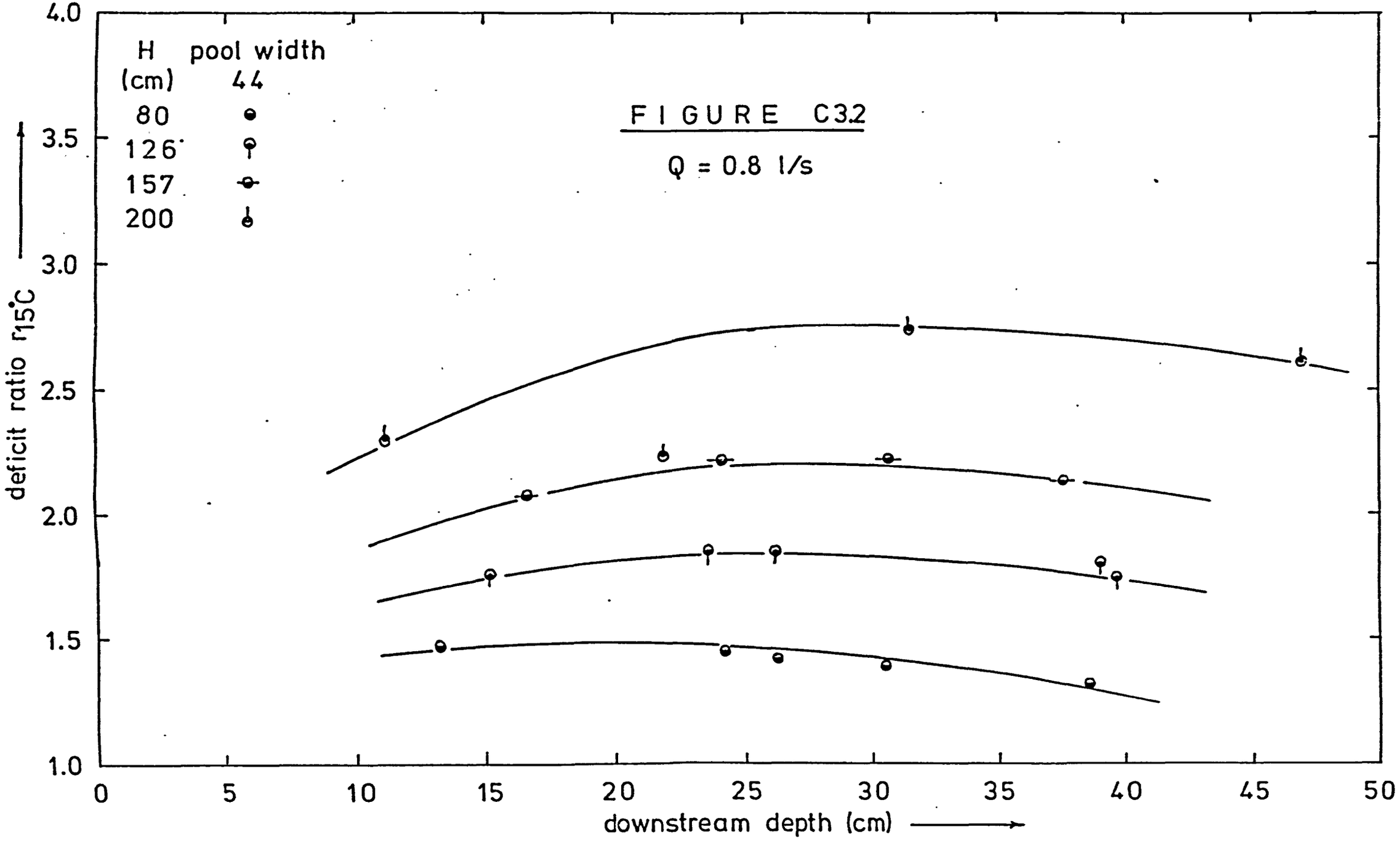
H (cm)
pool width 44
80
126
157
200
FIGURE C3.2
Q = 0.8 l/s
deficit ratio r15°C
downstream depth (cm)
4.0
3.5
3.0
2.5
2.0
1.5
1.0
0
5
10
15
20
25
30
35
40
45
50

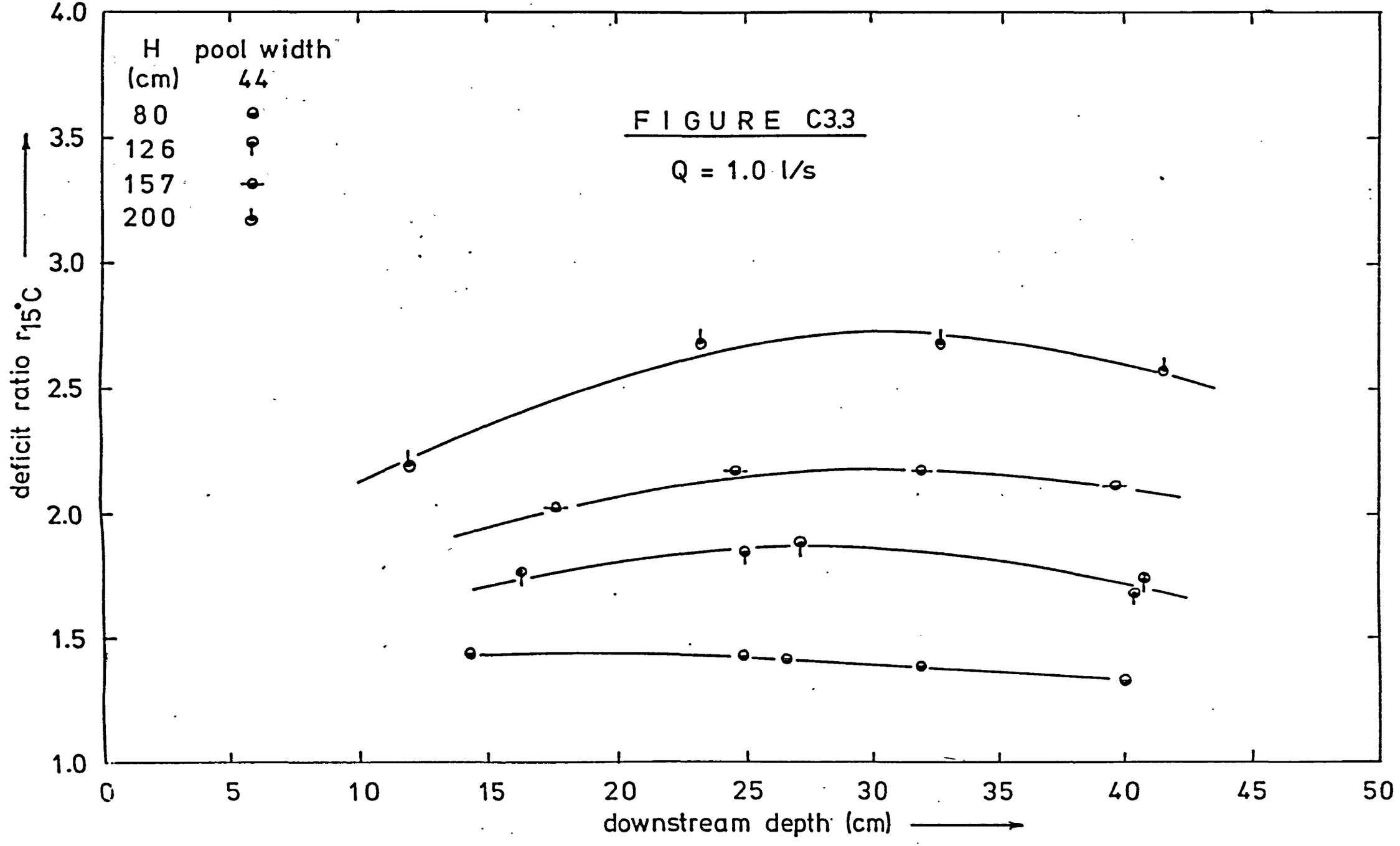
H (cm)
pool width 44
80
126
157
200
FIGURE C3.3
Q = 1.0 l/s
deficit ratio $r_{15°C}$
downstream depth (cm)
4.0
3.5
3.0
2.5
2.0
1.5
1.0
0
5
10
15
20
25
30
35
40
45
50

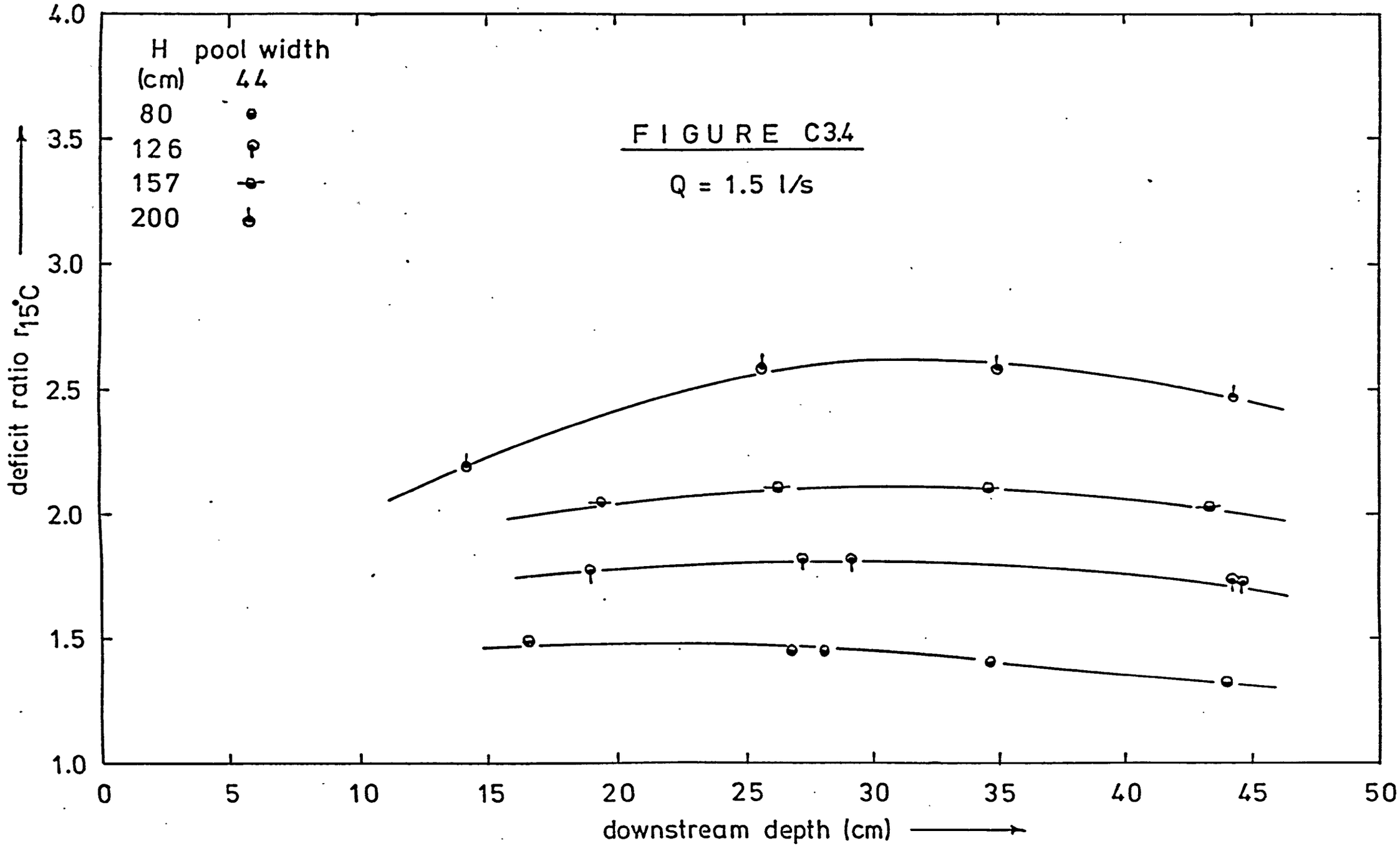
H pool width
(cm) 44
80
126
157
200
FIGURE C3.4
Q = 1.5 l/s
deficit ratio $r_{15°C}$
downstream depth (cm)
4.0
3.5
3.0
2.5
2.0
1.5
1.0
0
5
10
15
20
25
30
35
40
45
50

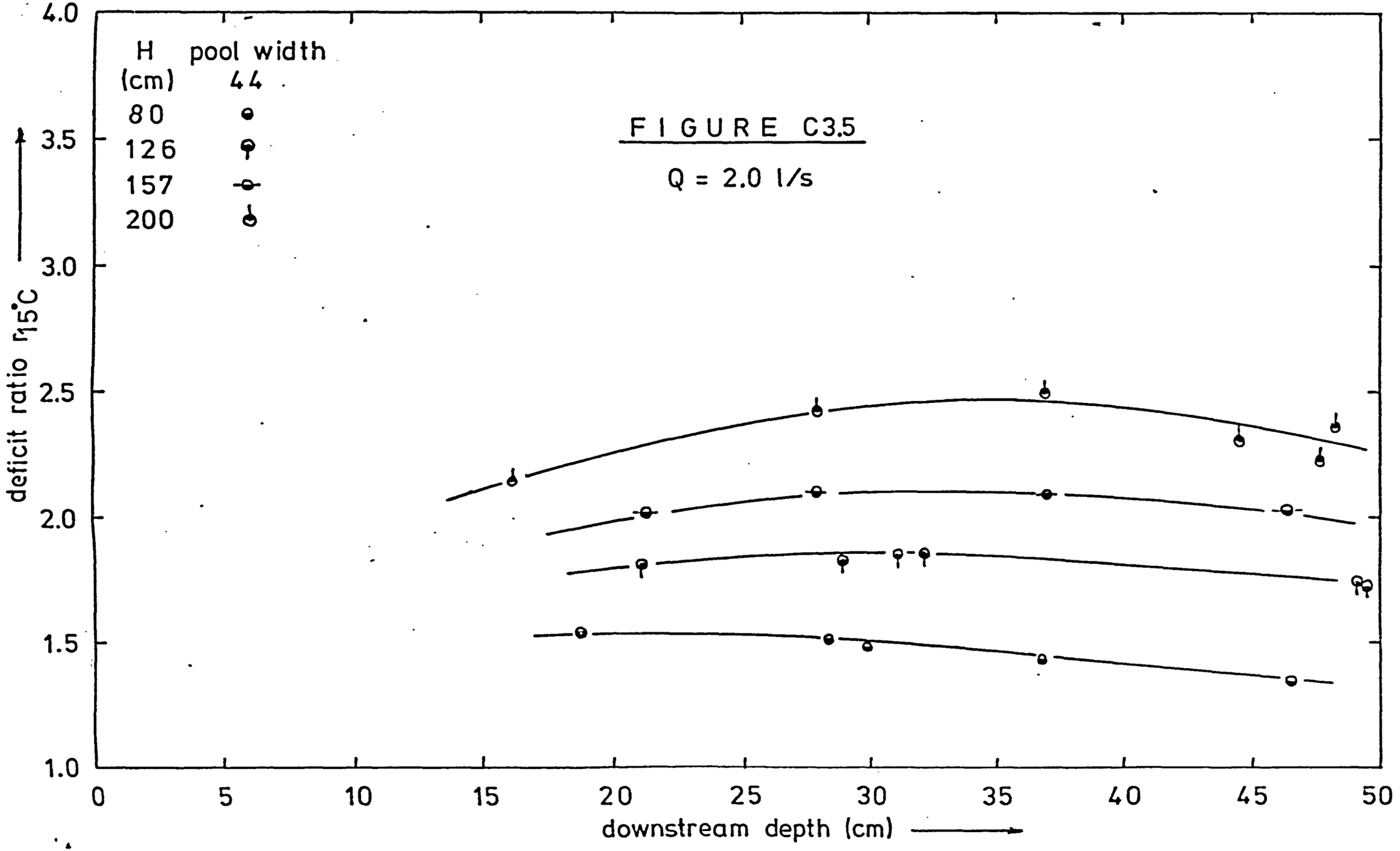
H (cm)
pool width 44
80
126
157
200
FIGURE C3.5
Q = 2.0 l/s
deficit ratio r15°C
downstream depth (cm)
4.0
3.5
3.0
2.5
2.0
1.5
1.0
0
5
10
15
20
25
30
35
40
45
50

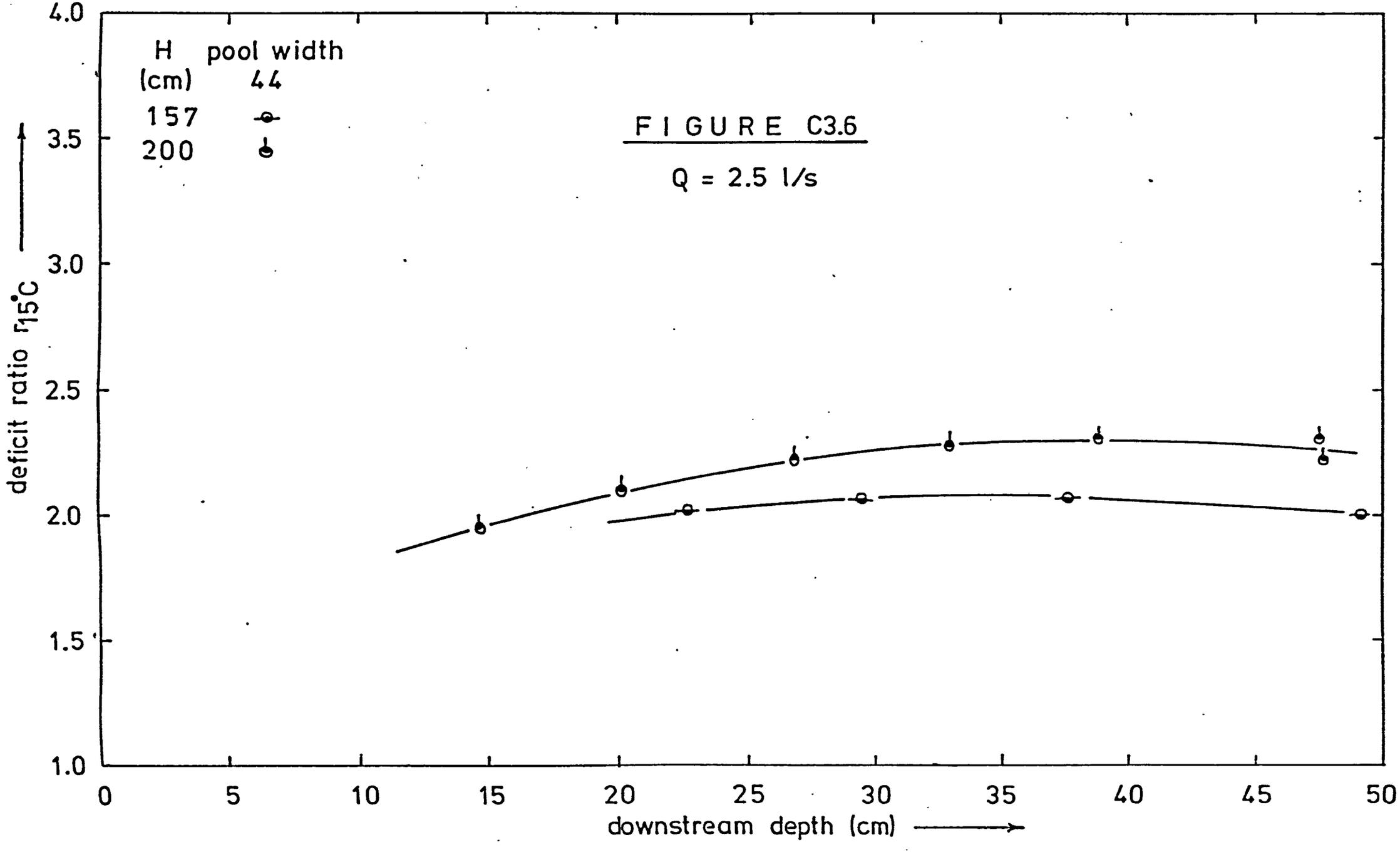
H (cm)
pool width 44
157
200
FIGURE C3.6
Q = 2.5 l/s
deficit ratio r15°C
4.0
3.5
3.0
2.5
2.0
1.5
1.0
0
5
10
15
20
25
30
35
40
45
50
downstream depth (cm)

APPENDIX D

FREE OVERFALL DATA - 220MM WIDE RECTANGULAR NOTCH

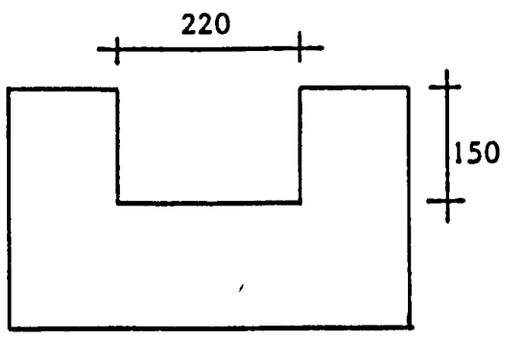

Figures D1.1 to D1.4 Tests with tap water + 0.3% $NaNO_3$

Figures D2.1 to D2.3 Tests with tap water

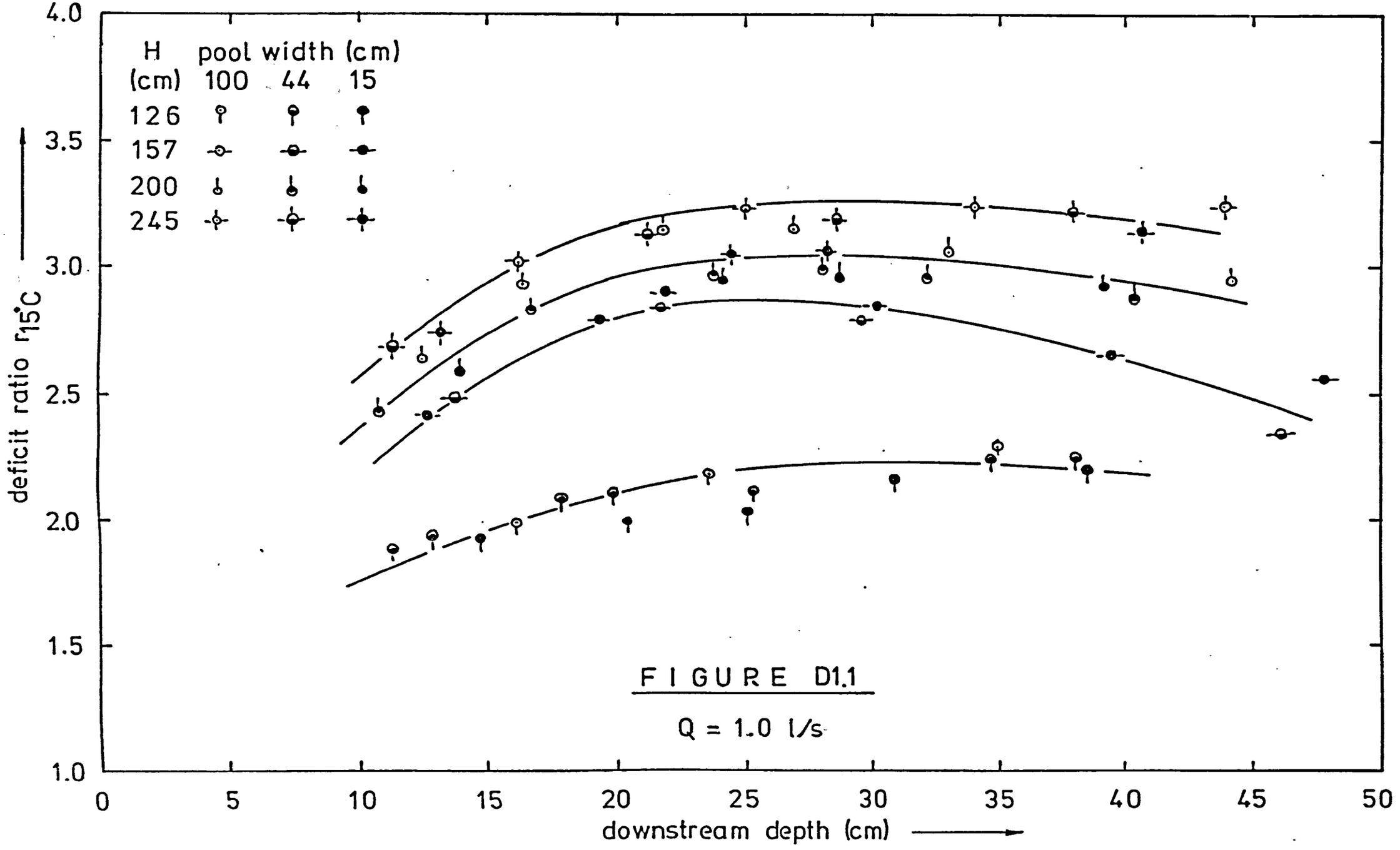

FIGURE D1.1

Q = 1.0 l/s

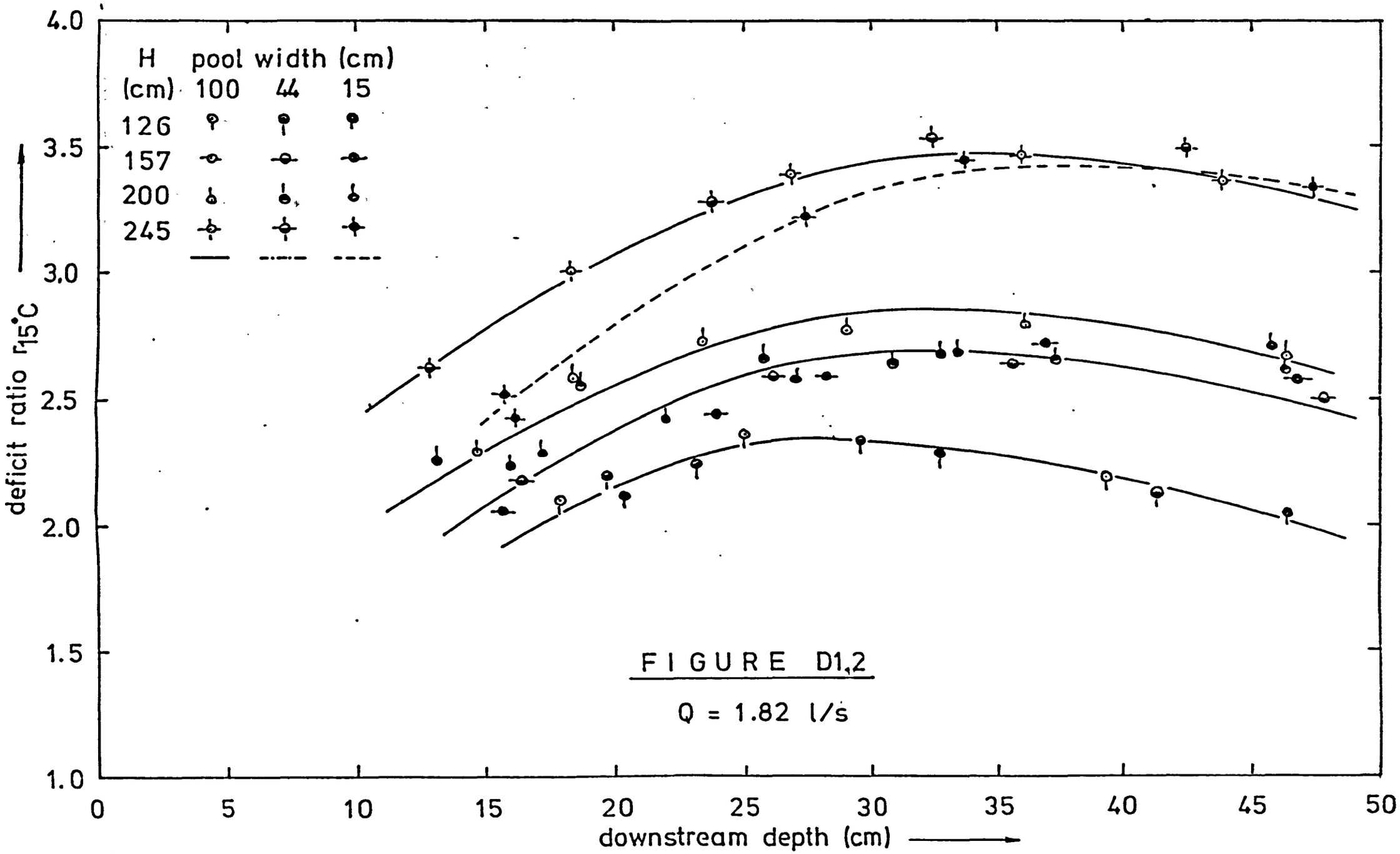

FIGURE D1,2

Q = 1.82 l/s

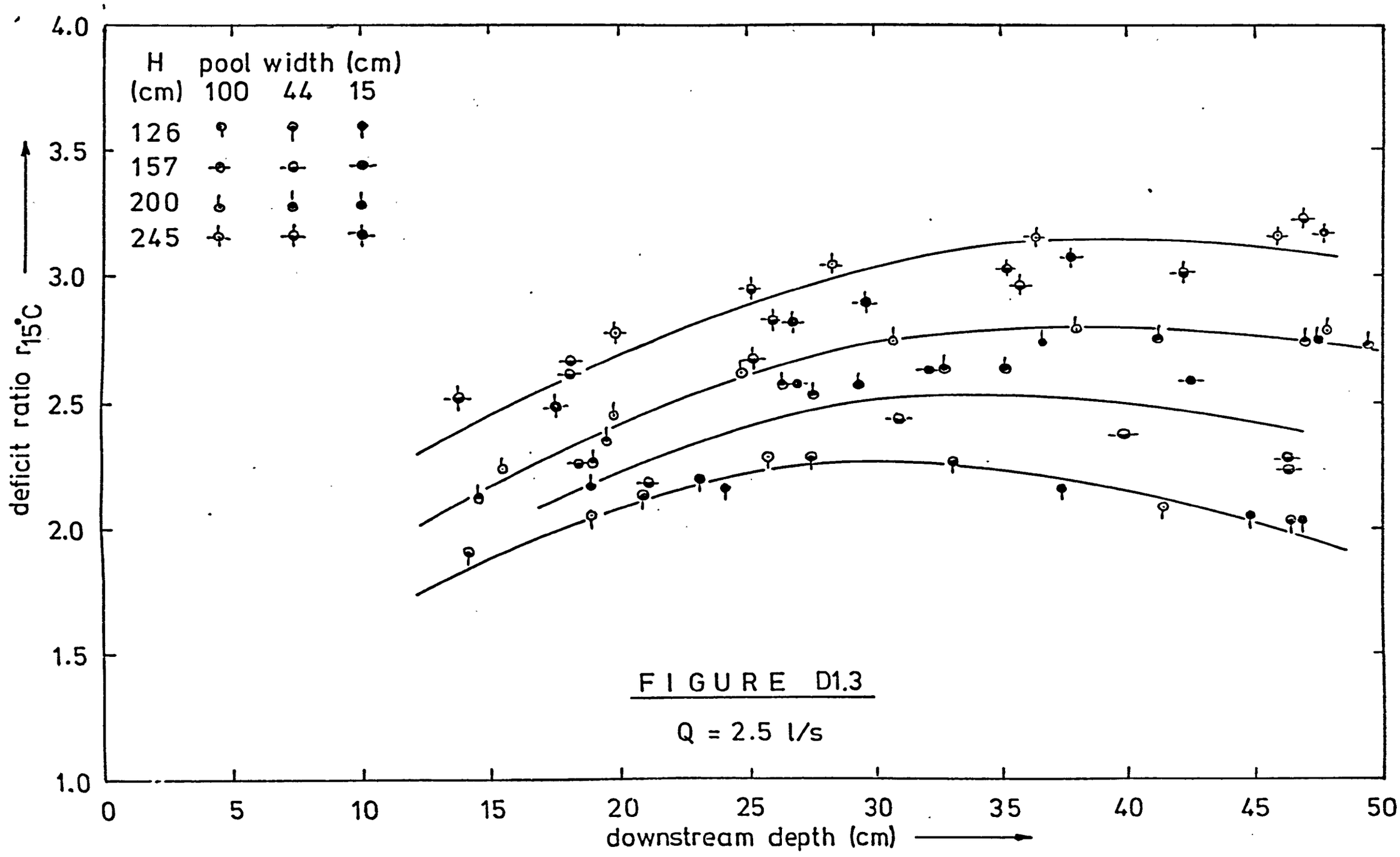

FIGURE D1.3

Q = 2.5 l/s

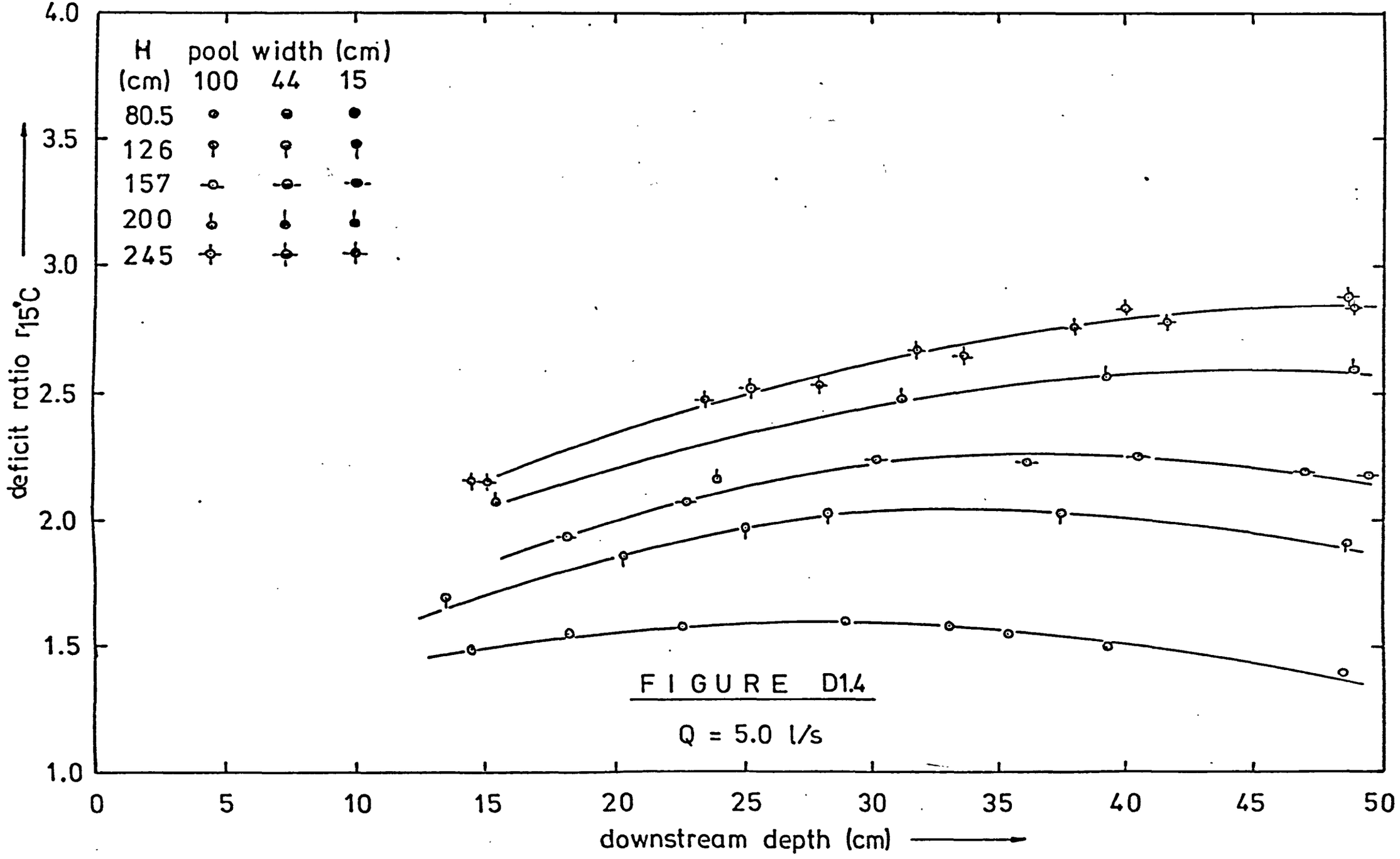

FIGURE D1.4

Q = 5.0 l/s

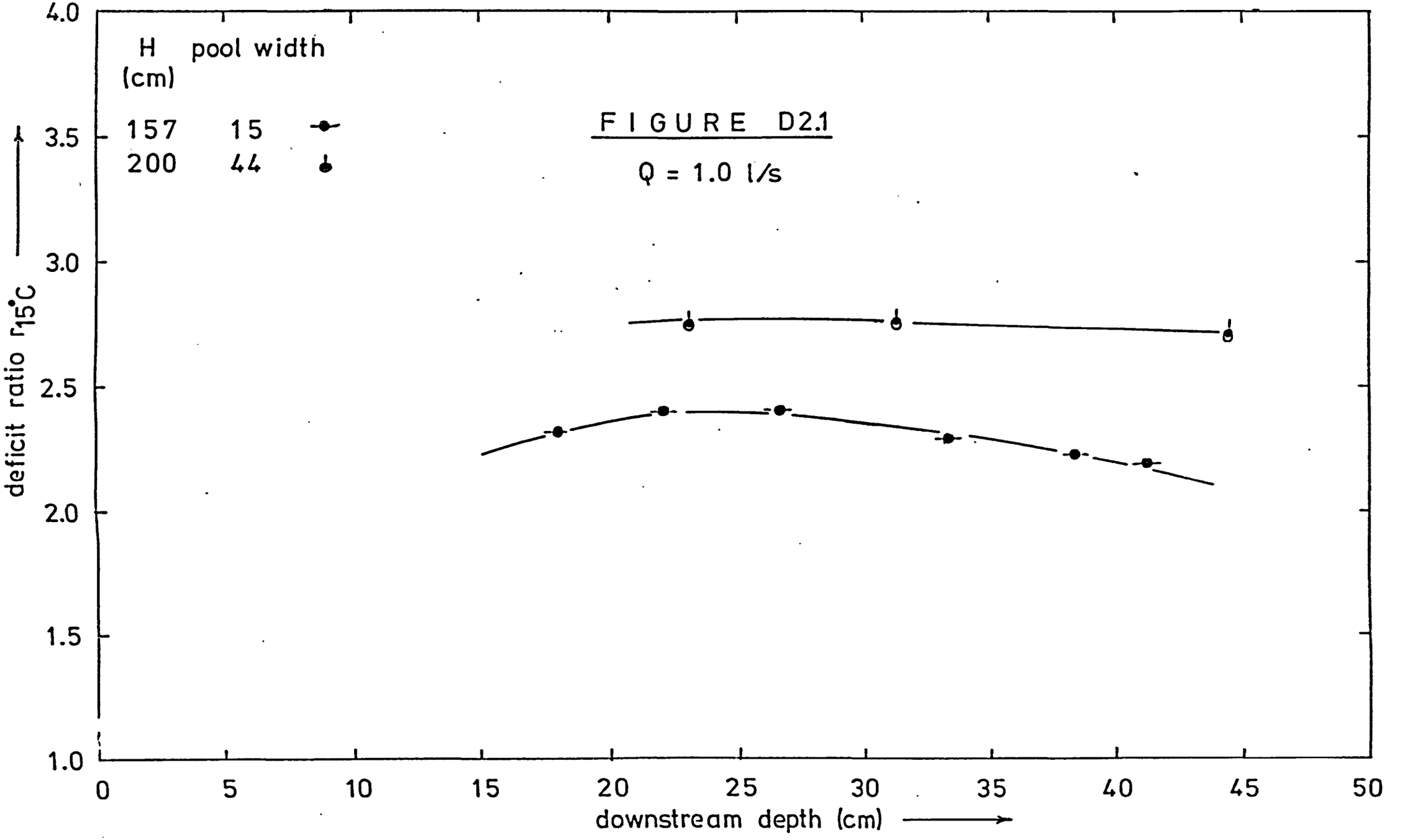
FIGURE D2.1
Q = 1.0 l/s
H (cm)
pool width
157 15
200 44
deficit ratio r15°C
downstream depth (cm)
4.0
3.5
3.0
2.5
2.0
1.5
1.0
0
5
10
15
20
25
30
35
40
45
50

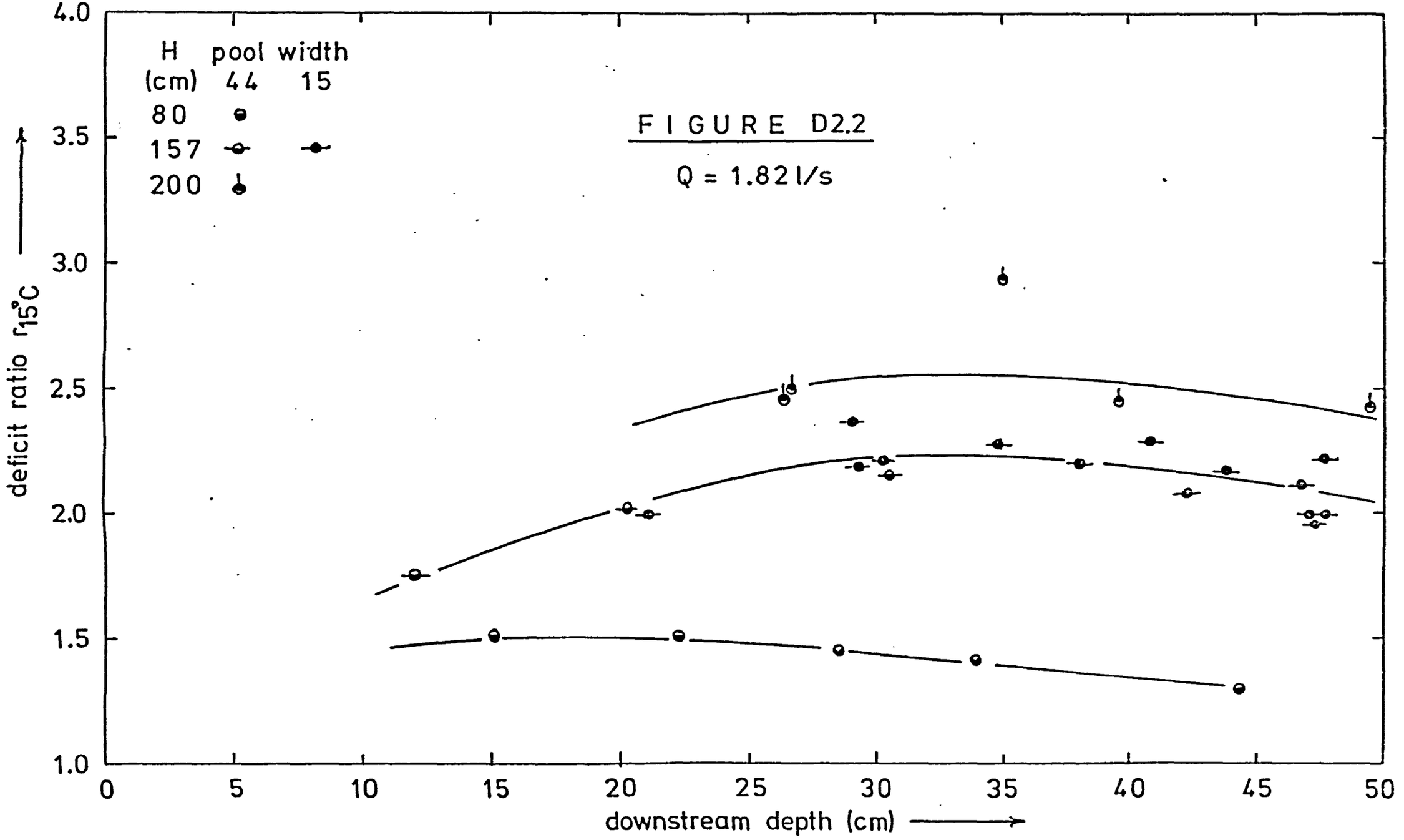
H pool width
(cm) 44 15
80
157
200
FIGURE D2.2
Q = 1.82 l/s
deficit ratio $r_{15°C}$
downstream depth (cm)
4.0
3.5
3.0
2.5
2.0
1.5
1.0
0
5
10
15
20
25
30
35
40
45
50

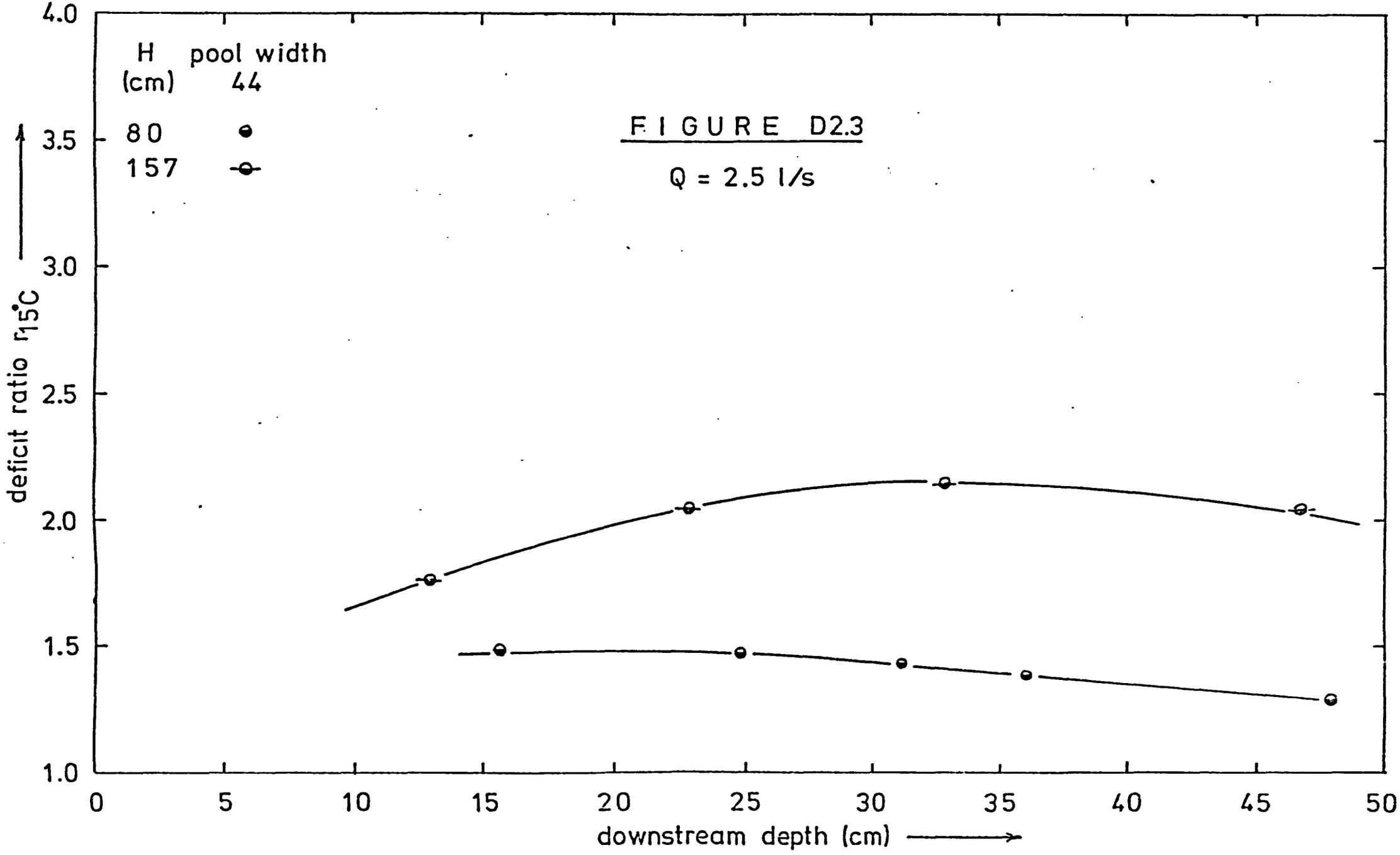
H (cm)
pool width 44
80
157
FIGURE D2.3
Q = 2.5 l/s
deficit ratio $r_{15°C}$
downstream depth (cm)
4.0
3.5
3.0
2.5
2.0
1.5
1.0
0
5
10
15
20
25
30
35
40
45
50

APPENDIX E

FREE OVERFALL DATA - 300MM WIDE RECTANGULAR NOTCH

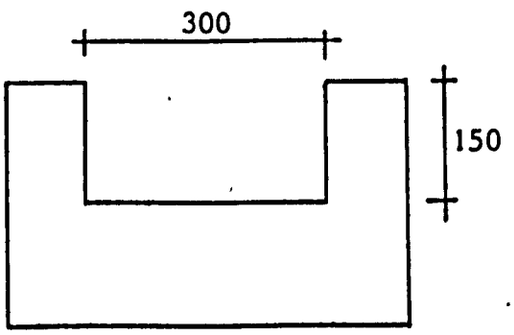

Figures E1.1 to E1.4 Tests with tap water + 0.3% $NaNO_3$

Figure E2.1 Tests with tap water

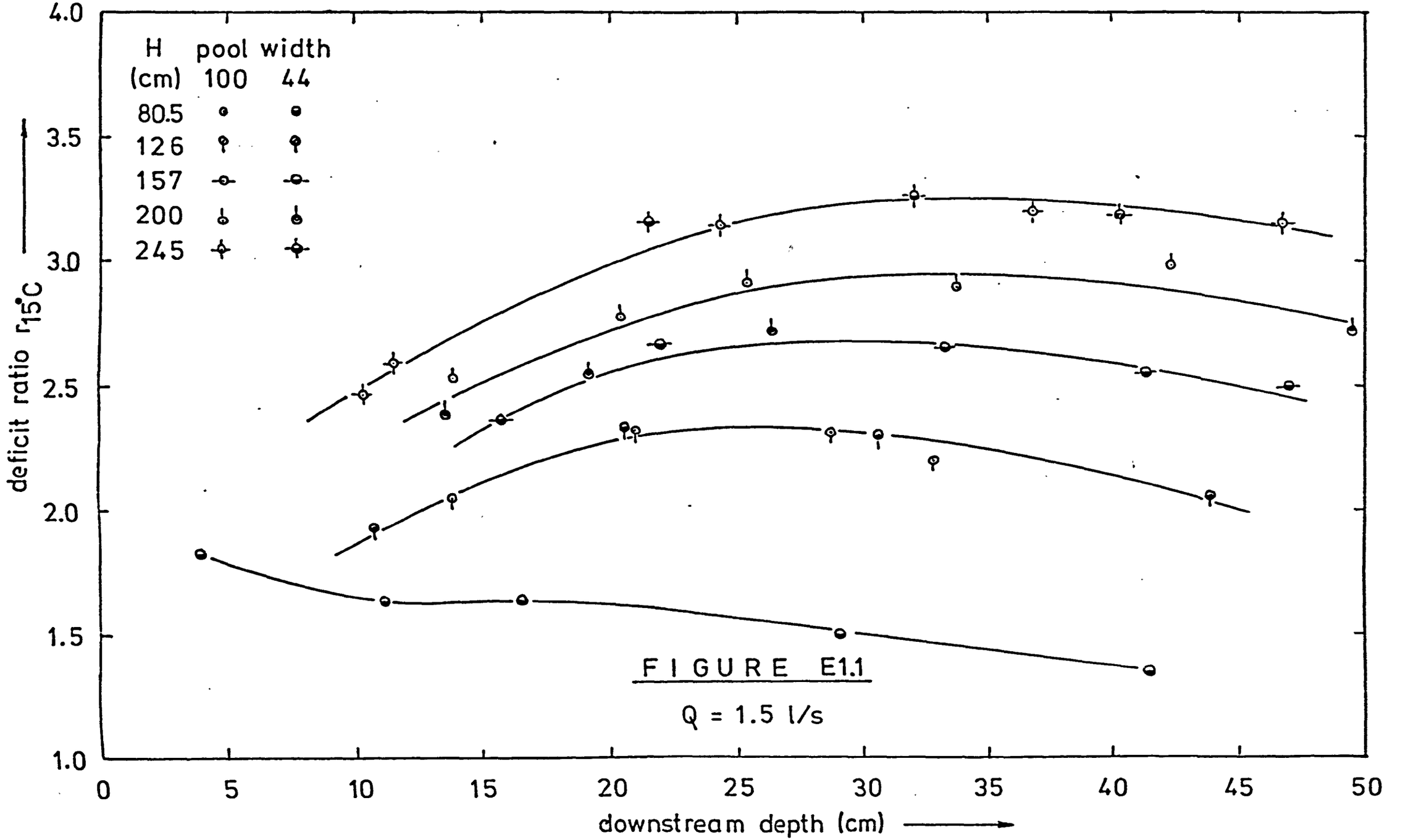

FIGURE E1.1

Q = 1.5 l/s

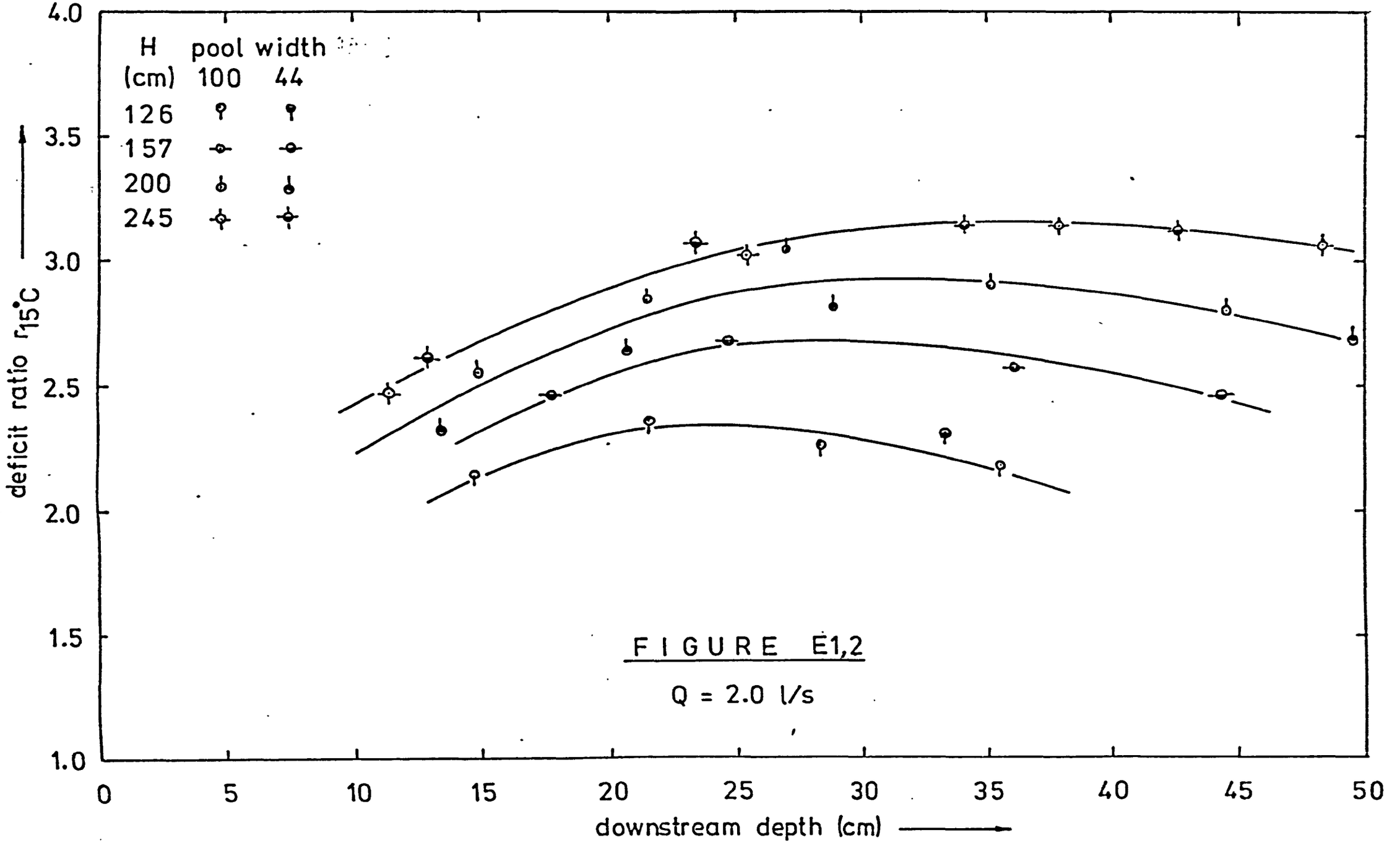

FIGURE E1,2

Q = 2.0 l/s

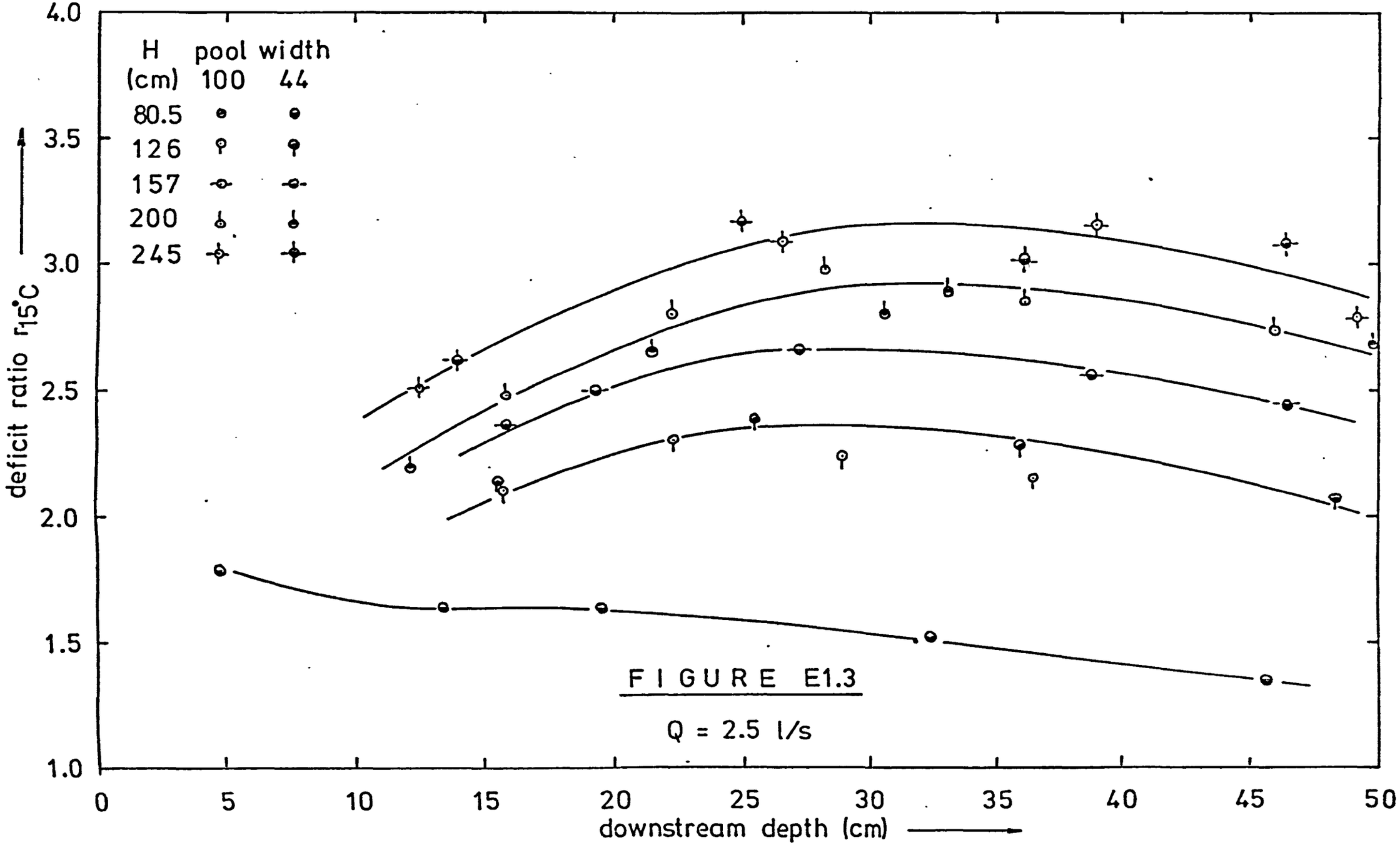

FIGURE E1.3

Q = 2.5 l/s

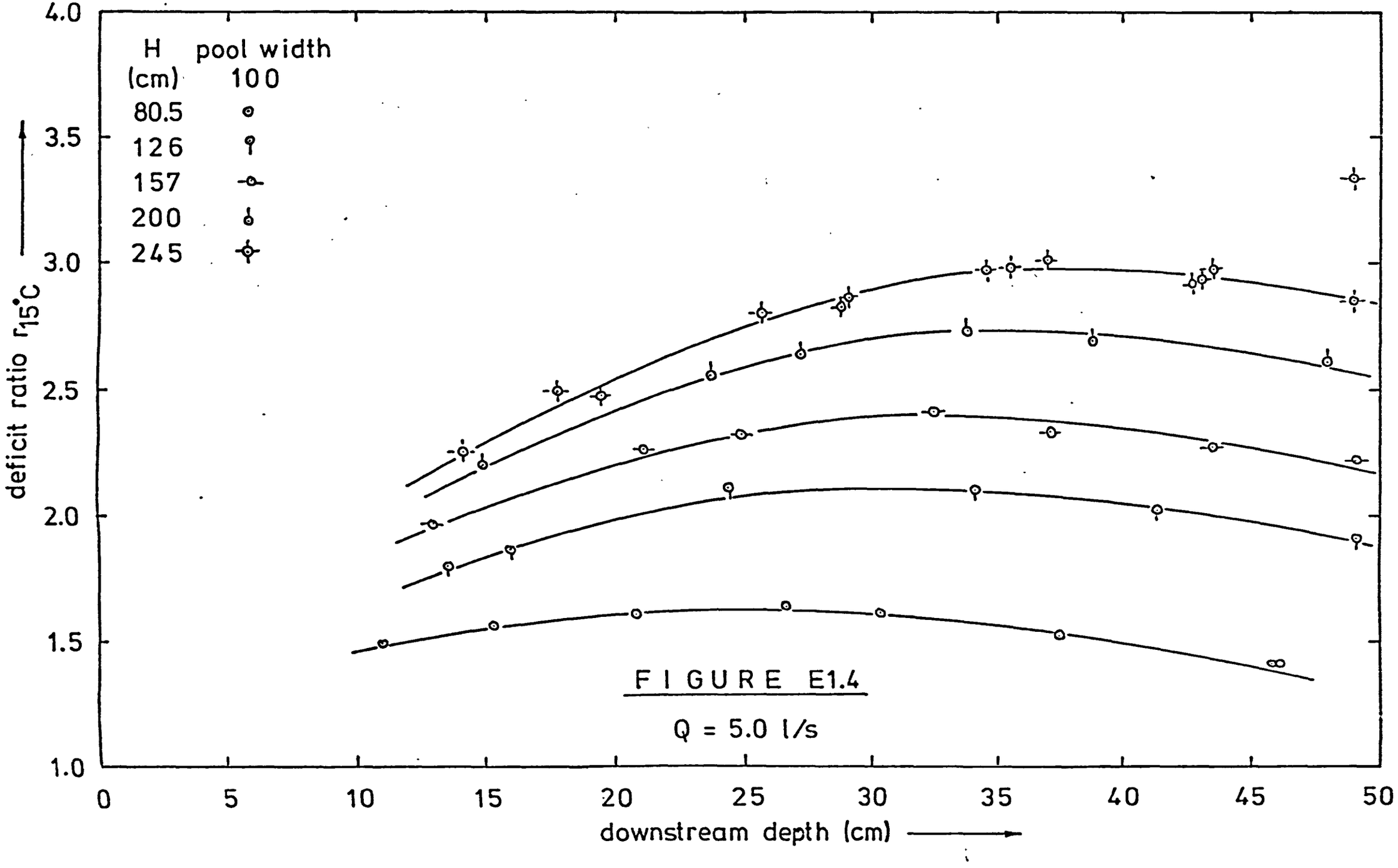

FIGURE E1.4

Q = 5.0 l/s

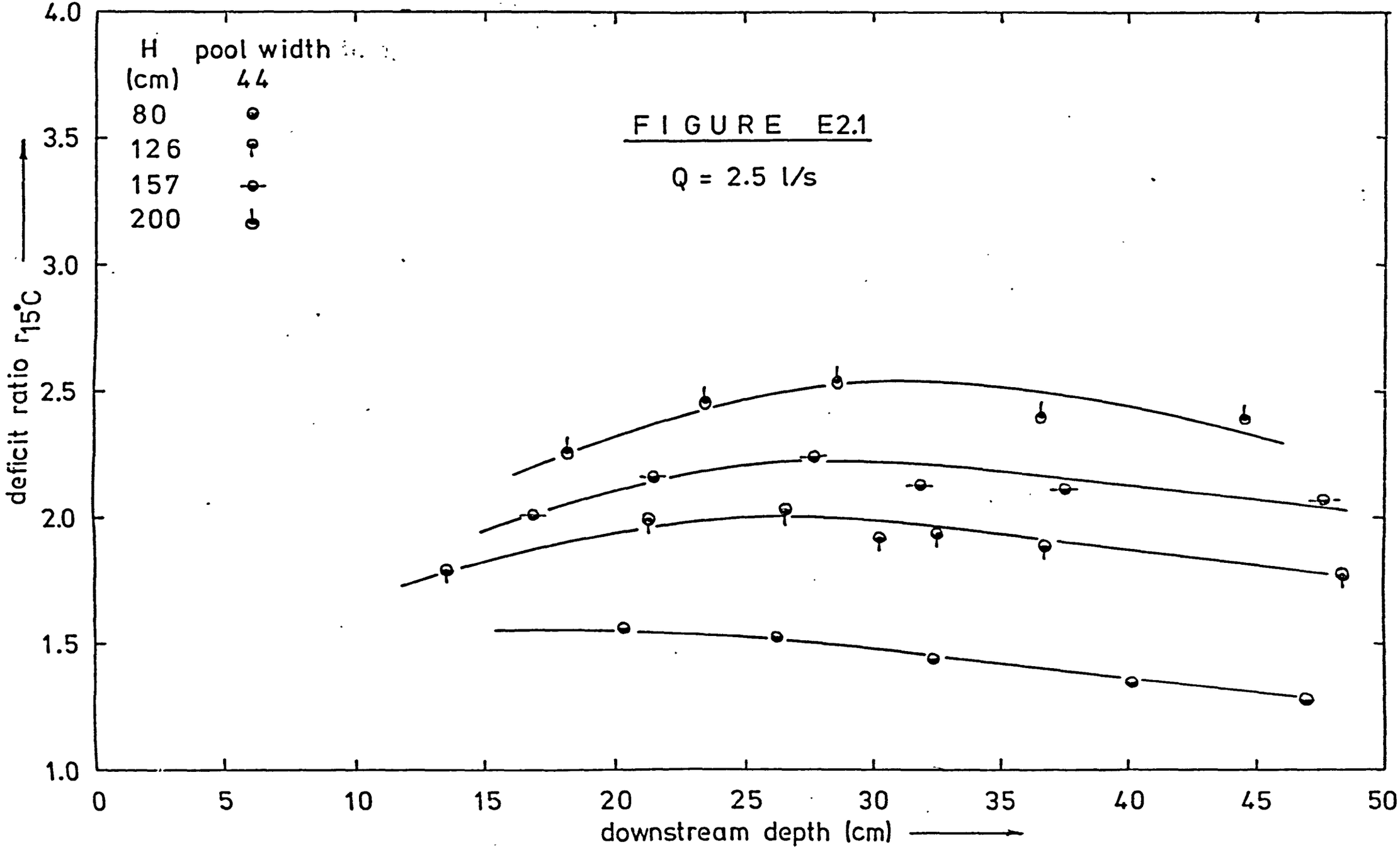
H (cm)
pool width
44
80
126
157
200
FIGURE E2.1
Q = 2.5 l/s
deficit ratio $r_{15°C}$
downstream depth (cm)
4.0
3.5
3.0
2.5
2.0
1.5
1.0
0
5
10
15
20
25
30
35
40
45
50

APPENDIX F

FREE OVERFALL DATA - TWIN CRESTED NOTCH

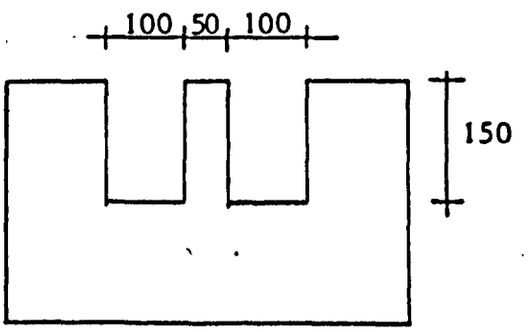

Figures F1 to F3 Tests with tap water

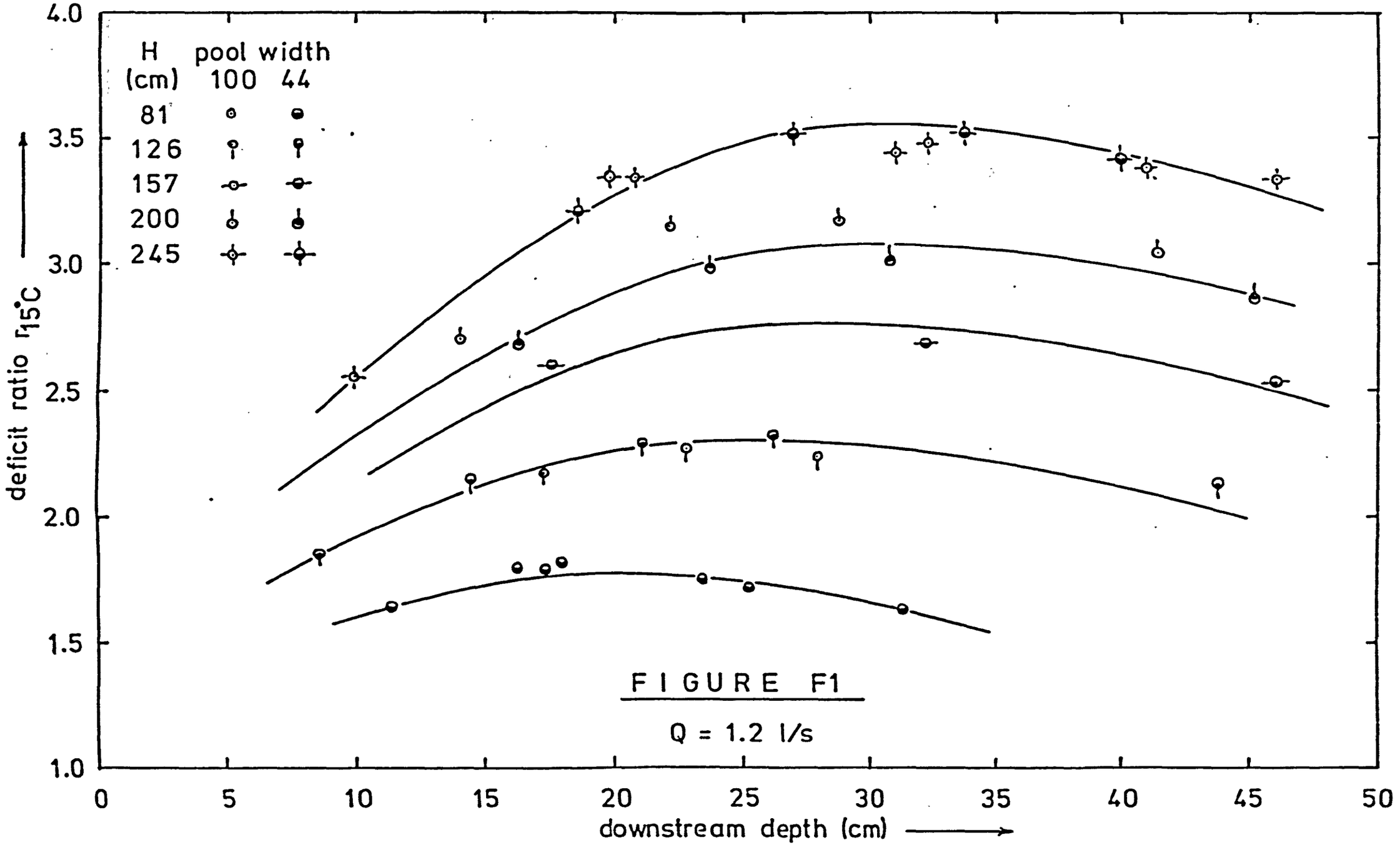

FIGURE F1

Q = 1.2 l/s

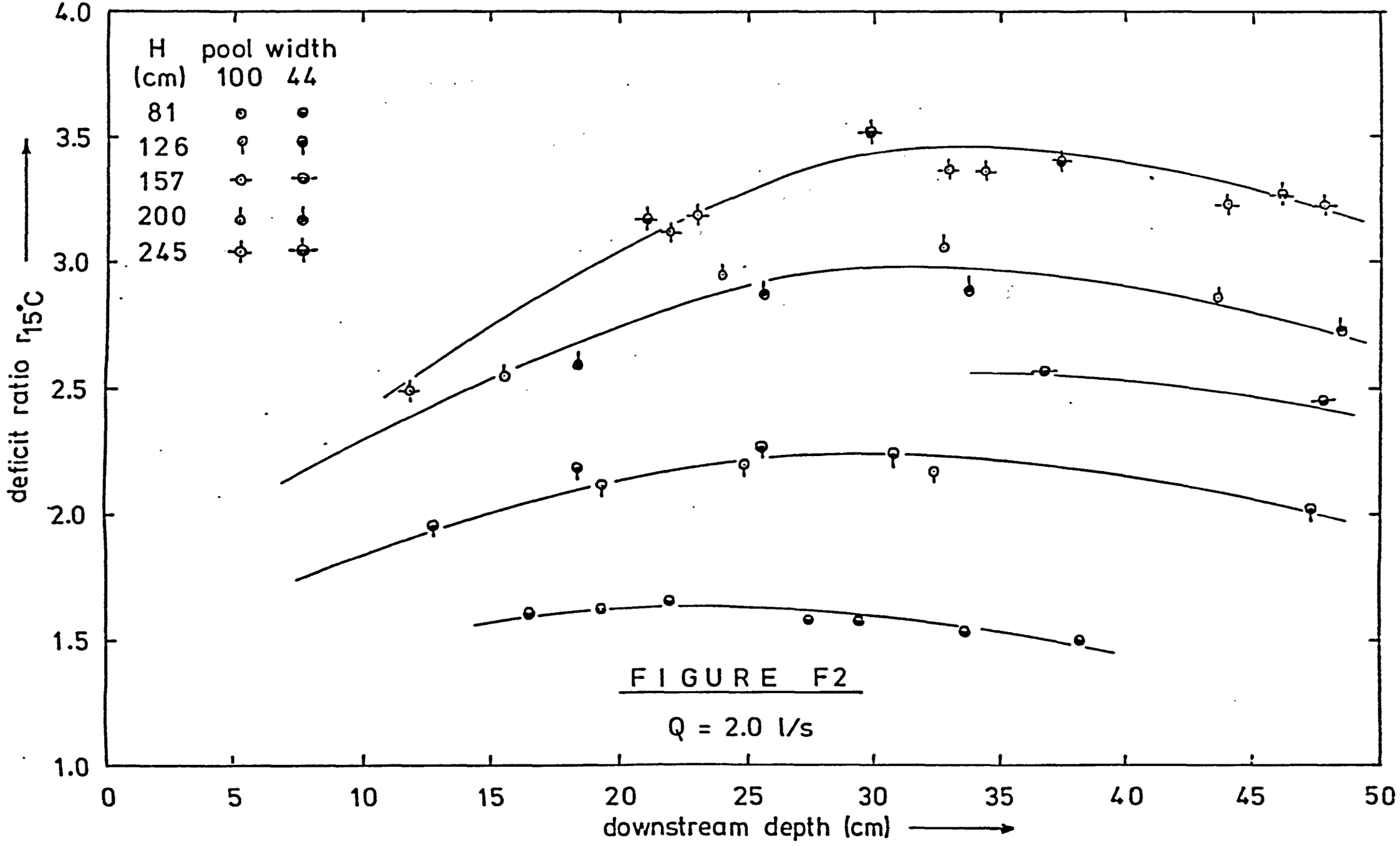

FIGURE F2

Q = 2.0 l/s

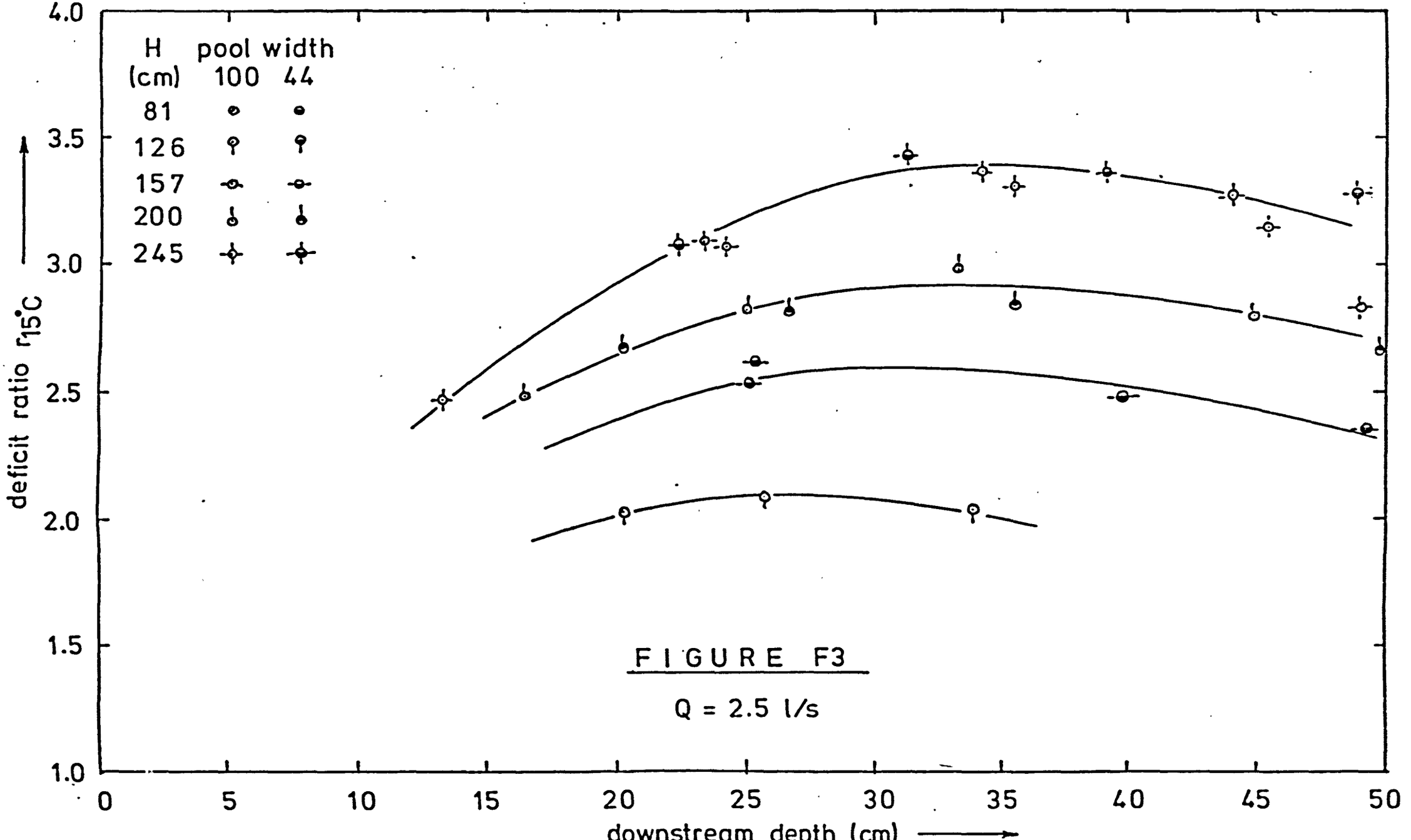

FIGURE F3

Q = 2.5 l/s

REFERENCES

ADENEY, W.E. and BECKER, H.G. (1919). The determination of the rate of solution o atmospheric nitrogen and oxygen by water. Part I. Phil. Mag. 38, 225, 317-337.

ADENEY, W.E. and BECKER, H.G. (1920). The determination of the rate of solution of atmospheric nitrogen and oxygen by water. Part II. Phil. Mag. 39, 232, 385-404.

ALBRECHT, D. (1968). Beluftung des Ruhrwassers am wehr Spillenburg. Die Wasserwirtschaft 11, 317-321.

APTED, R.W. (1975). The mechanics of aeration at weirs with special reference to river quality. M.Sc. thesis, University of Newcastle upon Tyne.

APTED, R.W. and NOVAK, P. (1973). Some studies of oxygen uptake at weirs. Proc. XV Congress I.A.H.R., Paper B23, 177-186.

AVERY, S. and NOVAK, P. (1975). Oxygen uptake in hydraulic jumps and at overfalls. Proc. XVI Congress I.A.H.R., Paper C38, 329-337.

BAIRD, M.H.I. and DAVIDSON, J.F. (1962). Annular jets. II Gas absorption. Chem. Engng Sci. 17, 473-480.

BARNHART, E.L. (1969). Transfer of oxygen in aqueous solutions. Proc. A.S.C.E. 95, SA3, 645-661.

BARRETT, M.J. and GAMESON, A.L.H. and OGDEN, C.G. (1960). Aeration studies at four weir systems. J. Wat. Wat. Engng 64, 207-213.

BENSON, B.B. and PARKER, P.D.M. (1961). Relations among the solubilities of nitrogen, argon, and oxygen in distilled water. J. Phys. Chem. 65, 1489-1496.

BEWTRA, J.K. and NICHOLAS, W.R. (1964). Oxygenation from diffused air in aeration tanks. J. WPCF 36, 10, 1195-1224.

BEWTRA, J.K. and NICHOLAS, W.R. and POLOKOWSKI, L.B. (1970). Effect of temperature on oxygen transfer in water. Wat. Research 4, 115-123.

BLACK, W.M. and PHELPS, E.B. (1911). The discharge of sewage into New York harbour. Report made to the Board of Estimate and Appointment, New York City.

BOWERS, R.H. (1955). The mechanics of bubble formation. J. appl. Chem. 5, 542-8.

BRIERLEY, M.R. and STEEL, R. (1959). Agitation-Aeration in submerged fermentation. II Effect of solid disperse phase on oxygen absorption in a fermentor. Appl. Microbio. 7, 57-61.

BRIUZN, J. and TUINZAAD, H. (1958). The relationship between depth of U-Tubes and the aeration process. J. Am. Wat. Wks Assn 50, 879.

CAMPBELL, F.B. and GUYTON, B. (1953). Air demand in gated outlet works. Proc. Minnesota Int. Hydraulics Convention, 529-532.

CHARLTON, J.A. (1970). The air control of self priming siphon spillways. Ph.D thesis, King's College, London.

CHURCHILL, M. (1961). Effect of water temperature on stream reaeration. 31. Progress Report on sanitary engineering research. Proc. A.S.C.E. 87, SA6, 59-71.

CHURCHILL, M.A. and ELMORE, H.L. and BUCKINGHAM, R.A. (1962). The prediction of stream reaeration rates. Proc. A.S.C.E. 88, SA4, 1-46.

COPPOCK, P.P. and MEIKLEJOHN, G.T. (1951). The behaviour of gas bubbles in relation to mass transfer. Trans. Inst. Chem. Engrs 29, 75-86.

DANCKWERTS, P.V. (1951). Significance of liquid film coefficients in gas absorption. Ind. Engng Chem. 43, 1460-7.

DEPARTMENT OF THE ENVIRONMENT (1973). Notes on water pollution, No. 61.

DEPARTMENT OF SCIENTIFIC AND INDUSTRIAL RESEARCH (1958). Water pollution research, 1957. H.M.S.O., 15-16.

DOBBINS, W.E. (1962). Mechanisms of gas absorption by turbulent liquids. Advances in Wat. Poll. Research 1.

DOWNING, A.L. (1958). Aeration in relation to water treatment. Proc. Soc. Wat. Treatm. Exam. 7, 66-101.

DOWNING, A.L. and TRUESDALE, G.A. (1955). Some factors affecting the rate of solution of oxygen in water. J. appl. Chem. 5, 570-581.

DRESNACK, R. and METZGER I. (1968). Oxygen response and aeration in streams. Proc. 23rd Ind. Waste Conf., Purdue Univ., Part I, 262-274.

ECKENFELDER, W.W. (1959). Factors affecting the aeration efficiency of sewage and industrial wastes. Sew. Ind. Wastes 31, 1, 60-70.

ECKENFELDER, W.W. and BARNHART, E.L. (1961). Effect of organic substances on the transfer of oxygen from air bubbles in water. J. Amer. Inst. Chem. Engng 7, 631-4.

ECKOLDT, M. (1962). Die Künstliche belüftung der flüsse. Deutsche Gewässerkundliche Mitteilungen, No.1, p.1.

ERVINE, D.A. and ELSAWY, E.M. (1975). The effect of a falling nappe on river aeration. Proc. XVI Congress I.A.H.R., Paper C45, 390-398.

FASSO (1956). Experimental research on air entrainment in gates outlet works. Milano.

FOX, C.J.J. (1909). On the coefficients of absorption of nitrogen and oxygen in distilled water and sea water, and of atmospheric carbonic acid in sea water. Trans. Far. Soc. 5, 68-87.

FOULK, C.W. and MILLER, J.N. (1931). Ind. Engng Chem. 23, 1283.

GAMESON, A.L.H. (1957). Weirs and the aeration of rivers. J. Inst. Wat. Engrs, 11, 477-490.

GAMESON, A.L.H. and ROBERTSON, K.G. (1955). The solubility of oxygen in pure water and sea water. J. appl. Chem. 5, 502.

GAMESON, A.L.H., VANDYKE, K.G. and OGDEN, C.G. (1958). The effect of temperature on aeration at weirs. Wat. Wat. Engng 62, 489-492.

GANNON, J. (1967). Aeration of waste treatment plant outfall structures. J. Wat. Wastes Engng 4, 4, 62-65.

GREEN, E.J. (1965). A redetermination of the solubility of oxygen in sea water and some thermodynamic implications of the solubility relations. D.S.R. 9337, Contract GP-486 Nat.Sci. Foundation, Dept. Geol. Geoph., Mass. Inst. Tech.

GUYTON, B. (1958). Field investigation of spillways and outlet works. Proc. A.S.C.E. 84, HY1, Paper 1532.

HABERMAN, W.L. and MORTON, D.K. (1956). Experimental study of bubbles moving in liquids. Trans. A.S.C.E. 121, 227-250.

HAINDL, K. (1958). Theory of the hydraulic jump in closed conduits and its use in practice. Výzkumný ústav vodohospodářský práce a studie, Sešit 98, Praha-Podbaba.

HAINDL, K. and SOTORNIK, V. (1957). Quantity of air drawn into a conduit by the hydraulic jump and its measurement by gamma radiation. Proc. VII Congress I.A.H.R., Paper D31, 1-7.

HART, I.C. (1967). Nomograms to calculate the dissolved oxygen contents and exchange coefficients. Water Research 1, 391-5.

HATFIELD, W.D. (1941). Sew. Wks. J. 13, 557.

HENDERSON, F.M. (1967). Open Channel Flow. MacMillan, New York.

HIGBIE, R. (1935). The rate of absorption of a pure gas into a still liquid during short periods of exposure. Trans. Amer. Inst. Chem. Engrs 31, 365-389.

HISE, R.E. (1975). A model of gas dissolution in water. Symp. on Reaeration Research, A.S.C.E. Hyd. Div., Glenstone Lodge, Gatlinburg, Tennessee.

HOLLER, A.G. (1970). Reaeration of discharge through hydraulic structures. U.S. Army Corps of Engineers.

HOLLER, A.G. (1971). The mechanism describing oxygen transfer from the atmosphere to discharge through hydraulic structures. Proc. XIV Congress I.A.H.R., Paper A45, 373-382.

HOLROYD, A. and PARKER, H.B. (1949). Investigations on the dynamics of aeration. J. and Proc. Inst. Sew. Purif., Part 3, 292-323.

HORENI, P. (1956). Disintegration of a free jet of water in air. Výzkumny ūstav vodohospodářský práce a studie, Sešit 93, Praha-Podbaba.

IMHOFF, K.R. and ALBRECHT, D. (1972). Influence of temperature and turbulence on the oxygen transfer in water. Advances in Wat. Poll. Research, Jerusalem.

INTERNATIONAL CRITICAL TABLES (1925). McGraw-Hill Book Co., New York.

IPPEN, A.T. and CARVER, C.E. (1954). Basic factors of oxygen transfer in aeration systems. Sew. Ind. Wastes, 26, 7, 813-827.

ISAACS, W.P. (1967). Atmospheric oxygenation and biological deoxygenation in an idealised streamflow model. Ph.D. thesis, Oklahoma State University.

ISAACS, W.P. and MAAG, J.A. (1968). Investigation of the effects of channel geometry and surface velocity on the reaeration rate coefficient. Proc. 23rd Ind. Waste Conf., Purdue Univ., 619-639.

JARVIS, P.J. (1970). A study in the mechanics of aeration at weirs. M.Sc. thesis, University of Newcastle upon Tyne.

JOHNSON, P.L. and KING, D.L. (1975). Prediction of dissolved gas at hydraulic structures. Symp. on Reaeration Research, A.S.C.E. Hyd. Div., Glenstone Lodge, Gatlinburg, Tennessee.

KALINSKE, A.A. and ROBERTSON, J.M. (1942). Entrainment of air in flowing water - closed conduit flow. Proc. A.S.C.E. 68, 1141-1153.

KAPLOVSKY, WALTERS and SOSEWITZ (1964). Artificial aeration of canals in Chicago. J. WPCF 36, 463-474.

KARTHA, C.V. (1968). Effects of inflow conditions on the hydraulic jump. Master of Applied Science thesis, University of Toronto.

KISHINEVSKI, M. (1955). Two approaches to the theoretical aspects of gas absorption. J. Appl. Chem. Russia.

KLOTS, C.E. and BENSON, B.B. (1963). Solubilities of nitrogen, oxygen and argon in distilled water. J. Mar. Research 21, 48-57.

KRENKEL, P.A. and ORLOB, G.T. (1962). Turbulent diffusion and the reaeration coefficient. Proc. A.S.C.E. 88, SA2, 53-83.

LEUTHEUSSER, H.J. and KARTHA, V.C. (1972). Effects of inflow condition on hydraulic jump. Proc. A.S.C.E. 98, HY8, 1367-85.

LEUTHEUSSER, H.J., RESCH, F.J. and ALEMU, S. (1973). Water quality enhancement through hydraulic aeration. Proc. XV Congress I.A.H.R. 2, Paper B22, 167-175.

LEWIS, W.K. and WHITMAN, W.G. (1924). Principles of gas absorption. Ind. Engng Chem. 16, 1215-1220.

LE BOSQUET, M. Discussion of "The oxygen sag and DO relationships in streams" by H.W. STREETER in "Oxygen relationships in streams" Tech. Rept W58-2, Robert A. Taft Sanitary Engng Centre, U.S. Public Health Service.

LIN, T.J. and DONNELLY, H.G. (1966). Gas bubble entrainment by plunging laminar jets. A.I. Ch. E. Journal 12, 3, 563-571.

LONDONG, D. (1967). Flusswasserbelüftung an der Lippe. Lecture given in the "Haus der Technik", Meeting No. 104, May 17 & 18, Essen.

MANCY, K.H. and OKUN, D.A. (1960). Effects of surface active agents on bubble aeration. J. WPCF 32, 4, 351.

MANCY, K.H. and OKUN, D.A. (1965). The effects of surface active agents on aeration. J. WPCF 37, 212-227.

MANCY, K.H. and OKUN, D.A. (1968). Discussion of a paper by VAN DER KROON (1968). 4th Int. Conf. on Wat. Poll. Research, 231-239.

MASTROPIETRO, M.A. (1968). Effects of dam reaeration on waste assimilative capacities of the Mohawk river. Proc. 23rd Ind. Waste Conf., Purdue University, 754-765.

MITCHELL, R.C. (1973). U-Tube aeration. EPA-670/2-73-031, Environmental Protection Techn. Series Project No. 17050 DVT, U.S. Govt. Printing Office, Washington D.C.

MONTGOMERY, H.A.C., THOM, N.S. and COCKBURN, A. (1964). Determination of dissolved oxygen by the Winkler method and the solubility of oxygen in pure water and sea water. J. appl. Chem. 14, 280.

MOORE, W.L. (1941). Energy loss at the base of a free overfall. Proc. A.S.C.E. 67, 1697-1714.

NAKASONE, H. (1975). Derivation of aeration equation and its verification - Study on the aeration at falls and spillways (1). Trans. J.S.I.D.R.E., 42-48.

NATERMAN, E. (1952). Eine neue berechnungsweise des sauerstoffhaushaltes veruntreinigter flüsse nebst einigen folgerungen. G.W.F., No 16.

NEGULESCU, M. and ROJANSKI, V. (1969). Recent research to determine reaeration coefficient. Water Research 3, 189-202.

O'CONNOR, D.J. and DOBBINS, W.E. (1956). Mechanics of reaeration in natural streams. Proc. A.S.C.E. 82, SA6, Paper 1115.

OGDEN, C.G., GIBBS, J.W. and GAMESON, A.L.H. (1959). Some factors affecting the aeration of flowing saline water. Wat. Waste Treatm. Journal 7, 392-6.

OWENS, M. and EDWARDS, R.W. (1963). Some oxygen studies in the river Lark. Proc. Soc. Wat. Treatm. Exam. 12, 126-145.

OWENS, M., EDWARDS, R.V. and GIBBS, J.W. (1964). Some reaeration studies in streams. Int. Jour. Air and Water Poll. 8, 469-486.

PALLADINO, A.J. (1961). Investigations of methods of stream improvement. Ind. Water and Wastes 6, 3, 87.

PASVEER, A. (1955(i)). Research on activated sludge. VI Oxygenation of water with air bubbles. Sew. Ind. Wastes 27, 10, 1130.

PASVEER, A. (1955(ii)). Untersuchungen über das belebt schlammverfahren für die reinigung von abwasser. Ges.-Ing., P. 332.

PETERKA, A.J. (1963). Hydraulic design of stilling basins and energy dissipators. Engng. Monograph No. 25, U.S.B.R., U.S. Govt. Printing Office, Washington D.C.

PETRIKAT (1958). Vibration tests on weirs and bottom gates. Wat. Power.

PHILPOTT, J.A. (1952). Ph.D. thesis, University of London.

PÖPEL, H.J. (1972). Aeration and gas transfer. Delft Univ. of Techn. Depart. of Civ. Engng, Div. of San. Engng.

PYE, D.J. (1947). Chemical fixation of oxygen. J. Am. Wat. Wks Assn 39, 1121-7.

QUIRK, LAWLER and MATUSKY (1966). Study of the assimilation capacity of the St. Louis river from Cloquet, Minnesota to Lake Superior. Report to Northwest Paper and Wood Conversion Company.

RAO, N.S.L. and KOBUS, H.E. (1975). Characteristics of self-aerated free surface flows. Water and Waste Water Current Research and Practice, Vol. 10.

ROUSE, H.T., SIAIO, T.T., and NAGARATNAM, S. (1959). Turbulence characteristics of the hydraulic jump. Trans. A.S.C.E. 124, 926-950.

RAJARATNAM, N. (1962). An experimental study of air entrainment characteristics of the hydraulic jump. J. Inst. Engrs of India 42, No. 7.

RENNER, J. (1973). Lufteinmischung beim aufprall eines ebenen wasserstrahls auf eine wand. Doktor-Ingenieurs dissertation, Universität Karlsruhe.

RESCH, F.J. and LEUTHEUSSER, H.J. (1971). Mesures de turbulence dans le ressaut hydraulique. La Houille Blanche, No. 1, 17-32.

RESCH, F.J. and LEUTHEUSSER, H.J. (1972). Le ressaut hydraulique: mesures de turbulence dans la région diphasique. La Houille Blanche, No. 4, 279-294.

RYDER, R.A. (1972). Dissolved oxygen control of activated sludge aeration. Water Research, 6, pp 441-445.

SAWYER, C.N. and McCARTY, P.L. Chemistry for Sanitary Engineers. McGraw Hill Book Co., New York.

SCRIVEN, L.E. and PIGFORD, R.L. (1958). On phase equilibrium at the gas-liquid interface during absorption. A.I.Ch.E. Journal 4, 439-444.

SEELIGER, R. (1949). Die Naturwissenschaften 36, 41.

SETSCHENOW, J. (1875). Memoirs Acad. Imperial Sci. St. Petersburg 22, No. 6.

SHIRLEY, R.W. (1950). Entrainment of air by liquid jets. M.Sc. thesis, University of Iowa.

SHREIR, L.L. (1963). Corrosion. Vol. 1 - Corrosion of metals and alloys. George Newnes Ltd., London.

SPEECE, R.E., ADAMS, J.L. and WOOLDRIDGE (1969). U-Tube aeration operating characteristics. J. A.S.C.E., SA3, 563-574.

SPEECE, R.E. and RAYYAN, F. (1973). Hyplomnion aeration with commercial oxygen. Vol. 1 Dynamics of bubble plume. EPA - 660/2 - 73 - 025a, Environmental Protection Techn. Series Project 16080 FW, U.S. Govt. Printing Office, Washington D.C.

STREETER, H.W. and PHELPS, E.B. (1925). A study of the pollution and natural purification of the Ohio river. Public Health Bull. 146, U.S. P.H. Service, Washington D.C.

TEBBUTT, T.H.Y. (1971). Dissolved oxygen - its significance in effluents. Effl. and Wat. Treatm. J., 39-44.

TEBBUTT, T.H.Y. (1972). Some studies on reaeration in cascades. Wat. Research 6, 297-304.

THACKSTON, E.G. and KRENKEL, P.A. (1969. Reaeration prediction in natural streams. J. A.S.C.E. 95, SA1, 65.

THACKSTON, E.L. and SPEECE, R.E. (1966). Review of Supplemental reaeration of flowing streams. J. WPCF 38, 1614-1622.

TRUESDALE, G.A., DOWNING, A.L., LOWDEN, G.F. (1955). The solubility of oxygen in pure water and sea-water. J. appl. Chem. 5, 53-62.

TRUESDALE, G.A. and VANDYKE, K.G. (1958). The effect of temperature on the aeration of flowing water. Wat. Waste Treatm. J. 7, 9-11.

TSIVOGLOU, E.C. and WALLACE, J.R. (1972). Characterisation of stream reaeration capacity. EPA-R3-72-012, U.S. Environmental Protection Agency Ecological Research Series, Project No. 16050 EDT, Washington D.C.

TYLER, R.G. (1946). Polluted streams cleared up by aeration. Civil Eng. 16, 348.

VAN DER KROON, G.T.M. (1968). The influence of suspended solids on the rate of oxygen transfer in aqueous solutions. 4th Int. Conf. on Wat. Poll. Research, 219-229.

VAN DER KROON, G.T.M. and SCHRAM A.H. (1969). Weir aeration - Part 1: Single free fall. $H_2O(2)$, No. 22, 528-537.

VERSCHOOR, H. (1950). Some aspects of the motion of a swarm of gas bubbles rising through a vertical liquid column. Conference on formation and properties of gas bubbles. Trans. Inst. Chem. Eng. 28, 52-57.

WAGNER, H. (1958). Versuche mit der kunstlichen flubwasserbeluftung. Deutsche Gewasserkundliche Mitteilungen II, 4, 73.

WEST, J.M. (1970). Electrodeposition and Corrosion Processes. Van Nostrand Reinhold Co., London.

WILEY, A.J. and LUECK, B.F. (1960). Turbine aeration and other methods of aerating streams. Tappi 43, 241.

WILEY, A.J., LUECK, B.F., SCOTT, R.H. and WISNIEWSKI, T.F. (1960). Commercial scale operation of turbine aeration on Wisconsin rivers. J. WPCF 32, 2, 186.

WILHELMS, S.C. (1975). Reaeration through hydraulic structures. Symp. on Reaeration Research, A.S.C.E. Hyd. Div., Glenstone Lodge, Gatlinburg, Tennessee.

WINKLER, R.W. (1888) Ber. dtsch. chem. Ges. 21, 2843.

WISNER, P. (1965). On the role of the Froude number in the air entrainment by high velocity flow. Proc. XI Congress I.A.H.R., Paper 1.15.

YUKIO, M., ILGININ, S. and NAKAGAUR (1959). Air demand in conduits partly filled with flowing water. Proc. VIII Congress I.A.H.R.

ZIEMINSKI, S.A., GOODWIN, C.C. and HILL, R.L. (1960). The effect of some organic substances on oxygen absorption in bubble aeration. Tappi 43, 12, 1029-34.

Reprint from XVIth Congress, International Association for Hydraulic Research, São Paulo, 1975

INTERNATIONAL ASSOCIATION FOR HYDRAULIC RESEARCH

OXYGEN UPTAKE IN HYDRAULIC JUMPS AND AT OVERFALLS (Subject C.)

BY S. AVERY
Research Student

P. NOVAK
Professor of Civil & Hydraulic Engineering

Department of Civil Engineering,
University of Newcastle upon Tyne,
Great Britain

SYNOPSIS

This paper presents results of a continuation of oxygen uptake studies first reported at the XVth IAHR Congress in 1973. Experiments on hydraulic jumps have now been completed and the effects of discharge and upstream oxygen deficit have been taken into account; the results are presented in a dimensionless form and conclusions about similarity of oxygen uptake are drawn. The previous studies of oxygen uptake at a free overfall have been extended over a wide range of discharges and height of fall; the results for the deficit ratio for solid jets and optimum downstream depth are again expressed in a dimensionless generally applicable form and the validity of the derived relationship is tested against other published results. The study of oxygen uptake at overfalls is continuing.

RÉSUMÉ

Le bulletin contient les résultats de la continuation des études de l'augmentation d'oxygène présentés pour la première fois au XVIè Congrès AIHR en 1973. Les expériences sur le ressant hydraulique ont été completées et tiennent compte des effets du debit et du déficit d'oxygène en amont. Les résultats sont présentés dans une forme sans dimension, et les conclusions rapportant sur la similitude de l'augmentation d'oxygène. Les études préalables sur l'augmentation d'oxygène dans un déversoir libre ont été étendues pour embrasser une grande étendue de debits d'eau et hauteurs de chute. Les resultats du rapport des déficits d'oxygène pour jetssolides et de profondeur optimale en aval sont de nouveau exprimés en forme sans dimension et généralement applicable et la validité de la relation dérivée a été vérifiée contre les résultats déjà publiés. Les études sur l'augmentation d'oxygène quise passe en barrages, continuent.

1. OXYGEN UPTAKE IN A HYDRAULIC JUMP

1.1 Theory and previously reported experiments

Previously reported experiments on the oxygen uptake in a hydraulic jump{1} based on preliminary experiments with one discharge (4.0 1/s) and one upstream oxygen deficit (C_1 = 55%) expressed the results as a correlation between the deficit ratio r ($r = \frac{100 - C_1}{100 - C_2}$, where C_1 is the upstream oxygen concentration expressed as % of saturation concentration C_s and C_2 the downstream concentration) and the energy loss in the hydraulic jump ΔE (cm):

$$r = 10^{0.0024\Delta E} ; \qquad (1)$$

this is within the tested range of $0.02 < \Delta E < 0.30$m and up to $\Delta E \simeq 1.0$m approximately equal to (ΔEmm):

$$r = 1 + 0.70\ \Delta E \qquad (2)$$

Holler {2} conducted experiments on oxygen uptake in a hydraulic jump using a 380mm wide flume and a discharge of 890cm^2/s; C_1 was $35 < C_1 < 80$%. Holler summarised his results by the equation:

$$r_{20} - 1 = 0.0043\ \Delta v^2 \qquad (3)$$

where Δv is the difference in measured velocities before and after the jump (Δv in ft/s).

Equations 1 to 3 have of course the disadvantage of not being expressed in a dimensionless form throughout.

The air entrainment in a hydraulic jump is well documented and has been proved to be a function of Froude number. Kalinske and Robertson {3} established (for a hydraulic jump in an open channel) the following equation for air entrainment:

$$\beta = \frac{Q_a}{Q} = K\ (Fr_1 - 1)^{1.4} \qquad (4)$$

(where Q_a is the air discharge and Q the water discharge and K a coefficient given by the authors as K = 0.0066. Haindl {4} verified equation 4 for a jump in a closed conduit and found k to vary between 0.0066 and 0.012.

The basic equation for oxygen transfer can be expressed as:

$$V \frac{dC}{dt} = k\ A(C_s - C) \qquad (5)$$

where V is the volume of liquid $\frac{dC}{dt}$ the rate of change of oxygen concentration C, k the liquid film coefficient and A the area of air-liquid interface. Eq. 5 can be rewritten as

---

{1} APTED R.W., NOVAK P. (1973). Some studies of oxygen uptake at weirs, XV Congress IAHR, Paper B23.

{2} HOLLER A.G. (1971). The mechanism describing oxygen transfer from the atmosphere to discharge through hydraulic structures, XIV Congress IAHR, Paper A45.

{3} KALINSKE A.A., ROBERTSON J.M. (1943). Closed conduit flow. Trans. A.S.C.E., 108, 1435-1516.

{4} HAINDL K. (1958). Theory of the hydraulic jump in closed conduits and its use in practice, Výzkumny ústav Vodohospodářský Práce a Studie, 98, Prague.

$$\ln \frac{100 - C_1}{100 - C_2} = \ln r = k \frac{A}{V} t$$

where t is the time of contact.

Substituting for ln r a series and taking the first two terms only we get:

$$r - 1 = k \frac{A}{V} t \qquad (6)$$

Neglecting the free water surface the contact area for n spherical bubbles radius R can be expressed as $A = n/4\pi R^2$ and $n = \frac{Q_a t}{4/3\pi R^3}$. Thus

$$\frac{A}{V} = \frac{Q_a 4\pi R^2 t}{4/3\pi R^3 Qt} = \frac{3}{R} \beta$$

From 6:

$$r - 1 = k \frac{3}{R} \beta t \qquad (7)$$

1.2 Experimental procedure and results

A comprehensive study of the oxygen uptake in a hydraulic jump with variable parameters C_1 and y_1 (upstream supercritical depth) was carried out. The experiments were carried out in a glass walled flume 3000mm long and 100mm wide with a sluice gate near the flume inlet. By adjusting the gate position and tail water level a hydraulic jump was created in the flume close to the gate. Oxygen saturated water was supplied from the laboratory circuit; upstream of the flume inlet the water was deoxygenated to the required level by controlled dosing with sodium sulphite and cobalt chloride in a mixing tank. Care was taken to ensure adequate reaction. The discharge was measured by an orifice meter in the flume supply line and the oxygen concentration by E.I.L. Dissolved Oxygen Meters which recorded the oxygen concentration as a percentage of saturated levels automatically compensating for temperature and which were calibrated against the standard Winkler chemical titration method.

The range of Froude numbers $Fr_1 = \frac{v_1}{\sqrt{gy_1}} = \frac{Q}{by_1^{3/2} g^{1/2}}$ was $2 < Fr_1 < 9$, the range of upstream oxygen content was $10\% < C_1 < 70\%$ (of saturation concentration C_s) and the range of discharges was $1.45 < Q < 7.10$ ℓ/s or expressed in terms of specific discharge ($q = \frac{Q}{b}$) $145 < q < 710$ cm^2/s.

The temperature range of the water T was $14^\circ < T < 18^\circ$C.

The full experimental results (including those used in {1} for the derivation of eq. 1) are plotted in fig. 1, in terms of $\frac{\Delta E}{y_1}$ against r for various values of C_1 and q. The advantage of this plot is that it is dimensionless and that both axes are functions of Froude number as (for both the Boussinesque and Coriolis coefficients $\beta = \alpha = 1$):

$$\frac{\Delta E}{y_1} = \frac{(-3 + \sqrt{1 + 8 Fr_1^2})^3}{16(-1 + \sqrt{1 + 8 Fr_1^2})} \qquad (8)$$

and r is clearly a function of β which is a function of Froude number. All experimental results have been corrected to a temperature 15°C using a previously reported {5} temperature correction:

$$r_T - 1 = (r_{15} - 1)\,[1 + \alpha\,(T-15)] \text{ where } \alpha = 0.0271 \qquad (9)$$

It can be seen from Fig.1 that the results are practically independent of the upstream concentration C_1 but vary substantially with q as would be expected from equation 7 as both r and t will vary with q. All the results can be expressed by a single relationship:

$$r_{15} = 1.00 + 0.023\,\left(\frac{q}{345}\right)^{3/4}\,\left(\frac{\Delta E}{y_1}\right)^{4/5} \qquad (10)$$

(with q in cm^2/s)

If the jump is close to the vena contracta then $q = v_1\,y_1 \simeq \sqrt{2gh}\,y_1$ where h is the difference between the upstream water level and y_1. Equation 10 then results in:

$$r \simeq 1.00 + 0.88\,h^{3/8}\,\Delta E^{4/5}\,y_1^{-1/20} \quad (h_1\ y_1, \Delta E \text{ in m})$$

In our experiments h varied between the limits $0.17 < h < 0.46$m, and y_1 between the limits $0.013 < y_1 < 0.03$m. Using the mean values $h \simeq 0.30$m and $y_1 = 0.022$m the results can approximately be expressed by a simple expression (which is not dimensionless with ΔE in m):

$$r \simeq 1 + 0.54\,\Delta E^{4/5} \qquad (2a)$$

which is quite close to equation 2; the difference in the coefficients can be explained by an extension of Froude numbers in the presently reported experiments.

For comparison Holler's results (obtained by private correspondence) were recalculated for a temperature of 15°C and compared with equation 10. The results are summarised in the table on Fig.1; the resultant correlation is very good.

1.3 Similarity considerations

Hydraulic jumps are of course modelled according to the Froude law of similarity and for a constant value of Froude number, $\frac{\Delta E}{y_1}$ is constant (eq. 8). According to eq. 10 for two cases I and II

$$\frac{r_I - 1.00}{r_{II} - 1.00} = M_{(r-1)} = \left(\frac{qI}{qII}\right)^{3/4} = \left[(M_\ell)^{3/2}\right]^{3/4} = M_\ell^{9/8} \qquad (11)$$

where M_ℓ is the length scale $\left(\frac{\ell_I}{\ell_{II}}\right)$.

Comparing equations 10 and 7 we can draw further tentative conclusions about the scale of the liquid film coefficient k:

{5} GAMESON A.L.H., VANDYKE K.G., OGDEN C.G. (1958). The effect of temperature on aeration at weirs. Wat. & Wat. Eng., 62, 489-492.

$$\frac{3}{R} k\beta t \simeq 0.023 \left(\frac{q}{345}\right)^{3/4} \left(\frac{\Delta E}{y_1}\right)^{4/5}$$

For constant Froude numbers $\frac{\Delta E}{y_1}$ and β are constant (eq. 4) and R is also practically constant i.e. the size of air bubbles entrained in the hydraulic jump is constant and independent of scale M_ℓ {4}.

The scale of the time of contact M_t can be assumed to be approximately given by $M_t = M_\ell^{1/2}$.

Thus:

$$M_k M_\ell^{1/2} \simeq M_\ell^{9/8}$$

The scale of the liquid film coefficient is therefore approximately $M_k \simeq M_\ell^{5/8}$. This result is only approximate as actually $M_t \neq M_\ell^{1/2}$. The scale of contact time for the actual hydraulic jump may be given by $M_\ell^{1/2}$, but the scale for the contact time in the aerated zone beyond the hydraulic jump will be bigger than $M_\ell^{1/2}$ as for an unchanged bubble size this zone will extend further beyond the bigger jump than indicated by the length scale. Thus it is likely that $M_t > M_\ell^{1/2}$ and $M_k < M_\ell^{5/8}$. It is important to realise that the largest discharge used in the experiments on which equations 10 and 11 are based was 710cm^2/s. Although the authors are confident that these equations can be safely used for substantially bigger discharges there may be an upper limit of their validity (in terms of q). For a constant value of y_1 the energy loss ΔE increases with q; this in turn results in an increase of macroturbulence and may lead to a situation where the value of the liquid film coefficient k is likely to converge to a constant. The consequence of this would be $M_k \simeq 1$ and $M_{(r-1)} \simeq M_\ell^{1/2}$.

2. OXYGEN UPTAKE AT OVERFALLS

2.1 Previous Studies

Results of previous experiments in Newcastle, as well as of some other studies, were briefly reported in 1973 {1}. Since then the WPRL {6} published additional results, incorporating their previously reported results, which could be expressed as:

$$r_T = 1 + 0.38\, a\, h\, (1-0.11h)\, (1 + 0.046T) \qquad (12)$$

Equation 12 is applicable for jets from rectangular notches falling over height h(m) (difference of upstream and downstream water levels) into a pool where the depth d is equal to or greater than that required for maximum oxygen transfer {1}. The range of h tested was $0.15 < h < 3.05$m. The parameter a is a function of water quality and is approximately 1.8, 1.6, 1.0, 0.65 respectively for clean, slightly polluted, moderately polluted and grossly polluted water (sewage effluent). The discharge used was about 1.8 1/s flowing over a 0.22m wide notch into a pool 0.30 x 0.30m^2.

Jarvis {7} reported for a jet falling from a 22.5° notch into a pool 0.61 x 0.61m^2 and discharge 0.65 1/s (clean laboratory water) the equation:

$$r_{15} = 2.05\, h^{0.434} \qquad (13)$$

{6} WATER POLLUTION RESEARCH LABORATORY (England). Aeration at weirs. Notes on Water Pollution, No.61, June 1973.

{7} JARVIS P.J. (1970). A study in the mechanics of aeration at weirs, M.Sc. Thesis, University of Newcastle upon Tyne, England.

which over the tested range of $0.40 < h < 1.8$m gives practically the same result as equation 12 with $a = 1.8$. Previous experiments conducted at Newcastle {1} have further shown that the oxygen uptake at a free overfall is dependent on the discharge and downstream depth as well as the height of fall; it was shown qualitatively and only in a very limited way quantitatively that the optimum downstream pool depth required for maximum oxygen transfer increased with the height of fall h and also with the discharge Q. Some of these findings agreed with conclusions reached by Van der Kroon {8}. These studies have now been extended over a wide range of variables to enable a comprehensive analysis.

2.2 Experimental procedure and results

Experiments were conducted in the laboratory using the same process for creating oxygen deficit and the same instrumentation for measuring the oxygen concentrations as reported in par. 1.2. From the mixing tank the deoxygenated water flowed through a rotameter measuring the discharge to the "upstream" pool; from there the jet fell from a 100mm wide rectangular notch to a "downstream" pool, whose length, depth, width and distance below the notch could be varied. In the presently discussed experiments the pool length and width were kept constant at length 1.5m and width 1.00m; the mode of jet entry was also not controlled in any way and corresponded to that of a solid or disintegrated jet; the depth was $0.10 < d < 0.50$m and the height of fall $0.40 < h < 2.10$m. The discharge was $0.6 < Q < 2.5$ l/s. One experiment was also conducted with a discharge 5.8 l/s. The upstream oxygen concentration was $40\% < C_1 < 50\%$.

Fig. 2 shows the measured values of r (for the depth $\geq$ the optimum depth d') as a function of h and Q. For comparison equations 12, 13 and Van der Kroon's data for seven notches have also been plotted in fig. 2. Fig. 2 contains results both for solid and disintegrated jets; the point of disintegration is indicated on each curve and was obtained by using an equation given by Hořeni {9}:

$$L = 31.2\, q^{0.32} \text{(cm)} \qquad (14)$$

where L is the length of passage of the jet from a rectangular notch and $q = \frac{Q}{b}$ is the discharge per unit length of crest of the notch). This agreed well with results obtained by visual observation.

Concentrating on solid jets it was observed that for $Q \leq 1.5$ l/s these rapidly contracted into an approximately circular cross-section with diameter D. Analysing the "optimum" depth d' (the limiting depth beyond which the entrained air is permitted to penetrate unobstructed deep into the pool and for which thus the deficit ratio is a maximum) as a function of height of fall h and the jet Froude No.

$$Fr_D = \frac{v}{\sqrt{gD}},$$

where v is the velocity of the jet at impact with the downstream pool, fig. 3 was obtained resulting in the equation:

$$\frac{d'}{h} = \frac{5.39}{Fr_D^{1.24}} \qquad (15)$$

{8} VAN der KROON G.T.M., SCHRAM A.H. (1969). Weir Aeration - part 1: Single free fall, H_2O (2), nr. 22, 528-537.

{9} HOŘENÍ P. (1956). Disintegration of a free jet of water in air. Výzkumný ústav Vodohospodářsky Práce a Studie, 93, Prague.

The use of the jet Froude number Fr_D in these studies is justified by the fact that the air entrainment by the jet into the downstream pool will depend on the solid jet circumference at the point of impact. For a circular jet we could write $Q = q\pi D$; since $v = \sqrt{2gh}$ (assuming the coefficient of velocity C_v to be unity for small heights of fall) and $Q = \frac{\pi}{4} D^2 \sqrt{2gh}$. Then:

$$Fr_D = \frac{v}{\sqrt{gD}} = (\pi\sqrt{2})^{1/4} \left(\frac{\sqrt{gh^5}}{Q}\right)^{1/4} = 2^{-1/4} \left(\frac{gh^3}{q^2}\right)^{1/4} \qquad (16)$$

For non-circular jets (in our case $Q > 1.5$ 1/s) and for $q = R\sqrt{2gh}$ equation 16 in the form $Fr_D = \left(\frac{gh^3}{2q^2}\right)^{1/4}$ is also applicable; in this case $D = 4R$ is an equivalent jet diameter and for q we must substitute $q = \frac{Q}{p}$ where p is the perimeter of the jet. Using equation 16, equation 15 can be rewritten:

$$\frac{d'}{h} = 3.39 \left(\frac{Q}{\sqrt{gh^5}}\right)^{0.31} = 6.68 \left(\frac{q^2}{gh^3}\right)^{0.31} \qquad (17)$$

For solid jets the results shown on fig. 2 have been recalculated in terms of Fr_D, plotted on fig. 4, and expressed by the equation:

$$r = 1 + 0.004\ Fr_D^{2.5} \qquad (18)$$

As can be seen from fig. 4 Van der Kroon's results agree quite well with equation 18 (the number of notches must of course be taken into account as Fr_D for two notches is $\sqrt[4]{2}\ Fr_D$ for one notch at the same discharge); further , circular jets have been assumed which is reasonably correct only for the case of multiple notches. The jet from a V notch disintegrates quickly and only one point for a small height of fall (assuming a circular section) has been included in the figure, again with reasonable agreement.

The results for the higher values of Fr_D for the bigger discharge 5.8 1/s deviate somewhat from the others; for this discharge the solid jet remained flat throughout the height of fall before disintegration and considerable uncertainty persisted about the actual perimeter at higher values of h (high Fr_D), although an attempt was made to establish this from preliminary measurement.

The WPRL results are on a quite different curve; apart from the fact that these refer again to a flat jet (this was taken into account by measuring the jet width and estimating q), this difference is attributed to the retention and contact time in downstream pool which was substantially lower in the WPRL experiments than in the authors' or Van der Kroon's work. An overall analysis must thus - apart from the depth of the downstream pool - take into account the shape and volume of the pool as well as the mode of entry of the jet. These factors, as well as an analysis of the disintegrated jet, form the basis of further work at Newcastle.

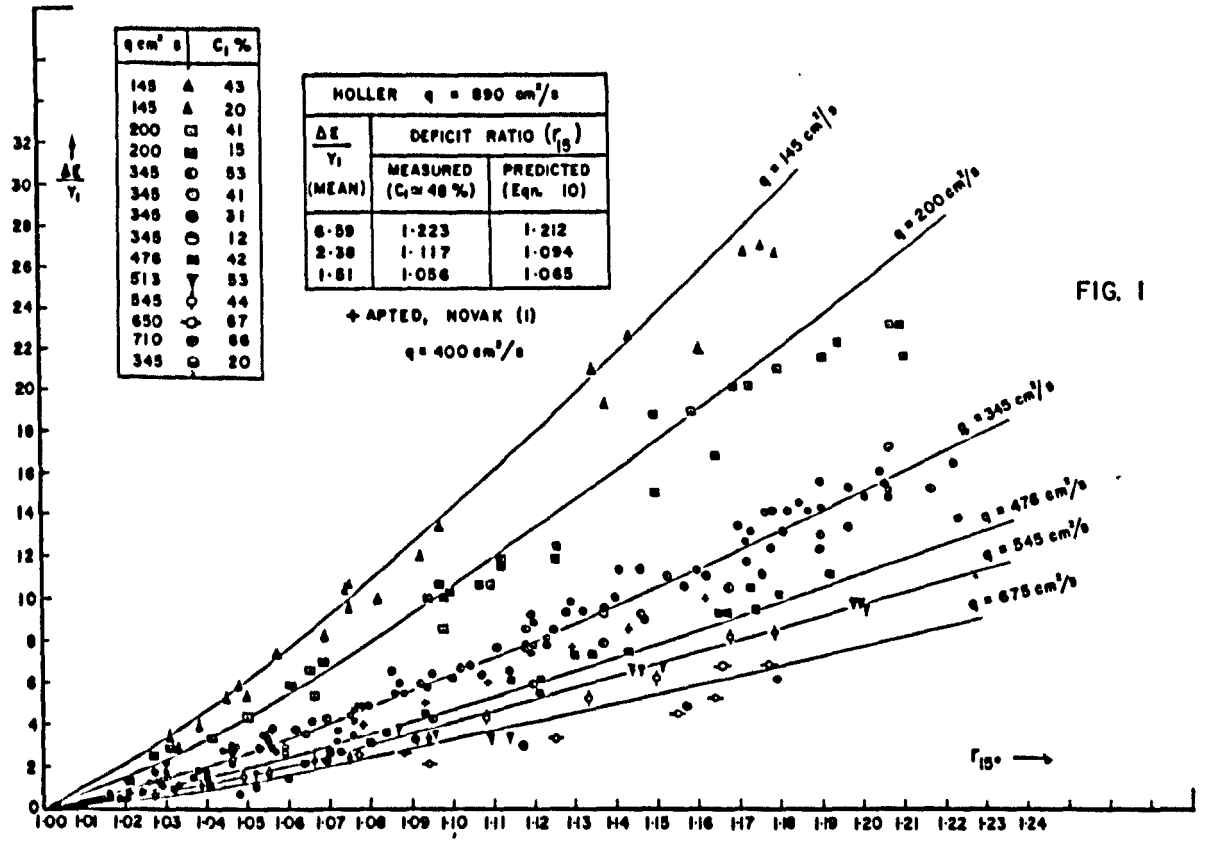
q cm²/s | C_1 %
148 43
145 20
200 41
200 15
345 53
345 41
345 31
345 12
476 42
513 53
545 44
650 67
710 66
345 20
HOLLER q = 890 cm²/s
ΔE/Y1 (MEAN) | DEFICIT RATIO (r15) MEASURED (C1≃48 %) | PREDICTED (Eqn. 10)
6·89 1·223 1·212
2·38 1·117 1·094
1·81 1·056 1·065
+ APTED, NOVAK (1)
q = 400 cm²/s
q = 145 cm²/s
q = 200 cm²/s
q = 345 cm²/s
q = 476 cm²/s
q = 545 cm²/s
q = 675 cm²/s
ΔE/Y1
r15° ⟶

FIG. 1

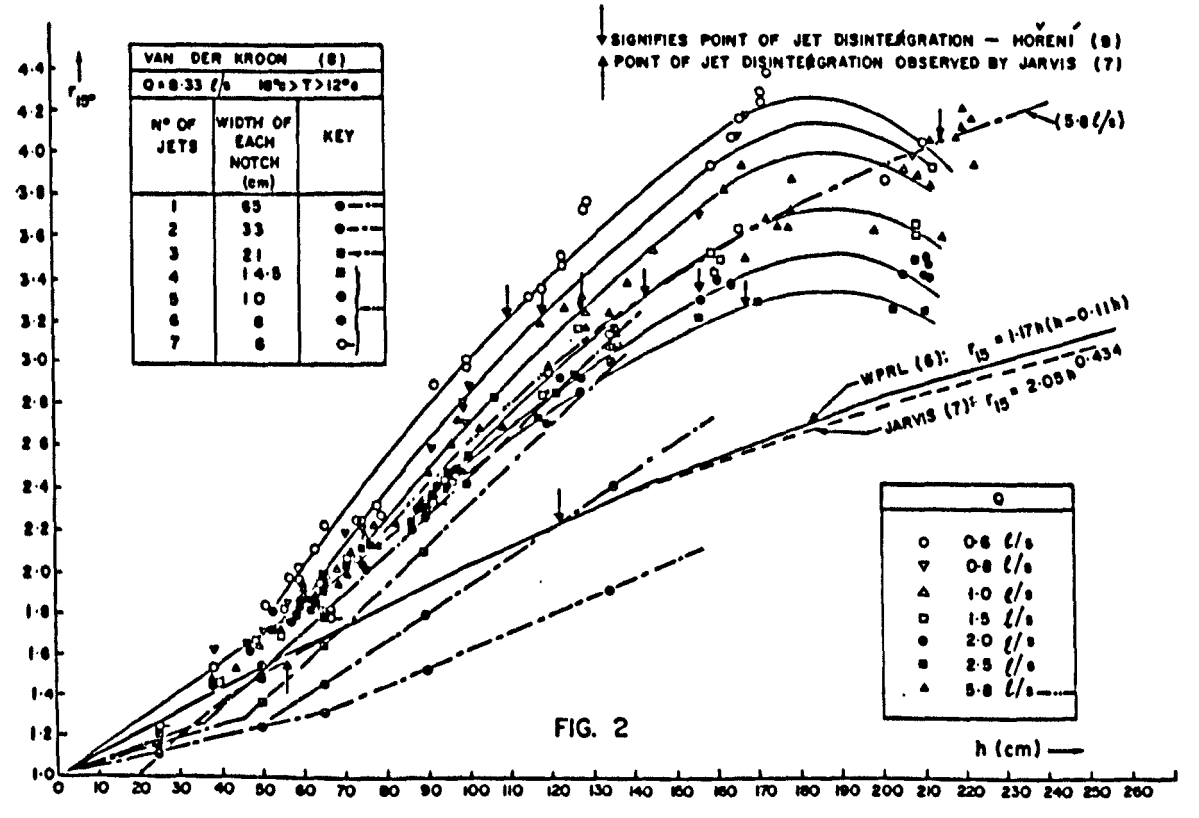
VAN DER KROON (8)
Q = 8·33 ℓ/s 18°C > T > 12°C
N° OF JETS | WIDTH OF EACH NOTCH (cm) | KEY
1 65
2 33
3 21
4 14·8
5 10
6 8
7 6
SIGNIFIES POINT OF JET DISINTEGRATION — HORENI (9)
POINT OF JET DISINTEGRATION OBSERVED BY JARVIS (7)
(5·8 ℓ/s)
WPRL (6): r15 = 1·17 h (h − 0·11 h)
JARVIS (7): r15 = 2·05 h^0·434
Q
0·6 ℓ/s
0·8 ℓ/s
1·0 ℓ/s
1·5 ℓ/s
2·0 ℓ/s
2·5 ℓ/s
5·8 ℓ/s
r15°
h (cm) ⟶

FIG. 2

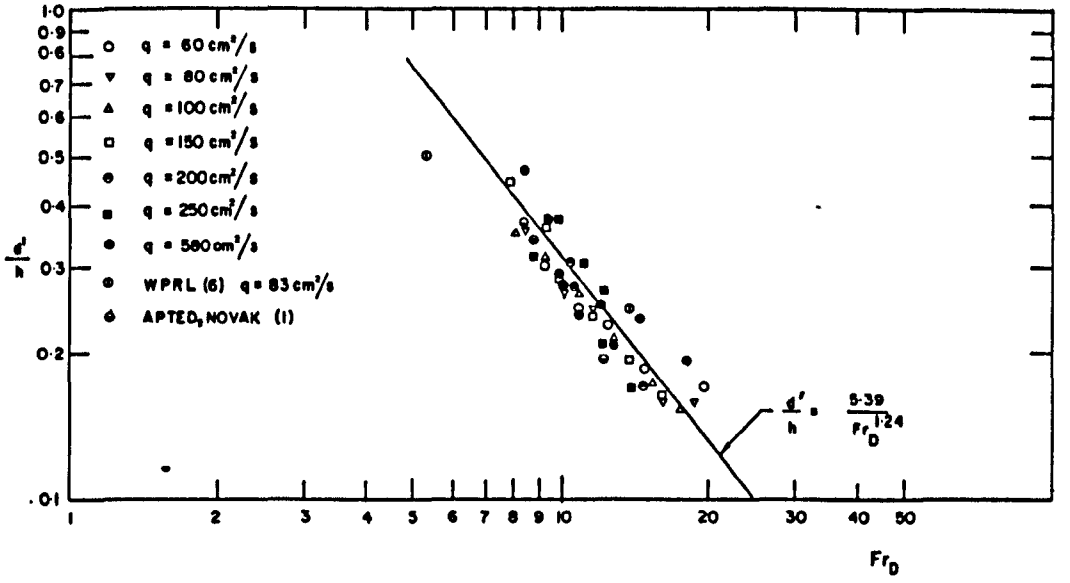
q = 60 cm²/s
q = 80 cm²/s
q = 100 cm²/s
q = 150 cm²/s
q = 200 cm²/s
q = 250 cm²/s
q = 560 cm²/s
WPRL (6) q = 83 cm²/s
APTED, NOVAK (1)
d'/h
Fr_D
d'/h = 5·39 / Fr_D^1·24

FIG. 3

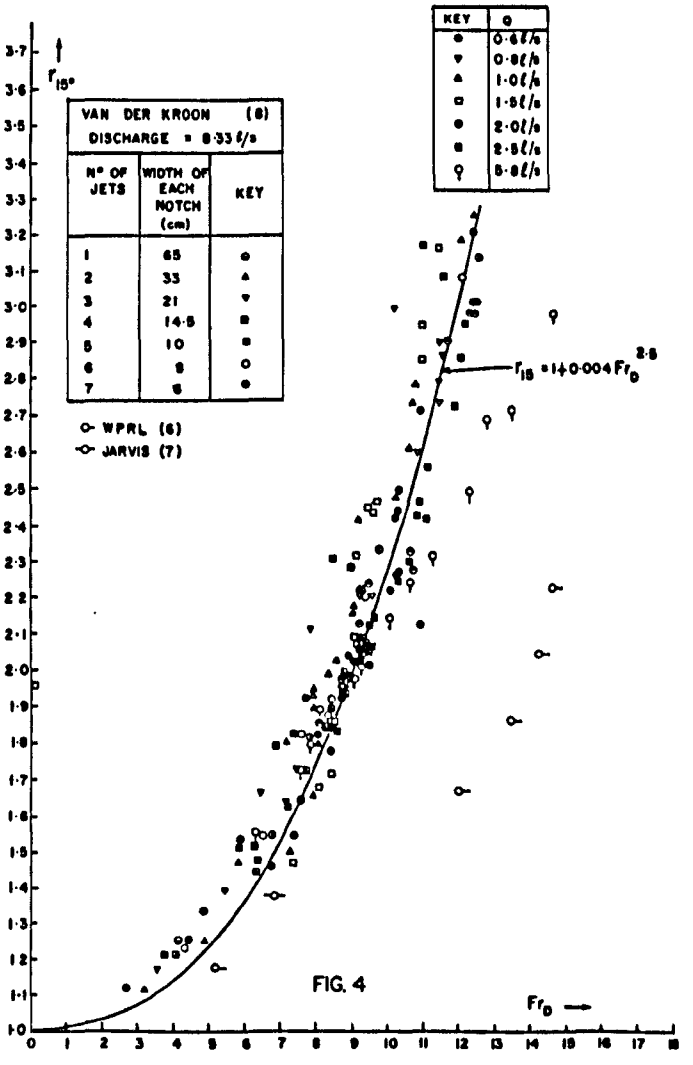
KEY
Q
0·6 ℓ/s
0·8 ℓ/s
1·0 ℓ/s
1·5 ℓ/s
2·0 ℓ/s
2·5 ℓ/s
3·8 ℓ/s
VAN DER KROON (8)
DISCHARGE = 8·33 ℓ/s
N° OF JETS
WIDTH OF EACH NOTCH (cm)
KEY
1 65
2 33
3 21
4 14·5
5 10
6 8
7 6
WPRL (6)
JARVIS (7)
r_15°
r_15° = 1·40·004 Fr_D^2·8
Fr_D

FIG. 4

E R R A T A

The following substitutions should be noted :

Figure 5.4 : "0.1 sec" for "0.01 sec"

Figure 7.13 : Legend

A, 1.0 l/s

A, 2.0 l/s

B, 1.82 l/s

B, 2.5 l/s

B, 5.0 l/s

C, 2.5 l/s

C, 5.0 l/s

Table 8.5 : "See Table 8.4" for "See Table 8.6"

Table 8.10, Column Eq. 2.11 : "5.21" for "4.21"

"6.33" for "5.33"

"3.28" for "2.28"

Table 8.10, Column Eq. 2.31 : "2.31" for "1.89"

"2.76" for "2.97

Table 8.10 : "Tables 8.4 and 8.5" for "Tables 8.6 and 8.7"

Page 199 : "tap water + 0.3% Na NO_3 " for "tap water"